Sterically-Hindered Derivatives of Pentacene: Synthesis, Properties, and Stability

by

Parisa Rezghi Rami

A thesis submitted in partial fulfillment of the requirements for the degree of

Master of Science

Department of Chemistry
University of Alberta

Abstract

Polycyclic aromatic hydrocarbons (PAHs), or more specifically pentacene derivatives, are promising candidates for solar energy conversion. Pentacenes can undergo π-stacking in solution and, consequently, can be poorly soluble. Furthermore, the pentacene moiety can react with oxygen, and it can participate in cycloaddition reactions with either itself or C_{60} used as an acceptor in a solar cell. This thesis focuses on the synthesis and characterization of monomeric and dimeric pentacenes with a focus to provide kinetic stability through substitution. All pentacene derivatives are characterized by ^{1}H NMR, ^{13}C NMR, IR, as well as mass spectroscopy. UV-vis spectroscopy, CV, DSC, and X-ray crystallography experiments have been used to study the effect of different substituents on photostability, electronic properties, thermal stability, and solid-state packing.

Chapter 1 of this thesis gives a short introduction into the synthesis of symmetrical and unsymmetrical functionalized pentacene derivatives and their application in solar cells.

Chapter 2 discusses the synthesis of sterically-hindered pentacene derivatives through substitution in 6- and 13-positions and the effects of the supertrityl substituent (tris(3,5-di-*tert*butylphenyl)methyl) on solubility, photostability, and thermal stability of symmetrical and unsymmetrical derivatives. The other functional groups that were used for substitutions are tri*iso*propylsilyl-, trimethylsilyl-, tri*iso*butylsilyl-, and phenylacetylene. The photostability of all derivatives has been studied via UV-vis in different solutions which are held in the presence of light and/or oxygen, as well as in the absence of light and/or oxygen. Interestingly, the compound bearing two bulky supertrityl groups was not

the most photostable derivative in solution, whereas it showed the greatest thermal stability in the liquid phase. The electrochemical and optical HOMO-LUMO gap calculated by CV and UV-vis data were in good agreement.

Chapter 3 focuses on the synthesis of two dimeric pentacene derivatives tethered by a *m*-phenylene spacer through connections at the 13-position of the pentacene scaffold via the Sonogashira cross-coupling reaction. Photo- and thermal stability comparisons of dimeric derivatives were not accomplished since one of the pentacene dimers was not sufficiently pure to give reliable results. In collaboration with the Torres group in Spain, SubPc-pentacene conjugates have been synthesized in order to explore intramolecular Förster resonance energy transfer (iFRET), and intramolecular singlet fission (iSF) is explored with the Guldi group in Germany.

Chapter 4 gives a brief conclusion and an outlook for the field of sterically-hindered pentacene monomers and dimers.

Chapter 5 gives the experimental details of all compounds discussed in the research work as well as the NMR spectra of all synthesized compounds and DSC scans of the final pentacene derivatives.

Preface

Parts of Chapter 2 of this thesis will be published as Adam, M.; Rami, P. R.; Hampel, F.; Tykwinski, R. R. “Sterically Shielded Pentacenes.” in preparation. Matthias Adam was responsible for several preliminary syntheses, characterization, data collection. I was responsible for the synthesis, experimental work, data collection, and characterization of compounds **1.47–1.49**, **2.1–2.5**, and **2.15–2.21** (numbering from Chapter 2), and compiling an initial draft of the manuscript. Rik R. Tykwinski is the supervisory author, and he has devised the concept and manuscript composition.

Parts of Chapter 3 of this thesis has been published as Lavarda, G.; Zirzlmeier, J.; Gruber, M.; Rami, P. R.; Tykwinski, R. R.; Torres, T.; Guldi, D. M. “Tuning Intramolecular Förster Resonance Energy Transfer and Activating Intramolecular Singlet Fission.” *Angew. Chem. Int. Ed.* **2018**, *57*, 16291–16295. Giulia Lavarda was responsible for synthesizing compound **3.8–3.10** and **3.11–3.13**. Marco Gruber was responsible for synthesizing of compounds **1.51**, **3.1**, **3.2**, and **TIPS-Pnc$_2$** and I was responsible for repeating the synthesis of **1.51**, **3.1**, **3.2**, and **TIPS-Pnc$_2$** (numbering from Chapter 3). Rik R. Tykwinski, Tomás Torres, and Dirk M. Guldi were the supervisory authors and were involved with concept formation and manuscript composition.

For

my greatest love,

Amin

Acknowledgements

First of all, I want to thank my parents for their endless support and encouragements, which give me this opportunity to come to the University of Alberta.

I would like to express my deepest gratitude to my supportive supervisor, Professor Rik R. Tykwinski, for giving me the opportunity to join his group. His unconditional supervision, encouragement, and guidelines through these three years, pushing me to be independent as a graduate student. Thank you for your never-ending patience, which helps me to build up my skills in organic chemistry.

Also, I would like to extend my million thanks to all former and current Tykwinski's group members who made my graduate study unforgettable by their kindness. In this context, I especially would like to express my gratitude to Dr. Jonathan Marshall, Dr. Marco Guber, Dr. Henrik Gotfredsen, Yueze Gao, Bozheng Sun, David Cameron, Matthew Johnson, Yuxuan Hou, and Lan Chen. Fortunately, some friends such as Funda Arslan, Shorena Gelozia, and Hansol Park were kind enough to make my life warm and friendly in the university and I thank them for all of their supports.

I express my gratitude to support staff of the chemistry department including Dr. Randy Whittal (the Mass Spectrometry Services), Dr. Michael J. Ferguson (X-ray Crystallographic Lab), Wayne Moffat and Jennifer Jones (Analytical and Instrumentation Laboratory), and Mark Miskolzie (NMR Facility).

However, the most important of my acknowledgments is addressed to my love, my best companion in my life, Amin, who always motivates me with his unconditional love and support. Thank you and I love all of you.

Table of Contents

List of Tables

CHAPTER 2

CHAPTER 3

CHAPTER 5

List of Figures

CHAPTER 1

CHAPTER 2

CHAPTER 3

CHAPTER 4

CHAPTER 5

List of Schemes

CHAPTER 1

CHAPTER 2

CHAPTER 3

List of Abbreviations and Symbols

°C	degree Celsius
1D	one-dimensional
2D	two-dimensional
Å	Angström
A	acceptor
APPI	atmospheric pressure photoionization
aq.	aqueous
BHJ	bulk heterojunction
br	broad (NMR, IR)
calcd	calculated
cm	centimeter(s)
cm^{-1}	wavenumber(s)
conc	concentrated
CV	cyclic voltammetry
d	doublet (NMR)
D	donor
D/A	donor/acceptor
decomp	decomposition
DRET	Dexter resonance energy transfer
DSC	differential scanning calorimetry
e	electron charge
e.g.	exempli gratia
$E_{gap}^{electro}$	electrochemical HOMO-LUMO gap
E_{gap}^{opt}	optical HOMO-LUMO gap
ESI	electrospray ionization (MS)
Et	ethyl
et al.	et alia
eV	electron volt
Fc^{+}/Fc	ferrocenium/ferrocene redox couple (CV)
FRET	Förster resonance energy transfer
g	gram(s)
h	hour(s)
HMBC	heteronuclear multiple bond correlation

HOMO	highest occupied molecular orbital
HRMS	high resolution mass spectrometry
Hz	Hertz
i.e.	id est (that is)
IR	infrared
ISC	intersystem crossing
iSF	intramolecular singlet fission
J	coupling constant (NMR)
K	Kelvin
LUMO	lowest unoccupied molecular orbital
μ	charge carrier mobility
m	multiplet (NMR), medium (IR)
m	meta
Mg	magnesium
m/z	mass-to-charge ratio (MS)
MALDI	matrix-assisted laser desorption/ionization (MS)
mg	milligram(s)
MHz	megahertz
min	minute(s)
mL	milliliter(s)
mmol	millimole(s)
mp	melting point
MS	mass spectrometry
MPA	traditional melting point analysis
n	normal
nm	nanometer(s)
NMR	nuclear magnetic resonance
n-type	negative-type
o	ortho
$^1O_2$	singlet oxygen
$^3O_2$	triplet oxygen
OE	organic electronic
OFET	organic field-effect transistor
OLED	organic light-emitting diode
OPV	organic photovoltaic
ORTEP	oak ridge thermal ellipsoid plot

OTFT	organic thin-film transistor
OX_1	first oxidation potential
OX_2	second oxidation potential
p	para
PAH	polycyclic aromatic hydrocarbon
PCBM	[6,6]-phenyl-C_{61}-butyric acid methyl ester
Ph	phenyl
Pnc_2	pentacene dimer
ppm	parts per million (NMR)
PQ	pentacene quinone
p-type	positive-type
ps	pico second(s)
Red_1	first reductive potential
R_f	retention factor
rt	room temperature
s	singlet (NMR), strong (IR)
S_1	first photoexcited singlet state
Satd	saturated
SF	singlet fission
Si*i*Bu_3	tri*iso*butylsilyl
Si*i*Pr_3	tri*iso*propylsilyl
$SiMe_3$	trimethylsilyl
SubPc	subphthalocyanines
T	temperature
t	triplet (NMR)
t	tertiary
$t_{1/2}$	half-life
T_1	first photoexcited triplet state
*t*Bu	tertiary butyl
tert	tertiary
TIPS	tri*iso*propylsilyl
THF	tetrahydrofuran
THF-d_8	tetrahydrofuran deuterated
TLC	thin-layer chromatography
Tr*	supertrityl (tris(3,5-di-*tert*butylphenyl)methyl)
Tr*-Pnc_2	pentacene dimer bearing two Tr* groups

UV-vis	ultraviolet-visible
V	volume
w	weak (IR)
α	alpha
β	beta
δ	chemical shift (NMR)
ε	molar extinction coefficient (UV-vis)
γ	gamma
λ	wavelength
λ_{max}	longest wavelength absorption

CHAPTER 1
INTRODUCTION

1.1 Acenes

Polycyclic aromatic hydrocarbons (PAHs) are a class of organic compounds that have been shown to be promising candidates for use in organic electronic (OE) devices. Acenes, i.e., linearly fused benzene rings, are the most extended class of PAHs and have a smaller HOMO-LUMO gap compared to other hydrocarbons with the same number of aromatic rings (**Figure 1.1**). Consequently, these molecules are the center of attention nowadays because of their electronic properties.[1a] Benzene **1.1**, with one aromatic ring, is the smallest and the most stable member of the acenes family.[2] The smaller acenes such as benzene **1.1**, naphthalene **1.2**, and anthracene **1.3** can be isolated and purified on large scales from petroleum resources, whereas larger acenes such as tetracene **1.4**, pentacene **1.5**, and hexacene **1.6**, can only be obtained by multistep synthesis due to their poor stability and high reactivity, which also explains the 100-fold increase in the cost of **1.4** compared to **1.3**.[1a]

Increased reactivity of other larger members of the acenes family, starting from heptacene **1.7**, has limited their synthetic accessibility and these compounds are most often studied by theory.[2] As a result, pentacene is the largest well-characterized acene.[1a,2]

Despite all drawbacks such as poor stability, low solubility, and the high price of larger acenes, some important electronic properties scale with the size of acenes, such as higher charge carrier mobility, stronger 2D electronic interactions in solid state, and lower HOMO energy level. More importantly, it has been established that the longer the acene the lower the exciton binding energy, thus acenes have attracted significant attention as promising organic semiconductors over the last decades.[2]

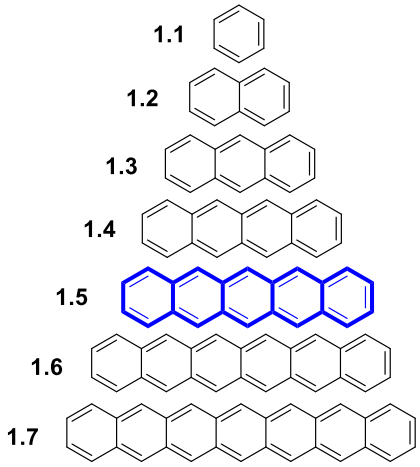

Figure 1.1. The Acene family.

Pentacene **1.5** has a relatively low HOMO-LUMO gap, π-cconjugated electronic structure. Pentacene is also one of the most popular p-type organic semiconductors in organic field-effect transistor (OFET) devices.[3] Due to the fact that the reactivity of pentacene is much higher than anthracene and tetracene, it needs to be synthesized rather than isolated from petrochemical sources. Nevertheless, commercially available pentacene used in devices has provided good field-effect mobilities on vacuum-deposition and they are compatible with flexible plastic materials.[1a]

1.2 History of Pentacene

Pentacene **1.5** (**Figure 1.2**) was first synthesized by Eric Clar in 1929.[4] Pristine pentacene **1.5** is sparingly soluble in common organic solvents, and it has a characteristic longest absorption maximum (λ_{max}) at 584 nm in EtOH and at 576 nm in benzene.[5, 6] Similar to tetracene **1.4**, compound **1.5** cannot be isolated from petroleum, but it can be formed from the combustion of carbon-rich polymers, or by organic synthesis.[1a] The synthesis of pentacene by Clar was accomplished through the Friedel-Craft acylations of *m*-xylene **1.8** by using benzoyl chloride **1.9** (**Scheme 1.1**).[4] Heating the diketone product **1.10** of the Friedel-Craft reaction in the presence of copper produces 6,13-dihydropentacene **1.11**, which can be converted to pentacene **1.5** by dehydrogenation in the presence of nitrobenzene ($PhNO_2$) and pentacenequinone **PQ**.

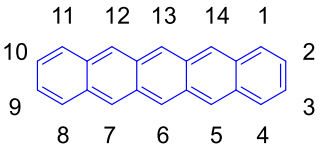

Figure 1.2. Chemical structure and numbering scheme of pentacene **1.5**.

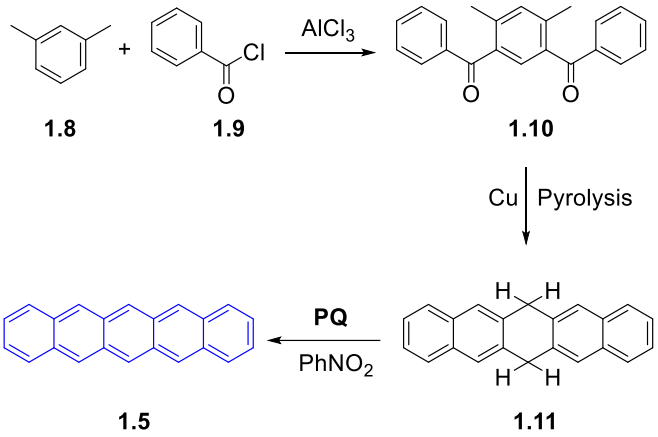

Scheme 1.1. The first reported synthesis of pentacene **1.5** by Clar.[4]

The most popular current method for the synthesis of pentacene was introduced by Bruckner and Tomasz in 1961 via the formation of basic precursor of **PQ** by a fourfold Aldol condensation of 1,4-cyclohexanedione **1.12** and *o*–phthalaldehyde **1.13** in a basic reaction environment (**Scheme 1.2**).[7] The advantages of this method are that it requires cheap and readily available starting materials and that is a high yielding reaction.[7] The dark blue pristine pentacene was then produced through the reductive aromatization of **PQ** with Al/$HgCl_2$ (Al-amalgam). However, because of the environmental risks of mercury, using $LiAlH_4$ is an alternative reductive reagent for reducing **PQ** to pentacene **1.5**.[7]

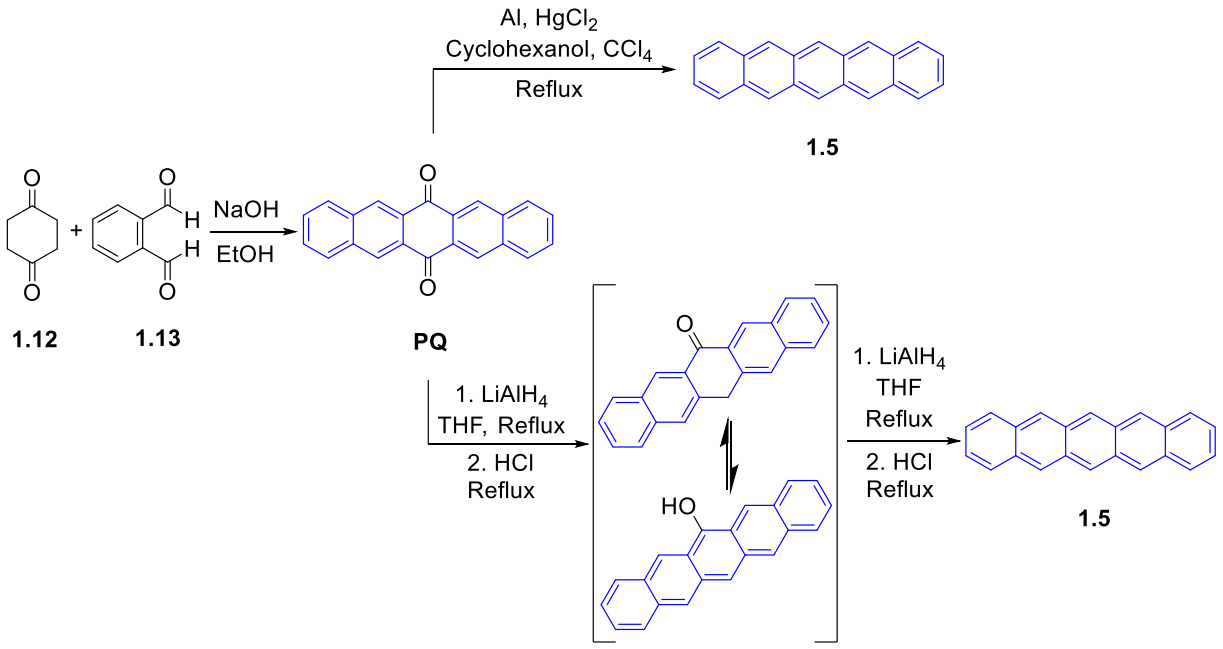

Scheme 1.2. Synthesis of pristine pentacene **1.5** via the formation of **PQ**.[4, 7]

1.3 Deficiencies of Pentacene

Poor solubility and low kinetic stability are the most challenging properties of pentacene, which can cause problems in purification and film deposition of pentacene from solution for device fabrication. Solubility issues are due to the strong intermolecular interactions between adjacent pentacene molecules in the solid state, while its instability is due to gradual decomposition upon exposure to air and light.[1a] The main oxidative by-product of decomposition of **1.5** is **PQ** which can result from endoperoxide **1.14** via two different possible routes, (a) energy transfer or (b) electron transfer (**Scheme 1.3**).[1a, 8, 9] In the first route, (a), pentacene can stimulate singlet oxygen formation. Typically, formation of singlet oxygen requires a sensitizer with a triplet energy that is larger than the energy of singlet-triplet gap in singlet oxygen (22.5 kcal mol^{-1}). Triplet pentacene with an energy of 17.9 kcal mol^{-1}, however, cannot sensitize singlet oxygen. Thus, pentacene must be thermally activated to the triplet state to sensitize singlet oxygen. Once formed, singlet oxygen leads to **1.14** as described in **Scheme 1.3**. In the second mechanism (b), **1.5** is excited to the singlet state, and subsequently transfers an electron to ground state oxygen to generate the pentacene radical cation and a superoxide radical anion ($O_2^{-\bullet}$) which is prone to further degradative reactions.[8, 9]

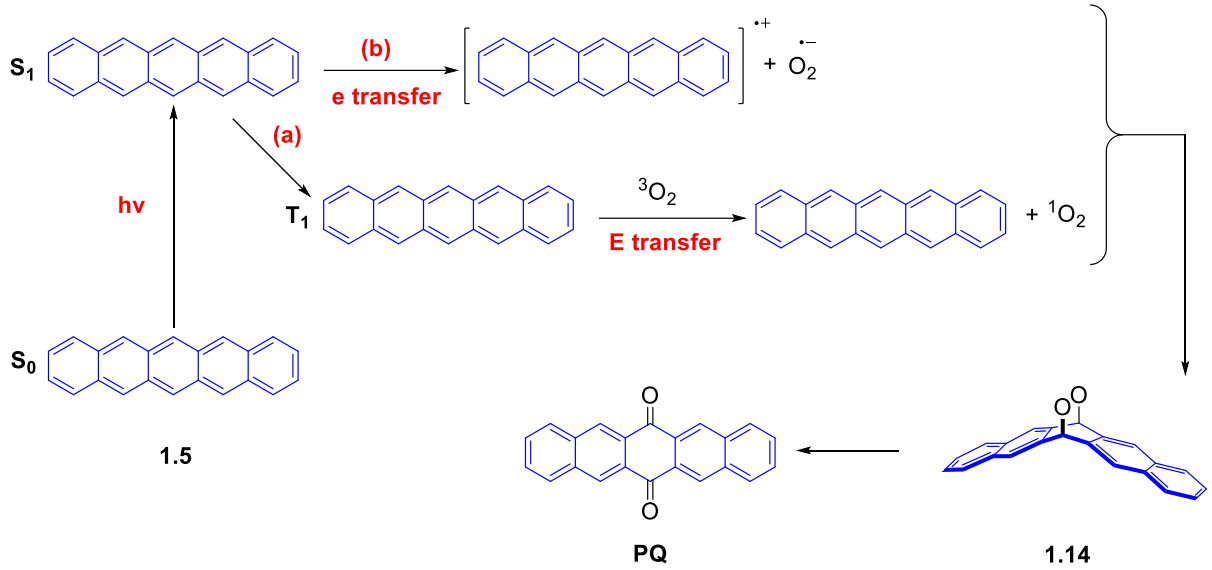

Scheme 1.3. Degradation mechanisms of pentacene **1.5** and pentacene derivatives in the presence of oxygen: (a) by energy transfer (E transfer) and (b) by electron transfer (e transfer).[8, 9]

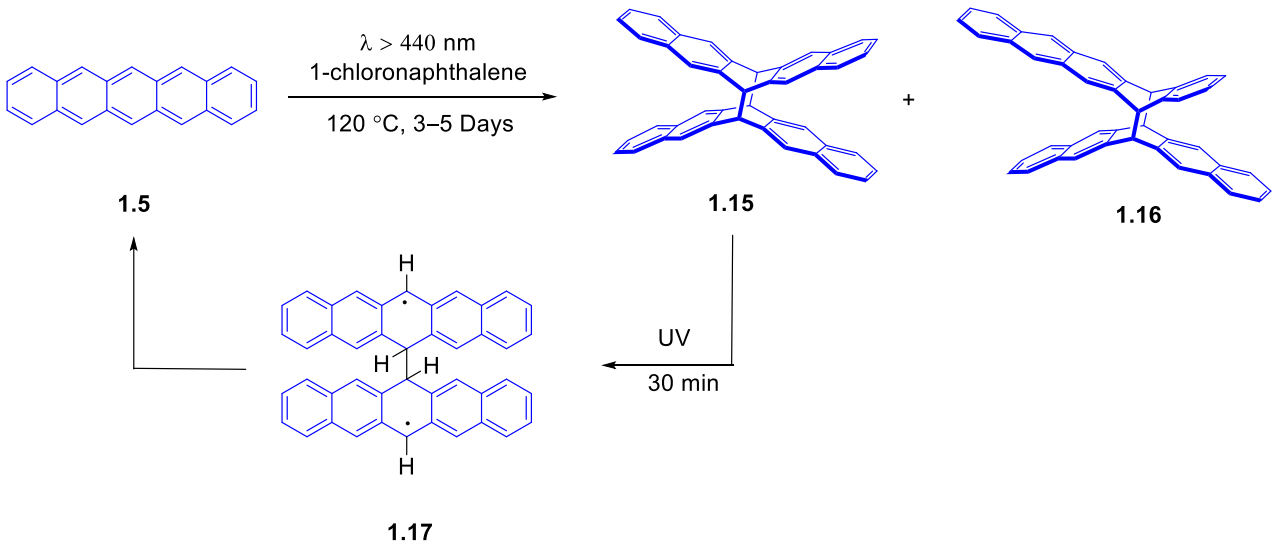

Scheme 1.4. Photodecomposition pathway of pentacene.[1b]

The symmetric butterfly dimer **1.15** and unsymmetrical dimer **1.16** are photodecomposition products formed in a deoxygenated solution of **1.5** irritated with light.[1b] The white solid, dimer **1.15** can be synthesized by irradiating a solution of **1.5** (λ > 440 nm) at 120 °C in deoxygenated 1-chloronaphthalene for 3–5 days (**Scheme 1.4**).[1b]

Although the dimer **1.15** is thermally stable, it can be converted into **1.5** by UV irradiation for 30 min via the intermediate **1.17**.[1a]

The conjugated backbone of pentacene can act as a diene and undergo a Diels-Alder reaction. In the case of applications to solar cells, for example, this can lead to a degradation process through a Diels-Alder reaction with fullerene.[1a] Studies have documented the reaction of pentacene **1.5** and fullerene in boiling toluene to generate a symmetric monoadduct **1.19** through cycloaddition across the 6- and 13-positions (**Figure 1.3**).[10] This reaction is regioselective and shows no evidence of either bis-fullerene-pentacene adducts *cis*-**1.20** / *trans*-**1.21** or any cycloaddition products across the 5- and 14-positions of pentacene. However, if the reactive 6- and 13-positions of pentacene are functionalized, rings adjacent to the central ring will undergo the Diels-Alder reaction with fullerene and produce a bisadduct **1.22** (**Figure 1.4**).[1a, 10]

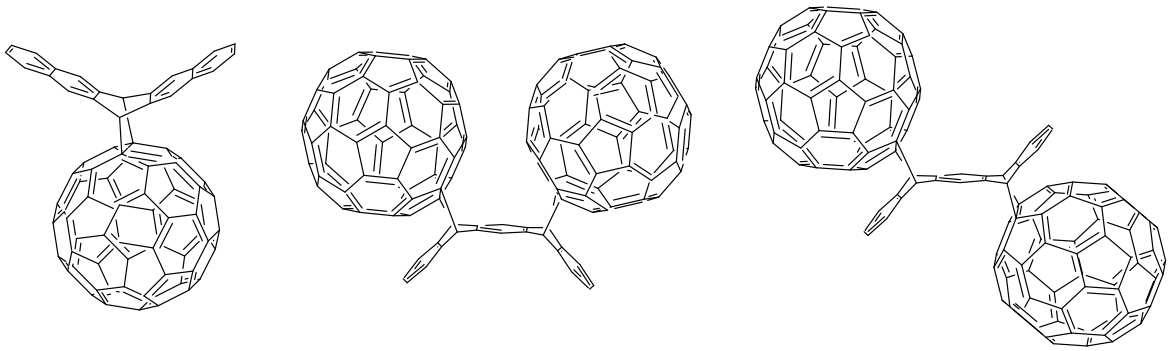

1.19 **1.20** **1.21**

Figure 1.3. Potential fullerene-pentacene adducts from the reaction of pristine pentacene and fullerene.[10]

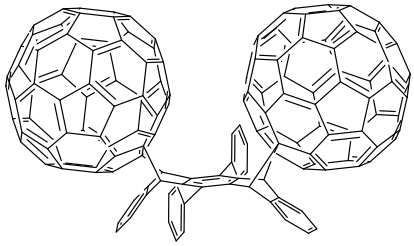

1.22

Figure 1.4. Fullerene-pentacene adduct from the reaction of 6- and 13-disubstituted pentacene and fullerene.[10]

1.4 Functionalization of Pentacene

1.4.1 Effects of Substitution on Pentacene

Lower fabrication costs, tunability of the HOMO and LUMO levels, solution processability, and even compatibility with flexible substrates are some of the benefits of organic materials compared to the inorganic counterparts. As a result of these advantages, polycyclic aromatic hydrocarbons (PAHs), such as pentacenes, are being used as organic semiconductors in organic field-effect transistors (OFETs), organic light-emitting diodes (OLEDs), solar cells, and beyond.[1]

To help address the problems of kinetic stability and solubility discussed above, functionalized pentacene has been targeted.[1] There are two goals for functionalization of pentacene. First, addition of solubilizing groups should simplify purification and processing. Second, substitution can be used toward optimization of intermolecular interactions in the solid state, in order to enhance intermolecular orbital overlap, which is important to most electronic applications.[11] The functionalization of pentacene is a broad topic that far exceeds the scope of this thesis, thus, this section focuses exclusively on substitution of pentacene in the 6- and 13-positions (*peri*-positions, pink substituents, **Figure 1.5**).[1] In general, substitutions at the *peri*-positions not only boost the solubility of pentacene derivatives, but also increase the π-stacking interactions in the solid state.[12] Regarding substituents at 2-, 3-, 9-, and 10-positions of the terminal ring (*pro-cata*-positions, blue substitutions, **Figure 1.5**), the electronic properties of pentacene derivatives can also be changed.[12]

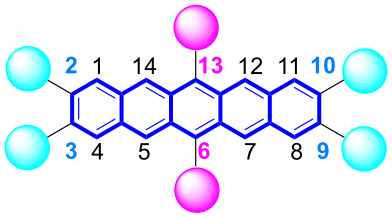

Figure 1.5. Schematic substitution of pentacene at *peri*-positions (pink circles) and *pro-cata*-positions (blue circles).

A breakthrough in the kinetic stability and solubility of pentacene was achieved by Anthony and coworkers in 2001 through the synthesis of a pentacene molecule bearing

tri*iso*propylsilylethynyl groups at 6- and 13-positions (**1.23**, so-called TIPS-pentacene) and at 5- and 14-positions **1.24** (**Figure 1.6**).[11] Interestingly, it was found that alkynyl groups at 6- and 13- positions can increase the stability of pentacene compared to alkyl-, phenyl-, or unsubstituted pentacene, and this effect is lessened when alkynyl groups are at 5- and 14-positions.[13] The increased stability of e.g., TIPS-pentacene, compared to **1.5**, has been attributed to two reasons: i) A low energy triplet state resulting from the presence of the ethynyl silanes which prevents singlet oxygen sensitization; and ii) Lowering the energy of the LUMO as a result of sp-alkynyl substitutions.[8]

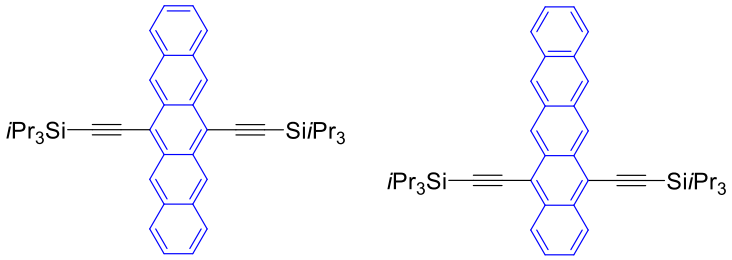

1.23 **1.24**

Figure 1.6. Chemical structure of disubstituted pentacenes bearing tri*iso*propylsilylethynyl groups at 6- and 13-positions **1.23** and 5- and 14-positions **1.24**.[11]

1.4.2 Symmetrical Alkyne-Functionalized Pentacenes

One of the most synthetically available classes of symmetrically functionalized pentacenes are derivatives with ethynyl groups in the 6- and 13-positions, which can be formed via a two-step protocol that starts from **PQ** (**Scheme 1.5**).[14, 15] The first step is nucleophilic addition of an ethynyllithium species (or an ethynyl Grignard reagent) to the **PQ**, followed by quenching the reaction mixture via the addition of water (or dilute acid) to yield a diol intermediate. The diol is then used in the second step and subjected to reductive elimination reactions[16] using $SnCl_2$ under a variety of conditions to give symmetrically disubstituted pentacene derivatives, usually in good yields. Examples include **1.23** and **1.25–1.31**.[1,14,15]

One of the earliest reported functionalized pentacene derivatives is 6- and 13-bis(phenylethynyl)pentacene **1.25**.[1, 17] Synthesis of soluble and stable 6- and 13-

disubstituted pentacene using trialkylsilyl groups such as **1.23** indicates that trialkylsilyl groups facilitate the isolation, purification, and processing steps. Altering the size of roughly spherical trialkylsilyl substituents provides excellent control over the π-stacking order in the solid state.[1, 14]

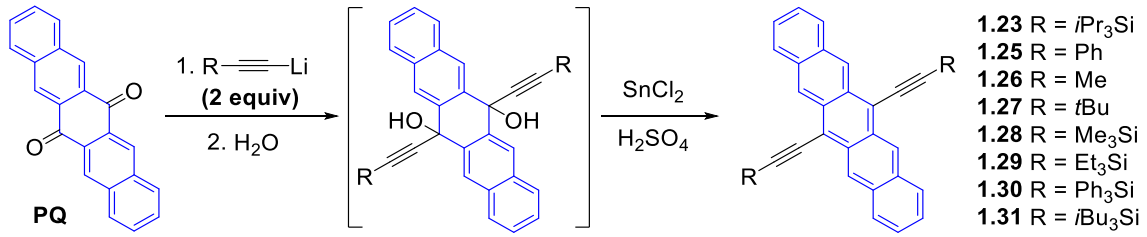

Scheme 1.5. General synthetic procedure for symmetrical 6- and 13-ethynyl pentacene derivatives **1.23** and **1.25–1.31**.[14,15]

1.4.3 Unsymmetrical Alkyne-Functionalized Pentacenes

A general, stepwise, synthetic route to unsymmetrically 6- and 13-disubstituted pentacene derivatives has been developed by Tykwinski and coworkers (**Scheme 1.6**).[17–19] The first step is used for desymmetrization of the pentacene backbone and can be achieved by using only one equivalent of an ethynyllithium (or Grignard reagent) in a reaction with **PQ** to yield a mono-ethynylated ketone intermediate, e.g., ketones **1.32–1.34**. In the next step, this ketone can be treated with different ethynyllithium (or Grignard reagent) to provide the diol intermediate. In the third step, the diol is subjected to a reductive elimination reaction by using $SnCl_2$ under acidic conditions to give unsymmetrically 6- and 13-disubstituted pentacene derivatives, such as **1.35–1.46**.[20]

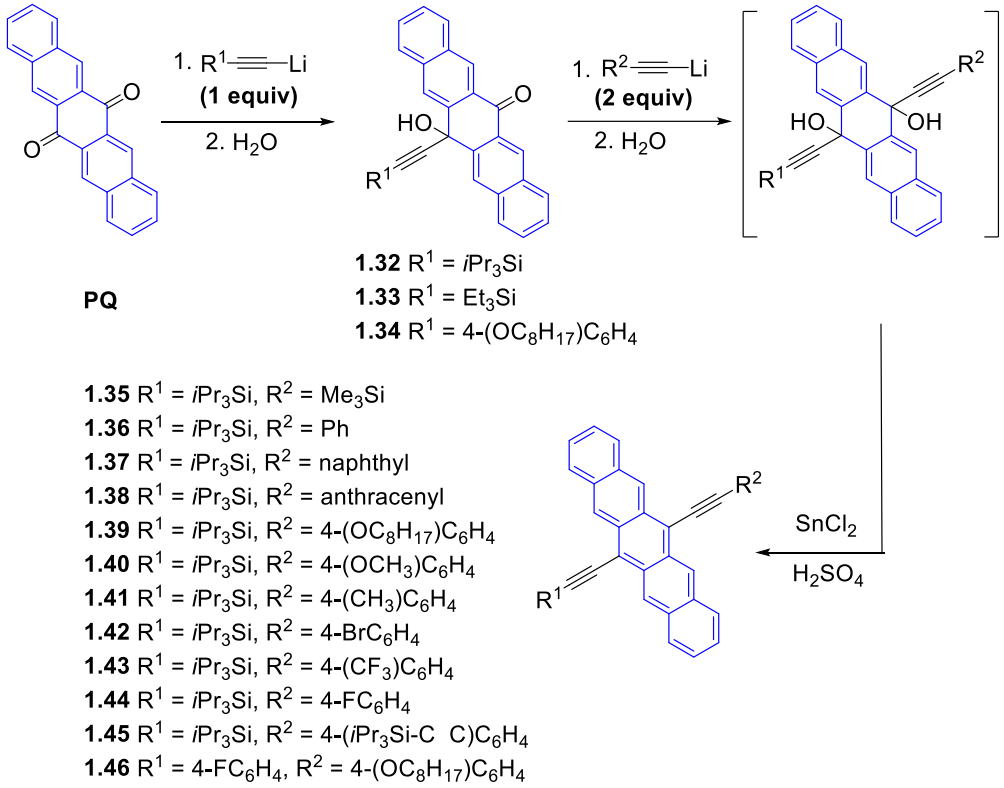

Scheme 1.6. General synthetic procedure for unsymmetrical 6- and 13-ethynyl pentacene derivatives **1.35–1.46**.[17–19]

As an example, attachment of two electronically varied substituents, i.e., electron-rich (donor) and electron-deficient (acceptor), produces an electronically polarized push-pull pentacene derivative, e.g., **1.44**. The substituents help to fine-tune of the electronic properties of the pentacene chromophores.[18, 21] Unfortunately, the nucleophilic addition step discussed in **Scheme 1.6** does not tolerate strong electron-rich and electron-deficient groups such as the aniline and nitrophenyl moieties.[21] This problem has been solved by a new synthetic procedure reported by Tykwinski and coworkers for unsymmetrically substituted pentacenes in which substitution is achieved by a palladium catalyzed Sonogashira cross-coupling reaction with aryl iodides (**Scheme 1.7**).[21] The key building blocks in these procedures are pentacenes bearing terminal acetylenes, such as **1.51** and **1.52**, which are synthesized from the desilylation of compounds **1.49** and **1.50**, respectively. Compounds **1.49** and **1.50** are synthesized by a nucleophilic addition of lithiated trimethylsilylacetylene to either ketone **1.47** or **1.48**, respectively, followed by quenching with excess MeI to protect the alcohol as the methyl ether. The Sonogashira

cross-coupling reaction between compounds **1.51** or **1.52** and an iodoarene yielded dimethyl ether derivatives **1.53–1.56**. Reductive elimination of dimethyl ether derivatives **1.53–1.56** with $SnCl_2$ gave pentacene derivatives **1.57–1.59**.

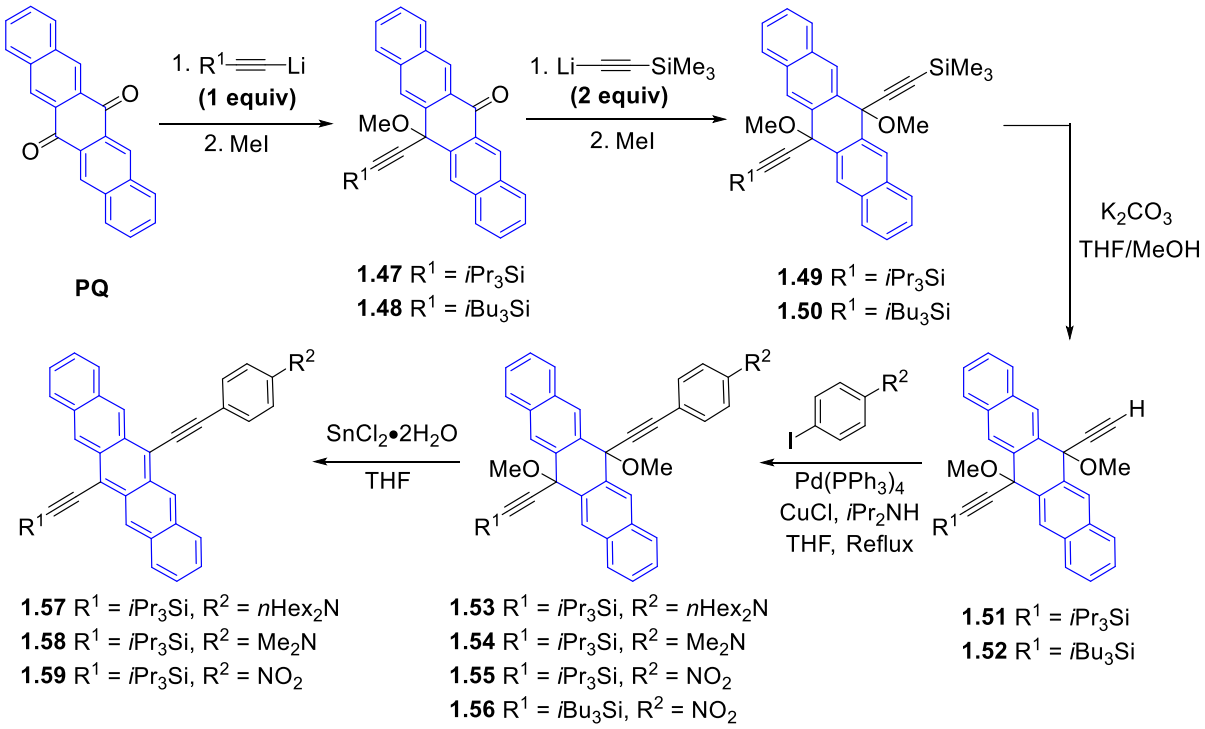

Scheme 1.7. Synthetic procedure for unsymmetrical 6- and 13-ethynyl pentacene derivatives **1.57–1.59**.[21]

The reported synthetic protocols by Anthony and Tykwinski have become a powerful tools for the synthesis of a variety of pentacene derivatives as organic semiconductors with promising properties for use in organic devices.[1, 21]

1.5 Pentacene Derivatives for Device Applications

Desirable organic semiconductors have several dominant characteristics such as easy synthesis, stability, efficient charge carrier mobility, and high capability in injecting and harvesting charges at interfaces of the device. Molecular structure, as well as optical, and electrical characteristics of organic semiconductors can be tailored through organic synthesis.[22]

Organic semiconductors typically have conjugated molecular structures and crystalline or amorphous thin films with a band gap of 1–4 eV.[23] These materials are intrinsically insulators but can function as semiconductors via charge injection from metal electrodes or through a photoexcitation process. The band gap in inorganic materials refers to the energy difference between the valence and conduction band, whereas in organic material, the band gap is often defined as the HOMO-LUMO gap which can be estimated via UV-vis spectroscopy or more accurately by cyclic voltammetry (CV).[24]

Charge carrier mobility (μ) is commonly used as an evaluation for semiconductor performance and relates the drift velocity of electrons/holes (cm s^{-1}) per unit of an electric field (cm V^{-1}) applied across a piece of semiconductor.[1] In principle, charge carrier mobility defines as how quickly a charge (electron or hole) can move through a metal or semiconductor in an applied electric field, and its value is reported as $cm^2\ V^{-1}\ s^{-1}$.[25]

Depending on the nature of the charge carrier, organic semiconductors are classified as either p-type (donor materials or hole conductors) or n-type (acceptor materials or electron conductors).[26] The p-type organic semiconductors are typically π-conjugated electron-rich molecules that have high HOMO levels.[25]

On the other hand, n-type organic semiconductors are typically π-conjugated, electron-poor molecules that have low-lying LUMO energy levels. Attachment of strong electron-withdrawing atoms/groups (e.g., fluorine or cyano) to conjugated molecules lowers the energy of the LUMO orbitals and generates an n-type semiconductor.[27] Due to the low charge carrier mobilities, instability, and poor solubility, the performance of n-type semiconductors is usually inferior to p-type materials.[28]

As a result of high hole carrier mobilities, PAHs, and particularly pristine pentacene **1.5**, are potential candidates for use in devices such as organic field-effect transistors (OFETs), organic light-emitting diodes (OLEDs), and solar cells. OFETs are a major focus area in the applications of acenes, while the increasing use of acenes in organic solar cells could someday provide cheaper, lighter, and more flexible alternatives compared to traditional silicon-base devices.[1]

1.5.1 Pentacene-Based Bulk Heterojunction Solar Cells

Organic molecules can be used as the active species in solar cells to convert solar energy to electricity. Although the efficiency of bulk heterojunction (BHJ) solar cells (10%)[31] is still much lower than conventional silicon based solar cells (35.8%),[29] organic solar cells have some potential advantages including the availability of functionalized organic molecules through short and cost effective synthetic routes, the possibility of creating flexible cells, and the solutions processability.[29–31]

A combination of a p-type and an n-type layer, and creating an internal electric field, is the main principle for these cells. The energy diagram for the conversion of light into electrical current in a BHJ solar cell with donor-acceptor (D/A) interfaces is shown in **Figure 1.7**.[31] Various polymers and small organic molecules can be used as either donor (hole transporting material) or acceptor (electron transporting material) in organic solar cells. Compared to the acceptor, the donor material has high-lying HOMO and LUMO levels and makes a contact with the anode electrode. The acceptor contacts the cathode electrode. Specifically, the conversion of solar irradiation to photocurrent requires four steps. The first step is irradiating the BHJ solar cell with photons of suitable energy to raise the energy of an electron in the HOMO level to the LUMO level and generates an electron-hole pair (exciton).[30, 31] Then, the exciton diffuses toward the donor-acceptor interface in the second step. The efficiency of this process is determined mainly by the exciton diffusion length and morphology of the D/A interface. In the third step, the exciton reaches the D/A interface and dissociates into a geminate pair (coulombically bound electron and hole) in the presence of the electric field. This pair can either dissociate into free carriers or recombine to the ground state. If dissociation occurs successfully, the electron moves to the LUMO of acceptor and the hole moves on the HOMO of the donor.[31, 32] Finally, the forth step completes the process as charges are collected.[32]

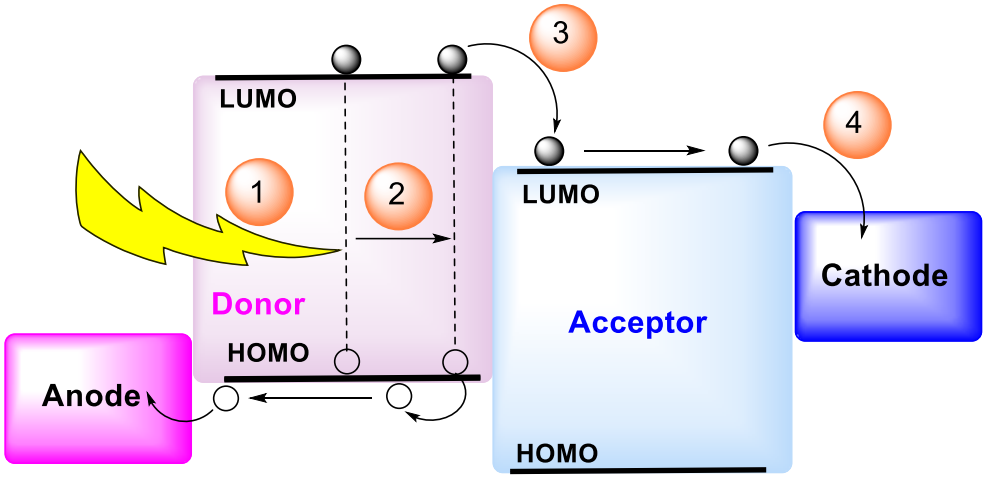

Figure 1.7. Generation of photocurrent in an organic solar cell with donor-acceptor (DA) interface: (1) absorption of a photon to create an exciton, (2) diffusion of the generated exciton toward D/A interface, (3) transfer of an electron to the acceptor and a hole to the donor, and (4) charge collection.[31]

Soluble conjugated molecules with strong intermolecular forces can be considered as efficient materials for OPVs. Soluble derivatives of pentacene, such as **1.23**, with a high hole mobility and reasonable air stability are common donor semiconductors that have been evaluated for use in OPVs. On the other hand, there is a scarcity of air-stable, conjugated molecules with high electron mobility. The exception is the performance of [6,6]-phenyl-C_{61}-butyric acid methyl ester (PCBM, a fullerene derivative, **Figure 1.8**), which is the prototypical n-type acceptor and features good stability.[30]

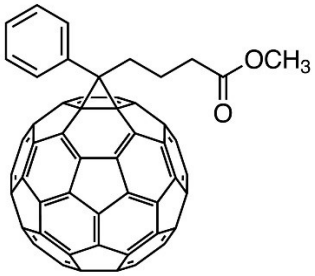

Figure 1.8. Molecular structure of [6,6]-phenyl-C_{61}-butyric acid methyl ester (PCBM).

In addition to the electron and hole transfer processes between the donor (pentacene derivatives) and acceptor (fullerene, C_{60}), however, these two materials can

undergo a Diels-Alder reaction. This incompatibility can potentially destroy the π-systems, as has been described in Section **1.3**.

1.5.2 Singlet Fission Solar Cells

Increasing the conversion efficiency of conventional solar cells is one of most challenging goals in current research. Shockley and Queisser have proposed that the upper theoretical limit of solar cells is ~32% because the excess energy of absorbed photons is lost, mostly as heat (**Figure 1.9**).[33] To overcome this limit, a new strategy, namely multiple exciton generation (MEG), has been explored. In the case of MEG, creation of more than one charge carrier is possible per absorbed photon.

Singlet fission (SF) is the molecular analogy to MEG, and it involves the spontaneous splitting of a photoexcited singlet state (S_1S_0) into a pair of lower triplet excited states $^1(T_1T_1)$. This process could increase the performance limit in OPVs to ~50% (**Figure 1.9**).[33]

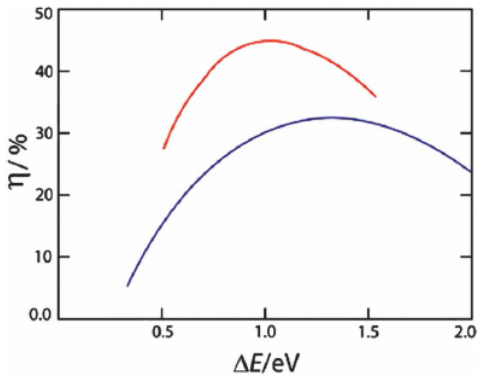

Figure 1.9. Theoretical efficiency of singlet fission solar cell (red) and conventional solar cell (blue) as a function of singlet-triplet band gap (S_0–T_1). Figure adapted from reference 33b.

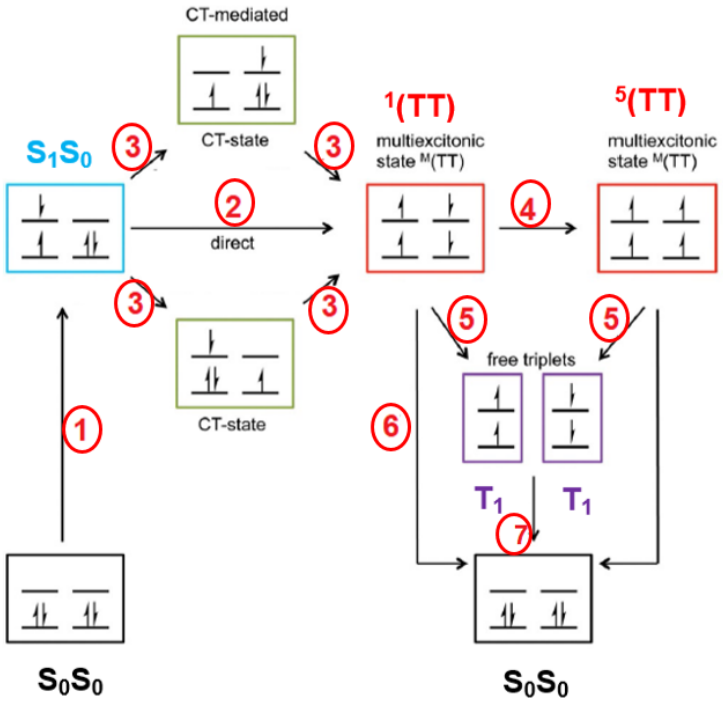

Figure 1.10. Mechanism of singlet fission: (1) generation of the (S_1S_0) state by photoexcitation of (S_0S_0) state, (2) formation of a multiexcitonic state ^{1}(TT) by a direct mechanism, (3) formation of a multiexciton state ^{1}(TT) by a two-step mechanism, (4) spin evolution from a multiexciton state ^{1}(TT) to a multiexciton state ^{5}(TT), (5) decoherence of the correlated multiexciton state ^{M}(TT) to two free triplets ^{1}T + ^{1}T, (6) decay to ground state (S_0S_0), and (7) decay to ground state (S_0S_0). Figure adapted from reference 33a.

Although an understanding of all processes of the SF mechanism is beyond the scope of this thesis, a general description of SF is shown in **Figure 1.10**.[33] The first step is initiated by absorption of a photon to excite one electron from the ground state (S_0S_0) to photoexcited singlet state (S_1S_0). The (S_1S_0) state transforms into a correlated triplet pair ^{1}(T_1T_1), likely via one of two mechanisms (although this is still argued): (a) The (S_1S_0) state can directly convert to the ^{1}(T_1T_1) state via a two-electron process (step 2), or (b) the (S_1S_0) state can convert to ^{1}(T_1T_1) state by formation of an charge-transfer intermediate via two consecutive one-electron processes (step 3). Formation of a quintet ^{5}(T_1T_1) state is possible via the spin evolution of the ^{1}(T_1T_1) state (step 4). The free triplet (^{1}T + ^{1}T) state is then generated by spin decoherence of either the ^{1}(T_1T_1) or ^{5}(T_1T_1) state

(step 5), or a combination of the two. Finally, the free triplets can be harvested, completing the process of solar energy conversion (not shown). In the absence of step 5 (spin decoherence of correlated triplet states) or triplet harvesting, the system can decay to the ground state (S_0S_0) (steps 6 and 7). The decay could be through triplet-triplet annihilation, thermal/emissive decay, or a combination of these two processes.[33]

In the past decade, there has been considerable effort toward the investigation of SF.[33] The efficiency and rate of SF depends strongly on electronic coupling and intermolecular arrangement of the two chromophores. More importantly, chromophores must meet the energetic requirement of $E(S_1) \geq 2E(T_1)$ to be suitable for SF. Pentacene and its derivatives are particularly useful for the study of SF since they fulfill the energetic requirement of $E(S_1) \geq 2E(T_1)$.

In 2013, Friend and coworkers reported a high triplet yield of 200% for SF in the study of concentrated solutions of TIPS-pentacene **1.23**. In contrast to the study of **1.23**, which required concentrated solutions to ensure close intermolecular interactions, intramolecular SF (iSF) in dimers (two chromophores tethered together by a spacer) offers the opportunity to study dilute solutions. Namely, challenges presented by intermolecular SF, such as low solubility, aggregation, and significant optical density, can be eliminated by using a dilute solution of dimers. The ability to modify the structure of the spacer in dimeric chromophores via synthesis allows for strategic tuning of the electronic coupling, distance, and geometric relationship between the two chromophores. Studies of different pentacene dimers (e.g., 6,6'-linked pentacene dimers and 2,2'-linked pentacene dimers) can help to elucidate the mechanism of iSF.[33] Only 6,6'-linked dimers will be discussed in this thesis.

1.5.2.1 6,6'-Linked Pentacene Dimers

Tykwinski and coworkers have reported the first dimers of pentacene for study of iSF in 2015, using of phenylene-linkers in **1.60–1.62**.[33] The general synthetic procedure for dimers **1.60–1.62** involves Sonogashira cross-coupling reactions between *o*-, *m*-, or *p*-diiodobenzene and pentacene **1.52** as shown in **Scheme 1.8**. The reductive aromatization of intermediates **1.63–1.65** using $SnCl_2$ and dilute acid yields dimers **1.60–1.62**. The orthogonal orientation of chromophores in **1.60** prevents strong linear

conjugation but favors through-space interactions. Dimer **1.61** has limited electronic coupling due to cross-conjugation through the *m*-phenylene spacer, and dimer **1.62** has strong linear conjugation between pentacene molecules. Transient absorption spectroscopy shows that dimer **1.61** shows the best performance for iSF, with a triplet yield of 156% in benzonitrile and 125% in toluene, whereas dimers **1.60** and **1.62** could not provide a meaningful triplet yield due to their triplet excited state kinetics including triplet-triplet annihilation. Therefore, successful iSF depends on the electronic coupling (either through-space or through-bond) and special proximity of pentacene chromophores. Studies with **1.60–1.62** suggested that reduced conjugation might be beneficial for iSF. Thus, dimer **1.66** was synthesized, as a non-conjugated analog to **1.61**, via the nucleophilic addition of lithiated 1,3-diethynyladamantane **1.67** to ketone **1.48**. Workup and reductive elimination of the intermediate yielded dimer **1.66**. Sufficiently weak electronic coupling between chromophores in non-conjugated dimer **1.66** facilitated the decoherence step and the formation of free triplet states, which increased to 188%. In addition, the studies of dimer **1.66** confirm that for an efficient iSF process, neither direct π–stacking (i.e., through-space coupling), nor strong linear or cross-conjugation (i.e., through-bond coupling) of pentacene chromophores was needed.[33]

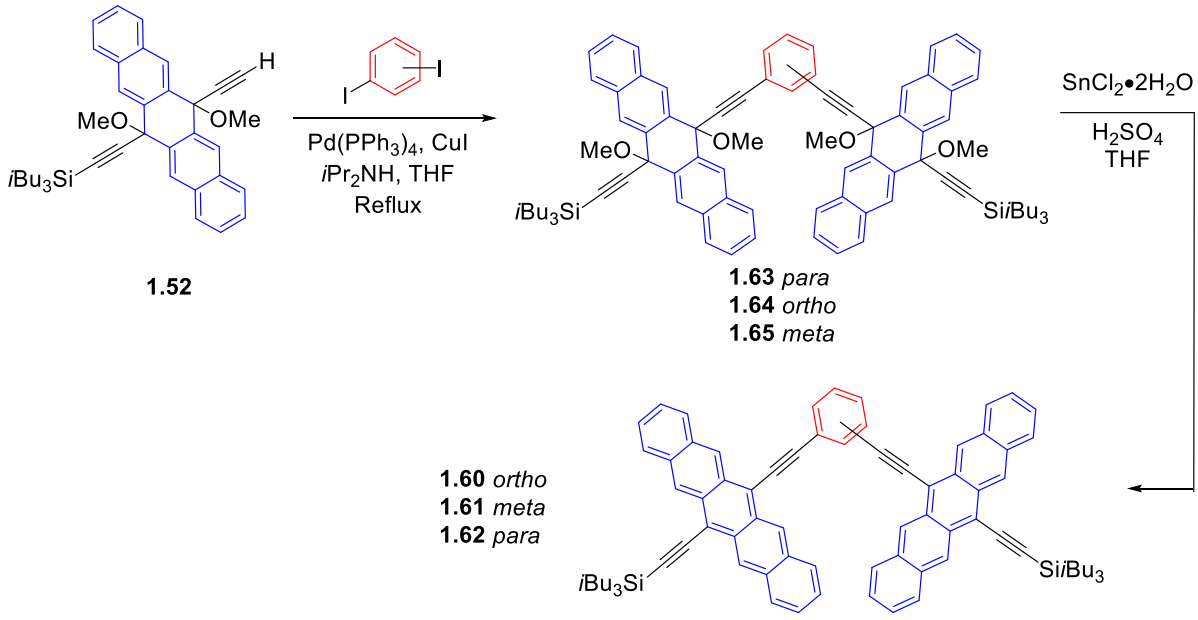

Scheme 1.8. General synthetic procedure for conjugated pentacene dimers **1.60–1.62**.[33]

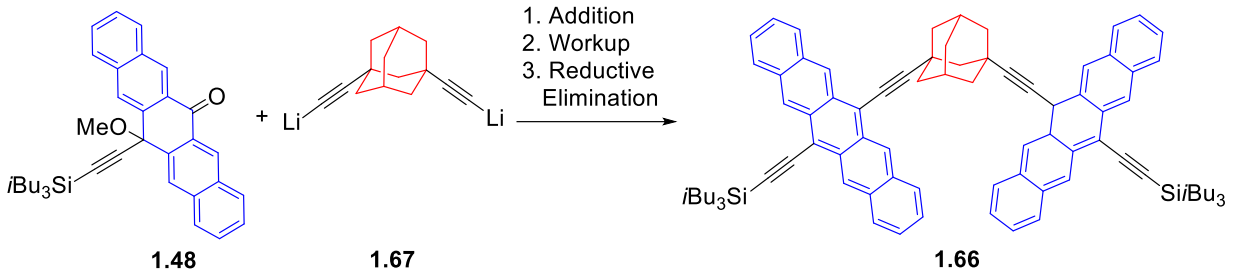

Scheme 1.9. General synthetic procedure for non-conjugated pentacene dimer **1.66**.[33]

1.6 SubPc Conjugates for Förster Resonance Energy Transfer

A donor chromophore (D) in its excited state can transfer energy to an acceptor chromophore (A) through two distinct mechanisms: i) Radiative energy transfer in which a photon is emitted by a the excited donor (D*) and then absorbed by the A. Upon photon emission, the D* returns to its ground state D whereas the ground state A will be promoted to its excited state (A*) though the absorption process; ii) Radiationless energy transfer from D* to A which can occur in two ways, Dexter Resonance Energy Transfer (DRET) and Förster Resonance Energy Transfer (FRET). In DRET, the excited electron of the D is exchanged with an A electron through electronic orbital collision and changing the spin of D and A. In FRET, deactivation of D* and excitation of A are coupled to each other by Coulombic dipole-dipole interaction based on virtual photon coupling. The term “virtual” is used because such photons cannot be observed.[34a] FRET is extremely sensitive to the D-A distance, and its efficiency is inversely proportional to the sixth power of D-A distance. Since FRET does not require a physical contact between the D and A chromophores, problems that may arise from the direct contact or conjugation between the two chromophores will be avoided.[34b]

Subphthalocyanines (SubPcs) **1.72** are cone-shaped molecules with 14 π-electrons that have a particular macrocyclic ring composed of three isoindole subunits connected by three azabridges that often accommodate a boron(III) ion within its central binding core (**Figure 1.11**).[35, 36] SubPcs with a (S_1) state energies of around 2.1 eV can act as energy-accepting components for chromophores that have higher energy (S_1) states, such as polycyclic aromatics.[35] In contrast, SubPcs can act as energy donors for chromophores with lower energy (S_1) states, including porphyrins (~2.0 eV) and fullerenes (~1.75).[35] Therefore, the SubPc acts as a light-harvesting antenna to transfer

the absorbed energy to the other chromophore.[35] The first example of a SubPc conjugate showing excitation energy transfer was SubPc-C_{60} systems **1.73** axially linked through phenoxy spacers to the fullerene (**Figure 1.11**).[35]

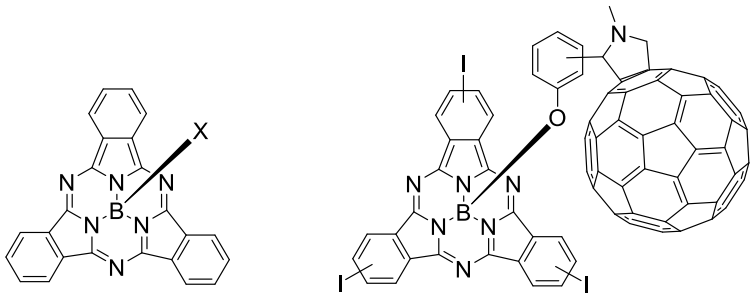

1.72 **1.73**

Figure 1.11. The molecular structure of SubPc **1.72** and SubPc-C_{60} conjugate **1.73**.

1.7 Motivation and Goal of This Thesis

The most challenging aspects of working with pentacene are poor solubility and facile photodegradation. Thus, numerous efforts have been directed to the synthesis of pentacene derivatives with improved solubility and kinetic stability. Synthetically, the reactive 6- and 13-positions of the pentacene backbone are the most promising sites for functionalization to optimize the solubility, stability, and electronic properties. Chapter **2** of this thesis explores the hypothesis that substitution can be used to form more stable pentacene derivatives. To do this, we have chosen groups of varying size and examine stability of the resulting pentacene derivatives based on the UV-vis spectroscopy and DSC. Chapter **3** describes the use of dimeric pentacene (Pnc_2) derivatives with different substitutions to test the stability based on the hypothesis explored in Chapter **2**. Since dimeric pentacene are promising candidates for the study of the mechanism of intramolecular singlet fission (iSF), synthesis of highly soluble dimeric pentacenes with improved stability in solution is the overarching goal.

CHAPTER 2
STERICALLY-HINDERED PENTACENE DERIVATIVES

2.1 Introduction

As reported by Anthony and coworkers, the stability and solubility of pentacene derivatives with silylethynyl substitutions at the 6- and 13-positions like TIPS-pentacene **1.23** is much greater than pristine pentacene **1.5**.[1] Surprisingly, the exact reason that contributes to stabilization in these pentacene derivatives is not completely known. For example, it is not clear that stabilization of silylethynyl functionalized pentacenes is through electronic or steric effects or a combination of the two factors.[8, 9, 37]

The work in this chapter explores several hypotheses toward answering the following basic questions:

- Does replacement of tri*iso*propylsilylethynyl groups at 6- and 13-positions in compound **1.23** with other sterically-hindered groups increase the solubility and stability of pentacene derivatives compared to pristine pentacene **1.5** or **1.23**?
- Can the supertrityl group (tris(3,5-di-*tert*butylphenyl)methyl, Tr*) play an important role in stabilizing pentacene derivatives?
- Can substitution of pentacenes with sterically-hindered groups inhibit or slow unfavored photooxidation and Diels-Alder reactions?

2.2 Design of Pentacene Monomers

In answering the questions proposed in the previous section and evaluating the effect of sterically-hindered groups on stability and solubility of pentacene derivatives, the goal is to synthesize pentacene monomers **2.1–2.5** with different alkyne endcapping groups at 6- and 13-positions (**Scheme 2.1**). Historically, silyl groups, such as Si*i*Pr$_3$, Si*i*Bu$_3$, and SiMe$_3$, have been used as substituents in the synthesis of a number of different pentacene derivatives. In addition to typical silyl groups, we want to have a sterically demanding stable group, such as Tr* group, to put on the periphery of the ethynyl

pentacene backbone. In recent studies by Tykwinski et al., Tr* has been used for effective stabilization of previously unrealized tetraethynyl[5]cumulene.[38a] So, we expected that Tr* could extend over the pentacene and prevent formation of the butterfly dimer.

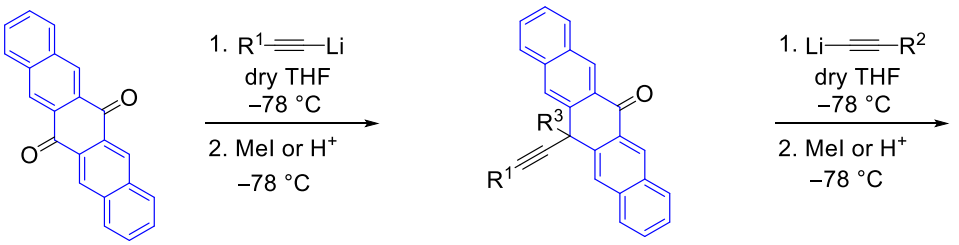

PQ

2.6 R^1 = *i*Pr_3Si
2.9 R^1 = Tr*
2.10 R^1 = *i*Bu_3Si

1.47 R^1 = *i*Pr_3Si, R^3 = OMe (97%)
1.48 R^1 = *i*Bu_3Si, R^3 = OMe (40%)
2.15 R^1 = Tr*, R^3 = OMe (39%)
2.16 R^1 = Tr*, R^3 = OH (58%)

2.7 R^2 = Me_3Si
2.8 R^2 = Ph
2.9 R^2 = Tr*

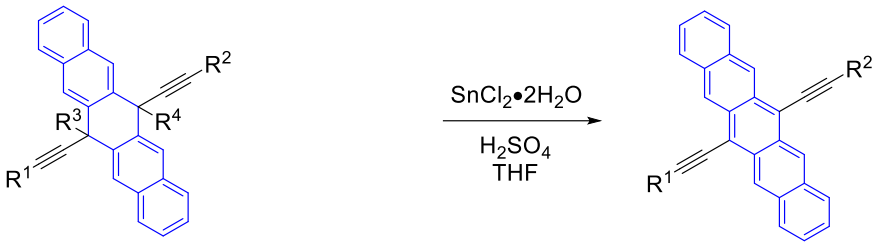

2.17 R^1 = Tr*, R^2 = Me_3Si, R^3 = R^4 = OMe (79%)
2.18 R^1 = *i*Pr_3Si, R^2 = Tr*, R^3 = OMe, R^4 = OH (45%)
2.19 R^1 = Tr*, R^2 = Tr*, R^3 = OMe, R^4 = OH (53%)
2.20 R^1 = *i*Bu_3Si, R^2 = Tr*, R^3 = OMe, R^4 = OH (36%)
2.21 R^1 = Tr*, R^2 = Ph, R^3 = OMe, R^4 = OH (33%)

2.1 R^1 = Tr*, R^2 = Me_3Si (88%)
2.2 R^1 = *i*Pr_3Si, R^2 = Tr* (68%)
2.3 R^1 = Tr*, R^2 = Tr* (73%)
2.4 R^1 = *i*Bu_3Si, R^2 = Tr* (74%)
2.5 R^1 = Tr*, R^2 = Ph (98%)

Scheme 2.1. Synthesis of functionalized pentacenes **2.1–2.5** from monosubstituted intermediates **1.47**, **1.48**, **2.15**, and **2.16** and 6- and 13-disubstituted intermediates **2.17–2.21**.

The synthesis of sterically-hindered pentacene derivatives **2.1–2.5** started from **PQ**, and substituents at 6- and 13-positions were introduced via the corresponding acetylenes **2.6–2.10**. Acetylenes bearing tri*iso*propylsilyl (**2.6**), trimethylsilyl (**2.7**), and phenyl (**2.8**) groups are commercially available, whereas alkynes bearing the supertrityl (**2.9**)[38b] and tri*iso*butylsilyl (**2.10**)[39] groups were synthesized on the basis of published protocols.

Supertritylacetylene **2.9** was synthesized from commercially available 1-bromo-3,5-di-*tert*butyl benzene **2.11** (**Scheme 2.2**).[38b] To freshly ground Mg in THF under an atmosphere of N_2 was added slowly a solution of compound **2.11** in THF. The reaction was stirred at reflux for 3–5 h. After cooling, a solution of diethyl carbonate in THF was slowly added and the reaction was stirred at rt for 2 days to give compound **2.12**. Without further purification, thionyl chloride was added to a solution of compound **2.12** in toluene. After heating at reflux for 20 h, the reaction was cooled, and the solvent was removed in vacuo. The resulting residue **2.13** was dissolved in benzene and ethynylmagnesium bromide was added. The mixture was stirred for 6 days at rt under an atmosphere of N_2. The solvent was removed in vacuo and the crude product was recrystallized from hexanes to obtain compound **2.9** as a tan solid (70% yield).

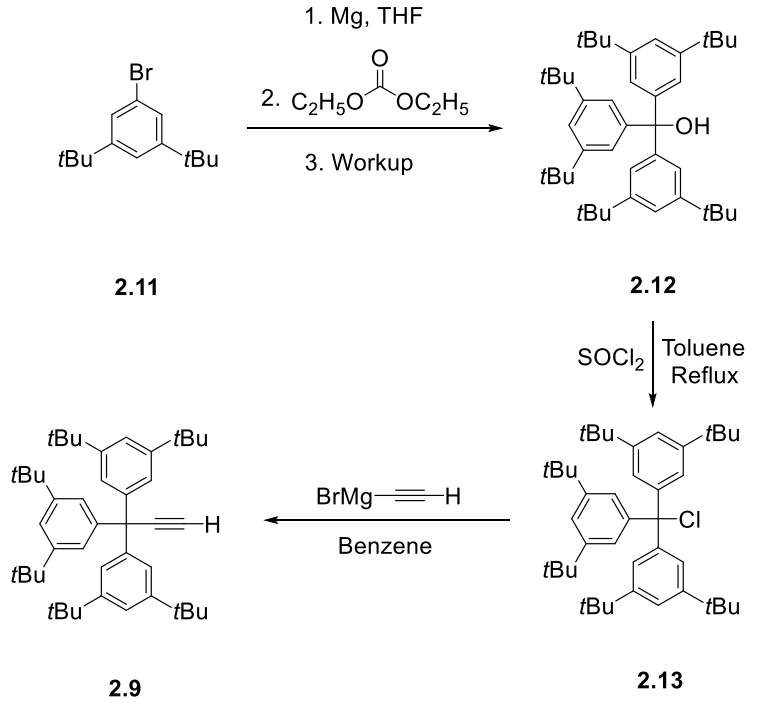

Scheme 2.2. Synthesis of supertritylacetylene **2.9**.[38b]

For the synthesis of compound **2.10** (**Scheme 2.3**),[39] commercially available tri*iso*butylchlorosilane **2.14** was added gradually to a cooled (–15 °C) solution of ethynylmagnesium bromide in THF, and after stirring for 2 h at rt. Workup and solvent removal gave compound **2.10** as a colorless liquid (85% yield).

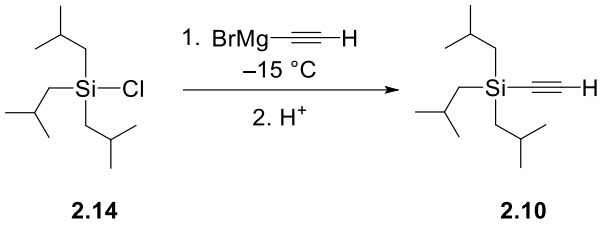

2.14 **2.10**

Scheme 2.3. Synthesis of tri*iso*butylsilylacetylene **2.10**.[39]

PQ was synthesized from the readily available reagents **1.12** and **1.13** by a fourfold Aldol condensation in a basic reaction environment (**Scheme 2.4**).[4]

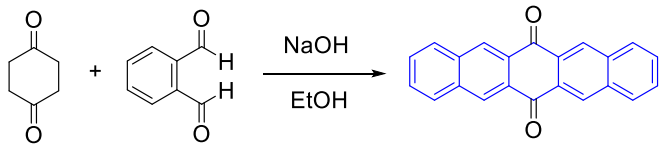

1.12 **1.13** **PQ** (90%)

Scheme 2.4. Synthesis of pentacenequinone **PQ**.[4]

The synthesis of functionalized pentacenes **2.1–2.5** required three steps: i) synthesis of 6-substituted intermediates **1.47**, **1.48**, **2.15**, and **2.16**; ii) synthesis of 6- and 13-disubstituted intermediates **2.17–2.21**; and iii) reductive aromatization. In the first step (**Scheme 2.1**), compound **1.47** was synthesized starting with the slow addition of lithiated tri*iso*propylsilylacetylene to a solution of **PQ** in dry THF over 5 min at –78 °C. After removing the cooling bath, the reaction mixture was allowed to warm and stirred for 4 h at rt. The reaction mixture was then cooled to –78 °C, and MeI (excess) was added slowly. The cooling bath was removed, the reaction mixture was allowed to warm to rt, and stirred for 18 h. After aq. workup and removing the solvent in vacuo, compound **1.47** was obtained by precipitation from CH_2Cl_2/MeOH and isolated as an off-white foamy solid (97% yield).[40]

The synthesis of compounds **1.48**, **2.15**, and **2.16** is analogous to the synthesis of compound **1.47**. Compound **1.48** was synthesized via slow addition of lithiated tri*iso*butylsilylacetylene via cannula into a suspension of **PQ** in dry THF over 5 min at –78 °C. After removing the cooling bath, the reaction mixture was warmed and stirred for 5 h

at rt. The reaction mixture was then cooled to –78 °C, and an excess of MeI was added slowly. The cooling bath was removed, the reaction mixture was allowed to warm to rt and stirred for 18 h. After aq. workup and removing the solvent in vacuo, compound **1.48** was obtained by precipitation from CH_2Cl_2/MeOH and isolated as a yellow solid (40% yield).[41]

Compound **2.15** was synthesized via slow addition of lithiated supertritylacetylene via cannula into a suspension of **PQ** in dry THF over 5 min at –78 °C. After removing the cooling bath, the reaction mixture was allowed to warm to rt while stirred for 1 day at rt. The reaction mixture was then cooled to –78 °C, and excess of MeI was added slowly. The cooling bath was removed, the reaction mixture was allowed to warm to rt and stirred for 4 h. After aq. workup and solvent removal in vacuo, compound **2.15** was purified by silica gel column chromatography to yield a pale-orange solid (39% yield). Although the yield was low, the advantage of this procedure was that both unreacted **PQ** and acetylene **2.9** could be recovered by filtration and column chromatography, respectively.

Compound **2.16** was synthesized via slow addition of lithiated supertritylacetylene via cannula into a suspension of **PQ** in dry THF over 5 min at –78 °C. After removing the cooling bath, the reaction mixture was warmed and stirred for 12 h at rt. After aq. workup and solvent removal in vacuo, compound **2.16** was purified by silica gel column chromatography to yield a pale-orange solid (58% yield).

In the second step, compound **2.17** was synthesized by dropwise addition of lithiated trimethylsilylacetylene into a solution of compound **2.15** in dry THF at −78 °C under an atmosphere of N_2. The reaction mixture was warmed and stirred at rt for 2 h before slow addition of MeI at −78 °C. After stirring at rt for 2 days, the reaction was quenched via the addition of saturated aq. NH_4Cl. Purification by silica gel column chromatography and removal of solvent in vacuo yielded compound **2.17** as a pale-green solid (79% yield).

Compound **2.18** was synthesized by dropwise addition of lithiated supertritylacetylene into a solution of compound **1.47** in dry THF at −78 °C under an atmosphere of N_2. The reaction mixture was warmed and stirred at rt for 2 days before quenching via the addition of saturated aq. NH_4Cl. Purification by silica gel column

chromatography and removal of solvent in vacuo yielded compound **2.18** as a bright green solid (45% yield).

Similarly, compound **2.19** was synthesized by dropwise addition of lithiated supertritylacetylene into a solution of compound **2.15** in dry THF at −78 °C under an atmosphere of N_2. The reaction mixture was warmed and stirred at rt for 19 h before quenching via the addition of saturated aq. NH_4Cl. Purification by silica gel column chromatography and removal of solvent in vacuo gave unreacted acetylene **2.9** and compound **2.19** (53% yield), the latter as a white solid that contained approximately 10% unknown/unidentified impurity.

Compound **2.20** was synthesized by dropwise addition of lithiated supertritylacetylene into a solution of compound **1.48** in dry THF at −78 °C under an atmosphere of N_2. The reaction mixture was warmed and stirred at rt for 1 day before quenching via the addition of saturated aq. NH_4Cl. Purification by silica gel column chromatography and removal of solvent in vacuo yielded compound **2.20** as an off-white solid (36% yield).

The final intermediate **2.21** was synthesized by dropwise addition of lithiated phenylacetylene to a solution of compound **2.15** in dry THF at −78 °C under an atmosphere of N_2. The reaction mixture was warmed and stirred at rt for 20 h before quenching via the addition of saturated aq. NH_4Cl. Purification by silica gel column chromatography and removal of solvent in vacuo yielded compound **2.21** as a pale-yellow solid (33% yield).

In the third step, the reductive aromatization, compound **2.1** was synthesized by addition of $SnCl_2 \bullet 2H_2O$ into a solution of compound **2.17** in dry THF under an atmosphere of N_2. The flask was wrapped in aluminium foil to limit light exposure, and the solution was stirred at rt for 6 h before being poured into H_2O. After workup and removal of the solvent in vacuo, purification by silica gel column chromatography yielded compound **2.1** as a deep-blue solid (88% yield).

Compound **2.2** was synthesized by addition of $SnCl_2 \bullet 2H_2O$ followed by 10% aq. H_2SO_4 into a solution of compound **2.18** in dry THF under an atmosphere of N_2. The flask was wrapped in aluminium foil to limit light exposure, and the solution was stirred at rt for

17 h. Removal of the solvent in vacuo and purification by silica gel column chromatography yielded compound **2.2** as a deep-blue solid (68% yield).

Compounds **2.3**, **2.4**, and **2.5** were synthesized in an analogous manner as compound **2.2**. to precursor **2.19**, **2.20**, or **2.21** in dry THF under an atmosphere of N_2 was added $SnCl_2 \bullet 2H_2O$ followed by 10% aq. H_2SO_4. The flask was wrapped in aluminium foil to limit light exposure, and the solution was stirred at rt for 16–24 h. Removal of the solvent in vacuo and purification by silica gel column chromatography yielded compound **2.3** (73% yield), compound **2.4** (74% yield), or compound **2.5** (98% yield) as deep-blue solids.

The purity of all 6-substituted intermediates **1.47**, **1.48**, **2.15**, and **2.16**, 6- and 13-disubstituted intermediates **2.17–2.21**, and final pentacene derivatives **2.1–2.5** was supported by ^{1}H NMR and ^{13}C NMR spectroscopy.

2.3 NMR Spectroscopic Comparison

To confirm the formation of the extended π-system during the reductive elimination to the pentacene derivatives **2.1–2.5**, ^{1}H NMR spectroscopy was the key method to use. The aromatic protons in derivatives **2.1–2.5** and their precursors **2.17–2.21** that are directly attached to the pentacene core (**a**, **a'**, **b**, **b'**, **c**, and **c'**) and the supertrityl group (**d** and **e**) can be compared and are more informative (and stronger) than signals in ^{13}C NMR spectra. Specific protons have not been assigned but they could be assigned by using 2D NMR spectroscopy techniques such as HMBC. Different substituents appended to the pentacene core cause slight changes in chemical shift of these aromatic protons. As the pattern of the aromatic protons is analogous for all derivatives, the spectra for compound **2.1** and its precursor **2.17** are compared and discussed (**Figure 2.1**), while other comparisons are presented in the Experimental Section (Sections **5.3.1–5.3.4**).

As can been observed in **Figure 2.1**, in the aromatic region of the ^{1}H NMR spectra of compounds **2.1** and **2.17**, **a** and **a'** protons are found as singlets since they are isolated from other protons. Protons **b** and **b'** and peripheral protons **c** and **c'** form a pseudo-second order splitting pattern and are observed as doublets and multiplets, respectively. Overall, in compound **2.1**, protons **a** and **a'** show a small downfield shift whereas protons

c and **c'** show a very small upfield shift in comparison to **2.17**. Aromatic protons of the supertrityl group, **d** and **e**, also show a very small downfield shifts in **2.1** relative to **2.17**.

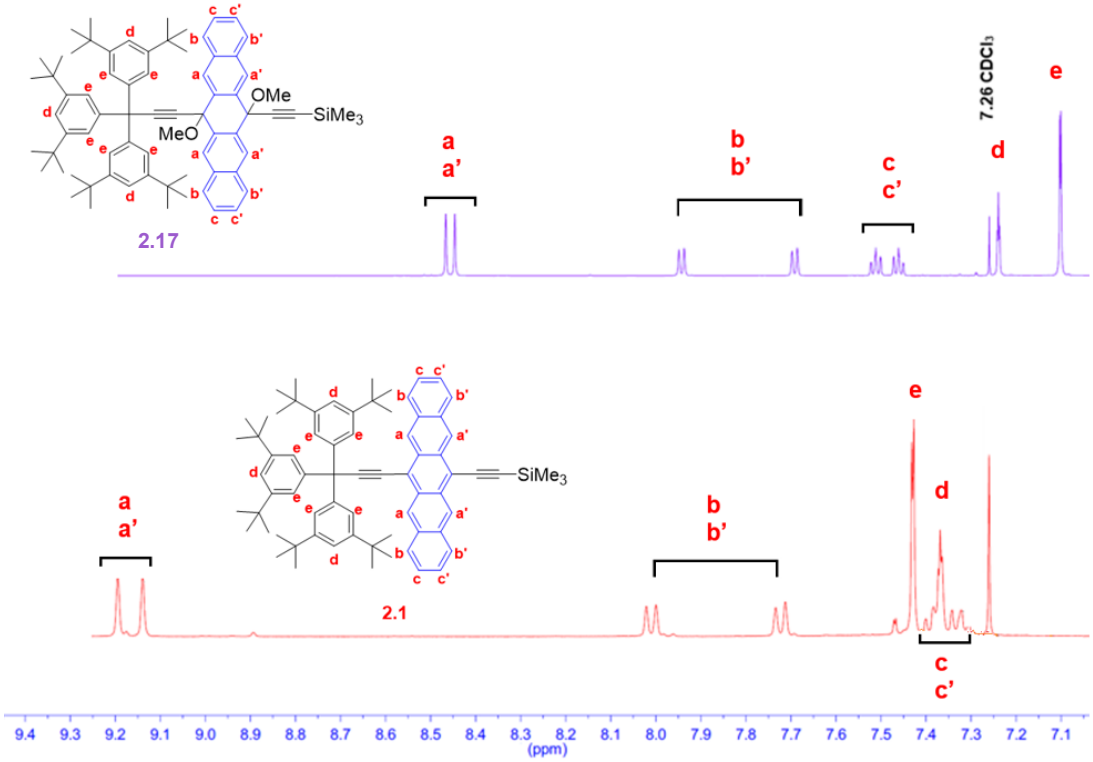

Figure 2.1. Comparison of the aromatic region of the ^{1}H NMR spectra of compounds **2.1** and **2.17** in $CDCl_3$.

As all sterically-hindered pentacene derivatives **2.1–2.5** have the supertritylethynyl group as a common substituent and other groups such as ethynyltrimethylsilyl ($SiMe_3$, **2.1**), ethynyltri*iso*propylsilyl (Si*i*Pr$_3$, **2.2**), supertritylethynyl (Tr*, **2.3**), ethynyltri*iso*butylsilyl (Si*i*Bu$_3$, **2.4**), and ethynylphenyl (Ph, **2.5**) as the second substituent, the next question is which group(s) might have an effect on the aromatic protons, perhaps revealing shielding of the acene framework.

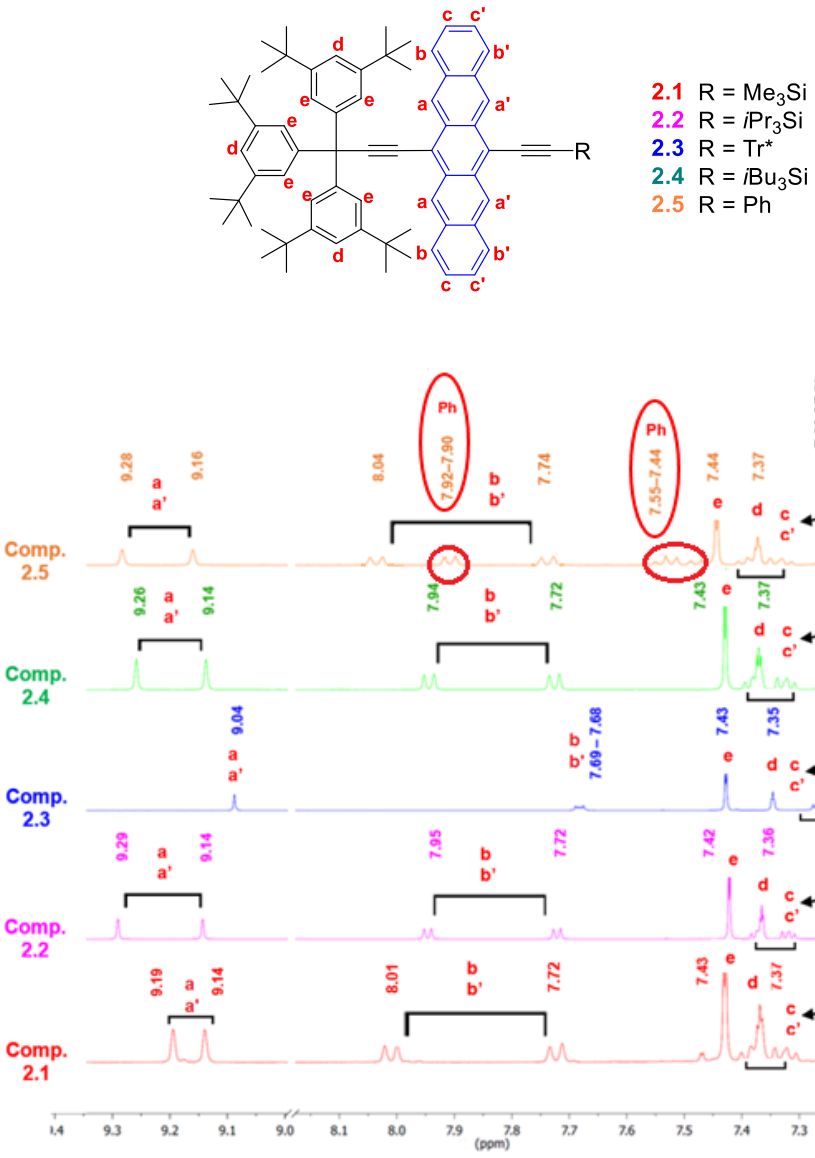

Figure 2.2. Comparison of the aromatic region of the ^{1}H NMR spectra of compounds **2.1–2.5** in $CDCl_3$.

^{1}H NMR spectroscopic comparison of the aromatic region of all sterically-hindered pentacene derivatives **2.1–2.5** indicates that there is little change in the shift of the protons of supertrityl groups (**Figure 2.2**). There are, however, small changes in the shift of the protons of the pentacene groups, and interestingly, compound **2.1** shows the most variance in chemical shift of protons **a** and **a'** in comparison to other derivatives. The aromatic protons in compound **2.3** are shifted slightly upfield compared to other derivatives, while protons **c** and **c'** are coincident with signals of the solvent. On the other

hand, protons **a**/**a'** and **b**/**b'** of **2.3** experience overall the most upfield shifts, perhaps due to interaction with the large Tr* groups. Finally, the ^{1}H NMR spectra of compound **2.5** showed two extra multiplet peaks at 7.92–7.90 and 7.55–7.44 ppm as expected the protons of the phenyl group.

2.4 Solid-State Analysis

Pentacene derivatives commonly pack in one of four arrangements: the 2D brick-layer, 1D slipped stack, herringbone, and sandwich-herringbone packing (**Figure 2.3**). Packing of acenes in the solid state generally depends on intermolecular π-π, C–H•••π, and H•••H interactions. The π-π interactions dominate for co-planar molecules, whereas C–H•••π interactions are important between edge-to-face molecules in solid state (e.g., herringbone arrangement). Both π-π and C–H•••π interactions are effective in sandwich structures.[42] Pristine pentacene shows a herringbone packing motif which is a simple combination of face-to-face and edge-to-face interactions (**Figure 2.4**). The hypothesis introduced by Anthony is to separate substituent from the acene backbone by a rigid alkyne spacer to disrupt the unfavored edge-to-face interactions.[14] Studies on pentacene crystals have shown that even slight changes in π-π interactions can dramatically affect device performance.[14]

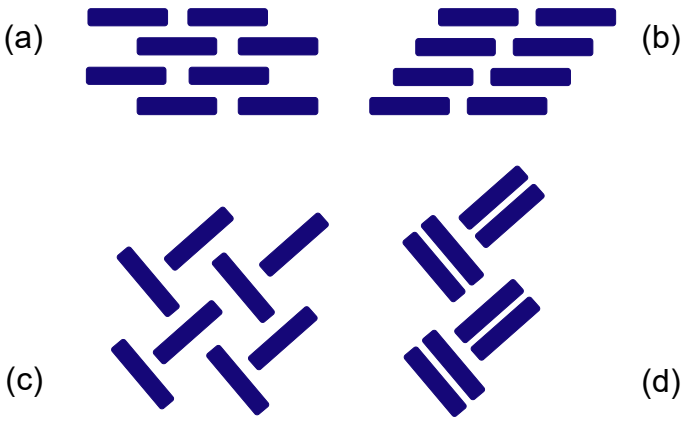

Figure 2.3. Typical packing modes of acenes in solid state: (a) 2D brick-layer, (b) 1D slipped stack, (c) herringbone, and (d) sandwich-herringbone packing.

Compared to pentacene **1.5**, TIPS-pentacene **1.23** with tri*iso*propylsilylethynyl groups at 6- and 13-positions, adopts 2D face-to-face brick-layer π-stacking in solid state with interplanar distance of 3.43 Å (**Figure 2.4**).[1b]

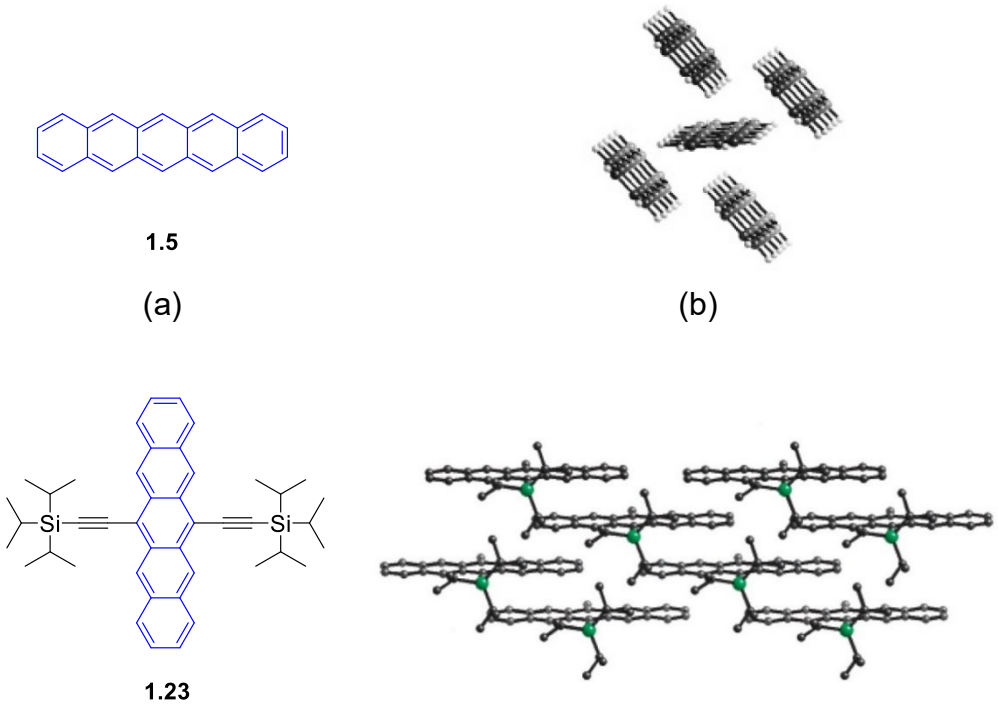

Figure 2.4. (a) Molecular structure of **1.5**, (b) Pentacene **1.5** with 2D edge-to-face arrangement, (c) Molecular structure of **1.23**, and (d) Pentacene **1.23** with 2D brick-layer arrangement.[1b]

Many efforts have been made to crystalize pentacene derivatives **2.1–2.5** to provide X-ray quality crystals, using a variety of solvents and conditions. Crystallographic analysis of compound **2.5** has been possible with crystals obtained by slow evaporation of a solution of **2.5** in CH_2Cl_2 layered with MeOH. Single-crystal X-ray crystallographic analysis of compounds **2.2** and **2.3** was accomplished by Matthias Adam during his research work in the group (see Chapter **5** for details), and these unpublished results have been used to compare π-stacking of these molecules in the solid state.[43] It was found that replacement of one of the Si*i*Pr$_3$ groups on compound **1.23** with the Tr* group

(compound **2.2**, **Figure 2.5**) affords a packing motif as shown in **Figure 2.5**, in which the π-systems do not significantly overlap.

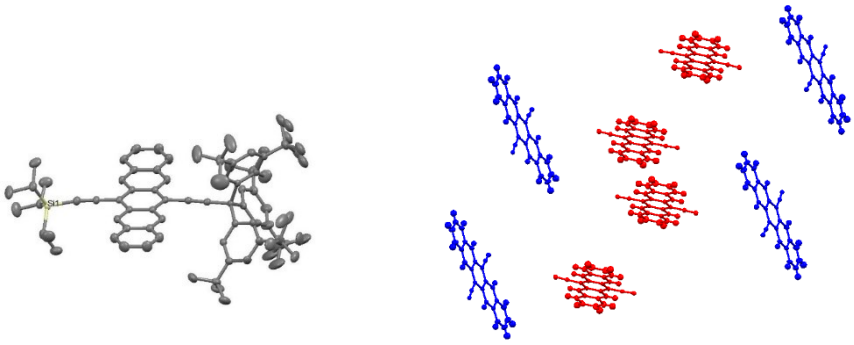

(a) (b)

Figure 2.5. X-ray crystallographic analysis showing (a) molecular structure of **2.2**, (b) packing motif (hydrogen atoms, tri*iso*propylsilyl, and Tr* groups omitted for clarity); ORTEPs drawn at 50% probability level.[43]

Formal replacement of both Si*i*Pr$_3$ groups with the Tr* groups provides compound **2.3** (**Figure 2.6**). Similar to compound **2.2**, **2.3** does not adopt a known motif as shown in **Figure 2.3**, and molecular arrangement in the solid state does not show significant π-overlap between neighboring pentacene moieties.

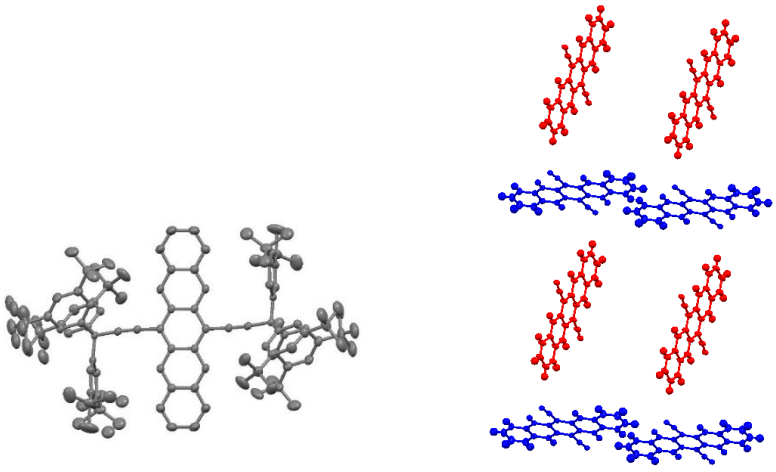

(a) (b)

Figure 2.6. X-ray crystallographic analysis showing (a) molecular structure of **2.3**, (b) packing motif (Tr* groups and hydrogen atoms omitted for clarity); ORTEPs drawn at 50% probability level.[43]

Compound **2.5**, with one Tr* group and one phenyl group pendent to the pentacene framework, crystalizes as a dimeric pair of molecules in the solid-state, and this is not an arrangement typically observed for pentacene derivatives. Each dimeric pair show an overlap of approximately three aromatic rings (**Figure 2.7**), but there is no long-range overlap between neighboring dimeric pairs. The interplanar distance between neighboring pentacenes is 3.39 Å as determined by generating planes through 22 atoms of each pentacene moiety.

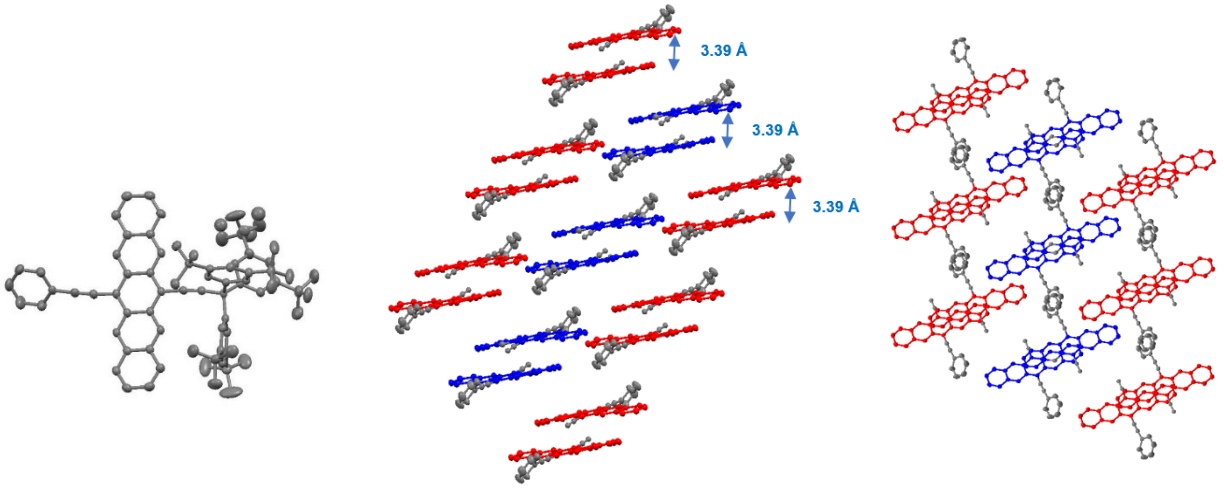

(a) (b) (c)

Figure 2.7. X-ray crystallographic analysis showing (a) molecular structure of **2.5**, (b) dimeric pair packing motif (Tr* group and hydrogen atoms omitted for clarity), and (c) illustration of the overlapping aromatic rings; ORTEPs drawn at 50% probability level.

2.5 UV-vis Spectroscopic Comparison

UV-vis spectra of compounds **2.1–2.5** have been measured in CH_2Cl_2 to explore the optical and electronic effects of substitutions on pentacene derivatives compared to compound **1.23**. **Figure 2.8** shows absorption spectra of compounds **2.1–2.5** in the range of 250–750 nm in CH_2Cl_2 with λ_{max} values labelled. The strongest absorption for compounds **2.1–2.4** is observed at λ_{max} = 310 nm (λ_{max} = 311 nm for **2.5**) with a series of low energy absorptions with λ_{max} = 642 nm (**2.1–2.3**) and λ_{max} = 644 nm (**2.4**). Compound

2.5 shows a red shift of the low energy absorption to λ_{max} = 652 nm due to the extended π-system relative to **2.1–2.4**.

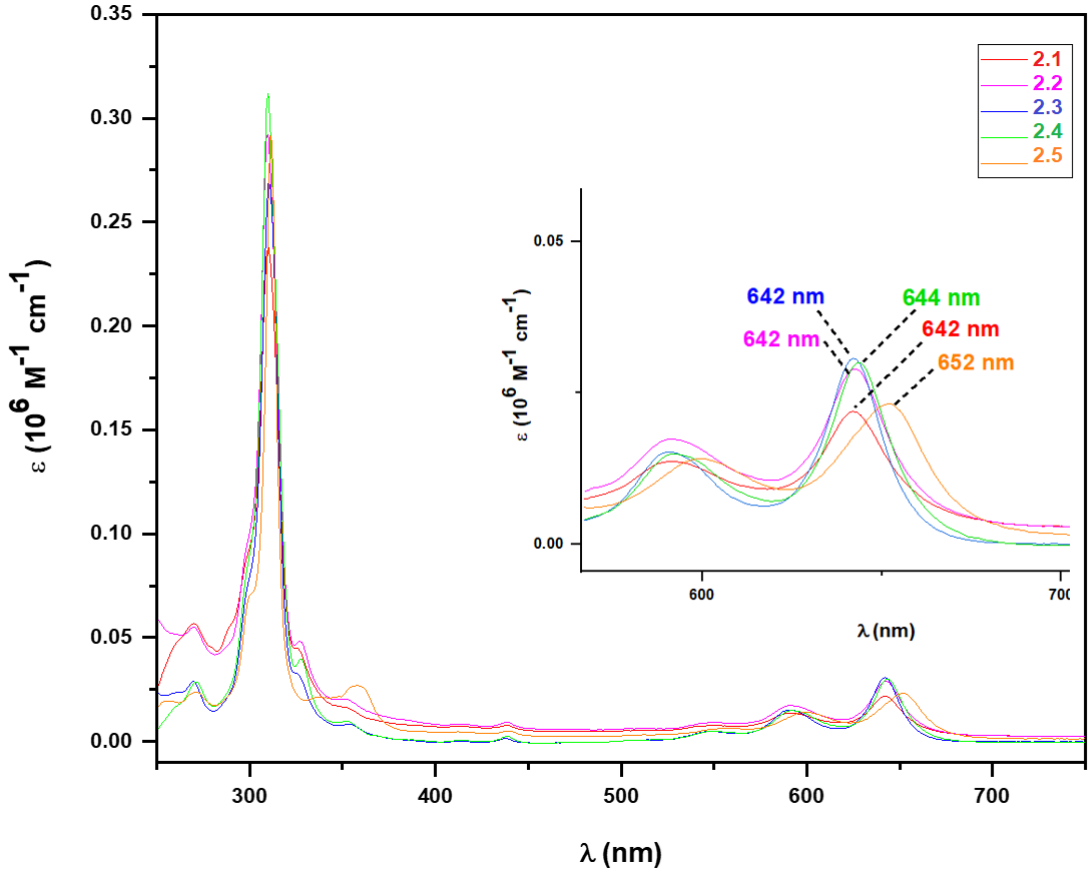

Figure 2.8. UV-vis absorption spectra for pentacenes **2.1–2.5** in CH_2Cl_2 (250–750 nm). Inset: Low energy absorption region with λ_{max} values.

As the results show in Table **2.1**, λ_{max} value of compounds **1.23**, **1.31**, **1.35**, and **2.1–2.4** are similar and basically the effect of supertrityl group is the same as the effect observed for the SiR_3 groups. Extending conjugation through the addition of Ph groups to replace the supertrityl or SiR_3 groups gives a slight red shift in λ_{max} values of compounds **1.36** and **2.5**, and a more substantial red shift of λ_{max} of compound **1.25**. Compared to pristine pentacene **1.5** which has λ_{max} = 584 nm in EtOH,[5] λ_{max} of compounds **2.1–2.3**, **2.4**, and **2.5** show a red shift of 58, 60, and 68 nm, respectively.

Table 2.1. UV-vis absorption data for selected pentacenes **2.1–2.5** in CH_2Cl_2 compared to compounds **1.23**, **1.25**, **1.31**, **1.35**, and **1.36**.

Compound	R^1	R^2	λ_{max} (nm)
1.23[4]	Si*i*Pr$_3$	Si*i*Pr$_3$	643
1.25[4]	Ph	Ph	660
1.31[4]	Si*i*Bu$_3$	Si*i*Bu$_3$	644
1.35[4]	Si*i*Pr$_3$	SiMe$_3$	642
1.36[4]	Si*i*Pr$_3$	Ph	652
2.1	SiMe$_3$	Tr*	642
2.2	Si*i*Pr$_3$	Tr*	642
2.3	Tr*	Tr*	642
2.4	Si*i*Bu$_3$	Tr*	644
2.5	Ph	Tr*	652

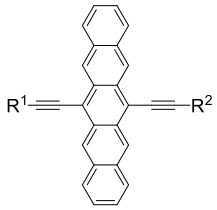

2.6 Electrochemical Properties

Investigation of the electronic properties of pentacene derivatives **2.1–2.5** was attempted using cyclic voltammetry (CV) with ferrocene as internal standard and tetrabutylammonium hexafluorophosphate (*n*Bu$_4$NPF$_6$) as the supporting electrolyte. It should be noted that in some cases the redox couples were not well resolved, and the following analysis is regarded as preliminary (Supporting Information, Section **5.5**). As shown in **Table 2.2**, pentacene derivatives **2.1–2.5** show a reversible oxidation potential (E_{OX1}) between 0.26–0.31 V. The second oxidation potential (E_{OX2}) of compounds **2.1** and **2.4** is quasi-reversible, whereas compounds **2.2**, **2.3**, and **2.5** have irreversible OX_2 events. Pentacene derivatives **2.1–2.3** and **2.5** show reduction potentials (E_{Red1}) in the range of –1.35 to –1.44 V that are irreversible for compound **2.1** and quasi-reversible for compounds **2.2**, **2.3**, and **2.5**.

Pentacenes **2.1–2.5** are slightly easier to oxidize compared to compound **1.23** (E_{ox1} = 0.39 V). More specifically, comparing the E_{OX1} potential of compounds **2.2** and **1.23** indicates that compound **2.2** is slightly more easily oxidized (~0.09 V) than compound **1.23**. Likewise, the oxidation of compound **2.3** with two Tr* group is easier than compounds **1.23** and **2.2**. Compounds **2.3** and **2.5** have the lowest E_{Red1} potential.

However, **1.36** and **1.23** with E_{Red1} potentials of –1.63 and –1.52 V are the most difficult to reduce.

As shown in **Table 2.2**, the range of E_{OX1} potentials is narrower than that of E_{Red1}, suggesting that alkynyl substituents at 6- and 13-positions have a larger impact on the energy of the LUMO than the HOMO. Overall, the electrochemical and optical HOMO-LUMO gap calculated from CV ($E_{gap}^{electro}$) and UV-vis data (E_{gap}^{opt}) are consistent with approximately 0.01–0.23 eV difference (**Table 2.2**). The $E_{gap}^{electro}$ values for **2.1–2.5** are in a range of 1.61–1.86 eV while E_{gap}^{opt} values are in a narrow range of 1.84–1.88 eV.

Table 2.2. Electrochemical properties of compounds **2.1–2.5** compared to compounds **1.36** and **1.23**.[a]

Compound	R^1	R^2	E_{ox1} (V)	E_{ox2} (V)	E_{red1} (V)	$E_{gap}^{electro}$ (eV)[b]	λ_{max} (CH_2Cl_2) (nm)[c]	E_{gap}^{opt} (CH_2Cl_2) (eV)[d]
1.23[19]	Si*i*Pr$_3$	Si*i*Pr$_3$	0.39	0.99	–1.52	1.91	643[42, 44]	1.84
1.36[19]	Si*i*Pr$_3$	Ph	0.34	0.87	–1.63	1.97	652	1.89
2.1	SiMe$_3$	Tr*	0.27	0.93	–1.44	1.71	642	1.87
2.2	Si*i*Pr$_3$	Tr*	0.30	0.62	–1.36	1.66	642	1.87
2.3	Tr*	Tr*	0.29	0.67	–1.35	1.64	642	1.88
2.4	Si*i*Bu$_3$	Tr*	0.31	0.79	[e]	1.86	644	1.87
2.5	Ph	Tr*	0.26	0.67	–1.35	1.61	652	1.84

[a] Cyclic voltammetry performed in CH_2Cl_2 solutions containing 0.1 M nBu$_4$NPF$_6$ as supporting electrolyte at a scan rate of 200 mV/s. Glassy carbon disc electrode was used as working electrode, Pt wire as counter electrode, and Ag/AgCl as reference electrode. The potential values (E) were calculated using the equation: $E = (E_{pc} + E_{pa})/2$, where E_{pc} and E_{pa} correspond to the cathodic and anodic peak potentials, respectively. Potentials are referenced to the ferrocene/ferrocenium (Fc/Fc^+) couple used as an internal standard.
[b] Electrochemical HOMO-LUMO gaps determined by $E_{gap}^{electro} = E_{ox1} - E_{red1}$.
[c] Lowest energy absorption maxima.
[d] E_{gap}^{opt} determined using the intercept of the x-axis and the tangent applied to the longest wavelength absorption peak.
[e] Unresolved.

2.7 Photochemical Stability

UV-vis spectroscopic characterization of compounds **2.1–2.5** is vital to evaluate substituted pentacenes as molecular targets for use in solar cells. Photochemical stability can be studied via UV-vis spectroscopy. To establish the solution stability of pentacene derivatives **2.1–2.5**, four different solutions in CH_2Cl_2 were made (see Supporting

Information, Sections **5.4.1–5.4.5**) for each compound and monitored by UV-vis spectroscopy over a period of time. The first two samples were made with deoxygenated CH_2Cl_2 as solvent, one of which was stored in the dark (no O_2/dark, ND) and the other stored under ambient light (no O_2/light, NL). The other two samples used non-deoxygenated CH_2Cl_2 as solvent, of which one was stored in the dark (air/dark, AD) whereas the other one was in the presence of ambient light (air/light, AL).

For semi-quantitative evaluation of decomposition of compounds **2.1–2.5**, a plot A_t/A_o against time is drawn in which A_t is the absorbance at λ_{max} at time t, and A_o is the absorbance at λ_{max} at $t = 0$. As observed in **Figure 2.9** and **Figures S5**, **S7**, **S9**, **S11**, and **S13** (see Supporting Information, Sections **5.4.1–5.4.5**), pentacene derivatives **2.1–2.5** decompose more rapidly when the solutions are exposed to ambient light, and the presence of oxygen in solution can accelerate the decomposition rate. On the other hand, samples kept in the dark are reasonably stable over time and all show similar behavior.

Based on an exponential fitting, only the half-life ($t_{1/2}$) of samples which have been exposed to light (AL and NL) could be estimated. In general, half-lives for AL samples are shorter than estimated half-lives for NL samples, and specifically samples of compounds **2.1–2.5** exposed to air and light show $t_{1/2}$ = 3.1, 14, 8.6, 7.7, and 74 h, respectively. On the other hand, NL samples show $t_{1/2}$ = 4.3, 22, 9.4, 14, and 94 h, respectively. Estimated A_t/A_o values of samples kept in dark (AD and ND) are effectively constant or close to constant over time, and the initial loss is likely due to the presence of residual O_2 in the solution. Thus, ND samples show the least decomposition, whereas AL samples show the greatest decomposition over time. Comparing the $t_{1/2}$ values of AL samples of compounds **2.1–2.5** shows the trend of photooxidation resistance as follows: **2.5** > **2.2** > **2.3** > **2.4** > **2.1**. Among compounds **2.1–2.5**, compound **2.1** bearing the Tr* and $SiMe_3$ groups (with the smallest substituent on 6-position) has the shortest half-life which is consistent with, for example, increased reactivity in cycloaddition reactions. The size of other substituents does not, however, appear to be the main contributor to stability of these pentacene derivatives. Compound **2.5** shows the highest stability in the solution although the reason is not clear yet but it can be distinguished in future. Compound **2.3** bearing two Tr* groups is not the most stabilized compound of the series, and, therefore, it can be concluded that the presence of Tr* groups is not sufficient to increase the stability

of pentacene derivatives. Thus, other factors, e.g., electronic contributions to stability, must also play a significant role, and the proposed hypothesis centered on substituent size can be rejected.

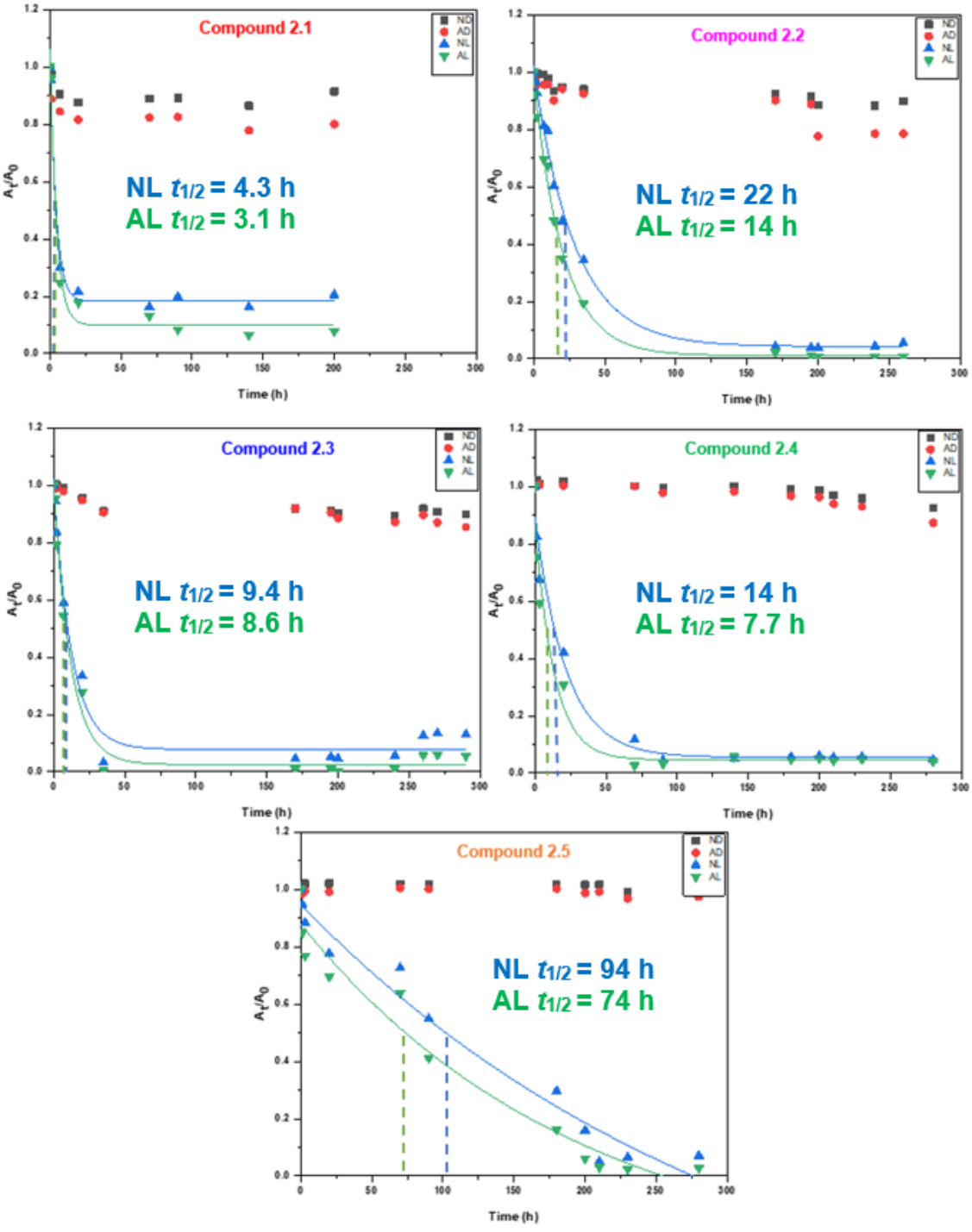

Figure 2.9. Absorbance-time profiles of compounds **2.1–2.5**; half-life of samples which were in the presence of light (NL and AL) indicated as $t_{1/2}$.

Finally, a logarithmic dependence of A_t/A_o against time would indicate that the degradation process of compounds **2.1–2.5** is not kinetically first-order. Since UV-vis absorption of all samples has not been monitored every hour in first 20 h, the calculated data is not particularly good, but the overall trends can still be discerned. Plotting $\ln(A_t/A_o)$ versus time for all compounds **2.1–2.5** (see Supporting Information, **Figures S6**, **S8**, **S19**, **S12**, and **S14**) is non-linear and it indicates that the degradation process of compounds **2.1–2.5** is not likely kinetically first-order. This observation is in agreement with the results of Miller et al.,[37] who concluded that the photooxidation reaction of most pentacene derivatives is non-linear over a significant percentage of the conversions.

2.8 Thermal Stability

Traditional melting point analysis (MPA) can be inconvenient for characterization of pentacene derivatives because the observation of small changes is difficult due to the dark color of the samples. Thus, differential scanning calorimetry (DSC) has been used to evaluate the thermal stability of compounds **2.1–2.5**, as shown in **Figure 2.10**. The comparison with compounds **1.23**, **1.31**, **1.35**, and **1.36** is described in **Table 2.3**.[39]

Table 2.3. Thermal properties of compounds **2.1–2.5** compared to compounds **1.23**, **1.31**, **1.35**, and **1.36**.

Compound	R^1	R^2	MPA (°C) [a]	DSC (°C) [b]		
				mp	dp/ onset	dp/ peak
1.23[39]	Si*i*Pr$_3$	Si*i*Pr$_3$	–	263	263	265
1.31[39]	Si*i*Bu$_3$	Si*i*Bu$_3$	213–215	213	213	215
1.35[39]	Si*i*Pr$_3$	SiMe$_3$	–	158	160	167
1.36[39]	Si*i*Pr$_3$	Ph	–	–	174	180
2.1	SiMe$_3$	Tr*	190–196	198	204	209
2.2	Si*i*Pr$_3$	Tr*	–	–	100	106
2.3	Tr*	Tr*	95–98	91	144	153
2.4	Si*i*Bu$_3$	Tr*	–	–	140	146
2.5	Ph	Tr*	–	–	109	135

[a] Traditional open capillary melting point analysis (MPA), measured under ambient conditions, uncorrected.
[b] Measured under an atmosphere of N_2, dp = decomposition point, shown as onset/peak temperatures.

Traditional MPA of compounds **2.1–2.5** have also been measured and when compared with the melting points obtained by DSC analysis, they are in good agreements. As the DSC results show, compounds **2.2**, **2.4**, and **2.5** decomposed directly as a solid before melting. In the case of compound **2.1**, melting is followed immediately by decomposition, similar to the behavior of compounds **1.23**, **1.31**, **1.35**, and **1.36**.[39] On the other hand, compound **2.3** melts at 91 °C and it is stable as a liquid up to 144 °C. Thus, the most obvious conclusion from the DSC data is that the two bulky supertrityl groups provide a pentacene derivative **2.3** that is stable in the liquid phase for around 50 °C after it melts.

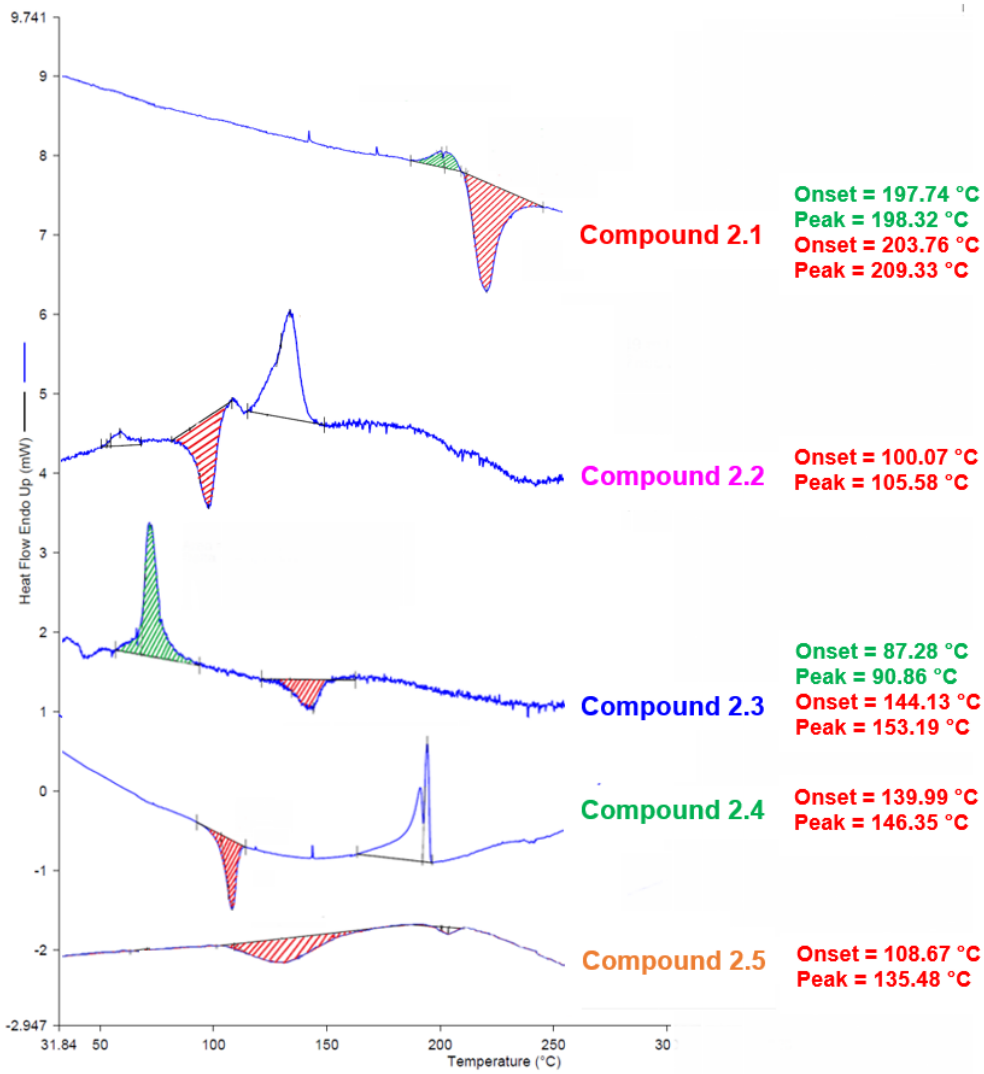

Figure 2.10. Differential scanning calorimetry of compounds **2.1–2.5** (melting in green, decomposition in red).

2.9 Summary and Conclusion

This chapter demonstrates success in the synthesis of symmetrical and unsymmetrical derivatives of pentacene with substituents in 6- and 13-positions, namely compounds **2.1–2.5**. All pentacene derivatives **2.1–2.5** are stable as solids for months when stored in the dark under refrigeration. As a result of substitution, **2.1–2.5** are soluble in common organic solvents such as THF, CH_2Cl_2, and hexanes. X-ray crystallographic analysis of compounds **2.2**, **2.3**, and **2.5** affords insight into the packing arrangements in the solid state. Compounds **2.2**, **2.3,** and **2.5** adopt packing motifs that are unusual for pentacene derivatives, and none show long range π-stacking interactions between pentacene groups. In solution, all of the derivatives show significant degradations in the presence of ambient light and oxygen, presumably via photodimerization and photooxidation reactions. According to UV-vis studies, the relative ordering of photooxidation stability is **2.5** > **2.2** > **2.3** > **2.4** > **2.1**, which leads to the conclusion that the size of substituents is not the main factor for stability of pentacene derivatives bearing Tr* groups. Namely, compound **2.3** bearing two Tr* groups is not the most stabilized compound of the series, and it is concluded that the presence of Tr* groups is not sufficient to increase the stability of pentacene derivatives. Thus, other factors such as electronic effects must play a role in stability of pentacenes. Analysis of thermal stability indicates that compound **2.3** bearing two Tr* groups is stable in the liquid phase for ~50 °C after the melting point, whereas compounds **2.2**, **2.4**, and **2.5** decomposed directly as a solid before melting, and compound **2.1** decomposed immediately after melting. From DSC results and photostability studies, it is concluded that steric shielding based on the presence of the Tr* group provides stabilization in liquid phase whereas the size of Tr* group is not an important factor to inhibit or slow down the photodegradation. As observed by cyclic voltammetry, the range of E_{OX1} potentials is much narrower in comparison to E_{Red1} potentials, which shows that alkynyl substituents at 6- and 13-positions has a larger effect on the energy of the LUMO than the HOMO. Overall, the electrochemical and optical HOMO-LUMO gap calculated from CV ($E_{gap}^{electro}$) and UV-vis data (E_{gap}^{opt}) are consistent.

CHAPTER 3
PENTACENE DIMERS

3.1 Introduction

Dimeric pentacene (Pnc_2) have the minimum number of chromophores required for iSF and allow for a molecular structure to be easily tailored by changing the spacer.[45–47] Pentacene precursors with terminal acetylene units that are formed in this chapter lend themselves to the synthesis of pentacene dimers via connections at the 13-positions of the pentacene through the Sonogashira cross-coupling reaction. The goal of the work in this chapter is to synthesize a series of pentacene dimers tethered by a 3,5-disubstituted benzoic acid spacer toward answering the following basic hypotheses:

- Can replacing the Si*i*Pr$_3$ groups in a dimer with bulky Tr* groups slow down the degradation process (dimerization or endoperoxide formation) and improve the stability of the dimer?
- Can replacing the Si*i*Pr$_3$ group with the bulky Tr* group in dimeric pentacenes slow down the hydrolysis of ester bond in subphthalocyanine-pentacene (SubPc-Pnc_2) dyads?
- Can SubPc-Pnc_2 dyads bearing Tr* groups be used for the study of iSF specially through incorporation of DSSC?

3.2 Synthesis of Pentacene Dimers

3.2.1 Synthesis of The Dimer TIPS-Pnc_2

The basic precursor for all of the target molecules in this chapter is **PQ**, which was synthesized as discussed in Chapter 2, Section **2.2** (**Scheme 2.2**).[4] Disubstituted intermediate **1.49** was synthesized by the similar procedure as was used for synthesis of 6- and 13-disubstituted intermediate **2.17** in Chapter 2, Section **2.2** (**Scheme 3.1**). To form compound **1.49**, lithiated trimethylsilylacetylene was added dropwise to a solution of compound **1.47** in dry THF at −78 °C under an atmosphere of N_2.[15] The reaction mixture

was warmed and stirred at rt for 15 h before slow addition of MeI at −78 °C. After stirring the reaction mixture at rt for 20 h, the reaction mixture was cooled to 0 °C and was quenched via the addition of saturated aq. NH_4Cl. Purification by silica gel column chromatography and removal of solvent in vacuo yielded compound **1.49** as an off-white solid (26% yield).

Terminal alkyne **1.51** was synthesized by following the procedure that was reported by Dan Lehnherr in reference 6. To a solution of **1.49** in THF/MeOH cooled to 0 °C was added K_2CO_3[15] The reaction mixture was maintained between 0 °C and 5 °C, stirred for 6 h, and then poured into saturated aq. NH_4Cl. After aq. workup and removing the solvent in vacuo, compound **1.51** was obtained by precipitation from CH_2Cl_2/MeOH and isolated as an off-white solid (63% yield).

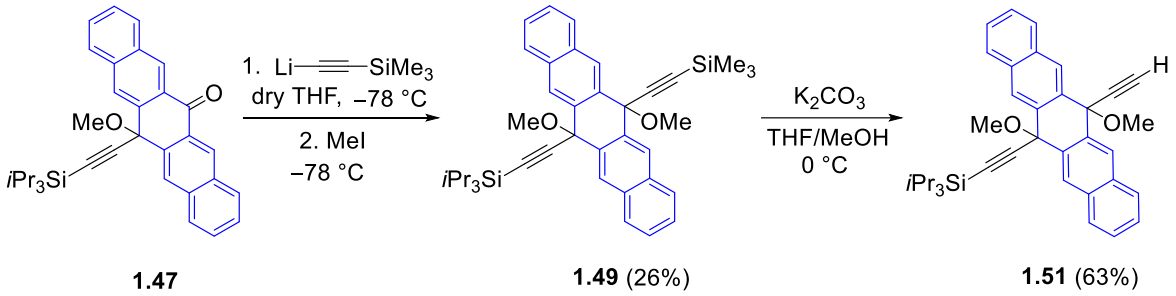

1.47 **1.49** (26%) **1.51** (63%)

Scheme 3.1. Synthesis of terminal alkyne **1.51**.[15]

Dimer **TIPS-Pnc$_2$** was synthesized in three steps according to the recently published paper by Tykwinski, Guldi, et al. (**Scheme 3.2**): i) Synthesis of ester intermediate **3.1** by Sonogashira cross-coupling reaction; ii) Synthesis of acid intermediate **3.2** via a saponification reaction; and iii) Reductive aromatization reaction.[48] The ester intermediate **3.1** was synthesized by dissolving the terminal alkyne **1.51** (excess) and methyl 3,5-dibromobenzoate in a mixture of dry THF and degassed Et_3N.[48] The mixture was purged with N_2 for 15 min. $Pd(PPh_3)_4$ and CuI were added as solids and the reaction mixture was purged with N_2 for 15 min. The reaction mixture was stirred for 16 h at reflux. After allowing to cool to rt, the mixture was poured onto a pad of silica gel and eluted with CH_2Cl_2. Purification by silica gel column chromatography and removal of solvent in vacuo yielded compound **3.1** as a light green solid (98% yield).

Saponification of 3,5-disubstituted methyl benzoate intermediate **3.1** was carried out by dissolving **3.1** in a mixture of THF/H_2O with aq. lithium hydroxide and stirring the reaction mixture at rt for 15 h.[48] Extracting the organic phase with CH_2Cl_2 and removing the solvent in vacuo yielded 3,5-disubstituted benzoic acid **3.2** as a green solid (92% yield).

Pentacene dimer **TIPS-Pnc$_2$** was synthesized by addition of $SnCl_2 \bullet 2H_2O$ and 10% aq. H_2SO_4 into a solution of compound **3.2** in dry THF under an atmosphere of N_2.[48] The flask was wrapped in aluminium foil to limit light exposure, and the solution was stirred at rt for 4 h. The reaction mixture was poured into MeOH, and the mixture was cooled to –18 °C for 20 h. The resulting dark blue precipitate was filtered, washed with cold MeOH and pentane, and dried in vacuo to yield dimer **TIPS-Pnc$_2$** as a dark blue solid (89% yield).

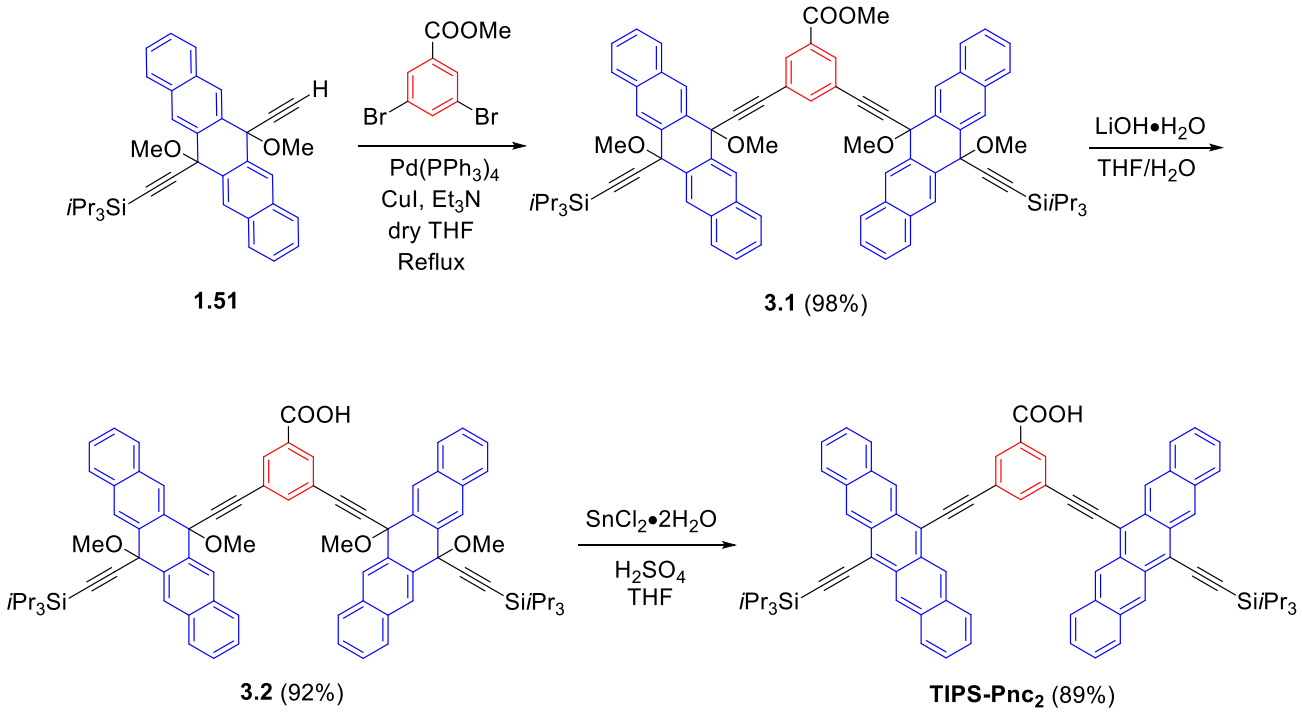

Scheme 3.2. Synthesis of the pentacene dimer **TIPS-Pnc$_2$**.[48]

3.2.2 Synthesis of The Dimer Tr*-Pnc$_2$

The first step toward the synthesis of pentacene dimer **Tr*-Pnc$_2$** required formation of the intermediate terminal alkyne **3.3** (**Scheme 3.3**) via desilylation of **2.17** (see Chapter 2, Section **2.2**). To this end, K_2CO_3 was added to a solution of compound **2.17** in

THF/MeOH at 0 °C. The reaction mixture was stirred for 6 h while the temperature maintained between 0 °C and 5 °C. The reaction mixture was then poured into saturated aq. NH_4Cl. Purification by silica gel column chromatography and removal of solvent in vacuo yielded compound **3.3** as a light green solid (74% yield).

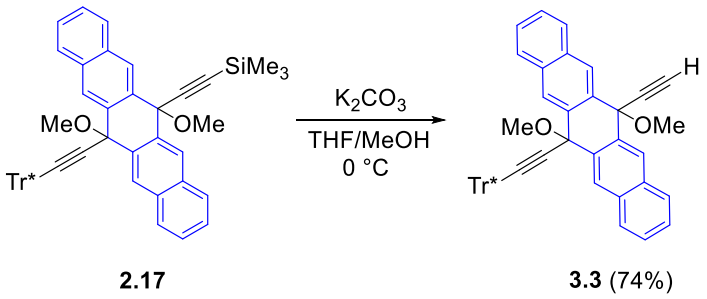

2.17 **3.3** (74%)

Scheme 3.3. Synthesis of terminal alkyne intermediate **3.3**.

The first attempt toward the synthesis of the dimer **Tr*-Pnc$_2$** (and the corresponding monomer **3.4)** relied on the same stepwise procedure as discussed for the synthesis of **TIPS-Pnc$_2$** in Section **3.2.1** using **3.3** and methyl 3,5-dibromobenzoate. These attempts were, unfortunately, unsuccessful (**Scheme 3.4**). Several modifications to the purification process, such as column chromatography and precipitation with different solvents, were tried but pure products from the Sonogashira cross-coupling, saponification, or reductive aromatization reactions could not be achieved. Indeed, TLC analysis showed a multiple of spots at each stage, with little hope of purification. This analysis was also confirmed by ^{1}H NMR spectra of the impure products in all three steps, which showed “a forest” of signals in the aromatic region. In desperation, the impure product of each step was used for the next step, in hopes that the final pentacene product might be achieved pure due to its decreased solubility and tendency to crystalize. In total, however, it was hard to support the synthesis of desired dimer **Tr*-Pnc$_2$** and monomer **3.4** by this procedure.

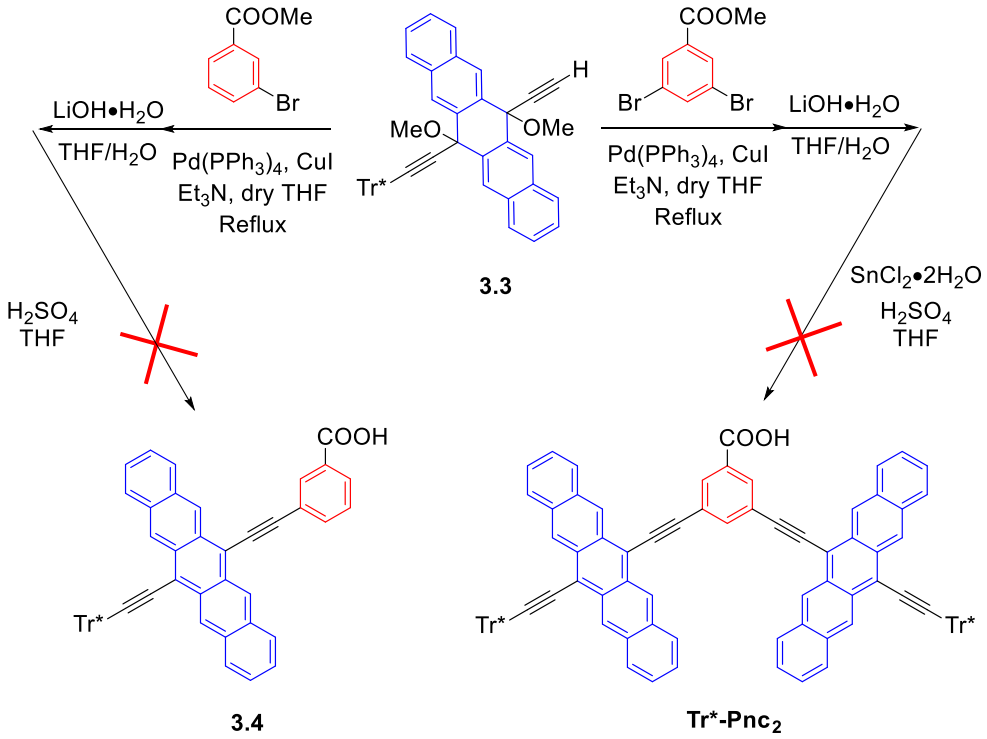

Scheme 3.4. Attempts toward the synthesis of the dimer **Tr*-Pnc$_2$** and monomer **3.4**.

A shorter and more direct method for synthesis of pentacene dimer **Tr*-Pnc$_2$** and monomer **3.4** was thus developed (**Scheme 3.5**). It is known that the choice of aryl halide substrate (sp^2-carbon) in the Sonogashira cross-coupling reaction is one of the most important factors that effects the reactivity.[49] More specifically, the reactivity of aryl iodides is superior to bromides, and 3,5-diiodobenzoic acid **3.5** and 3-iodobenzoic acid **3.6** were thus used toward the synthesis of dimer **Tr*-Pnc$_2$** and monomer **3.4**, respectively.

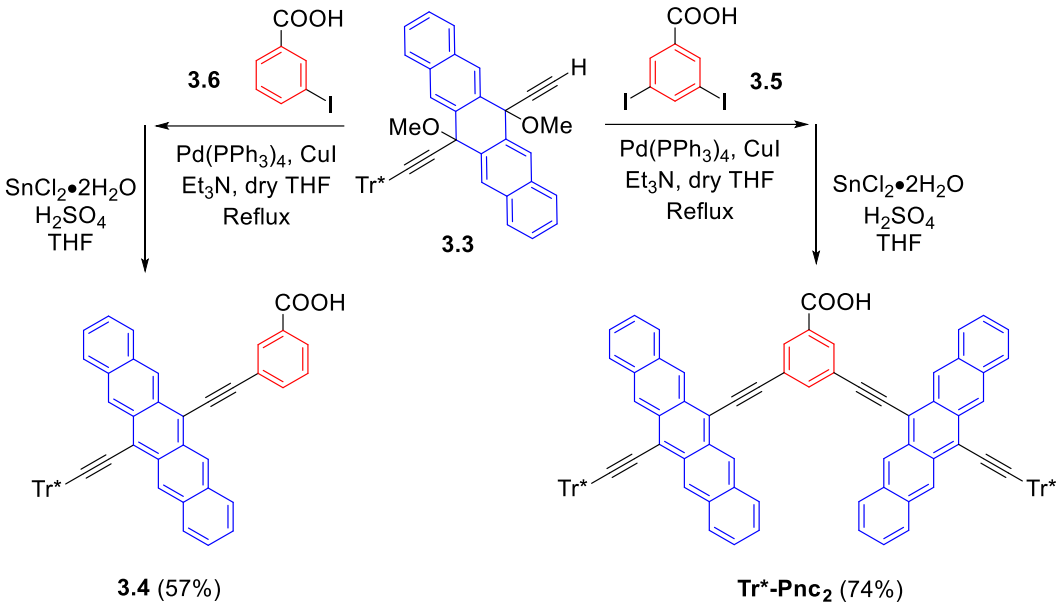

3.4 (57%) **Tr*-Pnc$_2$** (74%)

Scheme 3.5. Optimized conditions for synthesis of the dimer **Tr*-Pnc$_2$** and monomer **3.4**.

The aryl halide 3-iodobenzoic acid **3.6** was commercially available, whereas 3,5-diiodobenzoic acid **3.5** was synthesized as reported in the literature.[50] Sodium nitrite was added to an ice-cooled suspension of 3,5-diaminobenzoic **3.7** acid in H_2SO_4/H_2O mixture, and the reaction mixture was stirred for 1 h at 0 °C. The urea was added to the reaction mixture followed by dropwise addition of a cold solution of KI/H_2O. The black reaction mixture was stirred for an additional 3 h at 0 °C, warmed up to 60 °C for 30 min, and then poured into cold H_2O to precipitate as a brown solid. The solid was dissolved in diethyl ether and washed with aq. $Na_2S_2O_3$ until a pale-yellow color was observed. After removing the solvent in vacuo, compound **3.5** was purified by recrystallization from toluene and isolated as a pale-yellow solid (35% yield).

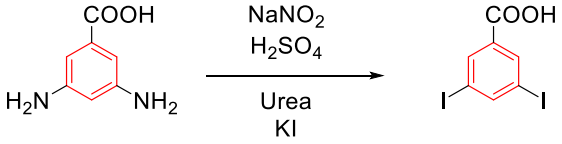

3.7 **3.5** (35%)

Scheme 3.6. Synthesis of 3,5-diiodobenzoic acid **3.5**.[50]

Under the new synthetic route (**Scheme 3.5**), dimer **Tr*-Pnc$_2$** was targeted by first dissolving terminal alkyne **3.3**, 3,5-diiodobenzoic acid **3.5**, $Pd(PPh_3)_4$, and CuI in degassed Et_3N and purging the reaction mixture with N_2 for 30 min. The reaction mixture was stirred for 25 h at reflux. After allowing to cool to rt, the mixture was poured onto a pad of silica gel and eluted with CH_2Cl_2 and MeOH. After removal of the solvent in vacuo and dissolving the crude sample in dry THF, $SnCl_2 \bullet 2H_2O$ and 10% aq. H_2SO_4 were added, and the reaction mixture was stirred in a flask wrapped in aluminium foil for 15 h at rt under an atmosphere of N_2. The reaction mixture was poured into MeOH, and the mixture was cooled to –18 °C for 20 h. The formed dark blue precipitate was filtered, washed with cold MeOH, and dried in vacuo to yield dimer **Tr*-Pnc$_2$** as a dark blue solid (74% yield) that contained approximately 10% monomer **3.4**. Although further purification was attempted by precipitation with different solvent mixtures, none of the attempts were successful. Dimer **Tr*-Pnc$_2$** is not stable on silica gel, and, thus, column chromatography did not help for further purification. Therefore, although the new synthetic procedure was useful for the synthesis of **Tr*-Pnc$_2$**, further actions are needed toward purification before the sample can be provided to our collaborators for photophysical characterization.

Monomer **3.4** was synthesized by dissolving the terminal alkyne **3.3**, 3-iodobenzoic acid **3.6**, $Pd(PPh_3)_4$, and CuI in degassed Et_3N and purging the reaction mixture with N_2 for 30 min. The reaction mixture was stirred for 2 days at reflux. After allowing to cool to rt, the mixture was poured onto a pad of silica gel and eluted with CH_2Cl_2 and MeOH. After removal of the solvent in vacuo and dissolving the crude sample in dry THF, $SnCl_2 \bullet 2H_2O$ and 10% aq. H_2SO_4 were added and the reaction mixture was stirred in an aluminium foil-wrapped flask for 1 day at rt under an atmosphere of N_2. After the removal of solvent in vacuo, precipitation from hexanes/MeOH afforded monomer **3.4** as a deep blue solid (57% yield).

3.3 SubPc-Pnc$_2$ Dyads

In collaboration with Guldi group (Erlangen, Germany) and the Torres group (Madrid, Spain), a sample of pentacene dimer **TIPS-Pnc$_2$** was sent to Spain for the synthesis of three SubPc-Pnc$_2$ conjugates **3.8–3.10** in order to explore intramolecular Förster resonance energy transfer (FRET) and singlet fission (SF) (**Scheme 3.7**).[36] While I did not synthesize the SubPc-Pnc$_2$ conjugates, this aspect of the study is briefly included here to emphasize the importance of the pentacene dimers.

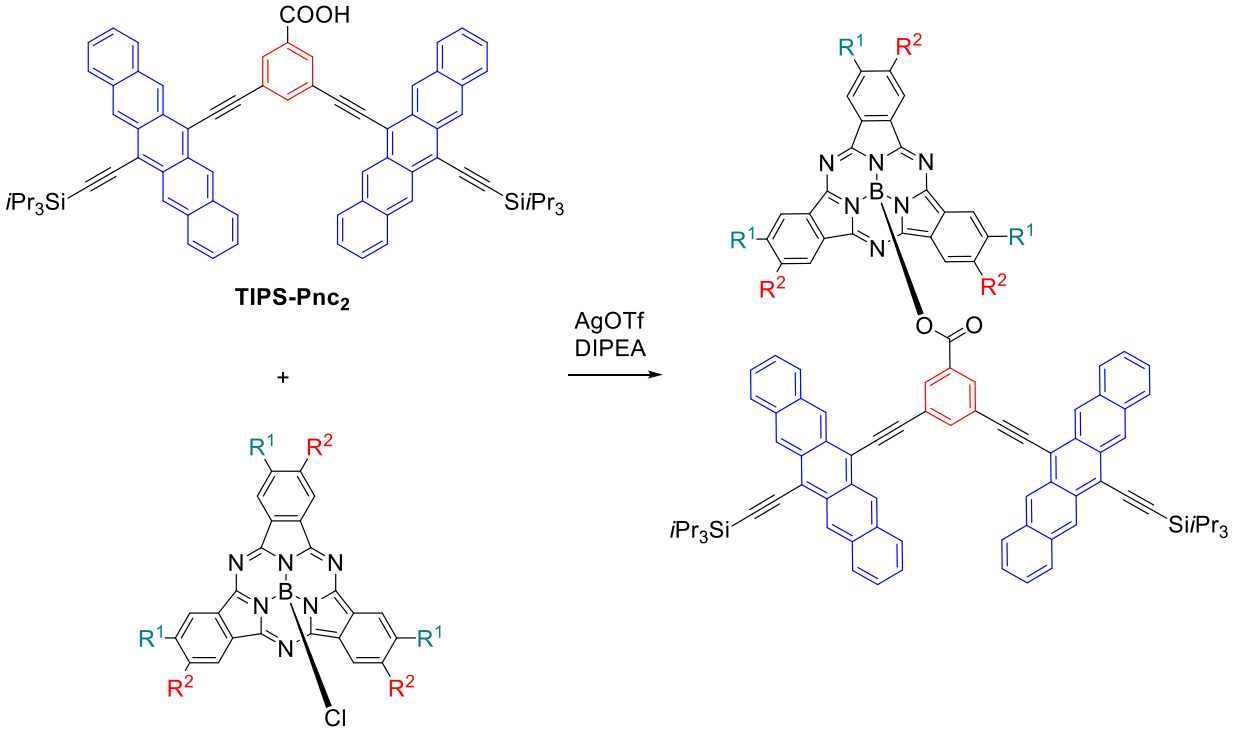

3.11 R^1 = H, R^2 = H
3.12 R^1 = OPh, R^2 = H
3.13 R^1 = SC_8H_{17}, R^2 = SC_8H_{17}

3.8 R^1 = H, R^2 = H
3.9 R^1 = OPh, R^2 = H
3.10 R^1 = SC_8H_{17}, R^2 = SC_8H_{17}

Scheme 3.7. Synthesis of SubPc-Pnc$_2$ dyads **3.8–3.10**.[36]

In this design, pentacene dimer **TIPS-Pnc$_2$** served as a SF material. The dimer was linked through a carboxylate group to the axial position of SubPcs **3.11–3.13**, which function as a light-harvesting antenna. Different peripheral substituents on SubPcs **3.11–3.13**, such as -H, -OPh, and -SC_8H_{17}, were used to influence and optimize the optical properties, and subsequently, the efficiency of intramolecular FRET. The UV-vis

absorption spectrum of dimer **TIPS-Pnc$_2$** shows that the dimer is almost transparent in the range of 450–550 nm, whereas SubPcs **3.11–3.13** and SubPc-Pnc$_2$ **3.8–3.10** have absorptions in this area (**Figure 3.1**). The SubPcs absorptions are complementary to pentacenes. The SubPc moiety in compounds **3.8–3.13** in toluene shows a Q-band at 565, 571, 602, 565, 572, and 601 nm, respectively, while the dimer **TIPS-Pnc$_2$** has major absorptions around 660 nm in low energy region in toluene.

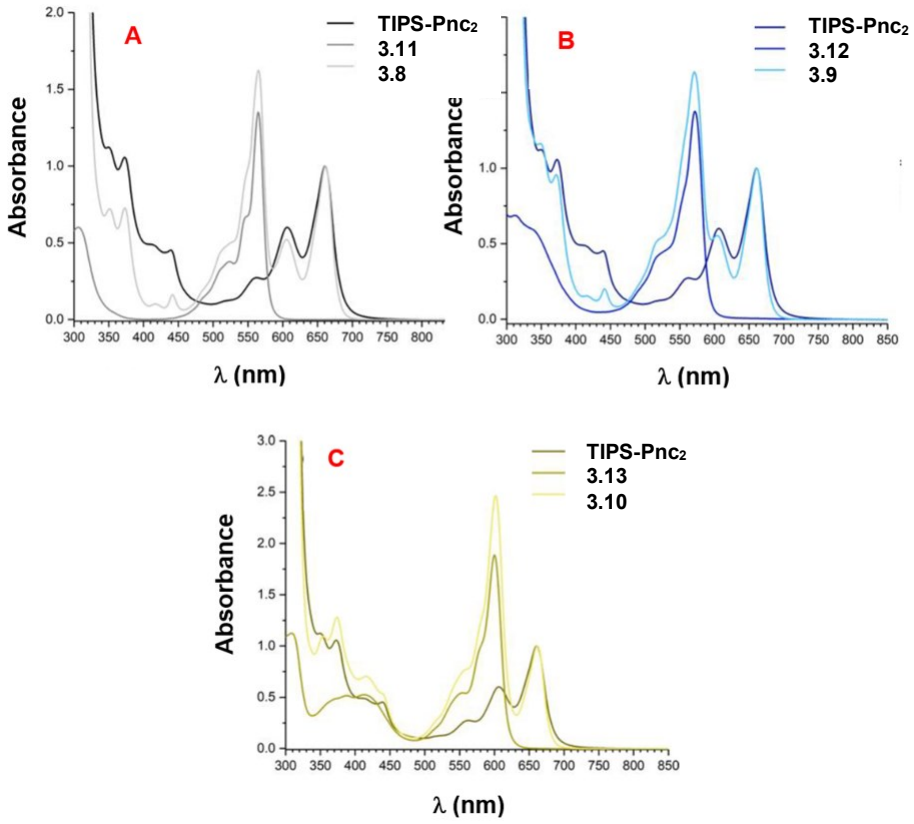

Figure 3.1. Absorption spectra of compounds **TIPS-Pnc$_2$**, **3.8**, and **3.11** (A), compounds **TIPS-Pnc$_2$**, **3.9**, and **3.12** (B), and compounds **TIPS-Pnc$_2$**, **3.10**, and **3.13** (C) in toluene. Figure adapted from reference 10.[36]

Excitation of **TIPS-Pnc$_2$** at 661 nm in toluene leads to fluorescence emission at 666 nm with a low fluorescence quantum yields of 0.02 (**Figure 3.2**).[36] Excitation at the wavelength of the Q-band of SubPcs **3.11–3.13** in toluene leads to strong fluorescence emission at 573 (**3.11**), 583 (**3.12**), and 609 (**3.13**) nm, and fluorescence quantum yields

of 0.30 (**3.11**), 0.31 (**3.12**), and 0.16 (**3.13**) with fluorescence lifetime of 3.30 (**3.11**), 3.01 (**3.12**), and 2.47 ns (**3.13**). The presence of sulfur in **3.13** caused a lower fluorescence quantum yields compared to **3.11** and **3.12** because sulfur is known to enhance the intersystem crossing (ISC).

In contrast, excitation of SubPc-Pnc_2 dyads **3.8–3.10** at their Q-band leads to a weak fluorescence emission (**Figure 3.2**)[36] at 573 (**3.8**), 583 (**3.9**), and 609 (**3.10**) nm, followed by a relatively good fluorescence emission at 666 nm (**3.8–3.10**), i.e., the same energy as the fluorescence emission of dimer **TIPS-Pnc_2** (666 nm). The weak fluorescence emissions indicate that SubPc-centered fluorescence of compounds **3.8–3.10** is quenched by about 90% compared to **3.11–3.13**. Thus, it is clear that the singlet excited state energy has been funneled from the SubPcs center to the **TIPS-Pnc_2** via ultrafast FRET.

Following excitation of the SubPc cores in dyads **3.8–3.10**, ultrafast FRET to ground state dimer **TIPS-Pnc_2** affords intramolecular SF (**Figure 3.3**). In other words, the initial **TIPS-Pnc_2** (S_1S_0) state, which is the product of FRET, is converted into the $^1(T_1T_1)$ state. More importantly, both fast FRET and SF compete with a slow intersystem crossing (ISC) process.[36] This observation is in agreement with iSF in pentacene dimers with phenylene spacers, in general, and a *m*-phenylene dimer, in particular.[36, 48] The same study on dimer **Tr*-Pnc_2** with Guldi group will be done in the future after further optimization of the purification of the dimer **Tr*-Pnc_2**.

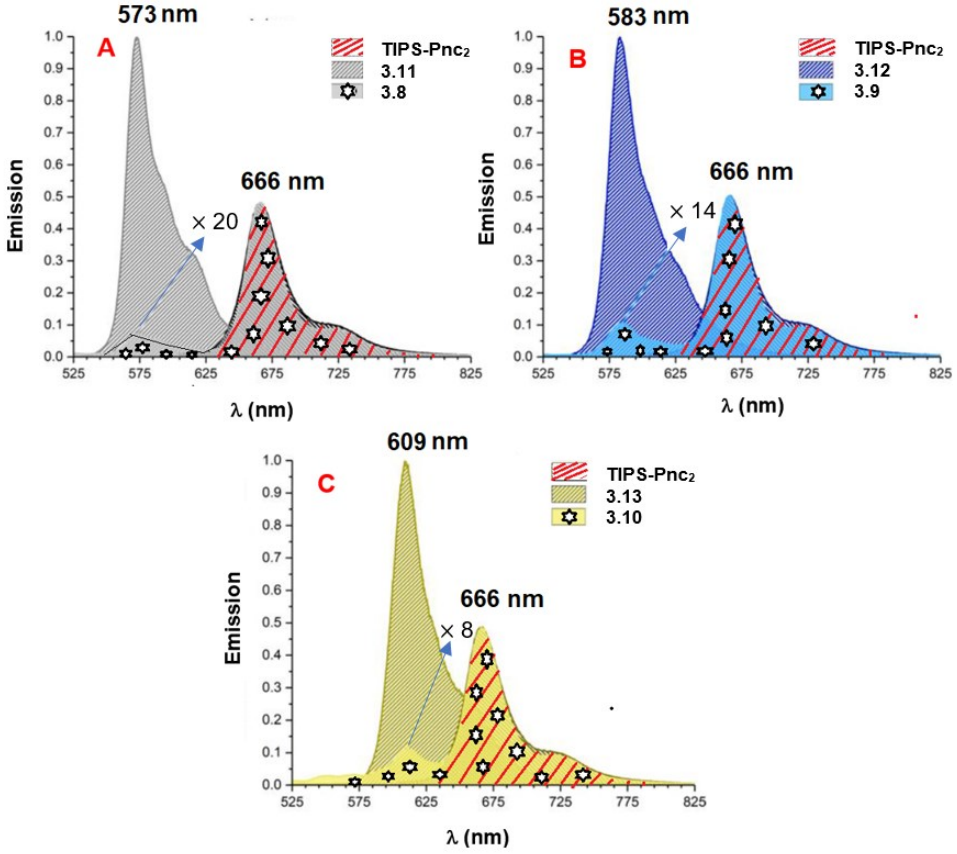

Figure 3.2. Fluorescence spectra of compounds **TIPS-Pnc$_2$**, **3.8**, and **3.11** (A), compounds **TIPS-Pnc$_2$**, **3.9**, and **3.12** (B), and compounds **TIPS-Pnc$_2$**, **3.10**, and **3.13** (C) in toluene. Figure adapted from reference 36.[36, 51]

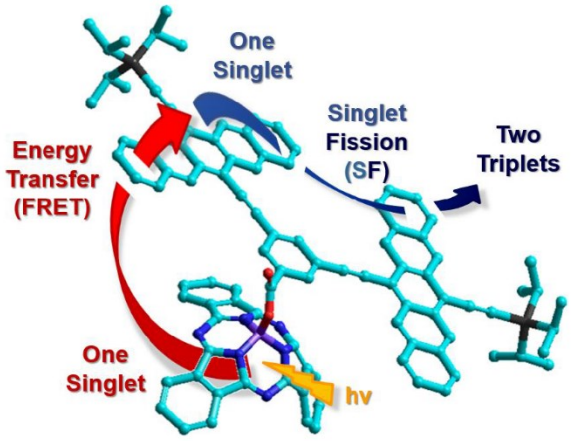

Figure 3.3. Illustration of intramolecular FRET and SF in SubPc-Pnc$_2$ dyads **3.8–3.10**.[36]

3.4 NMR Spectroscopic Comparison

The ^{1}H NMR spectroscopic comparison of dimers **TIPS-Pnc$_2$** and **Tr*-Pnc$_2$** in THF-d_8 indicates that the assigned aromatic protons of the pentacene core and the aromatic spacer in both compounds have similar shielding/deshielding pattern (**Figure 3.4**). In both dimers, the multiplicity pattern of the singlet for protons **a**,**a'** and doublet for protons **b**,**b'** are the same, whereas multiplets of protons **c**,**c'** show a slightly different second order pattern. As expected, dimer **Tr*-Pnc$_2$** shows two signals for supertrityl group (Tr*) at 7.47 and 7.55 ppm. Finally, protons **d** and **e** of the phenylene spacer group show both similar multiplicity and chemical shift in both dimers.

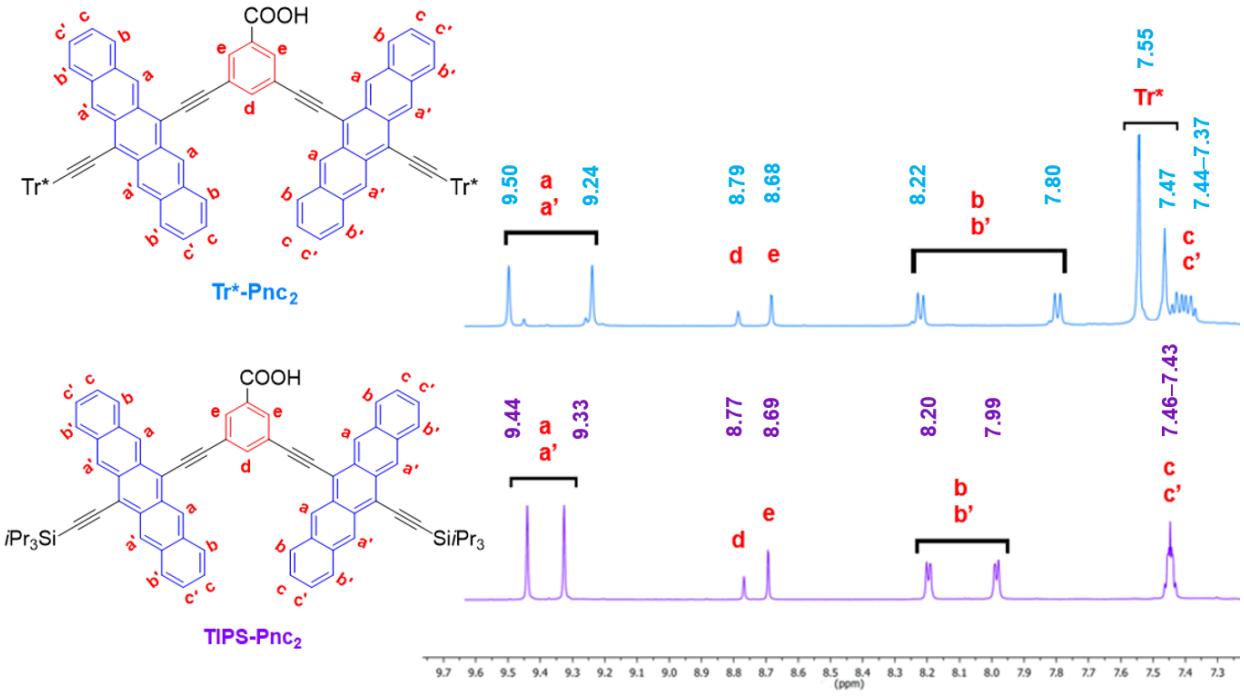

Figure 3.4. Comparison of the aromatic region of the ^{1}H NMR spectra of dimers **TIPS-Pnc$_2$** and **Tr*-Pnc$_2$** in THF-d_8.

3.5 UV-vis Spectroscopic Comparison

UV-vis spectra of dimers **TIPS-Pnc$_2$** and **Tr*-Pnc$_2$** and pentacene monomer **3.4** have been measured in the range of 250–750 nm in CH_2Cl_2 in order to explore the effect of different substitutions on the absorption properties (**Figure 3.5**). Although dimer **Tr*-**

Pnc_2 contained ~10% monomer **3.4** as an impurity, it has been studied by UV-vis spectroscopy and the result compared with UV-vis data of monomer **3.4**.

The strongest absorption for dimer **TIPS-Pnc_2** is observed at λ_{max} = 310 nm with a series of low energy absorptions and λ_{max} = 657 nm. The strongest absorption of the dimer **Tr*-Pnc_2** is observed at λ = 311 nm with a series of low energy absorptions at λ_{max} = 660 nm. The strongest absorption for the monomer **3.4** is also observed at λ = 312 nm with a series of low energy absorptions spanning as far as λ_{max} = 654 nm.

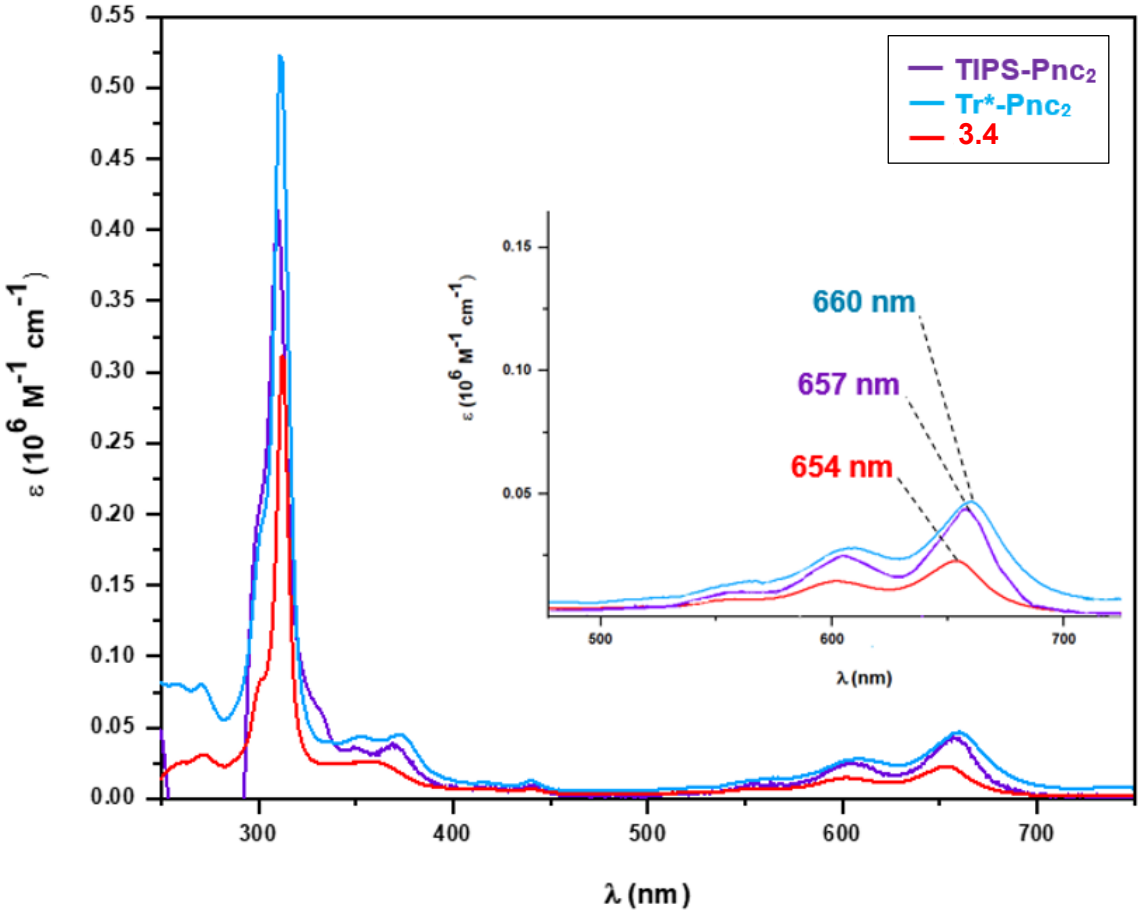

Figure 3.5. UV-vis absorption spectra for pentacene dimers **TIPS-Pnc_2**, **Tr*-Pnc_2**, and pentacene monomer **3.4** in CH_2Cl_2 (250–750 nm). Inset: Low energy absorption region with λ_{max} values.

Compared to the pentacene monomers **1.36** and **2.5** with λ_{max} = 652 nm in CH_2Cl_2 in the low energy region,[39] λ_{max} value of dimer **TIPS-Pnc$_2$** shows a minimal red shift of 5 nm at 657 nm and the λ_{max} value of dimer **Tr*-Pnc$_2$** shows a similar red shift of 8 nm at 660 nm (**Table 3.1**). Likewise, compared to monomer **3.4** with λ_{max} = 654 nm in CH_2Cl_2, λ_{max} value of dimers **TIPS-Pnc$_2$** and **Tr*-Pnc$_2$** show a red shift of 3 and 6 nm at λ_{max} = 657 and 660, respectively.

Cross-conjugated molecules, e.g., **TIPS-Pnc$_2$** and **Tr*-Pnc$_2$**, are molecules with three unsaturated groups from which only two π–bonds interact with each other by conjugation, whereas the third one is excluded from interaction. As it is known, cross-conjugation is less efficient in π-electron delocalization than linear conjugation. Therefore, linearly conjugated pentacene dimers tethered by a phenylene spacer have a redshifted absorption maxima in UV-vis, whereas *m*-phenylene dimers (cross-conjugated dimers) show a much weaker redshifted absorption. Consequently, **TIPS-Pnc$_2$** and **Tr*-Pnc$_2$** dimers show a slight red shift in their absorption maxima compared to the monomer **3.4**. The existence of six electron-donating *t*Bu groups on each supertrityl group in **Tr*-Pnc$_2$** likely raises the HOMO energy level, and results in a slight red shift in absorption maxima compared to the **TIPS-Pnc$_2$**.[50b]

Table 3.1. UV-vis absorption data for pentacene dimers **TIPS-Pnc$_2$** and **Tr*-Pnc$_2$** in CH_2Cl_2 compared to pentacene monomers **1.36**, **2.5,** and **3.4**.

Compound	R^1	R^2	λ_{max} (nm)
1.36[39]	Si*i*Pr$_3$	Ph	652
2.5[a]	Tr*	Ph	652
3.4	Tr*	C_6H_4COOH	654
TIPS-Pnc$_2$	Si*i*Pr$_3$	Si*i*Pr$_3$	657
Tr*-Pnc$_2$	Tr*	Tr*	660

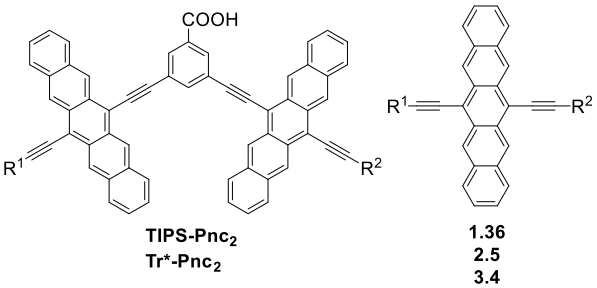

[a] Synthesis and UV-vis characterization of compound **2.5** has been presented in Chapter 2.

3.6 Photochemical Stability

The photochemical stability of dimer **TIPS-Pnc$_2$** has been studied via UV-vis spectroscopy. Following the same general protocol outlined in Chapter **2**, Section **2.7**, to establish the solution stability of the dimer **TIPS-Pnc$_2$**, four different solutions in CH_2Cl_2 were made (see Supporting Information, Section **5.4.6**) and monitored by UV-vis spectroscopy over a period of time. The first two samples were made with deoxygenated CH_2Cl_2 solvent, and one was stored in the dark (no O_2/dark, ND), whereas the other was stored under ambient light (no O_2 /light, NL). The other two samples used non-deoxygenated CH_2Cl_2 as solvent. One was stored in the dark (air/dark, AD), whereas the other remained exposed to ambient light (air/light, AL).

For semi-quantitative evaluation of the decomposition of dimer **TIPS-Pnc$_2$**, A_t/A_o plotted against time is drawn in which A_t is the absorbance at λ_{max} at time t, and A_o is the absorbance at the same λ_{max} at t = 0. As observed in **Figure 3.6** and **Figure 5.15**, (see Supporting Information, Section **5.4.6**), **TIPS-Pnc$_2$** decomposes more rapidly when the solutions are exposed to ambient light, and the presence of oxygen in solution can accelerate the decomposition rate. On the other hand, samples kept in the dark (AD and ND) are reasonably stable over time.

Based on an exponential fitting, the half-life ($t_{1/2}$) of samples that have been exposed to light (AL and NL) has been estimated. In general, the half-life for AL sample ($t_{1/2}$ = 50 h) is marginally shorter than estimated half-life for NL sample ($t_{1/2}$ = 53 h). Estimated A_t/A_o values of samples kept in dark (AD and ND) are effectively constant or very close to constant over time, and the initial loss is likely due to the reaction with residual O_2 in the solution. Thus, the ND sample shows the least decomposition, whereas AL sample shows the greatest decomposition over time. Plotting $\ln(A_t/A_o)$ versus time for dimer **TIPS-Pnc$_2$** (see Supporting Information, **Figure 5.16**) is non-linear and it indicates that the degradation process of dimer **TIPS-Pnc$_2$** is not kinetically first-order, and this observation is in agreement with the results of Miller et al.[52]

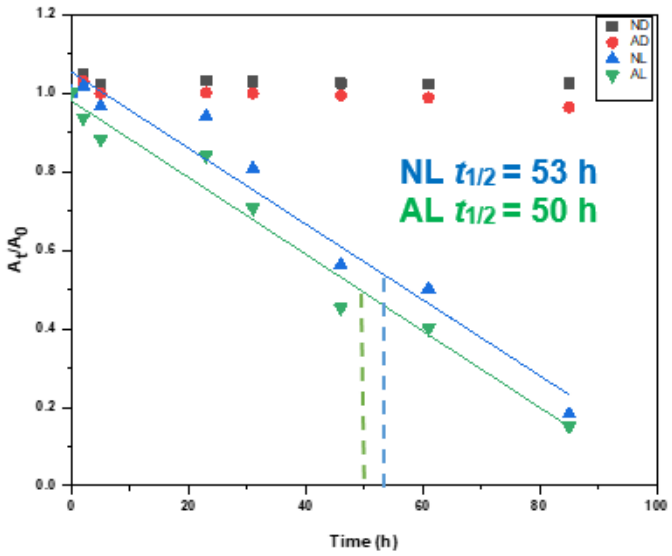

Figure 3.6. Absorbance-time profiles of dimer **TIPS-Pnc$_2$**; half-life of samples which were in the presence of light (NL and AL) indicated as $t_{1/2}$.

The stability results for dimer **TIPS-Pnc$_2$** led to the synthesis of dimer **Tr*-Pnc$_2$**, in order to see how the replacement of the Si*i*Pr$_3$ group in dimer **TIPS-Pnc$_2$** with a Tr* group can affect its stability. To be able to study the stability of dimers **Tr*-Pnc$_2$**, further purification is needed in future studies. Subsequently, answering to the proposed questions in the introduction section of this chapter will depend on the stability results of dimer **Tr*-Pnc$_2$** in future.

3.7 Summary and Conclusion

This chapter demonstrates success in the synthesis of monomer **3.4** and dimers **TIPS-Pnc$_2$** and **Tr*-Pnc$_2$**. The starting point for the synthesis of the dimers **TIPS-Pnc$_2$** and **Tr*-Pnc$_2$** is the synthesis of terminal alkynes **1.51** and **3.3**, respectively. All pentacene derivatives, **TIPS-Pnc$_2$**, **Tr*-Pnc$_2$**, and **3.4** are stable as solids for months when stored in the dark under refrigeration. As a result of substitution, **TIPS-Pnc$_2$**, **Tr*-Pnc$_2$**, and **3.4** are soluble in common organic solvents such as THF, CH_2Cl_2, and hexanes. Therefore the solubility of both dimers has increased compared to pristine pentacene **1.5**. However, when **TIPS-Pnc$_2$** was investigated in solution, it showed significant degradations in the presence of ambient light and oxygen, presumably via photodimerization and photooxidation reactions.

Since **Tr*-Pnc$_2$** could not be isolated pure, a stability test could not be accomplished and compared with a stability test of dimer **TIPS-Pnc$_2$**. Likewise, the thermal stability test comparison could not be accomplished.

A sample of **TIPS-Pnc$_2$** has been sent to the Torres group for synthesis of SubPc-Pnc$_2$ dyads **3.8–3.10** in order to explore intramolecular FRET and SF. Successfully, the results of photophysical studies indicates that the energy is funneled unidirectionally from the SubPc singlet excited state to the **TIPS-Pnc$_2$** ground state via FRET. Then, the excited **TIPS-Pnc$_2$** in converted into a pair of correlated **TIPS-Pnc$_2$** triplet excited states via iSF. The same study on dimer **Tr*-Pnc$_2$** with Guldi group will be done in future after further optimization on purification of dimer **Tr*-Pnc$_2$**.

CHAPTER 4
CONCLUSION AND OUTLOOK

4.1. Conclusion

This thesis, indeed, is a result of the collaboration of many people, and I acknowledge their contributions to the body of my master thesis. Personally, developing fellowship with the people that I have mentioned in the acknowledgment section has been by far one of the most meaningful achievement that I have made during these three years in University of Alberta. I hope that by writing this thesis, I have successfully summarized the scientific advances of our experiments in the synthesis of pentacene derivatives and their applications (Chapters 2–3).

Symmetrical and unsymmetrical derivatives of pentacenes with substituents in 6- and 13-positions, namely compounds **2.1–2.5** (Chapter 2) have been synthesized by the reaction of pentacenequinone **PQ** with lithiated acetylenes, followed by quenching the reaction mixture with MeI or via protonation, and, finally, reductive aromatization with $SnCl_2 \bullet 2H_2O$. All pentacene derivatives **2.1–2.5** are stable as solids for months when stored in the dark under refrigeration. Compounds **2.1–2.5** are soluble in common organic solvents such as THF, CH_2Cl_2, and hexanes as a result of substitution (~10 mg/mL). X-ray crystallographic analysis of **2.2**, **2.3**, and **2.5** shows unusual packing motifs for these pentacene derivatives, and none of the derivatives show long range π-stacking interactions between pentacene groups. The stability of **2.1–2.5** in solution has been evaluated by UV-vis spectroscopy, and these studies show significant degradation of the compounds in the presence of ambient light and oxygen. From the UV-vis results, it is concluded that the size of substituents is not the main factor for photostability, and the presence of Tr* groups is not sufficient to increase the photostability of pentacene derivatives. Thus, other factors such as electronic effects must play a role in stability of pentacene derivatives in solutions. DSC analyses showed that Tr* groups can increase the thermal stability of pentacene derivatives in the liquid phase. From DSC results and

photostability studies, it is concluded that steric shielding based on the presence of the Tr* group provides stabilization in liquid phase whereas the size of Tr* group is not an important factor to inhibit or slow down the photodegradation. Finally, cyclic voltammetric studies suggest that substituents at 6- and 13-positions have a larger effect on the energy of the LUMO than that of the HOMO.

Dimeric pentacenes **TIPS-Pnc$_2$** and **Tr*-Pnc$_2$** have been successfully synthesized (Chapter 3). Dimer **TIPS-Pnc$_2$** has been synthesized by the use of methyl 3,5-dibromobenzoate and terminal alkynes **1.51** via Sonogashira cross-coupling reaction followed by saponification and reductive aromatization. On the other hand, the synthesis of **Tr*-Pnc$_2$** has been devised, without purification of the intermediates. Specifically, dimer **Tr*-Pnc$_2$** has been formed using 3,5-diiodobenzoic acid and terminal alkynes **3.3** via Sonogashira cross-coupling reaction followed by reductive aromatization. Although the synthetic procedure was useful for the synthesis of **Tr*-Pnc$_2$**, further work is needed toward purification before the sample can be provided to our collaborators in Germany for photophysical characterization. Monomer **3.4** was also synthesized in two steps by Sonogashira cross-coupling reaction between **3.3** and 3-iodobenzoic acid **3.6**, followed by reductive aromatization. All pentacene derivatives, **TIPS-Pnc$_2$**, **Tr*-Pnc$_2$**, and **3.4** are stable as solids for months when stored in the dark under refrigeration. When the stability of **TIPS-Pnc$_2$** was investigated in solution, it showed significant degradation in the presence of ambient light and oxygen, presumably via photodimerization and photooxidation reactions. A sample of **TIPS-Pnc$_2$** has been sent to the group of Tomas Torres (Madrid) to be used in the synthesis of SubPc-Pnc$_2$ dyads **3.8–3.10**. Subsequent photophysical characterization of **3.8–3.10** by the group of Dirk Guldi (Erlangen) indicated that these dyads can be used to successfully tune intramolecular FRET and activate iSF. Since dimer **Tr*-Pnc$_2$** could not be achieved, stability test could not be accomplished and compared with stability of dimer **TIPS-Pnc$_2$**. Likewise, thermal stability was not evaluated for **Tr*-Pnc$_2$**.The photophysical study of dimer **Tr*-Pnc$_2$** will be done in future after further optimization on purification of dimer **Tr*-Pnc$_2$**.

4.2. Outlook

One of the most challenging problems that world is facing today, and in near future, is related to the growing needs for clean energy, particularly, converting the solar energy to the electricity. Collaborations between the material scientists and organic chemists is expected to play a crucial role in solving this challenge by increasing the stability and the efficiency of organic semiconductors for use in organic solar cells and electronic devices. To this point, although the main focus of this thesis has targeted toward the design and exploration of stable pentacene derivatives, further studies and efforts are needed for making sufficiently stable pentacene derivatives to be used in organic solar cells.

The crystals of pentacene monomers **2.1** and **2.4** and dimers **TIPS-Pnc$_2$** and **Tr*-Pnc$_2$** could not be grown to be able to compare the effect of the substitution on π-stacking interactions between pentacene backbones. Application of a broader variety of solvents may be helpful for growing suitable crystals in future for further studies. Interestingly, **2.3** is stable in liquid phase after melting, for 50 °C. This offers a potentially unique chance to study film formation and crystallization directly from a pure liquid, rather than from solution.

In order to increase the stability of pentacenes substituted in the 6- and 13-positions, substitutions with Tr* groups on *pro-cata*-positions, in addition to the *peri*-positions, may play a role by a complete shielding over pentacene backbone to prevent formation of the endoperoxide and butterfly structures. Alternatively, other large sterically shielding groups might also be used.

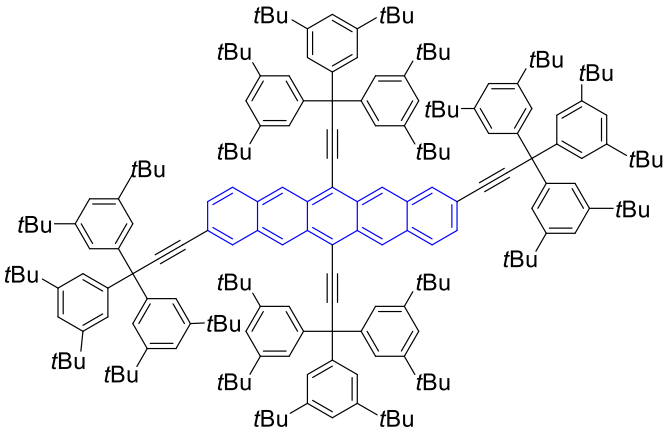

Figure 4.1. Substitution with Tr* groups on *peri*- and *pro-cata*-positions of pentacene backbone.

CHAPTER 5
EXPERIMENTAL SECTION

5.1 General Information

All reagents were purchased in reagent grade from commercial suppliers and used without further purification. Unless otherwise stated, all reactions were performed in standard, dry glassware under an inert atmosphere of N_2. THF and CH_2Cl_2 were dried under an atmosphere of N_2 in a commercial solvent purification system (LC Technology Solutions INC.). $MgSO_4$ was used after aq. workup as a drying agent. saturated aq. NH_4Cl and brine refer to saturated aq. solution of NH_4Cl and NaCl, respectively. Evaporation and concentration in vacuo was performed on a rotary evaporator equipped with a water bath at a maximum temperature of 45 °C. Deoxygenation of solvents or solutions was accomplished by purging N_2 gas through the solvent or solution for at least 30 min. A positive pressure of N_2 was essential to the success of all Sonogashira Pd-catalyzed reactions. Column chromatography was performed using silica gel Si-60 M (Merck, 230–400 mesh). Thin Layer Chromatography (TLC) analysis were carried out on pre-coated plastic sheets covered with 0.20 mm silica gel and visualized via UV-light (254/364 nm). Melting points (mp) were measured with Thomas-Hoover “uni-melt” apparatus. ^1H and ^{13}C NMR spectra were recorded on an Agilent/Varian Mercury 400 (^1H: 400 MHz, ^{13}C: 100 MHz), a Agilent/Varian Inova four-channel 500 (^1H: 500 MHz, ^{13}C: 125 MHz), an Agilent/Varian VNMRS two-channel 500 MHz (^1H: 500 MHz, ^{13}C: 125 MHz), and a Agilent VNMRS four-channel 700 (^1H: 700 MHz, ^{13}C: 175 MHz). NMR spectra were referenced to the residual solvent signal (^1H: $CDCl_3$: 7.26 ppm, THF-d_8: 1.72 or 3.58 ppm, DMSO-d_6: 2.50 ppm; ^{13}C: $CDCl_3$: 77.16 ppm, THF-d_8: 25.31 or 67.21 ppm, DMSO-d_6: 39.52 ppm) and recorded at ambient probe temperature. Coupling constants are reported as observed (±0.5 Hz). UV-vis measurements were carried out on a Varian Cary 400 in CH_2Cl_2 at rt with quartz cuvettes having 1 cm path length. λ_{max} refers to the lowest energy wavelength of significant absorption (nm), ε refers to molar absorptivity (L mol^{-1} cm^{-1}). IR

spectra were recorded on a Thermo Nicolet 8700 FTIR spectrometer and continuum FTIR microscope as CH_2Cl_2 cast films. For mass spectral analyses, low-resolution data are provided in cases when M^+ is not the base peak; otherwise, only high-resolution data are provided. MALDI HRMS were recorded on a Bruker 9.4T Apex-Qe FTICR instrument and using the matrix *trans*-2-[3-(4-*tert*butylphenyl)-2-methyl-2-propenylidene] malononitrile (DCTB). APPI HRMS were obtained from an Agilent 6220 oaTOF. Differential scanning calorimetry (DSC) measurements were measured on a Perkin Elmer Pyris 1 DSC instrument. All thermal analyses were carried out under a flow of N_2 with a heating rate of 10 °C/min. Melting points from DSC analysis are reported as the endothermic maxima, except in cases when the sample decomposed, in which case the onset temperature of the decomposition exothermic peak is reported, as well as the exothermic maxima corresponding to the decomposition. Cyclic voltammetry experiments were done using a BASi-Epsilon instrument. A three-electrode cell was used. A glassy carbon disc was used as working electrode, a platinum wire was used as counter electrode, and an Ag/AgCl electrode was used as reference electrode. Ferrocene/ferrocenium (Fc/Fc^+) was used as an internal standard. The potential values (E) were calculated using the following equation: $E = (E_{pc} + E_{pa})/2$, where E_{pc} and E_{pa} correspond to the cathodic and anodic peak potentials, respectively. The potential values obtained in reference to Ag/AgCl were converted to potentials versus ferrocene/ferrocenium (Fc/Fc^+). Cyclic voltammetry was performed using ca. 10 mg of the pentacene derivatives in CH_2Cl_2 (as noted in the Figure or Table captions) containing 0.1 M nBu$_4$NPF$_6$ as supporting electrolyte at a scan rate of 200 mV/s. All solutions were deoxygenated with a flow of N_2 before the measurement. The working electrode was polished with alumina polishing slurry and pad prior to each scan. X-ray crystallographic data for unpublished compounds are available from the X-ray Crystallographic Laboratory, Department of Chemistry, University of Alberta, Edmonton, Alberta, T6G 2G2, Canada; phone: 780-492-2485, fax 780-492-8231. All analysis was done on a Bruker PLATFORM/SMART 1000 CCD X-ray diffractometer.

5.2 Synthesis

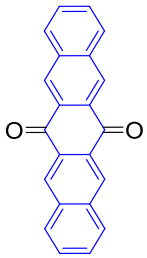

PQ was synthesized as reported in literature.[4]

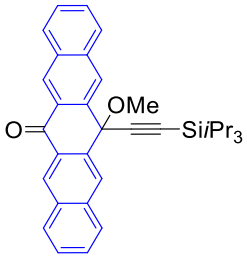

Compound 1.47 was synthesized as reported in the literature.[40]

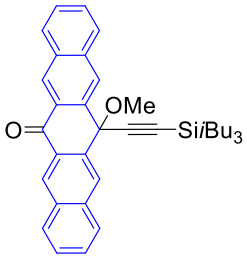

Compound 1.48 was synthesized as reported in the literature.[41]

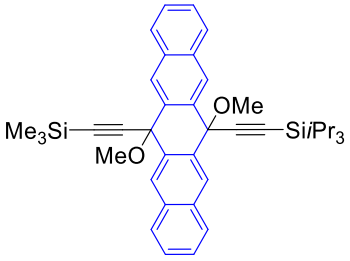

Compound 1.49 was synthesized as reported in the literature.[15]

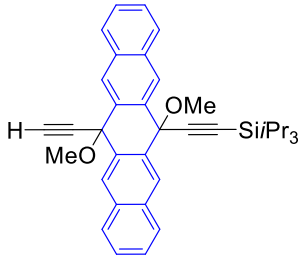

Compound 1.51 was synthesized as reported in the literature.[15]

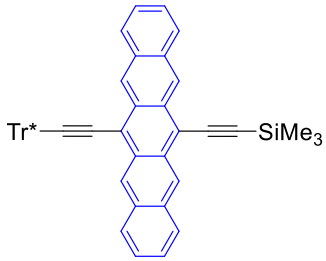

Compound 2.1: To a solution of **2.17** (145 mg, 0.139 mmol) in dry THF (10 mL) was added $SnCl_2 \bullet 2H_2O$ (110 mg, 0.487 mmol) under an atmosphere of N_2. The flask was wrapped in aluminium foil to limit light exposure, and the solution was stirred at rt for 6 h before being poured into H_2O (40 mL). The mixture was extracted with CH_2Cl_2 (3 x 30 mL), and the organic phase was washed with brine (50 mL), dried ($MgSO_4$), and the solvent removed in vacuo. Purification by silica gel column chromatography (CH_2Cl_2/hexanes 1:9) and removal of solvent in vacuo yielded **2.1** (120 mg, 88%) as a pure dark blue solid. Mp = 190–196 °C. R_f = 0.34 (hexanes/CH_2Cl_2 9:1). UV-vis (CH_2Cl_2) λ_{max} (ε) 271 (57900), 298 (sh, 83300), 310 (237000), 326 (sh, 40700), 351 (13200), 413 (4860), 439 (5690), 545 (5890), 591 (12200), 642 (20600) nm. IR (CH_2Cl_2, cast film) 3051 (vw), 2963 (s), 2904 (m), 2867 (m), 2131 (w), 1592 (m) cm^{-1}. ^1H NMR (400 MHz, $CDCl_3$) δ 9.19 (s, 2H), 9.14 (s, 2H), 8.01 (d, *J* = 8.5 Hz, 2H), 7.72 (d, *J* = 8.5 Hz, 2H), 7.43 (d, *J* = 1.8 Hz, 6H), 7.40–7.38 (m, 2H), 7.37 (t, *J* = 1.8 Hz, 3H), 7.34–7.31 (m, 2H), 1.25 (s, 54H), 0.53 (s, 9H). ^1H NMR (400 MHz, THF-d_8) δ 9.22 (s, 2H), 9.17 (s, 2H), 8.02 (d, *J* = 8.5 Hz, 2H), 7.75 (d, *J* = 8.5 Hz, 2H), 7.50 (d, *J* = 1.8 Hz, 6H), 7.44 (t, *J* = 1.8 Hz, 3H), 7.41–7.33 (m, 4H), 1.26 (s, 54H), 0.53 (s, 9H). ^{13}C NMR (100 MHz, $CDCl_3$) δ 150.2, 145.4, 132.4, 132.2, 130.8, 130.7, 128.9, 128.8, 126.6, 126.1, 126.0, 125.6, 124.2, 124.1, 120.3, 84.1, 58.6, 35.1, 31.7, 0.5 (four signals coincident or not observed). ^{13}C NMR (100 MHz, THF-d_8) δ 150.7, 146.2, 133.2, 133.0, 131.3, 131.2, 129.2, 126.8, 126.6, 126.5, 124.7, 120.8, 59.3, 35.5, 31.8, 0.1 (eight signals coincident or not observed). MALDI HRMS (DCTB) *m/z* calcd for $C_{72}H_{84}Si$ (M^+) 976.6337, found 976.6334. DSC: Mp = 198 °C, decomposition, 204 (onset), 209 °C (peak).

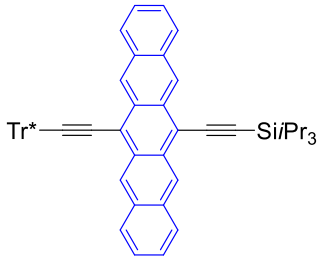

Compound 2.2: To the solution of **2.18** (230 mg, 0.207 mmol) in dry THF (12 mL) was added $SnCl_2 \bullet 2H_2O$ (135 mg, 0.598 mmol) followed by 10% aq. H_2SO_4 (0.1 mL) under an atmosphere of N_2. The flask was wrapped in aluminium foil to limit light exposure, and the solution was stirred at rt for 17 h. The solution was poured onto a pad of silica gel, eluted with a hexanes/CH_2Cl_2 5:1, and the solvent was removed in vacuo. Column chromatography (silica gel, hexanes/CH_2Cl_2 9:1) afforded **2.2** (150 mg, 68%) as a deep blue solid. Mp = 115–119 °C (decomp, dark blue to dark green color change). R_f = 0.37 (hexanes/CH_2Cl_2 9:1). UV-vis (CH_2Cl_2) λ_{max} (ε) 270 (47600), 298 (sh, 85400), 310 (278000), 327 (sh, 44400), 351 (21200), 414 (7320), 439 (8220), 547 (8310), 592 (16300), 642 (27700) nm. IR (CH_2Cl_2, cast film) 3050 (w), 2963 (s), 2865 (s), 2130 (m), 1592 (m) cm^{-1}. ^1H NMR (700 MHz, $CDCl_3$) δ 9.29 (s, 2H), 9.14 (s, 2H), 7.95 (d, *J* = 8.5 Hz, 2H), 7.72 (d, *J* = 8.5 Hz, 2H), 7.42 (d, *J* = 1.8 Hz, 6H), 7.38–7.36 (m, 5H), 7.33–7.31 (m, 2H), 1.43–1.33 (m, 21H), 1.24 (s, 54H). ^{13}C NMR (175 MHz, $CDCl_3$) δ 150.2, 145.4, 132.4, 132.2, 131.0, 130.8, 128.9, 128.7, 126.6, 126.3, 126.0, 125.6, 124.2, 120.3, 114.8, 112.7, 106.6, 97.2, 84.0, 58.5, 35.1, 31.7, 19.2, 11.9 (one signal coincident or not observed). MALDI HRMS (DCTB) *m/z* calcd for $C_{78}H_{96}Si$ (M^+) 1060.7276, found 1060.7258. DSC: decomposition, 100 (onset), 106 °C (peak).

A crystal of **2.2** suitable for X-ray crystallographic analysis has been grown by slow evaporation of a CH_2Cl_2 solution layered with hexanes. X-ray data for **2.2** ($C_{78}H_{96}Si \bullet CH_2Cl_2$), F_w = 1146.56; monoclinic crystal system; space group $P2_1/n$; *a* = 18.0377(4) Å, *b* = 14.1188(2) Å, *c* = 28.1271(5) Å; α = 90.00°, β = 100.7166(19)°, γ = 90.00°; *V* = 7038.2(2) $Å^3$; Z = 4; $\rho_{(calcd)}$ = 1.082 g/cm^3; $2\theta_{max}$ = 123.16°; μ = 1.285 mm^{-1}; *T* = 172.95 K; total data collected = 14108; R_1 = 0.0698 [8837 independent reflections with $I \geq 2\sigma(I)$]; ωR_2 = 0.1909 for 8837 data, 796 variables, and 45 restraints; largest difference, peak and hole = 0.70 and –0.78 e $Å^{-3}$. The three disordered *tert*butyl groups were refined with the following occupancies: C62/63/64:C65/66/67 = 54:46, C82/83/84:C85/86/87 = 52:48, C102/103/104:C105/106/107 = 51:49.[53]

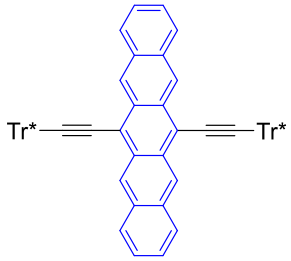

Compound 2.3: To the solution of **2.19** (200 mg, 0.130 mmol) in dry THF (8 mL) that had been purged with N_2 for 10 min was added $SnCl_2 \bullet 2H_2O$ (350 mg, 1.55 mmol) followed by 10% aq. H_2SO_4 (1.75 mL). The flask was wrapped in aluminium foil to limit light exposure, and the solution was stirred at rt for 16 h. The solution was poured onto a pad of silica gel, eluted with a hexanes/CH_2Cl_2 5:1, and the solvent was removed in vacuo. Column chromatography (silica gel, hexanes/CH_2Cl_2 1:9) afforded **2.3** (140 mg, 73%) as a deep blue solid. Mp = 95–98 °C. R_f = 0.86 (hexanes/CH_2Cl_2 1:9). UV-vis (CH_2Cl_2) λ_{max} (ε) 269 (29200), 300 (sh, 80200), 310 (268000), 326 (sh, 33100), 353 (8770), 415 (1410), 438 (1840), 548 (5160), 591 (15400), 642 (30800) nm. IR (CH_2Cl_2, cast film) 3054 (w), 2962 (s), 2904 (m), 2867 (m), 1591 (m) cm^{-1}. ^1H NMR (700 MHz, THF-d_8) δ 9.16 (s, 4H), 7.74–7.72 (m, 4H), 7.52 (d, J = 1.8 Hz, 12H), 7.44 (t, J = 1.8 Hz, 6H), 7.32–7.30 (m, 4H), 1.26 (s, 108H). ^{13}C NMR (175 MHz, THF-d_8) δ 150.8, 146.3, 133.0, 131.5, 129.3, 126.9, 126.6, 126.3, 124.7, 120.8, 35.5, 31.7 (three signals coincident or not observed). MALDI HRMS (DCTB) *m/z* calcd for $C_{111}{}^{13}CH_{138}$ (M^+) 1483.0793, found 1483.0779. DSC: Mp = 91 °C, decomposition, 144 (onset), 153 °C (peak).

A crystal of **2.3** suitable for X-ray crystallographic analysis has been grown by slow evaporation of a CH_2Cl_2 solution layered with hexanes. X-ray data for **2.3** ($C_{112}H_{138} \bullet 2CH_2Cl_2$), F_w = 1654.07; triclinic crystal system; space group P–1; a = 13.7545(5) Å, b = 20.7623(4) Å, c = 22.0601(7) Å; α = 80.869(2)°, β = 81.684(3)°, γ = 74.585(2)°; V = 5961.4(3) $Å^3$; Z = 2; $\rho_{(calcd)}$ = 0.921 g/cm^3; $2\theta_{max}$ = 123.62°; μ = 1.184 mm^{-1}; T = 172.9 K; total data collected = 29992; R_1 = 0.0888 [17957 independent reflections with $I \geq 2\sigma(I)$]; ωR_2 = 0.2855 for 17957 data, 1109 variables, and 55 restraints; largest difference, peak and hole = 0.832 and –0.681 e $Å^{-3}$. The four disordered *tert*butyl groups were refined with the following occupancies: C28/29/30:C28a/29a/30a = 74:26, C52/53/54:C52a/53a/54a = 73:27, C72/73/74:C72a/73a/74a = 63:37, C52b/53b/54b:C52c/53c/54c = 41:59.[53]

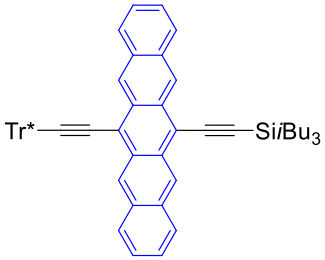

Compound 2.4: To a solution of **2.20** (350 mg, 0.303 mmol) in dry THF (10 mL) was added $SnCl_2 \bullet 2H_2O$ (684, 3.03 mmol) followed by 10% aq. H_2SO_4 (1.5 mL) under an atmosphere of N_2. The flask was wrapped in aluminium foil to limit light exposure, and the solution was stirred at rt for 20 h. The solution was poured onto a pad of silica gel, eluted with CH_2Cl_2 (20 mL), and the solvent was removed in vacuo. Column chromatography (silica gel, hexanes/CH_2Cl_2 1:1) afforded **2.4** (250 mg, 74%) as a deep blue solid. R_f = 0.92 (hexanes/CH_2Cl_2 1:1). UV-vis (CH_2Cl_2) λ_{max} (ε) 270 (43100), 299 (sh, 89900), 310 (315000), 327 (41700), 351 (10300), 415 (2120), 439 (2640), 550 (5250), 591 (15200), 644 (30200) nm. IR (CH_2Cl_2, cast film) 3051 (w), 2953 (s), 2902 (s), 2867 (s), 2128 (m), 1592 (m) cm^{-1}. ^1H NMR (500 MHz, $CDCl_3$) δ 9.26 (s, 2H), 9.14 (s, 2H), 7.94 (d, *J* = 8.5 Hz, 2H), 7.72 (d, *J* = 8.5 Hz, 2H), 7.43 (d, *J* = 1.8 Hz, 6H), 7.39–7.38 (m, 2H), 7.37 (t, *J* = 1.8 Hz, 3H), 7.34–7.31 (m, 2H), 2.21 (app nonet, *J* = 6.7 Hz, 3H), 1.25 (s, 54H), 1.20 (d, *J* = 6.5 Hz, 18H), 0.97 (d, *J* = 7.0 Hz, 6H). ^{13}C NMR (125 MHz, $CDCl_3$) δ 150.2, 145.4, 132.4, 132.1, 131.0, 130.8, 128.9, 128.6, 126.5, 126.2, 126.0, 125.6, 124.2, 120.3, 119.7, 117.5, 112.7, 109.3, 105.1, 84.0, 58.5, 35.1, 31.6, 26.7, 25.65, 25.62. APPI HRMS *m/z* calcd for $C_{81}H_{103}Si$ ($[M + H]^+$) 1103.7824, found 1103.7804. DSC: decomposition, 140 (onset), 146 °C (peak).

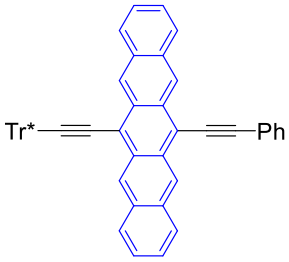

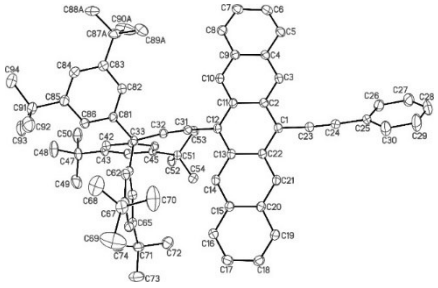

Compound 2.5: To a solution of **2.21** (80 mg, 0.078 mmol) in dry THF (12 mL) was added $SnCl_2 \bullet 2H_2O$ (176 mg, 0.780 mmol) followed by 10% aq. H_2SO_4 (1 mL) under an atmosphere of N_2. The flask was wrapped in aluminium foil to limit light exposure, and the solution was stirred at rt for 1 day. The solution was poured onto a pad of silica gel, eluted with CH_2Cl_2 (20 mL), and the solvent was removed in vacuo. Column chromatography (silica gel, hexanes/CH_2Cl_2 1:3) afforded **2.5** (75 mg, 98%) as a deep blue solid. Mp = 115−120 °C (decomp, observed dark blue to dark green color change). R_f = 0.78 (hexanes/CH_2Cl_2 1:1). UV-vis (CH_2Cl_2) λ_{max} (ε) 272 (16600), 300 (sh, 65700), 311

(291000), 337 (16500), 357 (22000), 440 (1540), 555 (3660), 599 (11600), 652 (21200) nm. IR (CH_2Cl_2, cast film) 3050 (w), 2963 (s), 2904 (m), 2867 (m), 2191 (vw), 1592 (m) cm^{-1}. ^1H NMR (400 MHz, $CDCl_3$) δ 9.28 (s, 2H), 9.16 (s, 2H), 8.04 (d, *J* = 8.5 Hz, 2H), 7.92–7.90 (m, 2H), 7.74 (d, *J* = 8.5 Hz, 2H), 7.55–7.47 (m, 3H), 7.44 (d, *J* = 1.7 Hz, 6H), 7.41–7.38 (m, 2H), 7.37 (t, *J* = 1.7 Hz, 3H), 7.35–7.31 (m, 2H) 1.25 (s, 54H). ^{13}C NMR (100 MHz, $CDCl_3$) δ 150.25, 150.20, 145.4, 144.1, 132.2, 131.9, 130.9, 129.0, 128.8, 128.7, 126.04, 125.96, 125.7, 124.2, 120.3, 110.1, 99.9, 82.0, 35.1, 31.7 (seven signals coincident or not observed). APPI HRMS *m/z* calcd for $C_{75}H_{81}$ ($[M + H]^+$) 981.6333, found 981.6321. DSC: decomposition, 109 (onset), 133 °C (peak).

A crystal of **2.5** (**RRT1909**) suitable for X-ray crystallographic analysis has been grown at 10 °C by slowly evaporation of a CH_2Cl_2 solution layered with MeOH. X-ray data for **2.5** ($C_{75}H_{80}\bullet C_6H_{14}$), F_w = 1067.56; triclinic crystal system; space group *P*–1 (No. 2); *a* = 13.1218(12) Å, *b* = 13.6776(13) Å, *c* = 20.3552(19) Å; α = 97.6201(17)°, β = 91.3622(17)°, γ = 113.4363(16)°; *V* = 3310.5(5) $Å^3$; Z = 2; $\rho_{(calcd)}$ = 1.071 g/cm^3; $2\theta_{max}$ = 51.51°; μ = 0.060 mm^{-1}; *T* = 193.15 K; total data collected = 25092; R_1 = 0.0505 [12585 independent reflections with $I \geq 2\sigma(I)$]; ωR_2 = 0.1486 for 12585 data, 692 variables, and 0 restraints; largest difference, peak and hole = 0.274 and –0.211 e $Å^{-3}$.

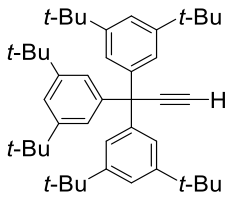

Compound 2.9 was synthesized as reported in the literature.[38]

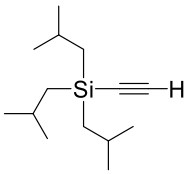

Compound 2.10 was synthesized as reported in Lehnherr's thesis.[39]

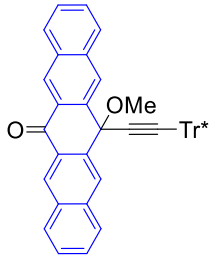

Compound 2.15: To a solution of **2.9** (3.1 g, 5.1 mmol) in dry THF (50 mL) cooled to −78 °C was added *n*-BuLi (2.5 mL, 2.5 M in hexanes, 6.1 mmol) slowly (over 5 min) under an atmosphere of N_2. The solution was stirred for 1 h and transferred via cannula dropwise into a suspension of **PQ** (2.2 g, 7.1 mmol) in dry THF (50 mL) at –78 °C. The reaction mixture was stirred at rt for 1 day. The solution was cooled to −78 °C, and MeI (1.30 mL, 20.9 mmol) was added slowly, and the reaction flask was wrapped in aluminium foil to limit light exposure. After stirring the reaction mixture at rt for 4 h, it was quenched via the addition of satd. aq. NH_4Cl (20 mL). The unreacted **PQ** (1.0 g, 3.2 mmol) was filtered and recovered. The filtrate was extracted with CH_2Cl_2 (3 x 50 mL). The combined organic phases were washed with brine (50 mL), dried over $MgSO_4$, filtered, and the solvent was removed in vacuo. Purification by silica gel column chromatography (CH_2Cl_2/hexanes 2:1 to 3:1) and removal of solvent in vacuo yielded **2.15** (1.87 g, 39%) as a pale-orange solid and recovered **2.9** (1.20 g, 1.98 mmol), R_f = 0.81, CH_2Cl_2 /hexanes 2:1. Mp = 204−206 °C. R_f = 0.40 (hexanes/CH_2Cl_2 1:2). IR (CH_2Cl_2, cast film) 3057 (w), 2963 (s), 2904 (m), 2868 (m), 1677 (m), 1593 (m), 1273 (m) cm^{-1}. ^1H NMR (700 MHz, $CDCl_3$) δ 8.82 (s, 2H), 8.46 (s, 2H), 8.04–8.02 (m, 2H), 7.68–7.67 (m, 2H), 7.58–7.54 (m, 4H), 7.30 (t, *J* = 1.8 Hz, 3H), 7.21 (d, *J* = 1.8 Hz, 6H), 3.12 (s, 3H), 1.17 (s, 54H). ^{13}C NMR (175 MHz, $CDCl_3$) δ 185.2, 150.1, 144.9, 137.0, 135.3, 133.0, 129.9, 129.8, 129.6, 128.7, 128.6, 128.3, 127.4, 123.9, 120.2, 98.5, 83.3, 75.0, 57.2, 52.4, 35.0, 31.6. MALDI MS (DCTB) *m/z* 926.6 (M^+, 10), 895.6 ($[M - OCH_3]^+$, 100). MALDI HRMS (DCTB) *m/z* calcd for $C_{68}H_{78}O_2$ (M^+) 926.5996, found 926.5995.

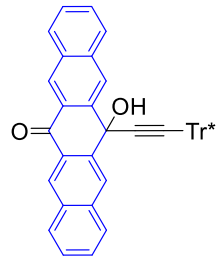

Compound 2.16: To a solution of **2.9** (2.0 g, 3.3 mmol) in dry THF (35 mL) cooled to −78 °C was added *n*-BuLi (1.3 mL, 2.5 M in hexanes, 3.3 mmol) slowly under an atmosphere of N_2. The solution was stirred for 1 h and then transferred via cannula dropwise into a suspension of **PQ** (3.1 g, 10 mmol) in dry THF (35 mL) at –78 °C. After stirring the reaction mixture at rt for 12 h, it was quenched via the addition of satd. aq. NH_4Cl (50 mL). The unreacted **PQ** (900 mg, 2.92 mmol) was filtered and recovered. The filtrate was extracted with CH_2Cl_2 (3 x 50 mL). The combined organic phases were washed with brine (50 mL),

dried over $MgSO_4$, filtered, and the solvent was removed in vacuo. Purification by silica gel column chromatography (CH_2Cl_2/hexanes 4:1) and removal of solvent in vacuo yielded **2.16** (1.75 g, 58%) as a pale-orange solid. Mp = 108–110 °C (decomp, pale-orange to green color change). R_f = 0.28 (hexanes/CH_2Cl_2 1:4). IR (CH_2Cl_2, cast film) 3415 (br, w), 3057 (w), 2963 (s), 2904 (m), 2868 (m), 2232 (vw), 1663 (m), 1628 (m), 1622 (m), 1592 (m) cm^{-1}. ^1H NMR (700 MHz, $CDCl_3$) δ 8.86 (s, 2H), 8.59 (s, 2H), 8.04 (d, *J* = 8.5 Hz, 2H), 7.78 (d, *J* = 8.5 Hz, 2H), 7.60–7.54 (m, 4H), 7.21 (t, *J* = 1.8 Hz, 3H), 6.93 (d, *J* = 1.8 Hz, 6H), 3.13 (s, 1H), 1.09 (s, 54H). ^{13}C NMR (175 MHz, $CDCl_3$) δ 184.2, 150.0, 144.7, 140.2, 136.1, 132.9, 129.9, 129.8, 128.8, 128.5, 128.4, 127.3, 127.0, 123.8, 120.0, 95.5, 86.6, 67.9, 56.7, 34.9, 31.5. MALDI MS (DCTB) *m/z* 935.6 ($[M + Na]^+$, 60), 912.6 (M^+, 20), 895.6 ($[M - OH]^+$, 100). MALDI HRMS (DCTB) *m/z* calcd for $C_{67}H_{76}O_2$ (M^+) 912.5840, found 912.5836. MALDI HRMS (DCTB) *m/z* calcd for $C_{67}H_{76}NaO_2$ ($[M + Na]^+$) 935.5738, found 935.5734.

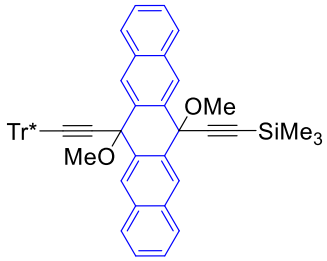

Compound 2.17: To a solution of **2.9** (2.80 mL, 19.7 mmol) in dry THF (15 mL) cooled to –78 °C was added *n*-BuLi (7.5 mL, 2.5 M in hexanes, 19 mmol) slowly under an atmosphere of N_2. After stirring for 5 min at –78 °C, the cooling bath was removed and this mixture was warmed to rt, stirred for 10 min, and then transferred via cannula dropwise into a solution of **2.15** (4.5 g, 4.8 mmol) in dry THF (30 mL) at –78 °C under an atmosphere of N_2. The cooling bath was removed after stirring for 10 min. The solution was warmed to rt and stirred for 2 h under an atmosphere of N_2. The solution was cooled to –78 °C and MeI (3.0 mL, 48 mmol) was added slowly, and the reaction flask was wrapped in aluminium foil to limit light exposure. The solution was allowed to warm to rt and stirred for 2 days. It was cooled to 0 °C and quenched via the addition of satd. aq. NH_4Cl (100 mL). H_2O (100 mL) was added and the reaction mixture was extracted with CH_2Cl_2 (3 x 100 mL). The combined organic phases were washed with brine (100 mL), dried over $MgSO_4$, filtered, and the solvent was removed in vacuo. Purification by silica gel column chromatography (CH_2Cl_2/hexanes 1:1) and removal of solvent in vacuo yielded **2.17** (4 g, 79%) as a bright green solid. Mp = 125–128 °C. R_f = 0.64 (hexanes/CH_2Cl_2 1:1). IR (CH_2Cl_2, cast film) 3058 (w), 2962 (s), 2904 (m), 2868 (m),

2170 (vw), 1593 (m), 1250 (m) cm^{-1}. ^1H NMR (700 MHz, $CDCl_3$) δ 8.47 (s, 2H), 8.45 (s, 2H), 7.94 (d, *J* = 9.4 Hz, 2H), 7.70 (d, *J* = 9.4 Hz, 2H), 7.52–7.50 (m, 2H), 7.47–7.46 (m, 2H), 7.24 (t, *J* = 1.8 Hz, 3H), 7.10 (d, *J* = 1.8 Hz, 6H), 3.16 (s, 3H), 2.73 (s, 3H), 1.12 (s, 54H), 0.14 (s, 9H). ^{13}C NMR (175 MHz, $CDCl_3$) δ 149.9, 145.2, 134.9, 133.9, 133.5, 133.2, 128.5, 128.2, 127.9, 127.5, 126.6, 126.4, 124.0, 119.9, 106.8, 96.8, 91.4, 84.9, 75.2, 74.2, 57.0, 52.6, 51.4, 34.9, 31.5, 0.1. MALDI MS (DCTB) *m/z* 1038.7 (M^+, 5), 1007.6 ($[M - OCH_3]^+$, 100). MALDI HRMS (DCTB) *m/z* calcd for $C_{74}H_{90}O_2Si$ (M^+) 1038.6705, found 1038.6701.

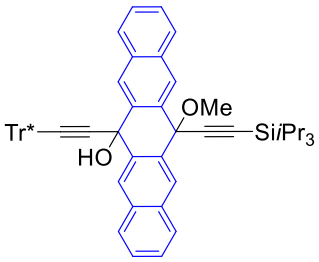

Compound 2.18: To a solution of **2.9** (600 mg, 0.992 mmol) in dry THF (15 mL) at −78 °C under an atmosphere of N_2 was added *n*-BuLi (0.40 mL, 2.5 M in hexanes, 0.99 mmol). After stirring for 5 min at −78 °C and 50 min at rt, it was added dropwise over 5 min to a solution of **1.47** (200 mg, 0.792 mmol) in dry THF (7 mL) at −78 °C under an atmosphere of N_2. The reaction mixture was warmed to rt and stirred for 2 days. After quenching the reaction via the addition of H_2O (5 mL) and satd. aq. NH_4Cl solution (5 mL), the resulting solution was extracted with CH_2Cl_2 (3 × 30 mL). The combined organic phases were washed with brine (40 mL), dried over $MgSO_4$, filtered, and the solvents removed in vacuo. Purification by silica gel column chromatography (CH_2Cl_2/hexanes 1:3) and removal of solvent in vacuo yielded **2.18** (200 mg, 45%) as a pure pale-green solid and recovered **2.9** (100 mg, 0.165 mmol, R_f = 0.95, CH_2Cl_2 /hexanes 1:1). Mp = 165−167 °C (decomp, pale-green to dark green color change). R_f = 0.68 (CH_2Cl_2 /hexanes 1:1). IR (CH_2Cl_2, cast film) 3056 (w), 2962 (s), 2904 (m), 2866 (m), 2169 (vw), 1593 (m), 1248 (m) cm^{-1}. ^1H NMR (700 MHz, $CDCl_3$) δ 8.63 (s, 2H), 8.50 (s, 2H), 7.90−7.89 (m, 2H), 7.85−7.83 (m, 2H), 7.51−7.48 (m, 4H), 7.08 (t, *J* = 1.8 Hz, 3H), 6.76 (d, *J* = 1.8 Hz, 6H), 3.30 (s, 1H), 2.38 (s, 3H), 1.27−1.26 (m, 21 H), 0.98 (s, 54H). ^{13}C NMR (175 MHz, $CDCl_3$) δ 149.6, 145.1, 139.3, 133.7, 132.9, 132.6, 128.3, 128.2, 128.1, 126.6, 126.3, 124.4, 124.1, 119.4, 105.2, 101.3, 91.5, 86.9, 67.8, 66.5, 56.2, 50.7, 34.8, 31.3, 19.0, 11.6. MALDI MS (DCTB) *m/z* 1148.7 ($[M + K]^+$, 6), 1131.7 ($[M + Na]^+$, 58), 1108.7 (M^+, 61), 1091.7 ($[M - OH]^+$, 76), 1077.7 ($[M - OCH_3]^+$, 100),

1060.7 ([M – OCH_3 – OH]$^+$, 43). MALDI HRMS (DCTB) *m/z* calcd for $C_{79}H_{100}O_2Si$ (M^+) 1108.7487, found 1108.7478.

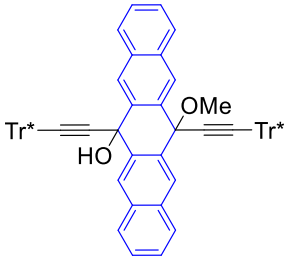

Compound 2.19: To a solution of **2.9** (890 mg, 1.47 mmol) in dry THF (10 mL) at −78 °C under an atmosphere of N_2 was added dropwise *n*-BuLi (0.60 mL, 2.5 M in hexanes, 1.5 mmol). After stirring for 5 min at −78 °C and 1 h at rt, this solution was added dropwise over 5 min to a solution of **2.15** (340 mg, 0.367 mmol) in dry THF (10 mL) at −78 °C under N_2. The reaction mixture was warmed to rt and stirred for 19 h. After quenching the reaction via the addition of satd. aq. NH_4Cl solution (10 mL), the resulting solution was extracted with CH_2Cl_2 (3 × 20 mL). The combined organic phases were washed with satd. aq. NH_4Cl solution (10 mL), brine (20 mL), dried over $MgSO_4$, filtered, and the solvents removed in vacuo. Purification by silica gel column chromatography (CH_2Cl_2/hexanes 1:1) and removal of solvent in vacuo recovered **2.9** (300 mg, 0.496 mmol, R_f = 0.95, CH_2Cl_2 /hexanes 1:1) and yielded **2.19** as a white solid (300 mg, 53%) containing approximately 10% unknown/unidentified impurity. Mp = 130–132 °C. R_f = 0.40 (hexanes/CH_2Cl_2 1:1). IR (CH_2Cl_2, cast film) 3052 (w), 2963 (s), 2905 (m), 2868 (m), 1593 (m), 1248 (m) cm^{-1}. ^{1}H NMR (700 MHz, $CDCl_3$) δ 9.00 (s, 2H), 8.89 (s, 2H), 8.35 (bs, 2H), 8.02 (bs, 2H), 7.92–7.43 (m, 22H), 3.76 (s, 1H), 2.88 (s, 3H), 1.68 (s, 54H), 1.46 (s, 54H). ^{1}H NMR (700 MHz, THF-d_8) δ 8.62 (s, 2H), 8.45 (s, 2H), 7.90 (d, *J* = 8.1 Hz, 2H), 7.54 (d, *J* = 8.1 Hz, 2H), 7.43–7.41 (m, 2H), 7.38 (t, *J* = 1.8 Hz, 3H), 7.37–7.35 (m, 8H), 7.08 (t, *J* = 1.8 Hz, 3H), 6.80 (d, *J* = 1.8 Hz, 6H), 5.73 (s, 1H), 2.39 (s, 3H), 1.19 (s, 54H), 0.95 (s, 54H). ^{13}C NMR (175 MHz, $CDCl_3$) δ 150.0, 149.8, 149.6, 145.3, 139.3, 133.9, 133.7, 132.7, 128.5, 128.2, 128.1, 126.4, 125.9, 124.6, 124.1, 124.0, 120.1, 119.4, 98.0, 91.6, 87.1, 84.2, 67.9, 57.4, 56.2, 51.1, 35.2, 34.8, 31.7, 31.3 (one signal coincident or not observed). ^{13}C NMR (175 MHz, THF-d_8) δ 150.6, 149.9, 146.5, 146.1, 141.9, 134.6, 134.5, 133.2, 128.9, 128.5, 128.3, 126.8, 126.1, 125.7, 124.8, 124.6, 120.6, 119.6, 84.8, 77.8, 58.0, 56.8, 51.4, 35.4, 35.1, 31.7, 31.4 (four signals coincident or not observed). MALDI MS (DCTB) *m/z* 1531.1 (M^+, 94), 1514.1 ([M – OH]$^+$, 71), 1500.1 ([M – OCH_3]$^+$, 100). MALDI HRMS (DCTB) *m/z* calcd for $C_{112}{}^{13}CH_{142}O_2$ (M^+) 1531.1004, found 1531.0994.

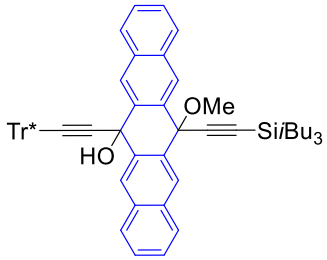

Compound 2.20: To a solution of **2.9** (1.66 g, 2.74 mmol) in dry THF (10 mL) at −78 °C under an atmosphere of N_2 was added dropwise *n*-BuLi (1.2 mL, 2.5 M in hexanes, 3.0 mmol). After stirring for 5 min at −78 °C and 15 min at rt, this solution was added dropwise over 5 min to a solution of **1.48** (500 mg, 0.914 mmol) in dry THF (10 mL) at −78 °C. The ice bath was removed and the reaction mixture warmed to rt and stirred for 1 day. After quenching the reaction via the addition of satd. aq. NH_4Cl solution (15 mL), the resulting solution was extracted with CH_2Cl_2 (3 × 30 mL). The combined organic phases were washed with brine (30 mL), dried over $MgSO_4$, filtered, and the solvents removed in vacuo. Purification by silica gel column chromatography (CH_2Cl_2/hexanes 1:1) and removal of solvent in vacuo yielded **2.20** (380 mg, 36%) as an off-white solid. Mp = 108−110 °C. R_f = 0.37 (hexanes/CH_2Cl_2 1:1). IR (CH_2Cl_2, cast film) 3057 (w), 2954 (s), 2903 (m), 2868 (m), 2167 (vw), 1593 (m), 1249 (m) cm^{-1}. ^1H NMR (700 MHz, $CDCl_3$) δ 8.57 (s, 2H), 8.50 (s, 2H), 7.90–7.89 (m, 2H), 7.85–7.84 (m, 2H), 7.51–7.48 (m, 4H), 7.08 (t, *J* = 1.8 Hz, 3H), 6.76 (d, *J* = 1.8 Hz, 6H), 3.29 (s, 1H), 2.35 (s, 3H), 2.09 (app nonet, *J* = 6.7 Hz, 3H), 1.12 (d, *J* = 6.6 Hz, 18H), 0.98 (s, 54H), 0.84 (d, *J* = 6.9 Hz, 6H). ^{13}C NMR (175 MHz, $CDCl_3$) δ 149.6, 145.2, 139.2, 133.7, 132.9, 132.7, 128.23, 128.19, 128.0, 126.6, 126.3, 124.5, 124.1, 119.4, 105.2, 94.9, 91.6, 86.9, 67.8, 56.2, 50.8, 34.8, 31.3, 26.6, 25.4 (two signals coincident or not observed). MALDI MS (DCTB) *m/z* 1189.8 ($[M + K]^+$, 8), 1173.8 ($[M + Na]^+$, 36), 1150.8 (M^+, 61), 1133.8 ($[M - OH]^+$, 53), 1119.8 ($[M - OCH_3]^+$, 100). MALDI HRMS (DCTB) *m/z* calcd for $C_{82}H_{106}O_2Si$ (M^+) 1150.7957, found 1150.7954.

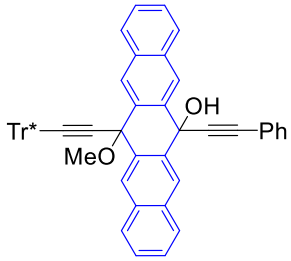

Compound 2.21: To a solution of **2.8** (0.31 mL, 2.8 mmol) in dry THF (10 mL) at –78 °C under an atmosphere of N_2 was added dropwise *n*-BuLi (1.1 mL, 2.5 M in hexanes, 2.7 mmol). After stirring for 5 min at −78 °C and 30 min at rt, this solution was added dropwise over 5 min to a solution of **2.15** (500 mg, 0.539 mmol) in dry THF (10 mL) at −78 °C. The reaction mixture was warmed to rt and stirred for 20 h. After quenching the reaction via the addition of satd. aq. NH_4Cl solution (30 mL), the

resulting solution was extracted with CH_2Cl_2 (3 × 30 mL). The combined organic phases were washed with brine (30 mL), dried over $MgSO_4$, filtered, and the solvents removed in vacuo. Purification by silica gel column chromatography (hexanes/EtOAc 10:1) and removal of solvent in vacuo yielded **2.21** (185 mg, 33%) as a pale-yellow solid. Mp = 125−130 °C (decomp, pale-yellow to pale-green color change). R_f = 0.55 (hexanes/EtOAc 10:1). IR (CH_2Cl_2, cast film) 3410 (br w), 3057 (w), 2963 (s), 2904 (m), 2867 (m), 2236 (vw), 1593 (m), 1248 (m) cm^{-1}. ^1H NMR (400 MHz, $CDCl_3$) δ 8.76 (s, 2H), 8.45 (s, 2H), 7.93 (d, *J* = 8.1 Hz, 2H), 7.80–7.78 (m, 2H), 7.56 (d, *J* = 8.1 Hz, 2H), 7.52–7.49 (m, 2H), 7.47–7.42 (m, 5H), 7.36 (t, *J* = 1.7 Hz, 3H), 7.33 (d, *J* = 1.7 Hz, 6H), 5.77 (s, 1H), 3.33 (s, 3H), 1.22 (s, 54H). ^{13}C NMR (100 MHz, $CDCl_3$) δ 154.5, 150.3, 144.8, 137.4, 133.9, 133.6, 132.6, 128.9, 128.63, 128.59, 128.5, 127.5, 127.1, 126.7, 123.9, 120.3, 78.9, 74.4, 72.3, 60.5, 57.5, 56.9, 52.4, 35.1, 31.6 (three signals coincident or not observed). ESI MS (CH_2Cl_2/CH_3OH) *m/z* 1051.6 ($[M + Na]^+$, 100), 1011.6 ($[M - OH]^+$, 8), 997.6 ($[M - OCH_3]^+$, 18). ESI HRMS (CH_2Cl_2/CH_3OH) *m/z* calcd for $C_{76}H_{84}NaO_2$ ($[M + Na]^+$) 1051.6364, found 1051.6346.

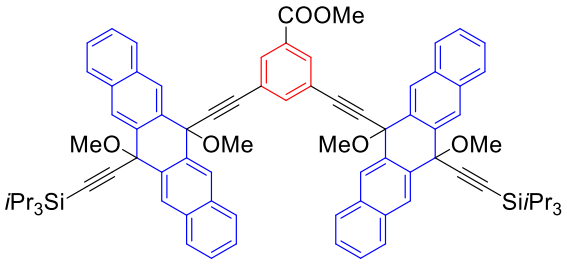

Compound 3.1 was synthesized as reported in the literature.[48]

Compound 1.51 (500 mg, 0.918 mmol) and methyl 3,5-dibromobenzoate (123 mg, 0.418 mmol) were dissolved in a mixture of dry THF (15 mL) and degassed Et_3N (7 mL), and the mixture was purged with N_2 for 15 min. $Pd(PPh_3)_4$ (107 mg, 92.6 µmol) and CuI (17 mg, 89 µmol) were added as solids and the mixture was purged with N_2 for 15 min. The reaction mixture was stirred for 16 h at reflux. After allowing to cool to rt, the mixture was poured onto a pad of silica gel and eluted with CH_2Cl_2 (250 mL). Purification by silica gel column chromatography (CH_2Cl_2/hexanes, 1:1 to 3:1) and removal of the solvent in vacuo gave **3.1** (500 mg, 98%) as a light green foamy solid. Mp 132–136 °C. R_f = 0.50 (CH_2Cl_2/hexanes, 2:1). IR (CH_2Cl_2, cast film) 3055 (m), 2943 (s), 2865 (m), 2166 (w), 1729 (m), 1595 (m), 1469 (m), 1249 (m) cm^{-1}. ^1H NMR (700 MHz, $CDCl_3$) δ 8.70 (s, 4H), 8.40 (s, 4H), 7.97–7.95 (m, 4H), 7.91–7.90 (m, 4H), 7.82 (d, *J* = 1.6 Hz, 2H), 7.56–7.53 (m, 8H), 7.46 (t, *J* = 1.6 Hz, 1H), 3.76 (s, 3H), 3.07 (s, 6H),

3.01 (s, 6H), 1.26–1.25 (m, 42H). ^{13}C NMR (175 MHz, $CDCl_3$) 165.7, 138.4, 134.0, 133.7, 133.3, 132.9, 132.5, 130.3, 128.44, 128.39, 128.3, 127.03, 127.01, 126.9, 123.5, 114.8, 105.3, 93.1, 92.3, 84.1, 76.3, 73.5, 52.3, 52.1, 19.0, 11.6. MALDI MS (DCTB) *m/z* 1190.6 ($[M - OCH_3]^+$, 34), 1243.6 ($[M + Na]^+$, 26). MALDI HRMS (DCTB) *m/z* calcd for $C_{82}H_{84}NaO_6Si_2$ ($[M + Na]^+$) 1243.5699, found 1243.5713.

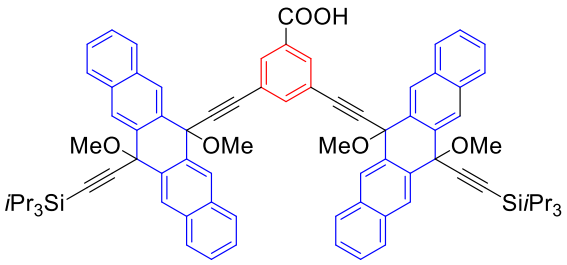

Compound 3.2 was synthesized as reported in the literature.[48]

To a solution of **3.1** (400 mg, 0.327 mmol) dissolved in a mixture of THF (15 mL) and H_2O (7 mL) was added $LiOH•H_2O$ (70 mg, 1.7 mmol) in one portion. The reaction was stirred at rt for 16 h. The mixture was poured into satd aq NH_4Cl (100 mL), extracted with CH_2Cl_2 (100 mL), washed with H_2O (100 mL) and brine (100 mL), dried ($MgSO_4$), and filtered. Removal of the solvent in vacuo afforded **3.2** (363 mg, 92%) as a green foamy solid that was subjected to reductive elimination without further purification. Mp 130–135 °C (decomp). R_f = 0.7 (EtOAc). IR (CH_2Cl_2, cast film) 3051 (m), 2942 (s), 2865 (s), 2165 (w), 1700 (m), 1592 (m), 1496 (m), 1274 (m) cm^{-1}. ^{1}H NMR (700 MHz, $CDCl_3$) δ 8.70 (s, 4H), 8.40 (s, 4H), 7.96–7.95 (m, 4H), 7.91–7.90 (m, 4H), 7.86 (d, *J* = 1.6 Hz, 2H), 7.55–7.52 (m, 8H), 7.47 (t, *J* = 1.6 Hz, 1H), 3.07 (s, 6H), 3.01 (s, 6H), 1.26–1.25 (m, 42H). ^{13}C NMR (175 MHz, $CDCl_3$) 143.5, 139.0, 133.9, 133.7, 133.2, 133.0, 132.9, 128.5, 128.4, 127.05, 127.01, 126.9, 123.7, 105.3, 93.2, 92.3, 83.9, 76.3, 73.6, 52.3, 52.1, 19.0, 11.6 (Two signal coincident or not observed). ESI HRMS (CH_2Cl_2/CH_3OH) *m/z* calcd for $C_{81}H_{81}O_6Si_2$ ($[M - H]^-$) 1206.5650, found 1206.5605.

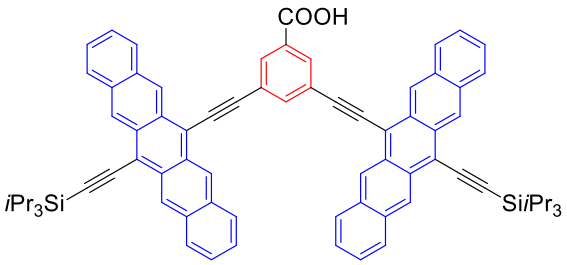

Compound TIPS-Pnc$_2$ was synthesized as reported in the literature.[48]

To a solution of **3.2** (330 mg, 0.273 mmol) in dry THF (20 mL) was added $SnCl_2•2H_2O$ (246 mg, 1.09 mmol) and 10% aq H_2SO_4 (1 mL). The reaction mixture was stirred for 4 h at rt. To minimize light exposure, the flask was wrapped in aluminum foil. The reaction mixture was poured into MeOH (200 mL) and the

mixture was cooled to –18 °C for 16 h. Upon completion the formed dark blue precipitate was filtered, the resulting solid was washed with ice-cold MeOH (30 mL) and pentane (30 mL) and dried in vacuo. Compound **TIPS-Pnc$_2$** (263 mg, 89%) was obtained as dark blue solid. R_f = 0.46 (EtOAc/hexanes, 9:1). UV/Vis (THF) λ_{max} (ε) 310 (413 000), 349 (36 000), 369 (39 000), 440 (9 190), 557 (10500), 603 (25 000), 657 (42 000) nm. IR (CH_2Cl_2, cast film) 3242 (br, m), 2960 (w), 1753 (m), 1591 (w), 1184 (3) cm^{-1}. ^{1}H NMR (700 MHz, THF-d_8) δ 9.44 (s, 4H), 9.33 (s, 4H), 8.77 (t, J = 1.6 Hz, 1H), 8.69 (d, J = 1.6 Hz, 2H), 8.20–8.19 (m, 4H), 7.99–7.98 (m, 4H), 7.46–7.43 (m, 8H), 1.44–1.42 (m, 42H). ^{13}C NMR (175 MHz, THF-d_8) δ 139.1, 133.64, 133.59, 133.5, 131.4, 131.2, 129.6, 129.2, 127.3, 127.2, 127.0, 126.8, 125.6, 119.6, 118.3, 108.1, 105.8, 103.9, 90.0, 19.4, 12.7 (two signals coincident or not observed). MALDI HRMS (DCTB) *m/z* calcd for $C_{77}H_{70}O_2Si_2$ (M^+) 1082.4909, found 1082.4913. DSC: decomposition, 98 (onset), 145 °C (peak).

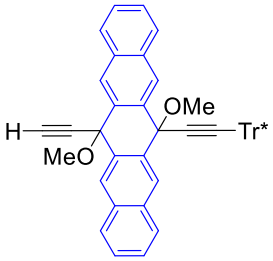

Compound 3.3: To a solution of **2.17** (650 mg, 0.625 mmol) in THF (10 mL) and MeOH (10 mL) was added K_2CO_3 (104 mg, 0.752 mmol) at 0 °C. The solution was stirred at 0 °C for 6 h, and quenched via addition of satd. aq. NH_4Cl solution (100 mL). The reaction mixture was extracted with hexanes (2 × 100 mL). Combined organic phases were washed with satd. aq. NH_4Cl solution (100 mL), brine (100 mL), dried over $MgSO_4$, filtered, and solvent removed in vacuo. Purification by silica gel column chromatography (CH_2Cl_2/hexanes 2:1) and removal of solvent in vacuo yielded **3.3** (445 mg, 74%) as a bright green solid. Mp = 103–105 °C. R_f = 0.44 (CH_2Cl_2 /hexanes 2:1). IR (CH_2Cl_2, cast film) 3268 (w), 3057 (w), 2962 (s), 2904 (m), 2868 (m), 2200 (vw), 1593 (m), 1248 (m) cm^{-1}. ^{1}H NMR (500 MHz, $CDCl_3$) δ 8.46 (s, 2H), 8.45 (s, 2H), 7.93 (d, J = 8.8 Hz, 2H), 7.67 (d, J = 8.8 Hz, 2H), 7.53–7.49 (m, 2H), 7.48–7.44 (m, 2H), 7.25 (t, J = 1.8 Hz, 3H), 7.13 (d, J = 1.8 Hz, 6H), 3.19 (s, 3H), 2.77 (s, 3H), 2.77 (s, 1H), 1.12 (s, 54H). ^{13}C NMR (125 MHz, $CDCl_3$) δ 149.9, 145.1, 134.6, 133.5, 133.4, 133.2, 128.5, 128.13, 128.09, 127.3, 126.7, 126.5, 124.0, 119.9, 97.3, 85.7, 84.4, 75.4, 74.7, 73.5, 57.1, 52.6, 51.5, 34.9, 31.5. ^{13}C NMR (APT, 125 MHz, $CDCl_3$) δ 149.9 (C), 145.1 (C), 134.6 (C), 133.5 (C), 133.4 (C), 133.2 (C), 128.5 (CH), 128.13 (CH), 128.10 (CH), 127.4 (CH), 126.7 (CH), 126.5 (CH), 124.0 (CH), 119.9 (CH), 97.3 (C), 84.4 (C), 75.4 (C),

74.7 (C), 73.5 (C), 57.1 (C), 52.6 (CH_3), 51.5 (CH_3), 34.9 (C), 31.5 (CH_3) (one signal coincident or not observed). MALDI MS (DCTB) *m/z* 966.6 (M^+, 8), 935.6 ($[M - OCH_3]^+$, 100). MALDI HRMS (DCTB) *m/z* calcd for $C_{71}H_{82}O_2$ (M^+) 966.6309, found 966.6314.

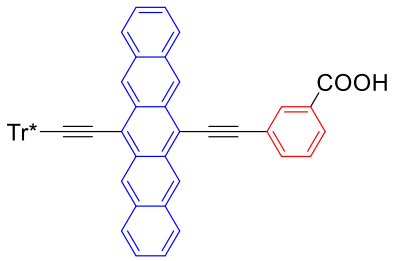

Compound 3.4: Compounds **3.3** (300 mg, 0.310 mmol), 3-iodobenzoic acid **3.6** (64 mg, 0.26 mmol), $Pd(PPh_3)_4$ (30 mg, 26 μmol), and CuI (5.0 mg, 26 μmol) were added to the flask and purged with N_2. The solids were dissolved in degassed Et_3N (30 mL) and stirred for 2 days at reflux over N_2. After allowing to cool to rt, the mixture was poured onto a pad of silica gel and eluted with MeOH (100 mL). After removal of the solvent in vacuo, the crude reaction mixture was dissolved in dry THF (15 mL) followed by addition of $SnCl_2 \bullet 2H_2O$ (290 mg, 1.29 mmol) and 10% aq. H_2SO_4 (1 mL). The flask was wrapped in aluminium foil to limit light exposure and the solution was stirred at rt for 1 day under an atmosphere of N_2. After removal of solvent in vacuo, recrystallization from hexanes/MeOH gave **3.4** (150 mg, 57%) as a deep blue solid. Mp = no visible change ≤ 250 °C. R_f = 0.91 (hexanes/CH_2Cl_2 1:1). UV-vis (CH_2Cl_2) λ_{max} (ε) 272 (28100), 302 (sh, 81100), 312 (306000), 355 (24100), 415 (5640), 441 (5910), 558 (6450), 601 (13800), 654 (25600) nm. IR (CH_2Cl_2, cast film) 3054 (w), 2963 (s), 2905 (m), 2868 (m), 1698 (m), 1592 (m) cm^{-1}. ^1H NMR (500 MHz, $CDCl_3$) δ 9.27 (s, 2H), 9.18 (s, 2H), 8.64 (s, 1H), 8.20 (d, *J* = 7.9 Hz, 1H), 8.13 (d, *J* = 7.7 Hz, 1H), 8.07 (d, *J* = 8.6 Hz, 2H), 7.74 (d, *J* = 8.6 Hz, 2H), 7.65 (t, *J* = 7.8 Hz, 1H), 7.45 (d, *J* = 1.8 Hz, 6H), 7.42–7.38 (m, 5H), 7.36–7.33 (m, 2H), 1.26 (s, 54H). ^{13}C NMR (125 MHz, $CDCl_3$) δ 150.2, 145.4, 136.8, 133.5, 132.5, 132.2, 130.8, 130.7, 130.2, 129.9, 129.1, 129.0, 128.7, 126.8, 126.2, 125.8, 125.7, 124.7, 124.1, 120.3, 116.4, 113.1, 102.6, 92.8, 84.2, 74.2, 58.6, 35.1, 31.7 (one signal coincident or not observed). ESI MS (CH_2Cl_2/MeOH) *m/z* 1023.6 ($[M - H]^-$, 100), 1024.6 (M^-, 84). ESI HRMS (CH_2Cl_2/MeOH) *m/z* calcd for $C_{76}H_{79}O$ ($[M - H]^-$) 1023.6086, found 1023.6079. DSC: decomposition, 175 (onset), 181 °C (peak).

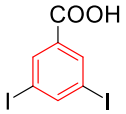

Compound 3.5 was synthesized as reported in the literature.[50a]

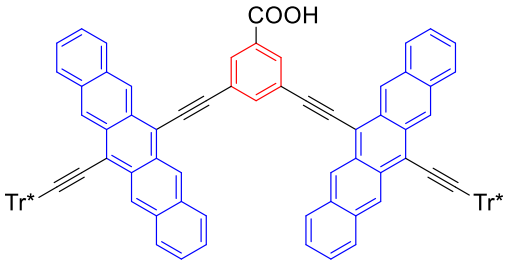

Tr*-Pnc$_2$

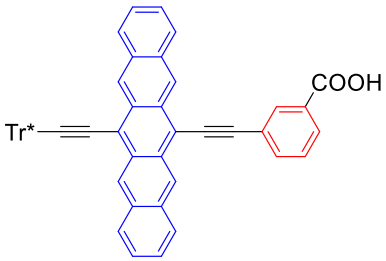

3.4

Compound Tr*-Pnc$_2$: Compounds **3.3** (300 mg, 0.310 mmol) and 3,5-diiodobenzoic acid **3.5** (53 mg, 0.14 mmol) were dissolved in degassed Et_3N (30 mL), and the mixture was purged with N_2 for 30 min. $Pd(PPh_3)_4$ (16 mg, 14 µmol) and CuI (2.7 mg, 14 µmol) were added to the solution and the mixture was purged with N_2 for an addition of 15 min. The reaction mixture was stirred for 25 h at reflux. After allowing to cool to rt, the mixture was poured onto a pad of silica gel and eluted with CH_2Cl_2 (250 mL). After removal of the solvent in vacuo and dissolving the crude sample in THF (70 mL), $SnCl_2 \bullet 2H_2O$ (450 mg, 1.99 mmol) was added followed by 10% aq. H_2SO_4 (2.5 mL). The flask was wrapped in aluminium foil to limit light exposure and the solution was stirred for 15 h at rt. The reaction mixture was poured into MeOH (500 mL) and the mixture was kept in a freezer at –30 °C for 16 h. The formed dark blue precipitate was filtered, the residue was washed with ice-cold MeOH (100 mL) and dried in vacuo, yielded **Tr*-Pnc$_2$** (200 mg, 74%) as dark blue solid containing approximately 10% of monomer **3.4**. Mp = 258–265 °C. R_f = 0.67 (hexanes/CH_2Cl_2 1:2). IR (CH_2Cl_2, cast film) 3051 (w), 2963 (s), 2905 (m), 2868 (m), 2186 (vw), 1699 (m), 1591 (m) cm^{-1}. ^1H NMR (500 MHz, $CDCl_3$) δ 9.37 (s, 4H), 9.21 (s, 4H), 8.70 (d, *J* = 1.5 Hz, 2H), 8.63 (t, *J* = 1.5 Hz, 1H), 8.15 (d, *J* = 8.5 Hz, 4H), 7.77 (d, *J* = 8.5 Hz, 4H), 7.47 (d, *J* = 1.8 Hz, 12H), 7.42–7.41 (m, 4H), 7.40 (t, *J* = 1.8 Hz, 6H), 7.37–7.34 (m, 4H), 1.28 (s, 108H). ^{13}C NMR (125 MHz, $CDCl_3$) δ 150.2, 145.4, 133.0, 132.6, 132.3, 130.83, 130.81, 130.7, 129.0, 128.8, 126.9, 126.3, 125.8, 125.8, 125.4, 124.2, 120.8, 120.3, 116.1, 113.3, 102.0, 90.3, 84.2, 58.6, 35.1, 31.7 (two signals coincident or not observed). MALDI HRMS *m/z* calcd for $C_{144}{}^{13}CH_{154}O_2$ $(M)^+$ 1927.1943, found 1927.1941. DSC: Mp = 294 °C (broad peak).

5.3 NMR Spectroscopic Comparison

5.3.1 Pentacene Monomer 2.2 and Intermediate 2.18

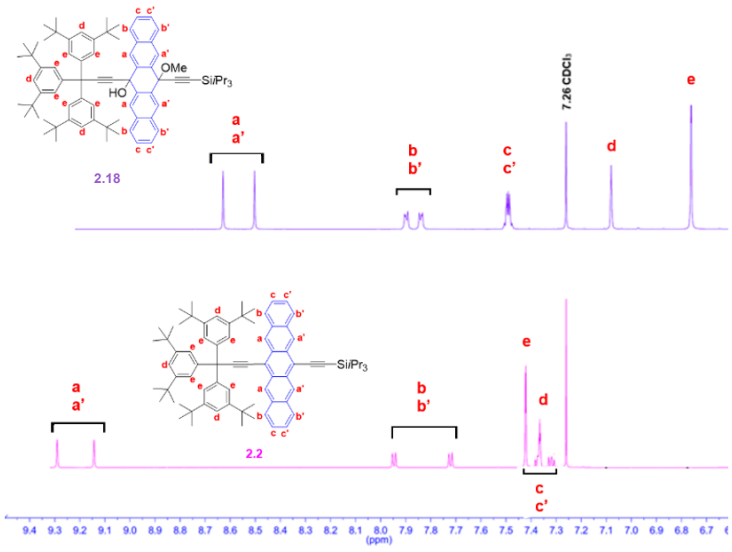

Figure 5.1. Comparison of the aromatic region of the ^{1}H NMR spectra of compounds **2.2** and **2.18** in $CDCl_3$.

5.3.2 Pentacene Monomer 2.3 and Intermediate 2.19

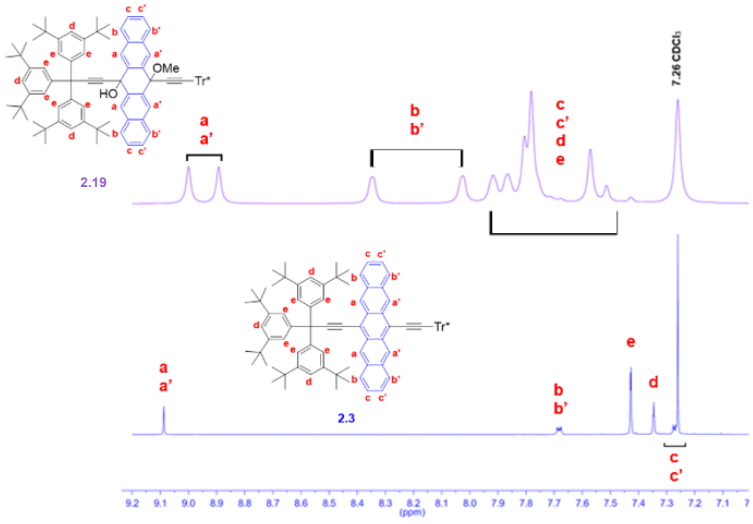

Figure 5.2. Comparison of the aromatic region of the ^{1}H NMR spectra of compounds **2.3** and **2.19** in $CDCl_3$.

5.3.3 Pentacene Monomer 2.4 and Intermediate 2.20

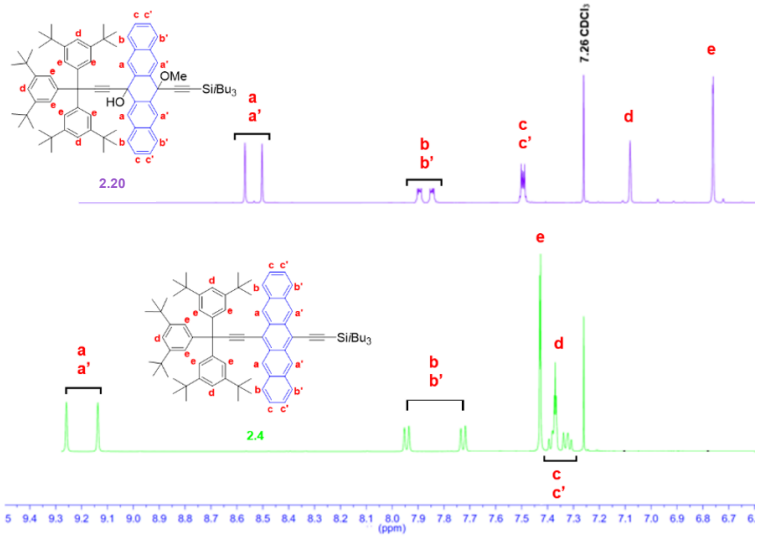

Figure 5.3. Comparison of the aromatic region of the ^{1}H NMR spectra of compounds **2.4** and **2.20** in $CDCl_3$.

5.3.4 Pentacene Monomer 2.5 and Intermediate 2.21

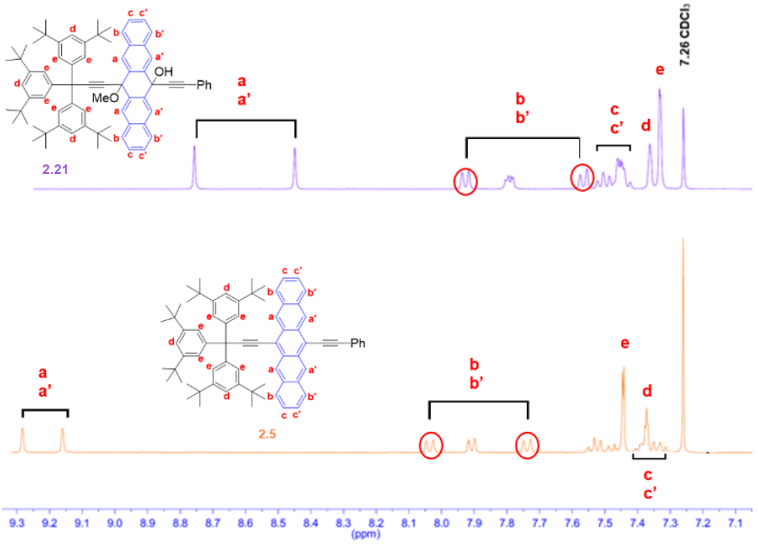

Figure 5.4. Comparison of the aromatic region of the ^{1}H NMR spectra of compounds **2.5** and **2.21** in $CDCl_3$.

5.4 Photochemical Stability of Pentacene Derivatives 2.1–2.5 and Dimer TIPS-Pnc$_2$

5.4.1 Photochemical Stability Test of Pentacene Monomer 2.1

After dissolving compound **2.1** (1.11 mg) in CH_2Cl_2 (100 mL), 5.0 mL of this solution was transferred into two separate volumetric flasks and diluted to 25 mL with CH_2Cl_2. One solution was purged with N_2 for 30 min to remove O_2 while the other one wasn't. The solvent lost from deoxygenation was replaced with deoxygenated CH_2Cl_2 and the solution used to fill two cuvettes. One cuvette was stored in the dark (no O_2/dark, ND), and the other one was stored under ambient light (no O_2/light, NL). Two further samples were prepared from the solution that was not deoxygenated and transferred into two cuvettes. One cuvette was stored in dark (air/dark, AD) whereas the other was stored under ambient light (air/light, AL). All four samples were monitored over a period of 200 hours by UV-vis spectroscopy, and the absorbance of the samples was plotted against the wavelength (**Figure 5.5**). For studying the photochemical stability of compound **2.1**, A_t/A_o against time was plotted where A_t is the absorbance at λ_{max} at time t and A_o is the initial absorbance at the same λ_{max}. Half-life ($t_{1/2}$) of compound **2.1** in AL and NL samples was calculated by exponential fitting through Origin pro 2018 software and the following equation:

$$A_t/A_o = be^{(-t/c)} + d \qquad \text{(Constants: } b\text{, } c\text{, and } d\text{)}$$

Table 5.1. Calculated A_t/A_o and $\ln(A_t/A_o)$ for ND, AD, NL, and AL for samples of compound **2.1**.

Time (h)	A_t/A_o				$\ln(A_t/A_o)$			
	ND	AD	NL	AL	ND	AD	NL	AL
0	1.0	1.0	1.0	1.0	0	0	0	0
1	0.97	0.89	0.95	0.96	–0.026	–0.12	–0.049	–0.04
7	0.90	0.84	0.30	0.25	–0.10	–0.17	–1.2	–1.4
20	0.88	0.82	0.22	0.18	–0.13	–0.2	–1.5	–1.7
70	0.89	0.82	0.16	0.13	–0.12	–0.19	–1.8	–2.0
90	0.89	0.83	0.20	0.083	–0.12	–0.19	–1.6	–2.5
140	0.86	0.78	0.16	0.064	–0.15	–0.25	–1.8	–2.7
200	0.91	0.80	0.21	0.078	–0.089	–0.22	–1.6	–2.6

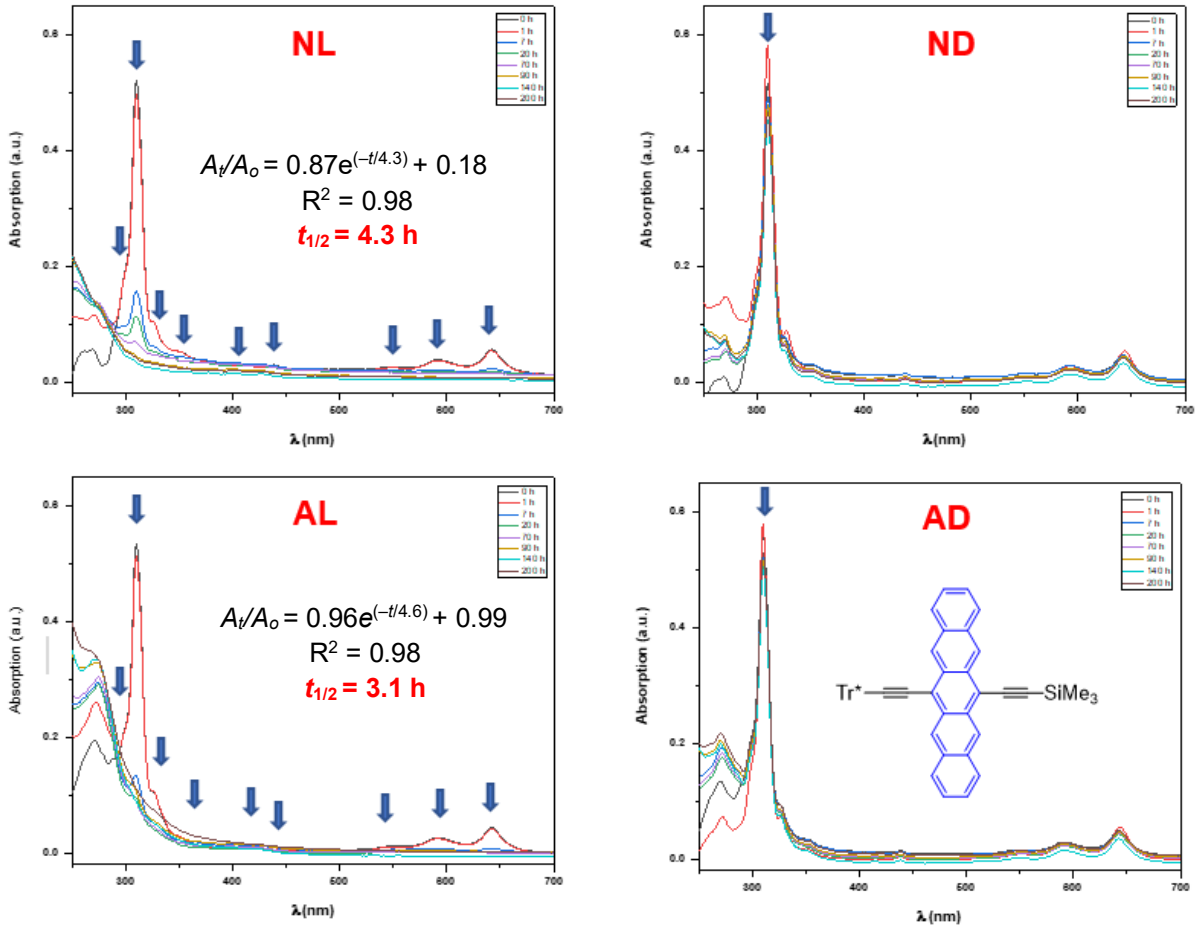

Figure 5.5. UV-vis spectra of no O_2/light (NL), no O_2/dark (ND), air/light (AL), and air/dark (AD) solutions of compound **2.1** in CH_2Cl_2 over a period of 200 hours. The arrows show the absorption trend at specific wavelengths.

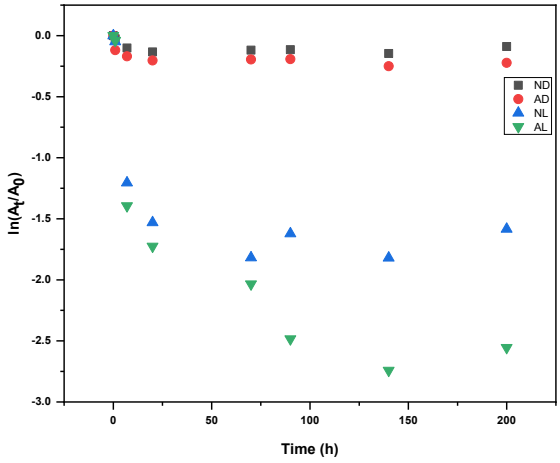

Figure 5.6. Logarithmic plot of A_t/A_o against time for compound **2.1**.

5.4.2 Photochemical Stability Test of Pentacene Monomer 2.2

After dissolving compound **2.2** (1.02 mg) in CH_2Cl_2 (100 mL), 5.0 mL of this solution was transferred into two separate volumetric flasks and diluted to 25 mL with CH_2Cl_2. One solution was purged with N_2 for 30 min to remove O_2 while the other one wasn't. The solvent lost from deoxygenation was replaced with deoxygenated CH_2Cl_2 and the solution used to fill two cuvettes. One cuvette was stored in the dark (no O_2/dark, ND), and the other one was stored under ambient light (no O_2/light, NL). Two further samples were prepared from the solution that was not deoxygenated and transferred into two cuvettes. One cuvette was stored in dark (air/dark, AD) whereas the other was stored under ambient light (air/light, AL). All four samples were monitored over a period of 260 hours by UV-vis spectroscopy, and the absorbance of the samples was plotted against the wavelength (**Figure 5.7**). For studying the photochemical stability of compound **2.2**, A_t/A_o against time was plotted where A_t is the absorbance at λ_{max} at time t and A_o is the initial absorbance at the same λ_{max}. Half-life ($t_{1/2}$) of compound **2.2** in AL and NL samples was calculated by exponential fitting through Origin pro 2018 software and the following equation:

$$A_t/A_o = be^{(-t/c)} + d \qquad \text{(Constants: } b\text{, } c\text{, and } d\text{)}$$

Table 5.2. Calculated A_t/A_o and $\ln(A_t/A_o)$ for ND, AD, NL, and AL for samples of compound **2.2**.

Time (h)	A_t/A_o				$\ln(A_t/A_o)$			
	ND	AD	NL	AL	ND	AD	NL	AL
0	1.0	1.0	1.0	1.0	0	0	0	0
1	0.97	0.97	0.97	0.92	–0.027	–0.029	–0.033	–0.083
2	1.0	0.96	0.93	0.84	–0.0040	–0.046	–0.075	–0.17
7	1.0	0.96	0.81	0.70	–0.0092	–0.046	–0.21	–0.36
10	0.98	0.96	0.79	0.67	–0.023	–0.045	–0.23	–0.40
14	0.93	0.90	0.60	0.48	–0.070	–0.10	–0.51	–0.73
20	0.95	0.94	0.48	0.35	–0.055	–0.061	–0.73	–1.0
35	0.94	0.92	0.34	0.19	–0.062	–0.080	–1.1	–1.6
170	0.92	0.90	0.042	0.022	–0.078	–0.10	–3.2	–3.8
195	0.91	0.90	0.039	0.012	–0.091	–0.12	–3.2	–4.4
200	0.89	0.78	0.039	0.0080	–0.12	–0.25	–3.3	–4.8
240	0.88	0.78	0.044	0.0079	–0.12	–0.24	–3.1	–4.8
260	0.90	0.78	0.054	0.0068	–0.11	–0.24	–2.9	–5.0

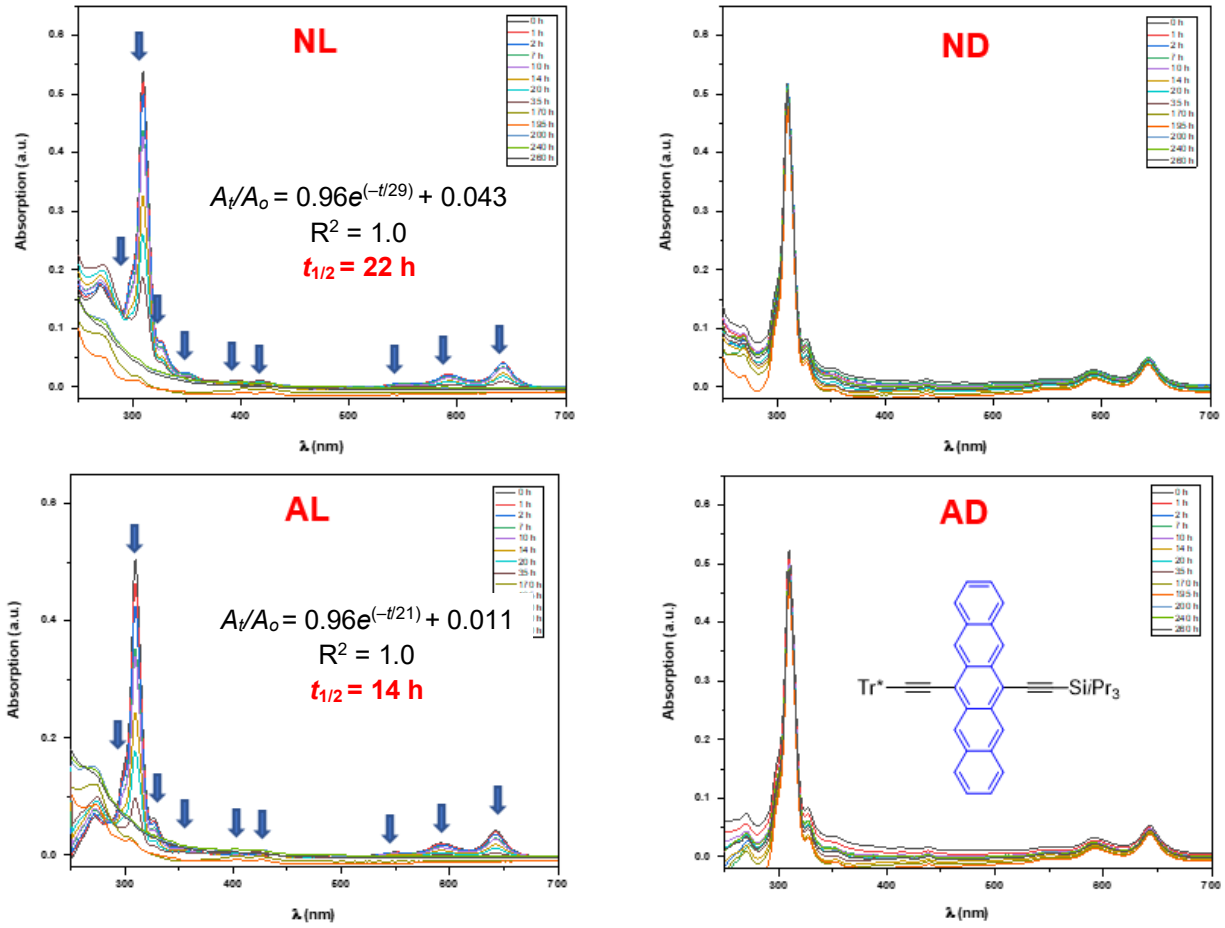

Figure 5.7. UV-vis spectra of no O_2/light (NL), no O_2/dark (ND), air/light (AL), and air/dark (AD) solutions of compound **2.2** in CH_2Cl_2 over a period of 260 hours. The arrows show the absorption trend at specific wavelengths.

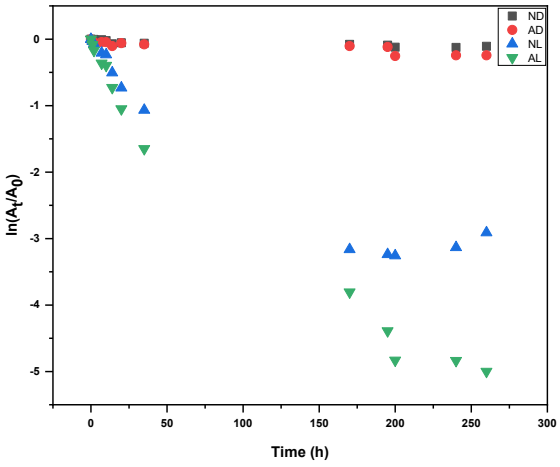

Figure 5.8. Logarithmic plot of A_t/A_o against time for compound **2.2**.

5.4.3 Photochemical Stability Test of Pentacene Monomer 2.3

After dissolving compound **2.3** (1.05 mg) in CH_2Cl_2 (100 mL), 10.0 mL of this solution was transferred into two separate volumetric flasks and diluted to 25 mL with CH_2Cl_2. One solution was purged with N_2 for 30 min to remove O_2 while the other one wasn't. The solvent lost from deoxygenation was replaced with deoxygenated CH_2Cl_2 and the solution used to fill two cuvettes. One cuvette was stored in the dark (no O_2/dark, ND), and the other one was stored under ambient light (no O_2/light, NL). Two further samples were prepared from the solution that was not deoxygenated and transferred into two cuvettes. One cuvette was stored in dark (air/dark, AD) whereas the other was stored under ambient light (air/light, AL). All four samples were monitored over a period of 290 hours by UV-vis spectroscopy, and the absorbance of the samples was plotted against the wavelength (**Figure 5.9**). For studying the photochemical stability of compound **2.3**, A_t/A_o against time was plotted where A_t is the absorbance at λ_{max} at time t and A_o is the initial absorbance at the same λ_{max}. Half-life ($t_{1/2}$) of compound **2.3** in AL and NL samples was calculated by exponential fitting through Origin pro 2018 software and the following equation:

$$A_t/A_o = be^{(-t/c)} + d \qquad \text{(Constants: } b\text{, } c\text{, and } d\text{)}$$

Table 5.3. Calculated A_t/A_o and $\ln(A_t/A_o)$ for ND, AD, NL, and AL for samples of compound **2.3**.

Time (h)	A_t/A_o				$\ln(A_t/A_o)$			
	ND	AD	NL	AL	ND	AD	NL	AL
0	1.0	1.0	1.0	1.0	0	0	0	0
1	0.99	0.99	0.94	0.95	–0.0079	–0.012	–0.057	–0.048
2	1.0	0.99	0.84	0.79	–0.0020	–0.0058	–0.18	–0.23
7	0.99	0.98	0.59	0.54	–0.0090	–0.022	–0.53	–0.61
20	0.95	0.95	0.33	0.28	–0.047	–0.054	–1.1	–1.3
35	0.91	0.90	0.032	0.0047	–0.095	–0.10	–3.4	–5.4
170	0.92	0.92	0.045	0.0093	–0.086	–0.085	–3.1	–4.7
195	0.91	0.90	0.053	0.0093	–0.094	–0.10	–2.9	–4.7
200	0.90	0.88	0.047	0.00090	–0.10	–0.12	–3.1	–7.0
240	0.89	0.87	0.056	0.0099	–0.12	–0.14	–2.9	–4.6
260	0.92	0.90	0.13	0.058	–0.086	–0.11	–2.1	–2.8
270	0.91	0.87	0.13	0.060	–0.097	–0.14	–2.0	–2.8
290	0.90	0.85	0.13	0.055	–0.11	–0.16	–2.0	–2.9

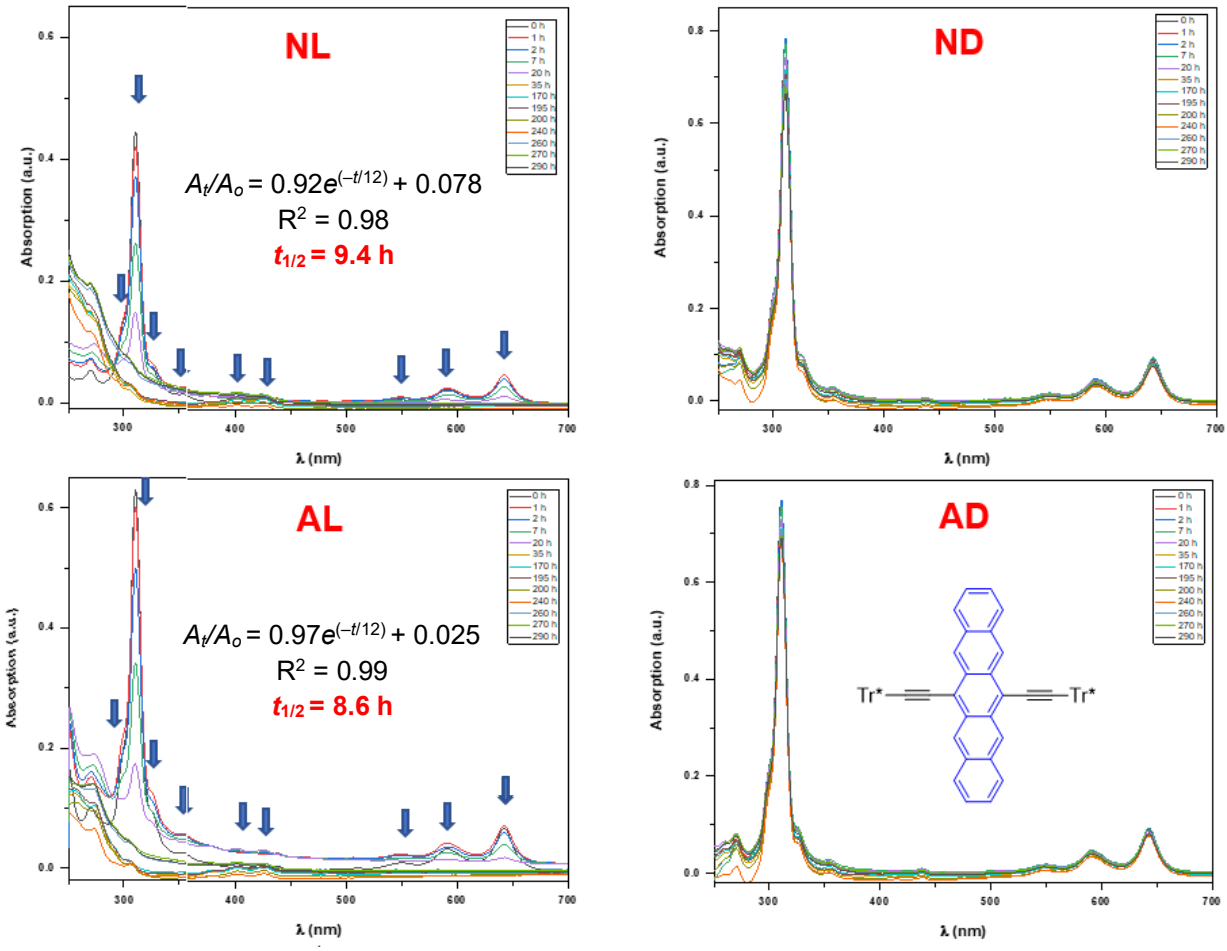

Figure 5.9. UV-vis spectra of no O_2/light (NL), no O_2/dark (ND), air/light (AL), and air/dark (AD) solutions of compound **2.3** in CH_2Cl_2 over a period of 290 hours. The arrows show the absorption trend at specific wavelengths.

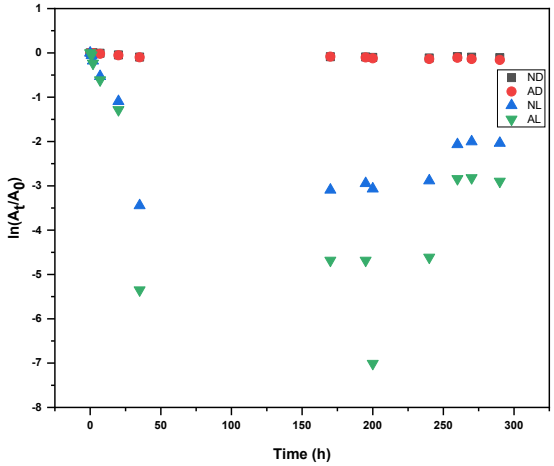

Figure 5.10. Logarithmic plot of A_t/A_o against time for compound **2.3**.

5.4.4 Photochemical Stability Test of Pentacene Monomer 2.4

After dissolving compound **2.4** (1.08 mg) in CH_2Cl_2 (100 mL), 5.0 mL of this solution was transferred into two separate volumetric flasks and diluted to 25 mL with CH_2Cl_2. One solution was purged with N_2 for 30 min to remove O_2 while the other one wasn't. The solvent lost from deoxygenation was replaced with deoxygenated CH_2Cl_2 and the solution used to fill two cuvettes. One cuvette was stored in the dark (no O_2/dark, ND), and the other one was stored under ambient light (no O_2/light, NL). Two further samples were prepared from the solution that was not deoxygenated and transferred into two cuvettes. One cuvette was stored in dark (air/dark, AD) whereas the other was stored under ambient light (air/light, AL). All four samples were monitored over a period of 280 hours by UV-vis spectroscopy, and the absorbance of the samples was plotted against the wavelength (**Figure 5.11**). For studying the photochemical stability of compound **2.4**, A_t/A_o against time was plotted where A_t is the absorbance at λ_{max} at time t and A_o is the initial absorbance at the same λ_{max}. Half-life ($t_{1/2}$) of compound **2.4** in AL and NL samples was calculated by exponential fitting through Origin pro 2018 software and the following equation:

$$A_t/A_o = be^{(-t/c)} + d \qquad \text{(Constants: } b\text{, } c\text{, and } d\text{)}$$

Table 5.4. Calculated A_t/A_o and $\ln(A_t/A_o)$ for ND, AD, NL, and AL for samples of compound **2.4**.

Time (h)	A_t/A_o				$\ln(A_t/A_o)$			
	ND	AD	NL	AL	ND	AD	NL	AL
0	1.0	1.0	1.0	1.0	0	0	0	0
1	1.0	1.0	0.82	0.75	0.023	0.00030	–0.19	–0.28
3	1.0	1.0	0.68	0.59	0.0091	0.0060	–0.39	–0.52
20	1.0	1.0	0.42	0.31	0.018	0.0019	–0.86	–1.2
70	1.0	1.0	0.12	0.026	0.0047	0.0011	–2.1	–3.6
90	0.99	0.98	0.045	0.032	–0.0077	–0.023	–3.1	–3.4
140	1.0	0.98	0.050	0.057	0.00314	–0.018	–3.0	–2.9
180	0.99	0.97	0.056	0.048	–0.0096	–0.033	–2.9	–3.0
200	0.99	0.96	0.059	0.050	–0.014	–0.039	–2.8	–3.0
210	0.97	0.94	0.055	0.043	–0.032	–0.063	–2.9	–3.1
230	0.96	0.93	0.056	0.049	–0.043	–0.074	–2.9	–3.0
280	0.92	0.87	0.046	0.040	–0.079	–0.14	–3.1	–3.2

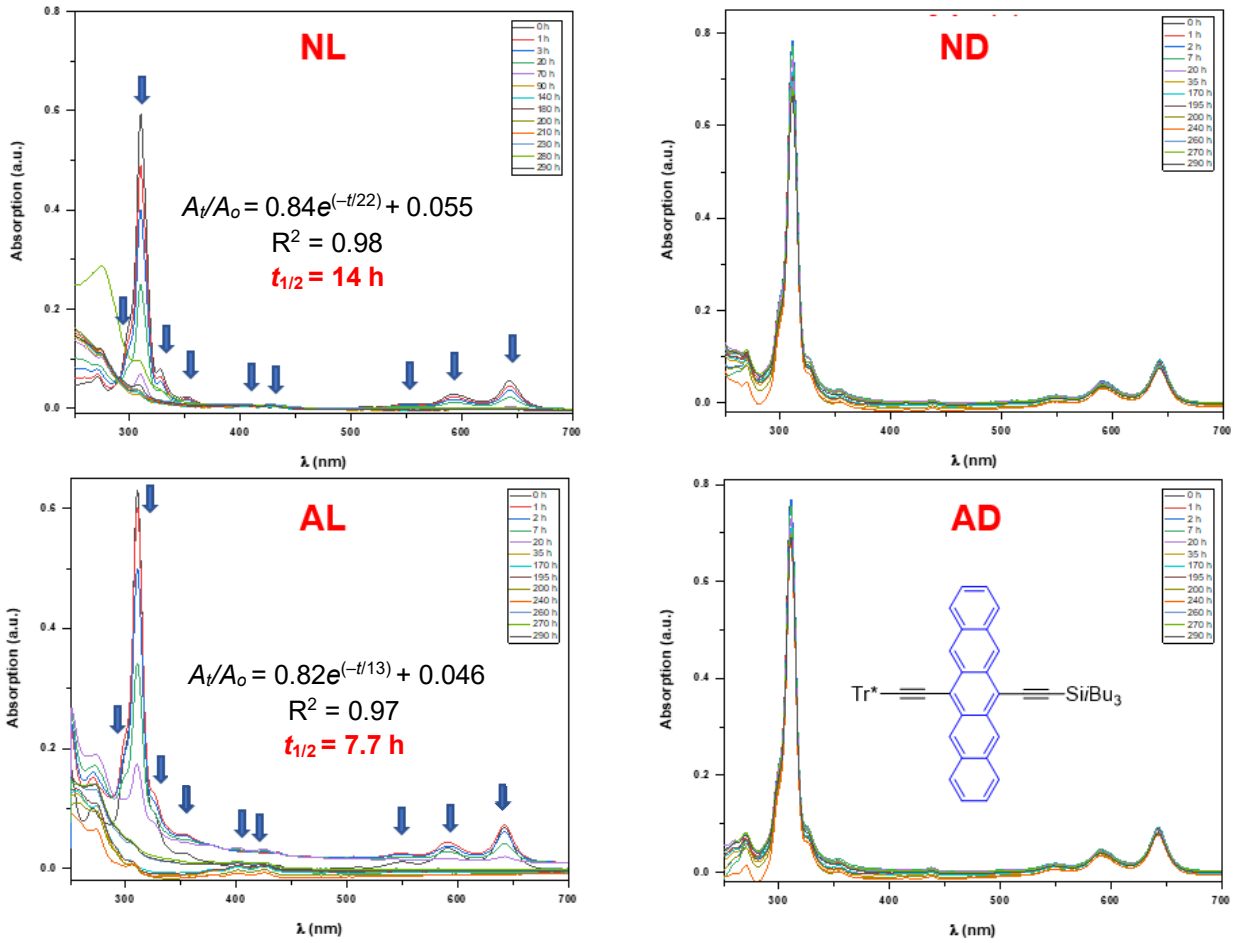

Figure 5.11. UV-vis spectra of no O_2/light (NL), no O_2/dark (ND), air/light (AL), and air/dark (AD) solutions of compound **2.4** in CH_2Cl_2 over a period of 280 hours. The arrows show the absorption trend at specific wavelengths.

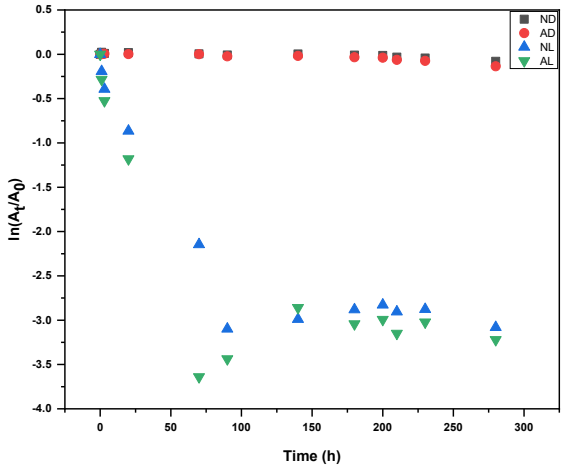

Figure 5.12. Logarithmic plot of A_t/A_o against time for compound **2.4**.

5.4.5 Photochemical Stability Test of Pentacene Monomer 2.5

After dissolving compound **2.5** (1.04 mg) in CH_2Cl_2 (100 mL), 5.0 mL of this solution was transferred into two separate volumetric flasks and diluted to 25 mL with CH_2Cl_2. One solution was purged with N_2 for 30 min to remove O_2 while the other one wasn't. The solvent lost from deoxygenation was replaced with deoxygenated CH_2Cl_2 and the solution used to fill two cuvettes. One cuvette was stored in the dark (no O_2/dark, ND), and the other one was stored under ambient light (no O_2/light, NL). Two further samples were prepared from the solution that was not deoxygenated and transferred into two cuvettes. One cuvette was stored in dark (air/dark, AD) whereas the other was stored under ambient light (air/light, AL). All four samples were monitored over a period of 280 hours by UV-vis spectroscopy, and the absorbance of the samples was plotted against the wavelength (**Figure 5.13**). For studying the photochemical stability of compound **2.5**, A_t/A_o against time was plotted where A_t is the absorbance at λ_{max} at time t and A_o is the initial absorbance at the same λ_{max}. Half-life ($t_{1/2}$) of compound **2.5** in AL and NL samples was calculated by exponential fitting through Origin pro 2018 software and the following equation:

$$A_t/A_o = be^{(-t/c)} + d \qquad \text{(Constants: } b\text{, } c\text{, and } d\text{)}$$

Table 5.5. Calculated A_t/A_o and $\ln(A_t/A_o)$ for ND, AD, NL, and AL for samples of compound **2.5**.

Time (h)	A_t/A_o				$\ln(A_t/A_o)$			
	ND	AD	NL	AL	ND	AD	NL	AL
0	1.0	1.0	1.0	1.0	0	0	0	0
1	1.0	0.99	0.95	0.85	0.0033	–0.015	–0.054	–0.16
3	1.0	0.99	0.88	0.77	0.019	–0.0069	–0.12	–0.26
20	1.0	0.99	0.78	0.70	0.021	–0.0095	–0.25	–0.36
70	1.0	1.0	0.73	0.64	0.024	0.0047	–0.32	–0.45
90	1.0	1.0	0.55	0.41	0.021	0.00083	–0.60	–0.89
180	1.0	1.0	0.30	0.16	0.022	0.0019	–1.2	–1.8
200	1.0	0.99	0.16	0.061	0.016	–0.013	–1.8	–2.8
210	1.0	0.99	0.050	0.031	0.016	–0.0093	–3.0	–3.5
230	0.99	0.97	0.066	0.024	–0.0082	–0.032	–2.7	–3.7
280	1.0	0.97	0.071	0.028	0.00071	–0.027	–2.6	–3.6

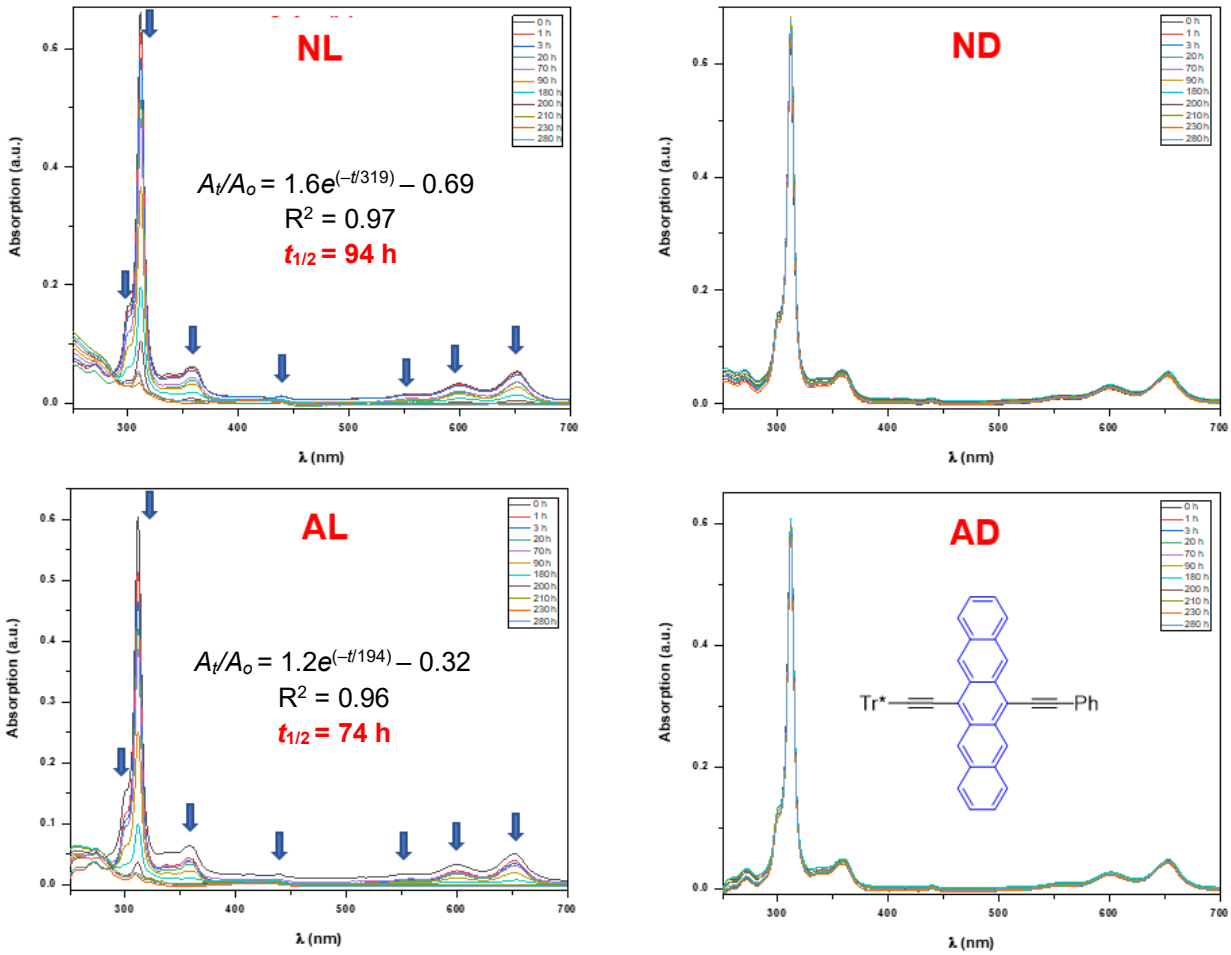

Figure 5.13. UV-vis spectra of no O_2/light (NL), no O_2/dark (ND), air/light (AL), and air/dark (AD) solutions of compound **2.5** in CH_2Cl_2 over a period of 280 hours. The arrows show the absorption trend at specific wavelengths.

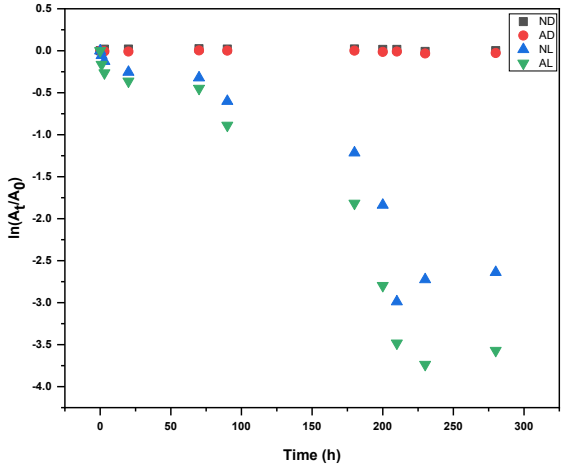

Figure 5.14. Logarithmic plot of A_t/A_o against time for compound **2.5**.

5.4.6 Photochemical Stability Test of Pentacene Dimer TIPS-Pnc$_2$

After dissolving compound **TIPS-Pnc$_2$** (3.00 mg) in CH_2Cl_2 (100 mL), 10.0 mL of this solution was transferred into two separate volumetric flasks and diluted to 100 mL with CH_2Cl_2. One solution was purged with N_2 for 30 min to remove O_2 while the other one wasn't. The solvent lost from deoxygenation was replaced with deoxygenated CH_2Cl_2 and the solution used to fill two cuvettes. One cuvette was stored in the dark (no O_2/dark, ND), and the other one was stored under ambient light (no O_2/light, NL). Two further samples were prepared from the solution that was not deoxygenated and transferred into two cuvettes. One cuvette was stored in dark (air/dark, AD) whereas the other was stored under ambient light (air/light, AL). All four samples were monitored over a period of 85 hours by UV-vis spectroscopy, and the absorbance of the samples was plotted against the wavelength (**Figure 5.15**). For studying the photochemical stability of compound **TIPS-Pnc$_2$**, A_t/A_o against time was plotted where A_t is the absorbance at λ_{max} at time t and A_o is the initial absorbance at the same λ_{max}. Half-life ($t_{1/2}$) of compound **TIPS-Pnc$_2$** in AL and NL samples was calculated by exponential fitting through Origin pro 2018 software and the following equation:

$$A_t/A_o = be^{(-t/c)} + d \qquad \text{(Constants: } b, c, \text{ and } d\text{)}$$

Table 5.6. Calculated A_t/A_o and $\ln(A_t/A_o)$ for ND, AD, NL, and AL for samples of compound **TIPS-Pnc$_2$**.

Time (h)	A_t/A_o				$\ln(A_t/A_o)$			
	ND	AD	NL	AL	ND	AD	NL	AL
0	1.00	1.00	1.00	1.00	0	0	0	0
2	1.05	1.02	1.02	0.936	0.0453	0.0295	0.0168	–0.0659
5	1.02	0.998	0.966	0.882	0.0201	–0.00187	–0.0348	–0.126
23	1.03	1.00	0.941	0.841	0.0300	0.00146	–0.0612	–0.174
31	1.03	0.999	0.807	0.707	0.0288	–0.00122	–0.214	–0.347
46	1.03	0.993	0.562	0.453	0.0253	–0.00675	–0.575	–0.792
61	1.02	0.988	0.502	0.401	0.0212	–0.0125	–0.690	–0.914
85	1.02	0.963	0.181	0.151	0.0243	–0.0375	–1.70	–1.89

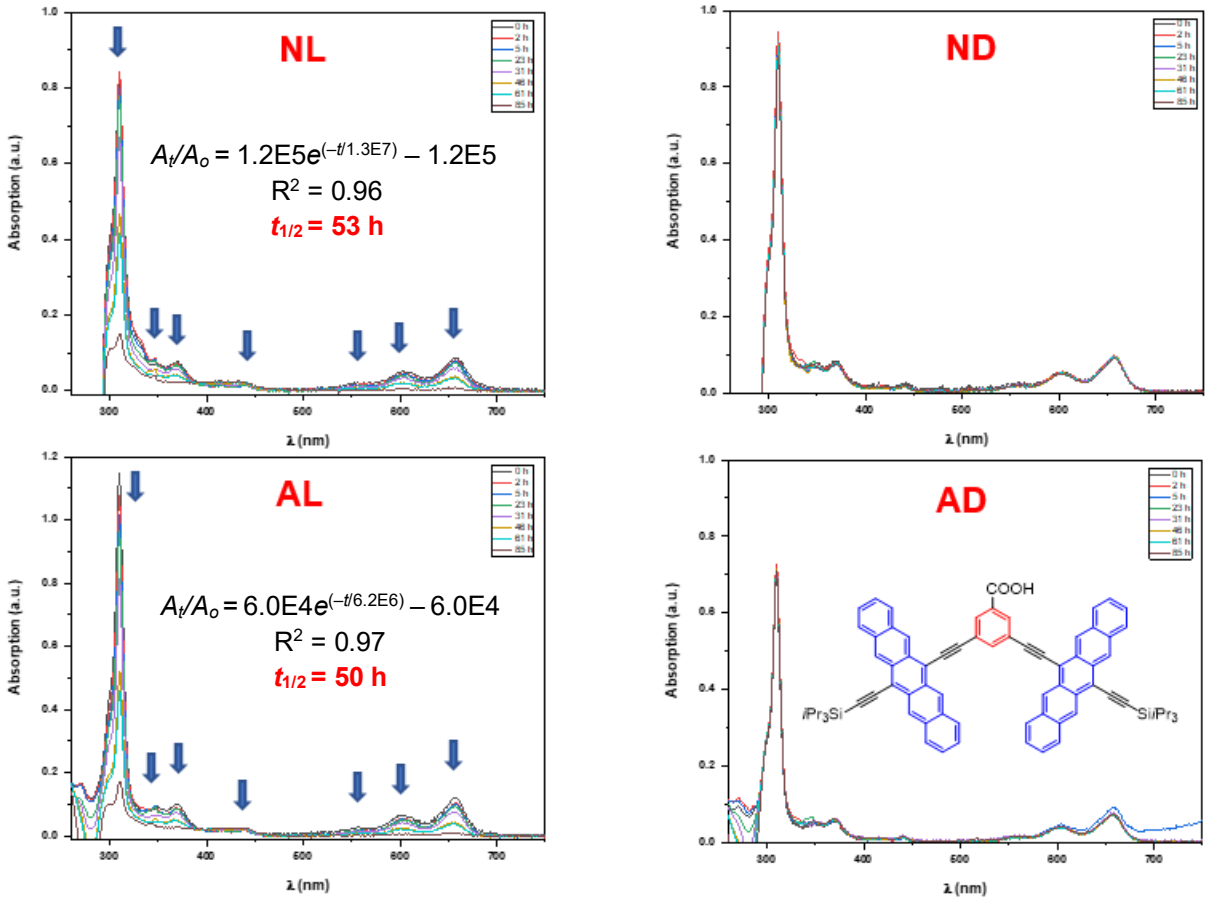

Figure 5.15. UV-vis spectra of no O_2/light (NL), no O_2/dark (ND), air/light (AL), and air/dark (AD) solutions of compound **TIPS-Pnc$_2$** in CH_2Cl_2 over a period of 85 hours. The arrows show the absorption trend at specific wavelengths.

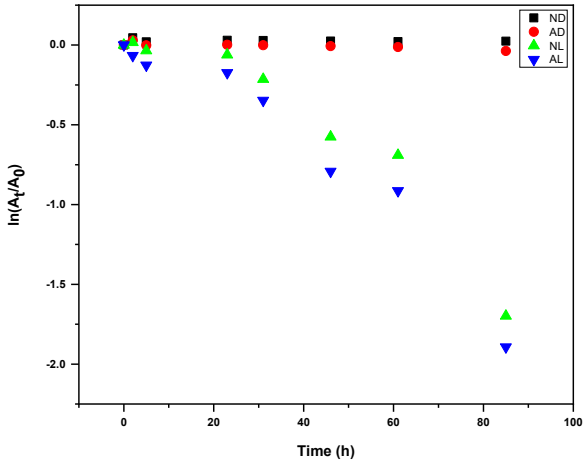

Figure 5.16. Logarithmic plot of A_t/A_o against time for compound **TIPS-Pnc$_2$**.

5.5 Electrochemical Characterization of Pentacene Derivatives 2.1–2.5

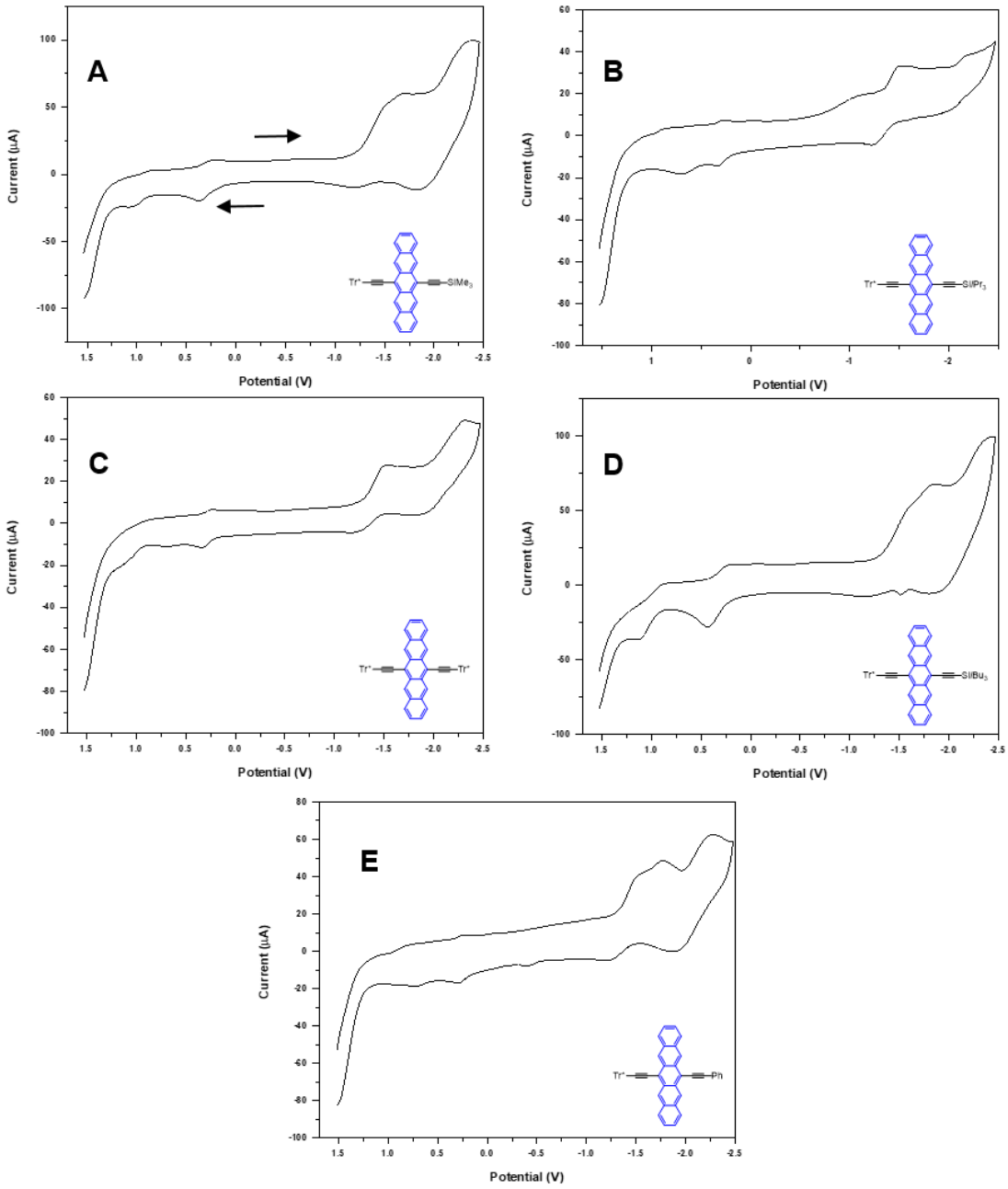

Figure 5.17. Cyclic voltammogram of pentacene derivatives **2.1–2.5** in CH_2Cl_2 solutions containing 0.1 M nBu$_4$NPF$_6$ as supporting electrolyte at a scan rate of 200 mV/s. Potentials are referenced to the ferrocene/ferrocenium (Fc/Fc^+) couple used as an internal standard. The arrows indicate the direction of the scan for compounds. (A) **2.1**, (B) **2.2**, (C) **2.3**, (D) **2.4**, and (E) **2.**

References

[1] (a) Anthony, J. E. The Larger Acenes: Versatile Organic Semiconductors. *Angew. Chem. Int. Ed.* **2008***, 47* (3), 452–483. (b) Berg, O.; Chronister, E. L.; Yamashita, T.; Scott, G. W.; Sweet, R. M.; Calabrese, J. s-Dipentacene: Structure, Spectroscopy, and Temperature- and Pressure-Dependent Photochemistry. *J. Phys. Chem. A* **1999**, *103* (14), 2451–2459.

[2] Bendikov, M.; Wudl, F.; Perepichka, D. F. Tetrathiafulvalenes, Oligoacenenes, and Their Buckminsterfullerene Derivatives: The Brick and Mortar of Organic Electronics. *Chem. Rev.* **2004***, 104* (11), 4891–4945.

[3] Kobayashi, Y. Organic Semiconductors for Organic Field-Effect Transistors. *Sci. Technol. Adv. Mater*. **2009**, *10* (2), 024313.

[4] Pramanik, C.; Miller, G. P. An Improved Synthesis of Pentacene: Rapid Access to a Benchmark Organic Semiconductor. *Molecules* **2012***, 17* (4), 4625–4633.

[5] Goodings, E. P.; Mitchard, D. A.; Owen, G. Synthesis, Structure, and Electrical Properties of Naphthacene, Pentacene, and Hexacene Sulphides. *J. Chem. Soc., Perkin Trans. 1,* **1972**, 1310–1314.

[6] Maulding, D. R.; Roberts, B. G. Electronic Absorption and Fluorescence of Phenylethynyl-Substituted Acenes. *J.Org. Chem.* **1969***, 34* (6), 1734–1736.

[7] Vets, N.; Smet, M.; Dehaen, W. Synthesis and Thermolysis of a Diels–Alder Adduct of Pentacene and Thiophosgene. *Tetrahedron Lett.* **2004***, 45* (39), 7287–7289.

[8] Maliakal, A.; Raghavachari, K.; Katz, H.; Chandross, E.; Siegrist, T. Photochemical Stability of Pentacene and a Substituted Pentacene in Solution and in Thin Films. *Chem. Mater.* **2004***, 16* (24), 4980–4986.

[9] Northrop, B. H.; Houk, K. N.; Maliakal, A. Photostability of Pentacene and 6,13-Disubstituted Pentacene Derivatives: A Theoretical and Experimental Mechanistic Study. *Photochem. Photobiol. Sci.* **2008***, 7* (12), 1463–1468.

[10] Briggs, J. B.; Miller, G. P. [60]Fullerene-Acene Chemistry: A Review. *C.R. Chim.* **2006***, 9* (7–8), 916-927.

[11] Bhatia, R.; Wadhawa, D.; Gurtu, G.; Gaur, J.; Gupta, D. Methodologies for the Synthesis of Pentacene and Its Derivatives. *J. Saudi Chem. Soc.* **2019**, https://doi.org/10.1016/j.jscs.2019.04.001.

[12] (a) Anthony, J. E.; Brooks, J. S.; Eaton, D. L.; Parkin, S. R. Functionalized Pentacene: Improved Electronic Properties from Control of Solid-State Order. *J. Am. Chem. Soc.* **2001**, *123* (38), 9482–9483. (b) Swartz, C. R.; Parkin, S. R.; Bullock, J. E.; Anthony, J. E.; Mayer, A. C.; Malliaras, G. G. Synthesis and Characterization of Electron-Deficient Pentacenes. *Org. Lett.* **2005**, *7* (15), 3163–

3166. (c) Anthony, J. E. Functionalized Acenes and Heteroacenes for Organic Electronics. *Chem. Rev.* **2006**, *106* (12), 5028–5048.

[13] Fudickar, W.; Linker, T. Why Triple Bonds Protect Acenes from Oxidation and Decomposition. *J. Am. Chem. Soc.* **2012***, 134* (36), 15071–15082.

[14] Anthony, J. E.; Eaton, D. L.; Parkin, S. R. A Road Map to Stable, Soluble, Easily Crystallized Pentacene Derivatives. *Org. Lett.* **2002**, *4* (1), 15–18.

[15] Lehnherr, D.; Murray, A. H.; McDonald, R.; Tykwinski, R. R. A Modular Synthetic Approach to Conjugated Pentacene Di-, Tri-, and Tetramers. *Angew. Chem. Int. Ed.* **2010***, 49* (35), 6190–6194.

[16] Marshall, J. L.; Lehnherr, D.; Lindner, B. D.; Tykwinski, R. R. Reductive Aromatization/Dearomatization and Elimination Reactions to Access Conjugated Polycyclic Hydrocarbons, Heteroacenes, and Cumulenes. *ChemPlusChem.* **2017**, *82* (7), 967–1001.

[17] (a) Lehnherr, D.; Gao, J.; Hegmann, F. A.; Tykwinski, R. R. Synthesis and Electronic Properties of Conjugated Pentacene Dimers. *Org. Lett.* **2008***, 10* (21), 4779–4782. (b) Rauhut, M. M.; Roberts, B. G.; Maulding, D. R.; Bergmark, W.; Coleman, R. Infrared Liquid-Phase Chemiluminescence from Reactions of Bis(2,4,6-Trichlorophenyl) Oxalate, Hydrogen Peroxide, and Infrared Fluorescent Compounds. *J. Org. Chem.* **1975**, *40* (3), 330–335.

[18] Lehnherr, D.; McDonald, R.; Tykwinski, R. R. Exploring Electronically Polarized Pentacenes. *Org. Lett.* **2008***, 10* (19), 4163–4166.

[19] Waterloo, A. R.; Sale, A.; Lehnherr, D.; Hampel, F.; Tykwinski, R. R. Aryl Substitution of Pentacenes. *Beilstein J. Org. Chem.* **2014**, *10*, 1692–1705.

[20] Tykwinski, R. R. Synthesis of Unsymmetrical Derivatives of Pentacene for Materials Applications. *Acc. Chem. Res.* **2019**, *52* (8), 2056–2069.

[21] Lehnherr, D.; Adam, M.; Murray, A. H.; McDonald, R.; Hampel, F.; Tykwinski, R. R. Synthesis, Physical Properties, and Chemistry of Donor–Acceptor-Substituted Pentacenes. *Can. J. Chem.* **2017***, 95* (3), 303–314.

[22] Anthony, J. E.; Facchetti, A.; Heeney, M.; Marder, S. R.; Zhan, X. N-Type Organic Semiconductors in Organic Electronics. *Adv. Mater.* **2010***, 22* (34), 3876–3892.

[23] Pope, M.; Swenberg, C. E. Electronic Processes in Organic Crystals and Polymers; Oxford University Press: New York, 1999.

[24] Bredas, J. L. Mind the Gap. *Mater. Horiz.* 2014*, 1,* 17–19.

[25] Shirota, Y.; Kageyama, H. Charge Carrier Transporting Molecular Materials and Their Applications in Devices. *Chem. Rev.* **2007***, 107* (4), 953–1010.

[26] Zhu, X.; Peng, J.; Cao, Y.; Roncali, J. Solution-Processable Single-Material Molecular Emitters for Organic Light-Emitting Devices. *Chem. Soc. Rev.* **2011***, 40* (7), 3509–3524.

[27] Tang, M. L.; Oh, J. H.; Reichardt, A. D.; Bao, Z. Chlorination: A General Route toward Electron Transport in Organic Semiconductors. *J. Am. Chem. Soc.* **2009***, 131* (10), 3733–3740.

[28] Meng, Q.; Hu, W. Recent Progress of N-type Organic Semiconducting Small Molecules for Organic Field-Effect Transistors. *Phys. Chem. Chem. Phys.* **2012***, 14* (34), 14152–14164.

[29] Sharp Develops Solar Cell with World's Highest Conversion Efficiency of 35.8%: Press Releases. http://www.sharp-world.com/corporate/news/091022.html (accessed Sep 28, 2019).

[30] Lloyd, M. T.; Anthony, J. E.; Malliaras, G. G. Photovoltaics from Soluble Small Molecules. *Mater. Today* **2007***, 10* (11), 34–41.

[31] Heremans, P.; Cheyns, D.; Rand, B. P. Strategies for Increasing the Efficiency of Heterojunction Organic Solar Cells: Material Selection and Device Architecture. *Acc. Chem. Res.* **2009***, 42* (11), 1740–1747.

[32] Clarke, T. M.; Durrant, J. R. Charge Photogeneration in Organic Solar Cells. *Chem. Rev.* **2010***, 110* (11), 6736–6767.

[33] (a) Hetzer, C.; Guldi, D. M.; Tykwinski, R. R. Pentacene Dimers as a Critical Tool for the Investigation of Intramolecular Singlet Fission. *Chem. Eur. J.* **2018***, 24* (33), 8245–8257. (b) Smith, M. B.; Michl, J. Singlet Fission. *Chem. Rev.* **2010**, *110* (11), 6891–6936.

[34] (a) Andrews, D. A Unified Theory of Radiative and Radiationless Molecular Energy Transfer. *Chem.Phys.* **1989**, *135* (2), 195–201. (b) Basham, J. I.; Mor, G. K.; Grimes, C. A. Förster Resonance Energy Transfer in Dye-Sensitized Solar Cells. *ACS Nano* **2010***, 4* (3), 1253–1258.

[35] Claessens, C. G.; González-Rodríguez, D.; Rodríguez-Morgade, M. S.; Medina, A.; Torres, T. Subphthalocyanines, Subporphyrazines, and Subporphyrins: Singular Nonplanar Aromatic Systems. *Chem. Rev.* **2014***, 114* (4), 2192–2277.

[36] Lavarda, G.; Zirzlmeier, J.; Gruber, M.; Rami, P. R.; Tykwinski, R. R.; Torres, T.; Guldi, D. M. Tuning Intramolecular Förster Resonance Energy Transfer and Activating Intramolecular Singlet Fission. *Angew. Chem. Int. Ed.* **2018**, *57* (50), 16291–16295.

[37] Kaur, I.; Jia, W.; Kopreski, R. P.; Selvarasah, S.; Dokmeci, M. R.; Pramanik, C.; McGruer, N. E.; Miller, G. P. Substituent Effects in Pentacenes: Gaining Control over HOMO−LUMO Gaps and Photooxidative Resistances. *J. Am. Chem. Soc.* **2008**, *130* (48), 16274–16286.

[38] (a) Marshall, J. L.; Arslan, F.; Januszewski, J. A.; Ferguson, M. J.; Tykwinski, R. R. A Tetraethynyl[5]Cumulene. *Helv. Chim. Acta* **2019**, *102* (3) e1900001. (b) Khuong, T. V.; Zepeda, G.; Ruiz, R.; Khan, S. I.; Garcia-Garibay, M. A. Molecular

Compasses and Gyroscopes: Engineering Molecular Crystals with Fast Internal Rotation. *Cryst. Growth Des.* **2004***, 4* (1), 15–18.

[39] Lehnherr, D. *Ph. D. Thesis*, University of Alberta, Edmonton, Canada, **2010**.

[40] Basel, B. S.; Hetzer, C.; Zirzlmeier, J.; Thiel, D.; Guldi, R.; Hampel, F.; Kahnt, A.; Clark, T.; Guldi, D. M.; Tykwinski, R. R. Davydov splitting and singlet fission in excitonically coupled pentacene dimers. *Chem. Sci.* **2019***, 10* (13), 3854–3863.

[41] Basel, B. S.; Zirzlmeier, J.; Hetzer, C.; Phelan, B. T.; Krzyaniak, M. D.; Reddy, S. R.; Coto, P. B.; Horwitz, N. E.; Young, R. M.; White, F. J.; Hampel, F.; Clark, T.; Thoss, M.; Tykwinski, R. R.; Wasielewski, M. R.; Guldi, D. M. Unified model for singlet fission within a non-conjugated covalent pentacene dimer. *Nat. Commun.* **2017***, 8* (1), 1–8.

[42] Desiraju, G. R.; Gavezzotti, A. Crystal structures of polynuclear aromatic hydrocarbons. Classification, rationalization and prediction from molecular structure. *Acta Crystallogr. Sect B* **1989***, 45*, 473–482.

[43] Crystal of compounds **2.2** and **2.3** have been grown and analyzed by Matthias Adam, a former master student in Tykwinski group: Adam, M. *M. Sc. Thesis*, FAU Erlangen-Nürnberg, Erlangen, Germany, **2010**.

[44] Lehnherr, D.; Tykwinski, R. R. Oligomers and Polymers Based on Pentacene Building Blocks. *Materials* **2010***, 3* (4), 2772–2800.

[45] Miyata, K.; Conrad-Burton, F. S.; Geyer, F. L.; Zhu, X. Triplet Pair States in Singlet Fission. *Chem. Rev.* **2019***, 119* (6), 4261–4292.

[46] Basel, B. S.; Papadopoulos, I.; Thiel, D.; Casillas, R.; Zirzlmeier, J.; Clark, T.; Guldi, D. M.; Tykwinski, R. R. Pentacenes: A Molecular Ruler for Singlet Fission. *Trends in Chemistry* **2019**, *1* (1), 11–21.

[47] Zirzlmeier, J.; Casillas, R.; Reddy, S. R.; Coto, P. B.; Lehnherr, D.; Chernick, E. T.; Papadopoulos, I.; Thoss, M.; Tykwinski, R. R.; Guldi, D. M. Solution-based intramolecular singlet fission in cross-conjugated pentacene dimers. *Nanoscale* **2016***, 8* (19), 10113–10123.

[48] Kunzmann, A.; Gruber, M.; Casillas, R.; Zirzlmeier, J.; Stanzel, M.; Peukert, W.; Tykwinski, R. R.; Guldi, D. M. Singlet Fission for Photovoltaics with 130 % Injection Efficiency. *Angew. Chem. Int. Ed.* **2018***, 57* (33), 10742–10747.

[49] Chinchilla, R.; Najera, C. The Sonogashira Reaction: A Booming Methodology in Synthetic Organic Chemistry. *Chem. Rev.* **2007***, 107* (3), 874–922.

[50] (a) Xiaoyong Zhao; Kirk S. Schanze Meta-Linked Poly(phenylene ethynylene) Conjugated Polyelectrolyte Featuring a Chiral Side Group: Helical Folding and Guest Binding. *Langmuir* **2006**, *22* (10), 4856–4862. (b) Christensen, M. A.; Pia, E. A. D.; Houmøller, J.; Thomsen, S.; Wanko, M.; Bond, A. D.; Rubio, A.; Nielsen, S. B.; Nielsen, M. B. Cross-Conjugation vs. Linear Conjugation in Donor-Bridge-

Acceptor Nitrophenol Chromophores. *Eur. J. Org. Chem.* **2014**, *2014* (10), 2044–2052.

[51] The emission spectra of **TIPS-Pnc$_2$** have been normalized to the **TIPS-Pnc$_2$** related emission of the SubPc-Pnc$_2$ conjugates **3.8**–**3.10** to visualize the analogy between the acene emission of dyads **3.8**–**3.10** and the emission of **TIPS-Pnc$_2$**. The emission depicted in spectra for **3.8**–**3.10** have been recorded with wider entrance and exit slits compared to **3.11**–**3.13** to ensure a reasonable signal-to-noise ratio. Subsequently, the respective intensities have been corrected.

[52] Kaur, I.; Jia, W.; Kopreski, R. P.; Selvarasah, S.; Dokmeci, M. R.; Pramanik, C.; McGruer, N. E.; Miller, G. P. Substituent Effects in Pentacenes: Gaining Control over HOMO−LUMO Gaps and Photooxidative Resistances. *J. Am. Chem. Soc.* **2008**, *130* (48), 16274–16286.

[53] Crystals of compounds **2.2** and **2.3** have been grown and analyzed by Matthias Adam, a former student in Tykwinski group: Adam, M. *M. Sc. Thesis*, FAU Erlangen-Nürnberg, Erlangen, Germany, **2010**.

Appendix I – NMR Spectroscopy

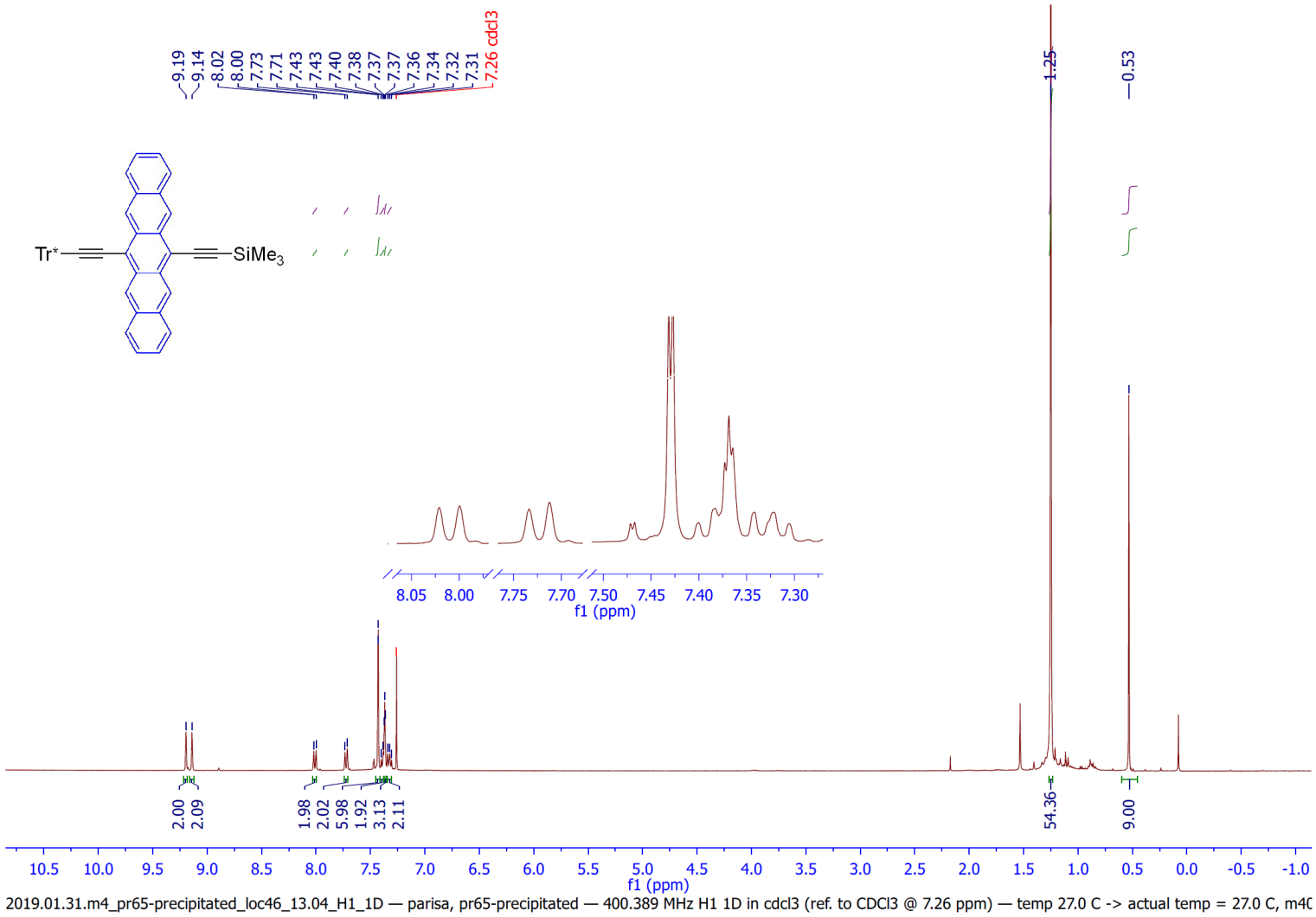

Figure N1. ^{1}H NMR spectrum of compound **2.1** by MestReNova software, 400 MHz, $CDCl_3$.

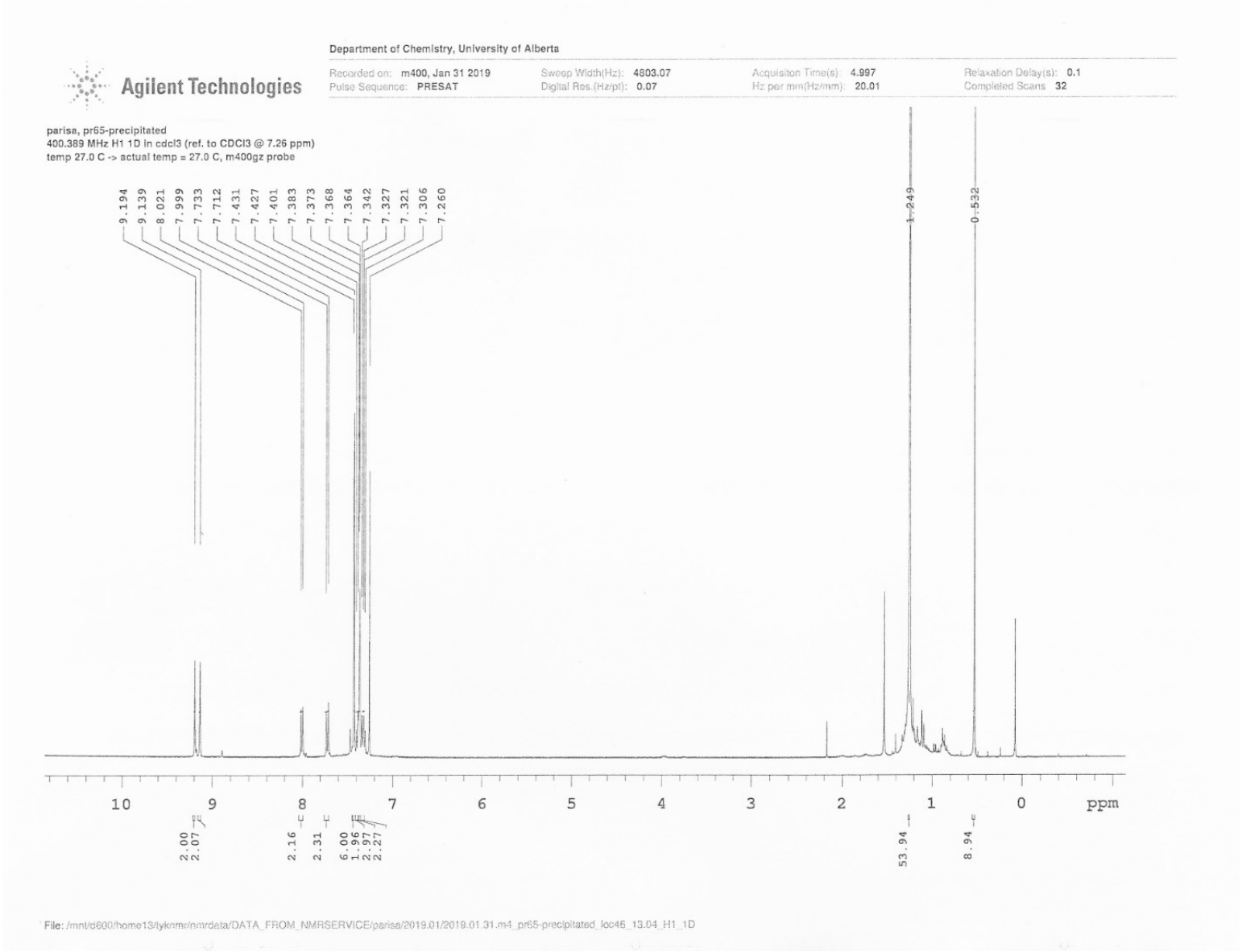

Figure N2. Original ^{1}H NMR spectrum of compound **2.1**, 400 MHz, $CDCl_3$.

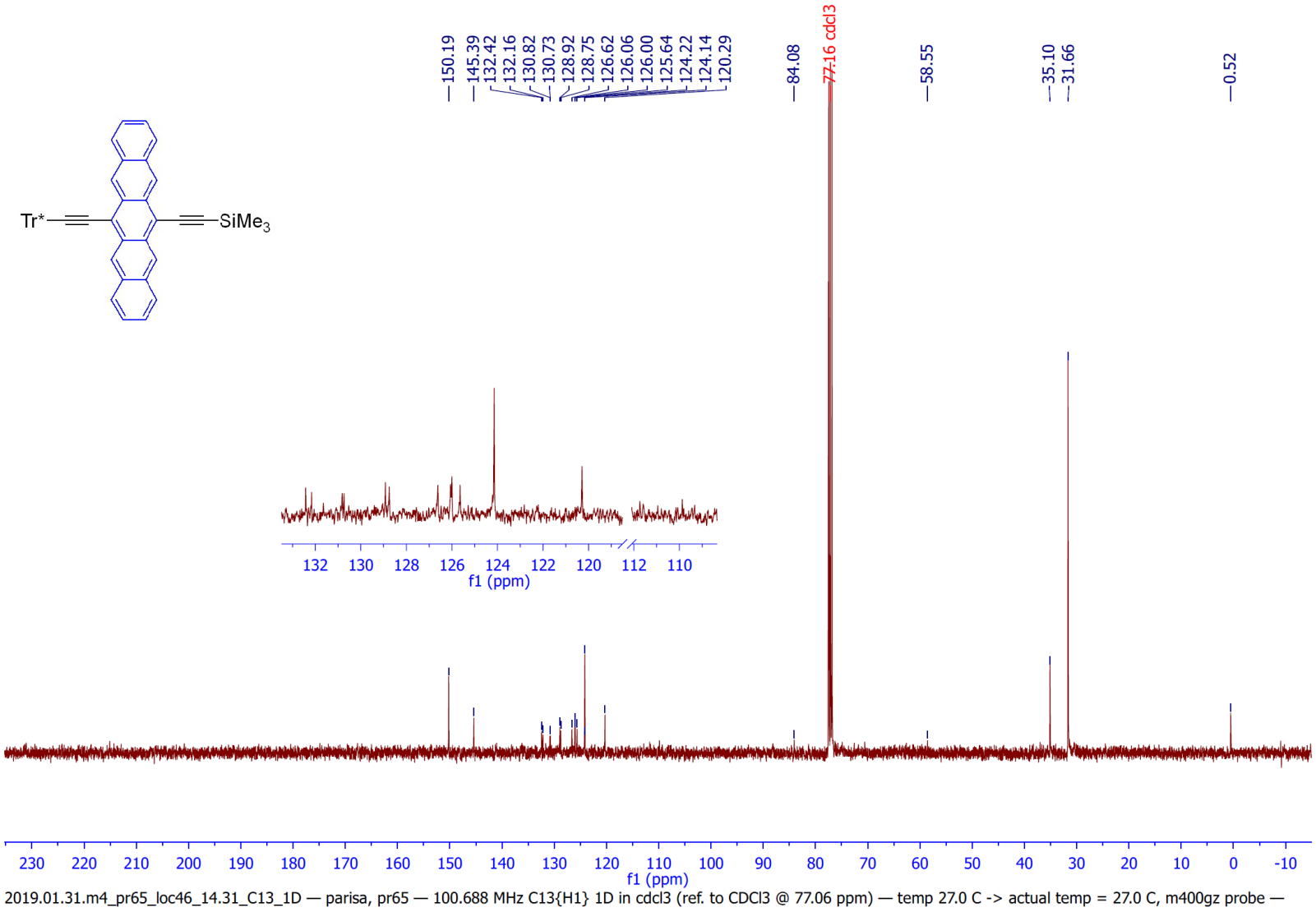

Figure N3. ^{13}C NMR spectrum of compound **2.1** by MestReNova software, 100 MHz, $CDCl_3$.

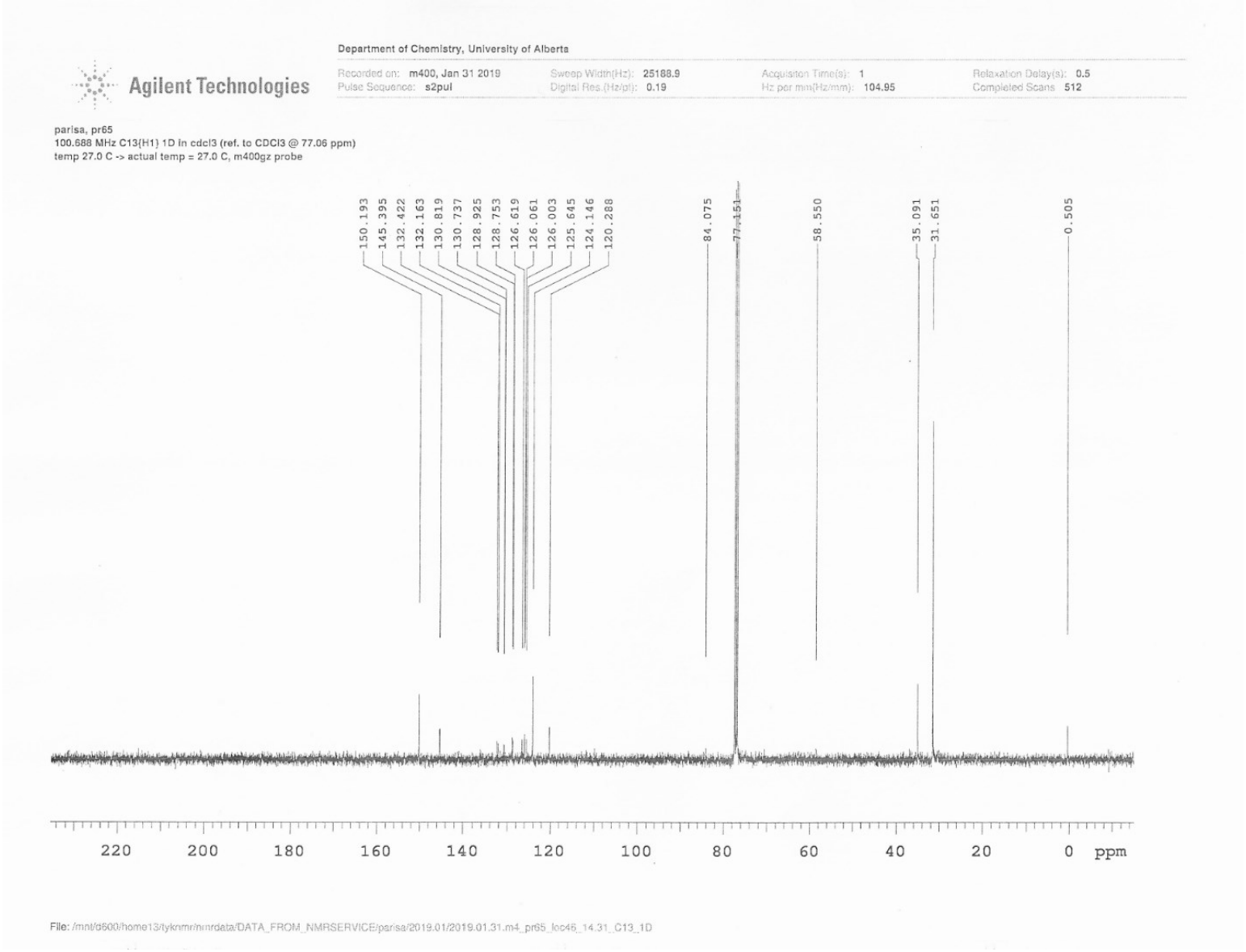

Figure N4. Original ^{13}C NMR spectrum of compound **2.1**, 100 MHz, $CDCl_3$.

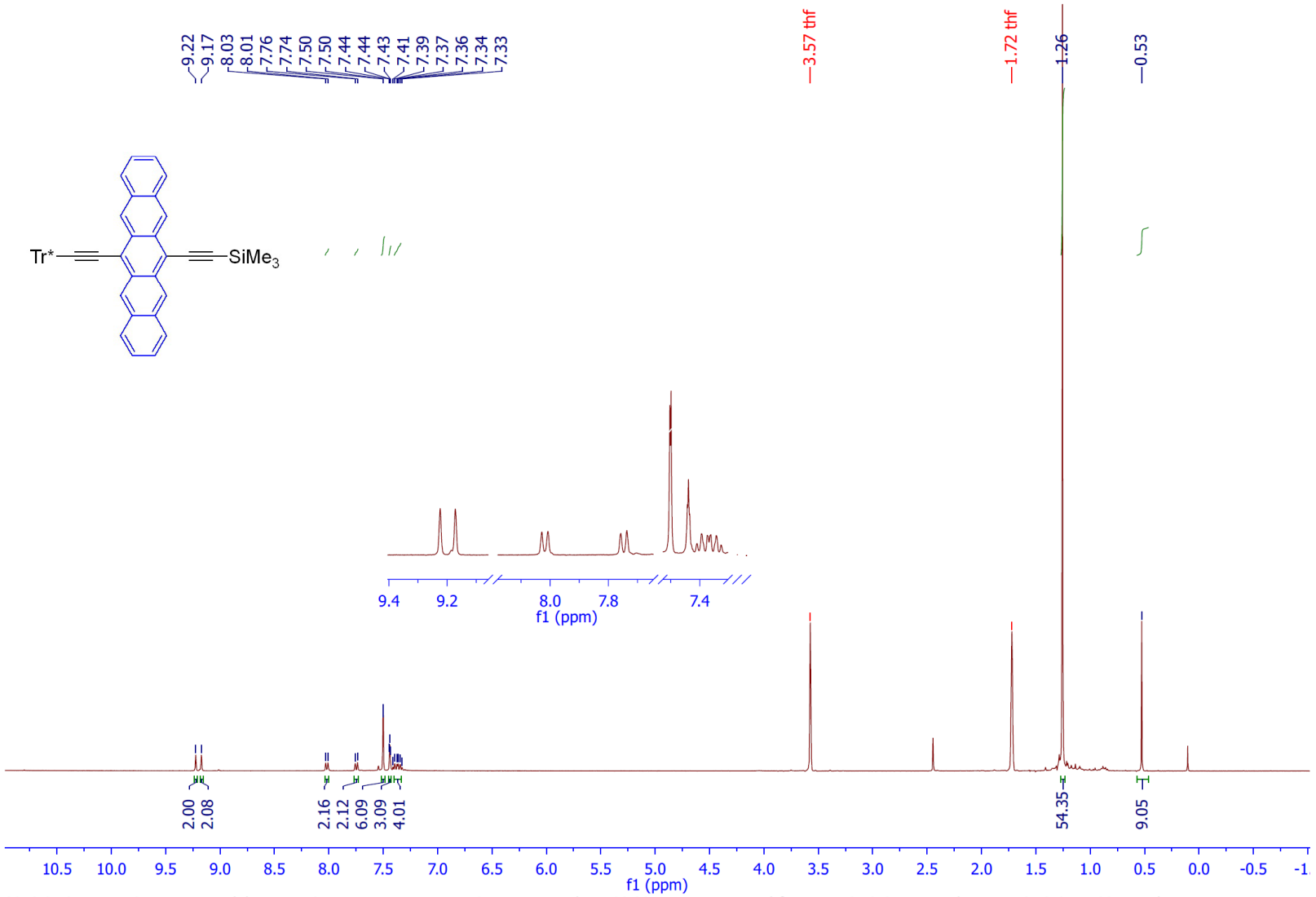

Figure N5. ^{1}H NMR spectrum of compound **2.1** by MestReNova software, 400 MHz, THF-d_8.

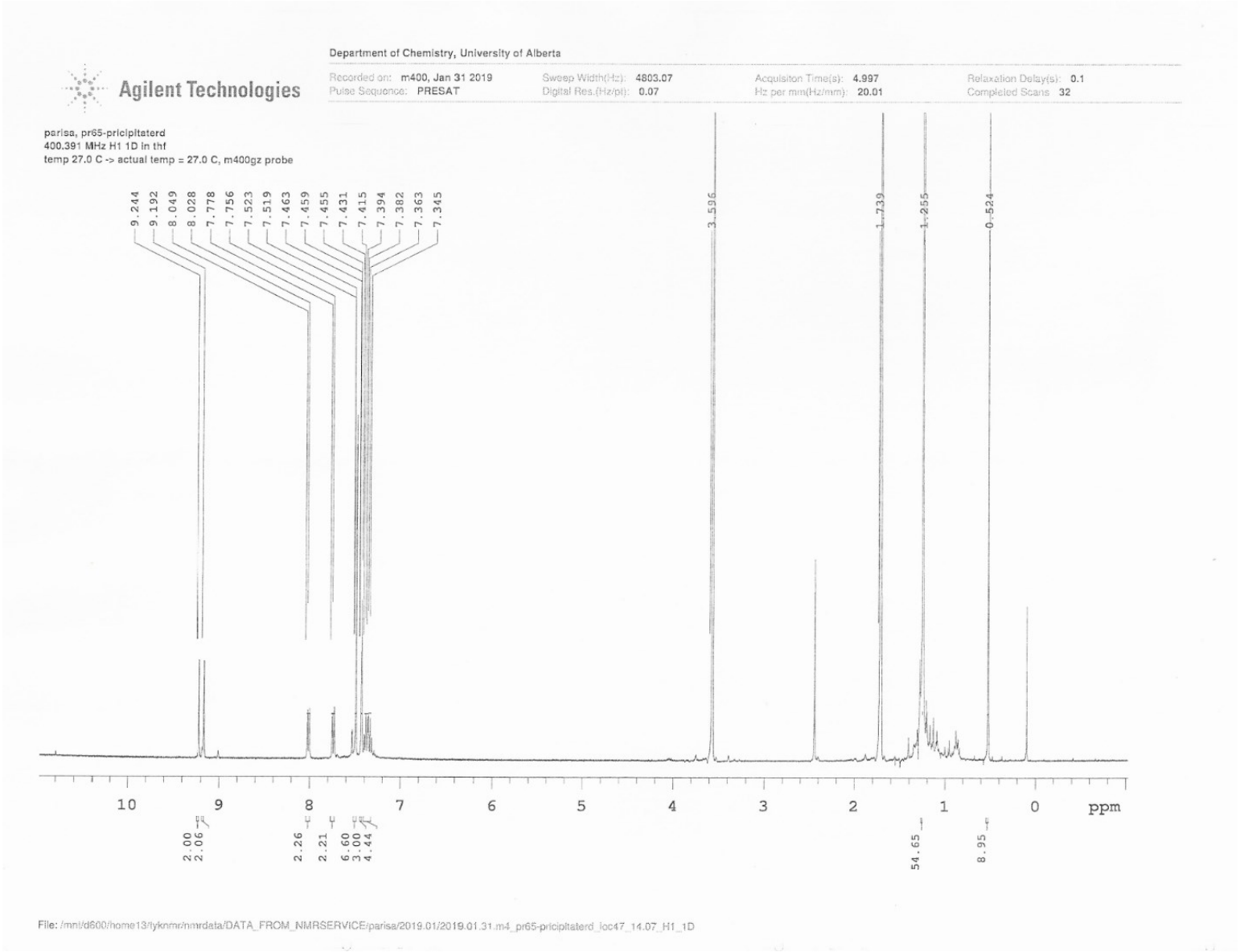

Figure N6. Original ^{1}H NMR spectrum of compound **2.1**, 400 MHz, THF-d_8.

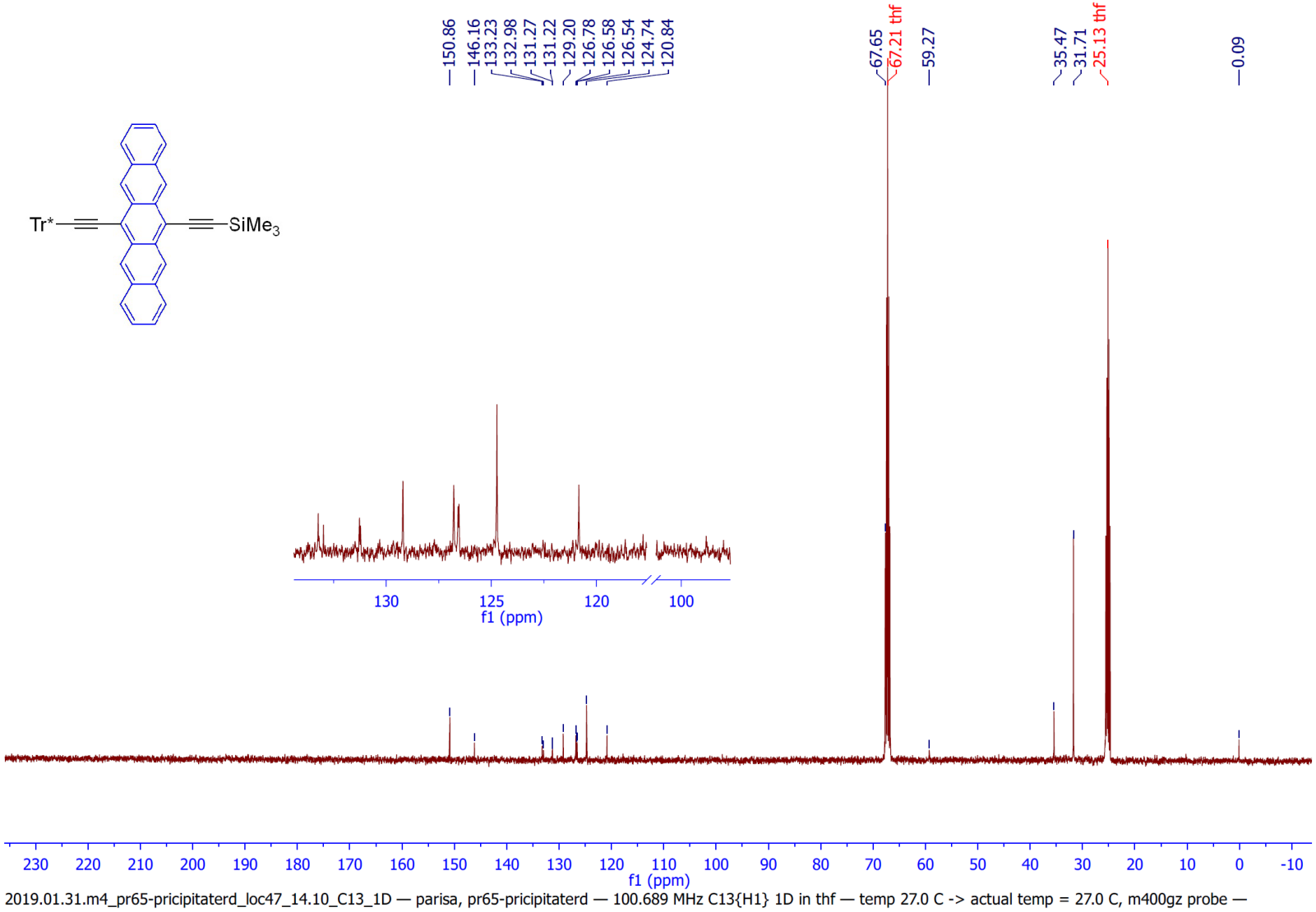

Figure N7. ^{13}C NMR spectrum of compound **2.1** by MestReNova software, 100 MHz, THF-d_8.

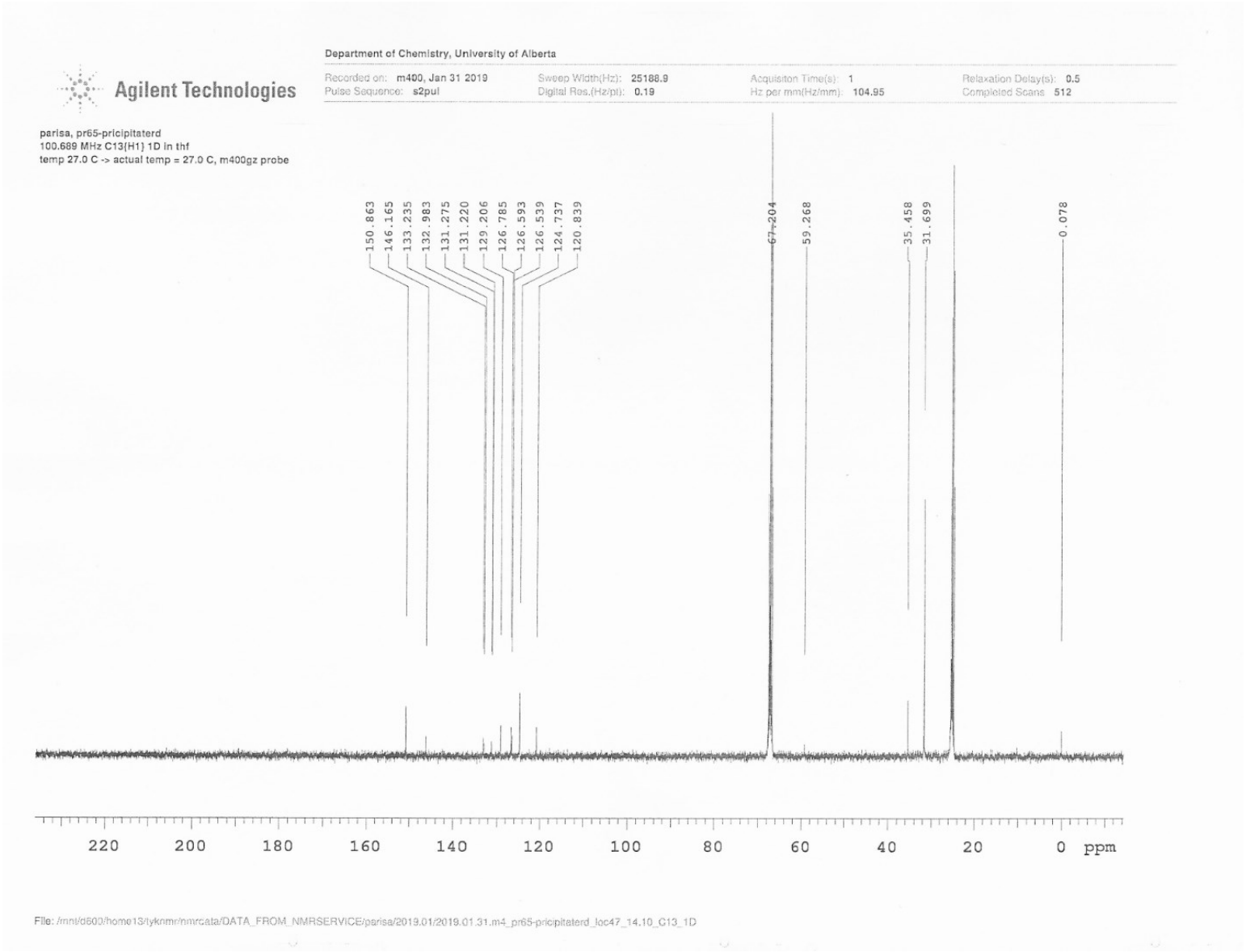

Figure N8. Original ^{13}C NMR spectrum of compound **2.1**, 100 MHz, THF-d_8.

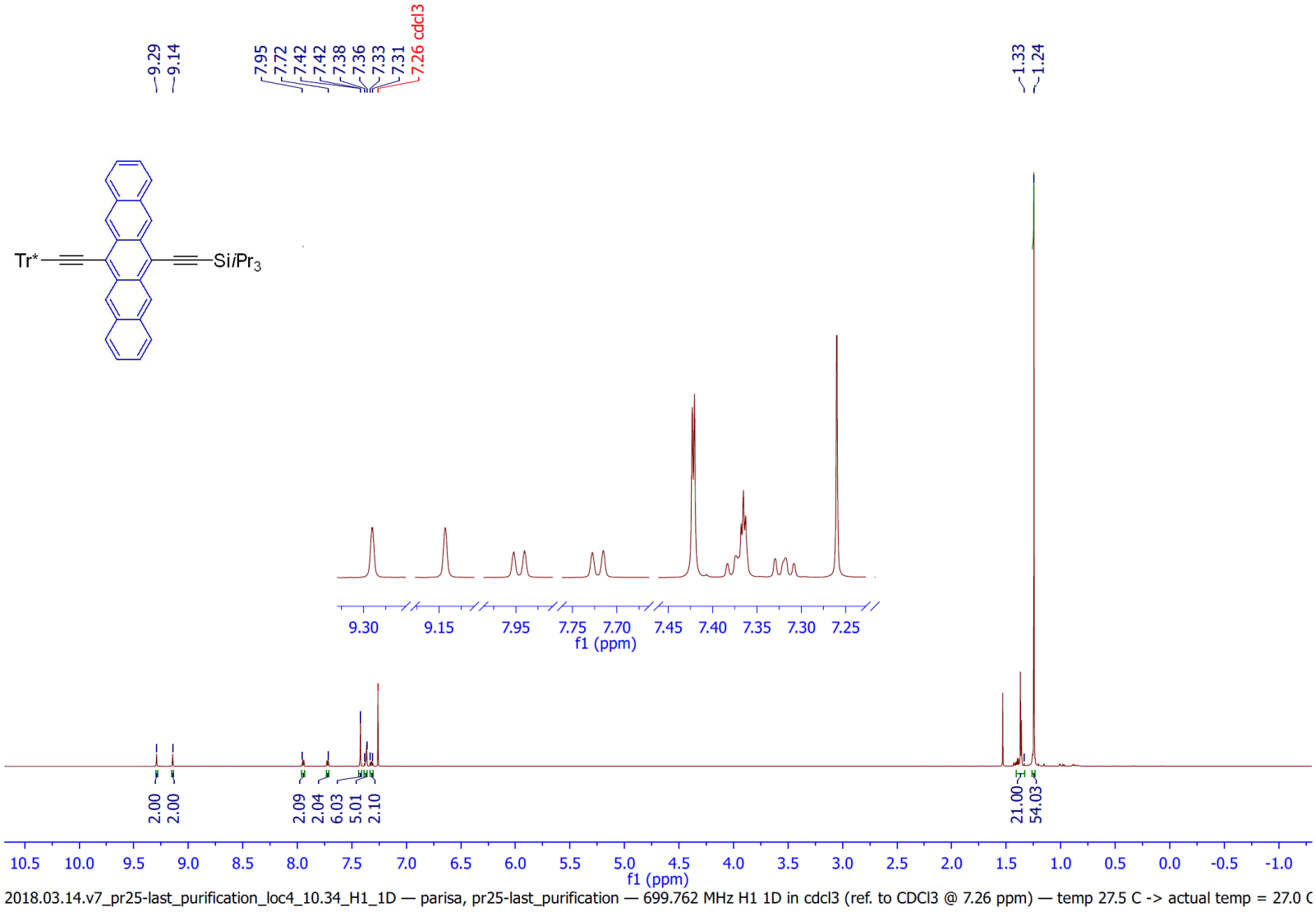

Figure N9. ^{1}H NMR spectrum of compound **2.2** by MestReNova software, 700 MHz, $CDCl_3$.

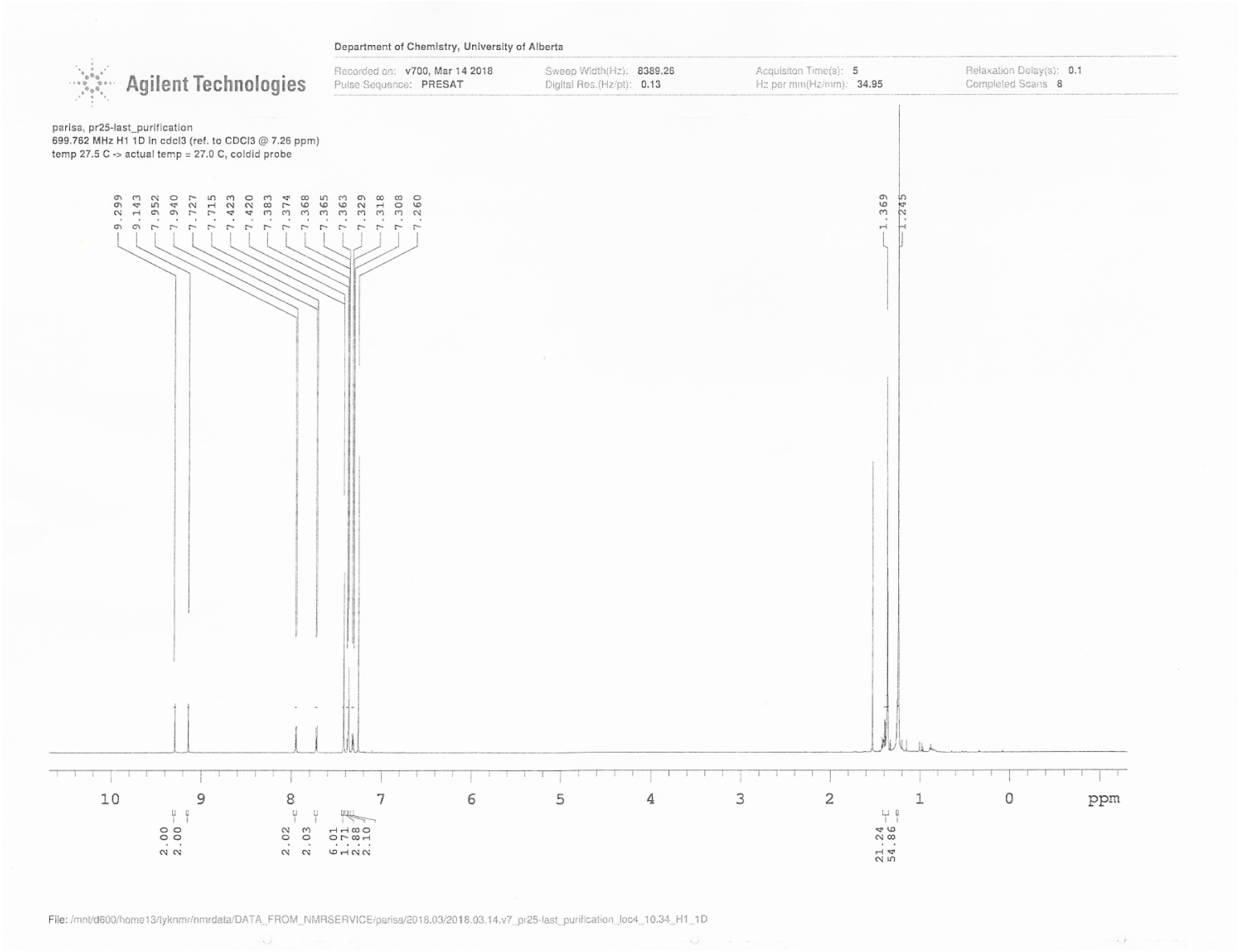

Figure N10. Original ^{1}H NMR spectrum of compound **2.2**, 700 MHz, $CDCl_3$.

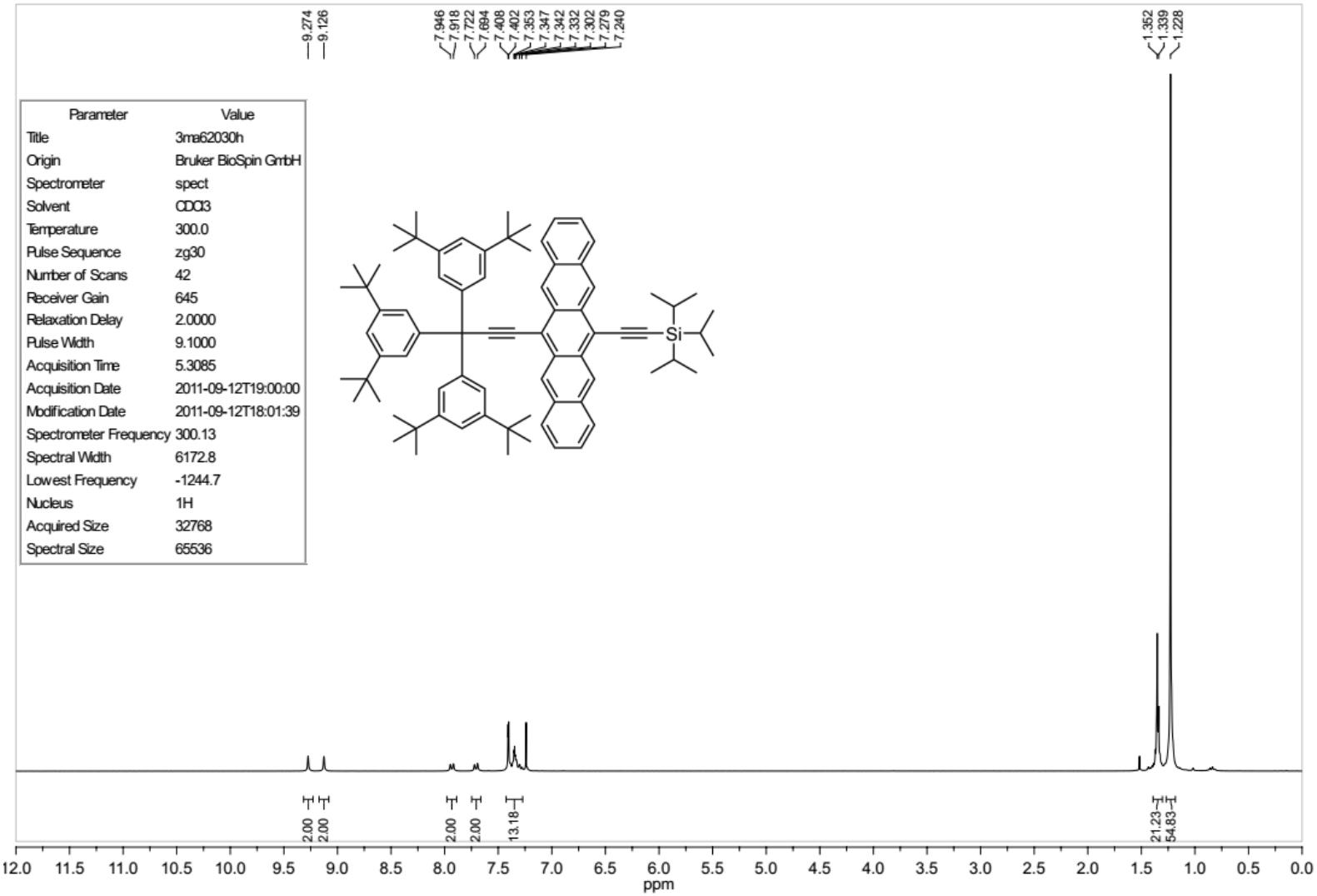

Figure N11. Original ^{1}H NMR spectrum of compound **2.2**, 300 MHz, $CDCl_3$.[10]

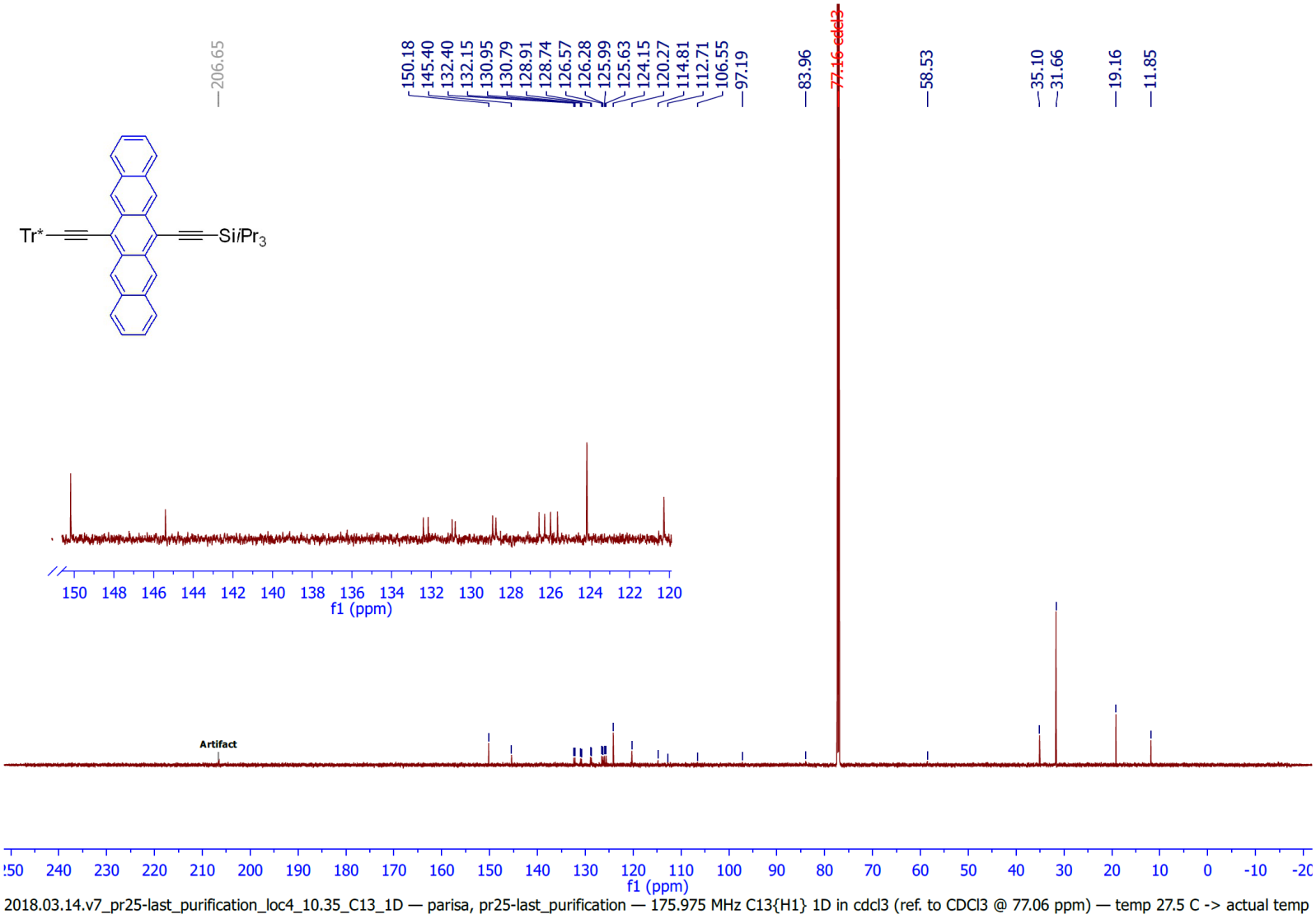

Figure N12. ^{13}C NMR spectrum of compound **2.2** by MestReNova software, 175 MHz, $CDCl_3$.

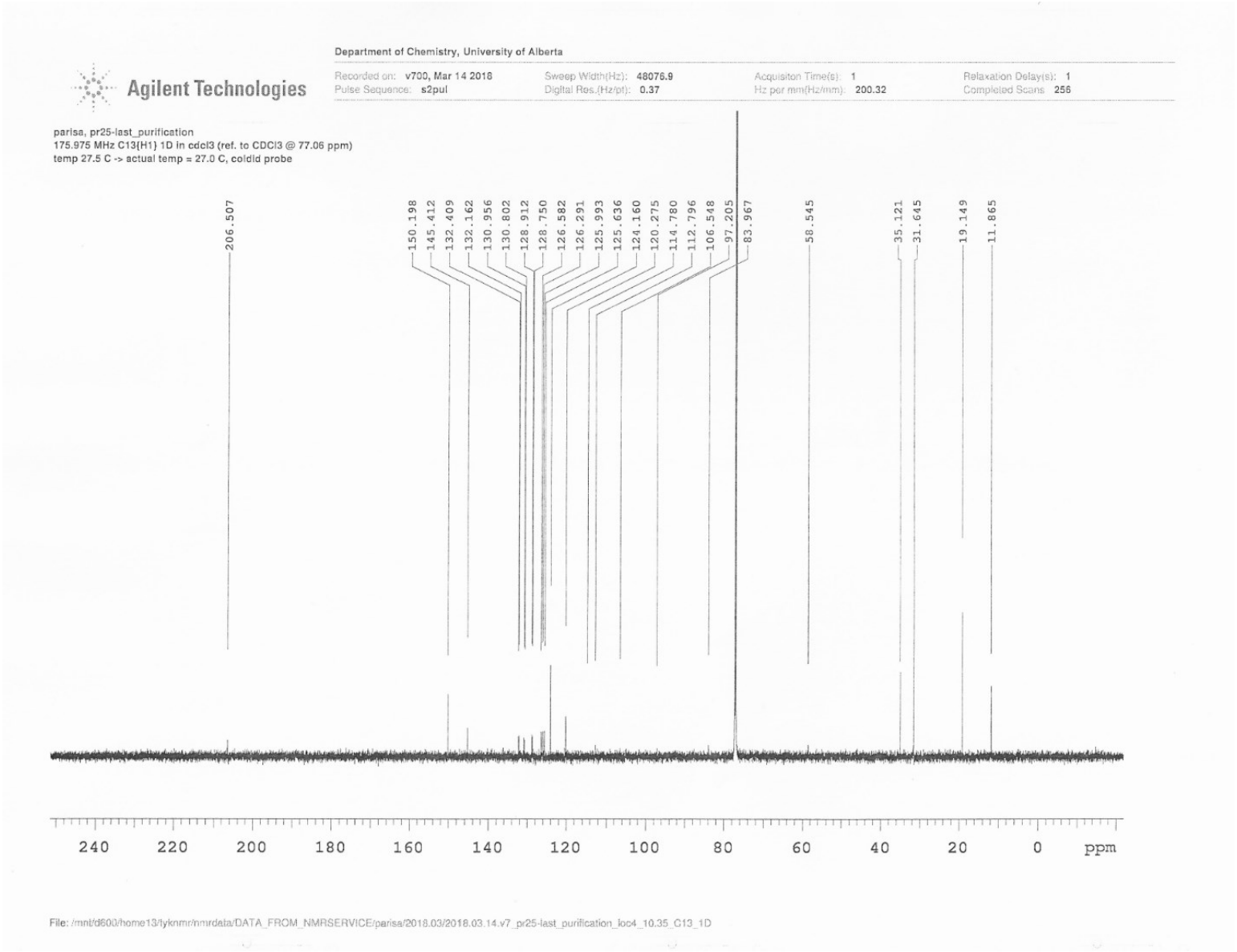

Figure N13. Original ^{13}C NMR spectrum of compound **2.2**, 175 MHz, $CDCl_3$.

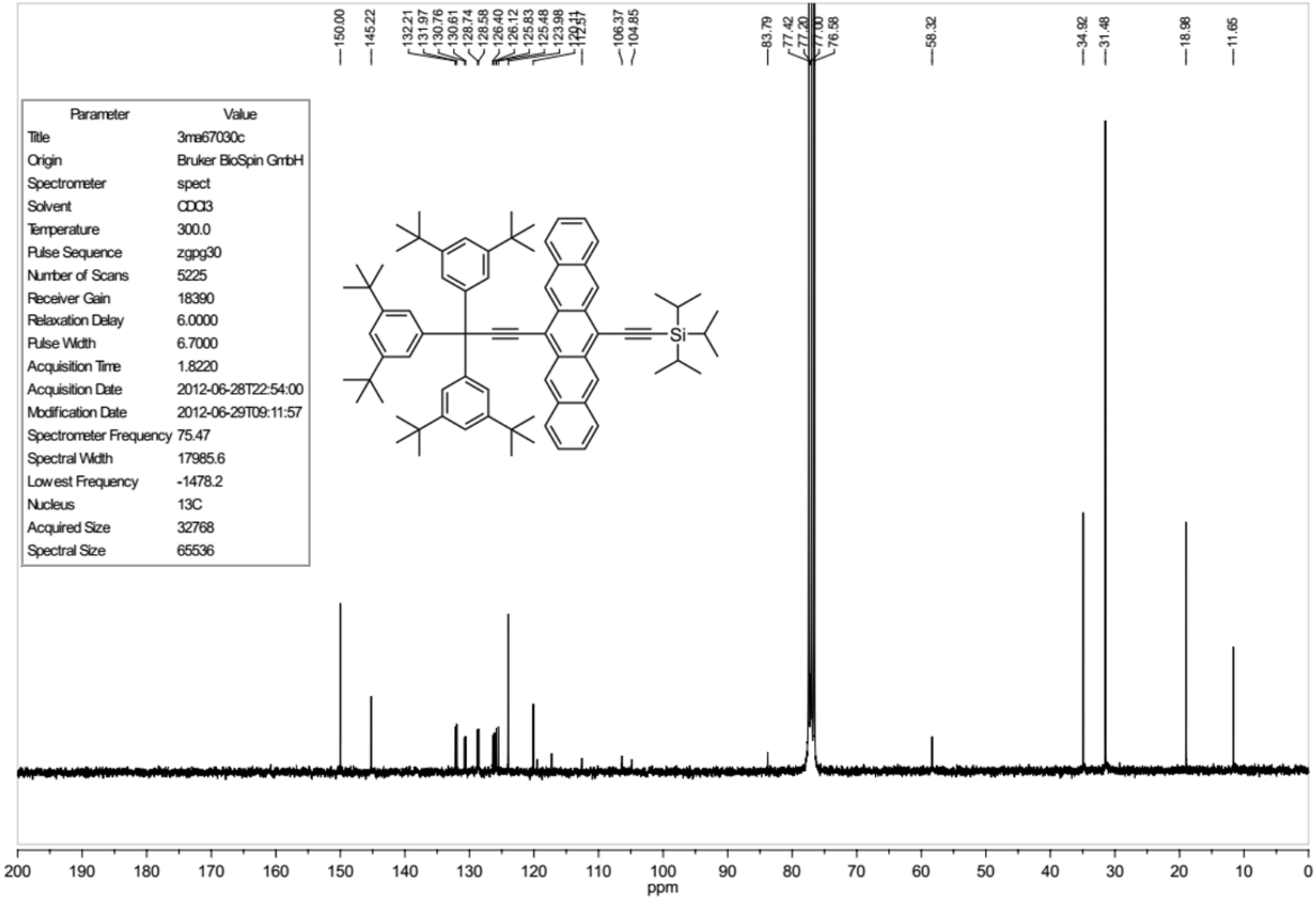

Figure N14. Original ^{13}C NMR spectrum of compound **2.2**, 75 MHz, $CDCl_3$.[10]

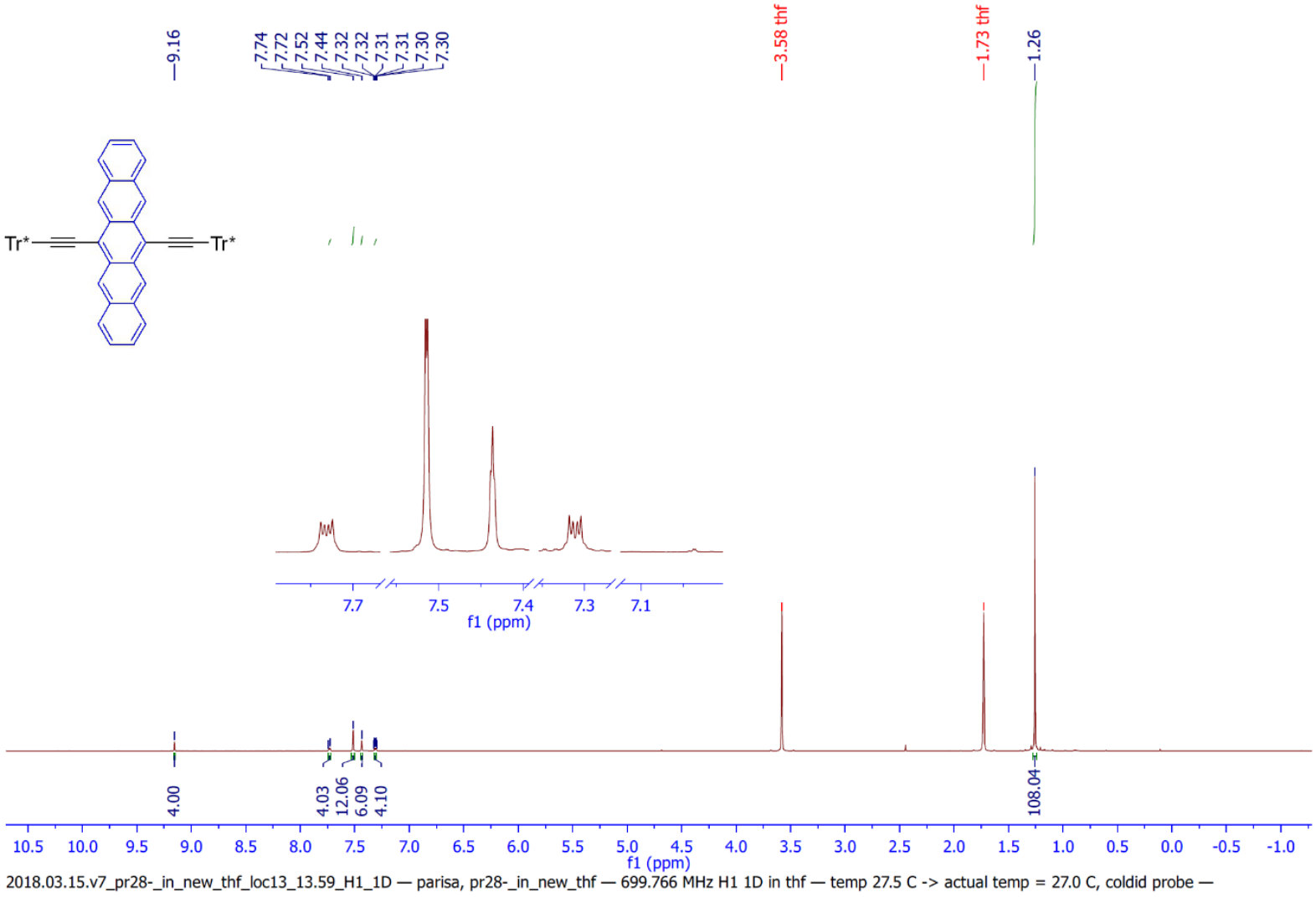

Figure N15. ^{1}H NMR spectrum of compound **2.3** by MestReNova software, 700 MHz, THF-d_8.

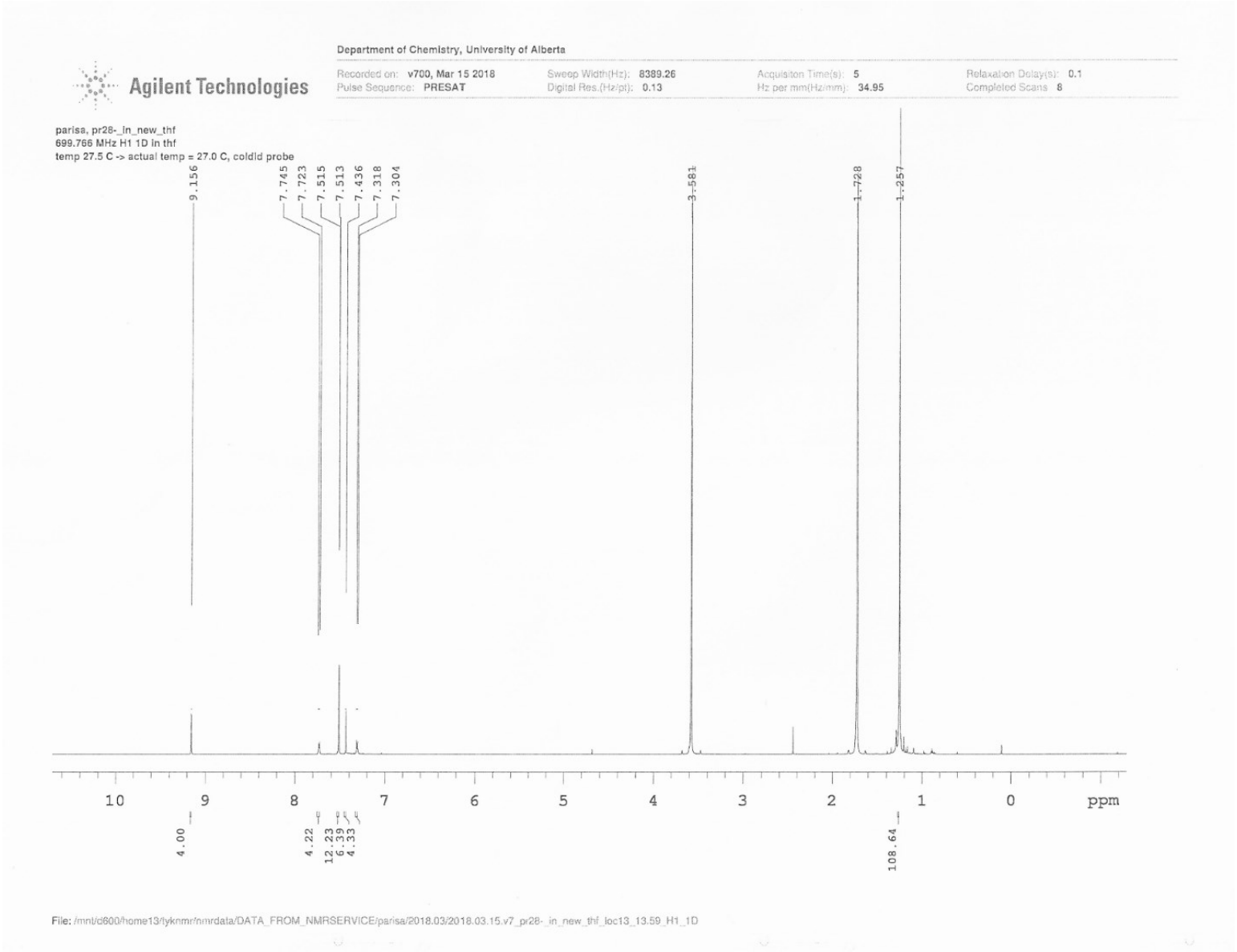

Figure N16. Original ^{1}H NMR spectrum of compound **2.3**, 700 MHz, THF-d_8.

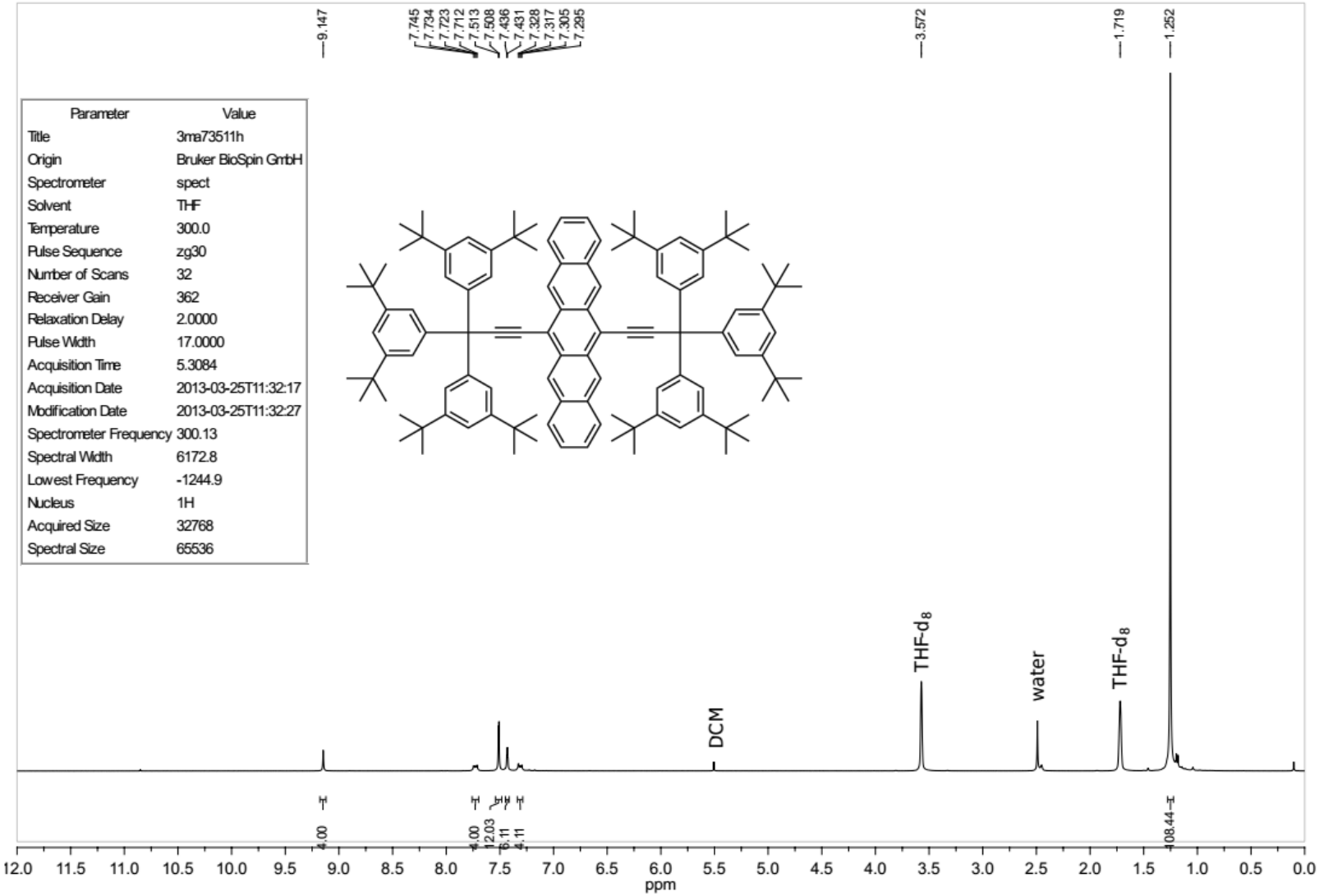

Figure N17. Original ^{1}H NMR spectrum of compound **2.3**, 300 MHz, THF-d_8.[10]

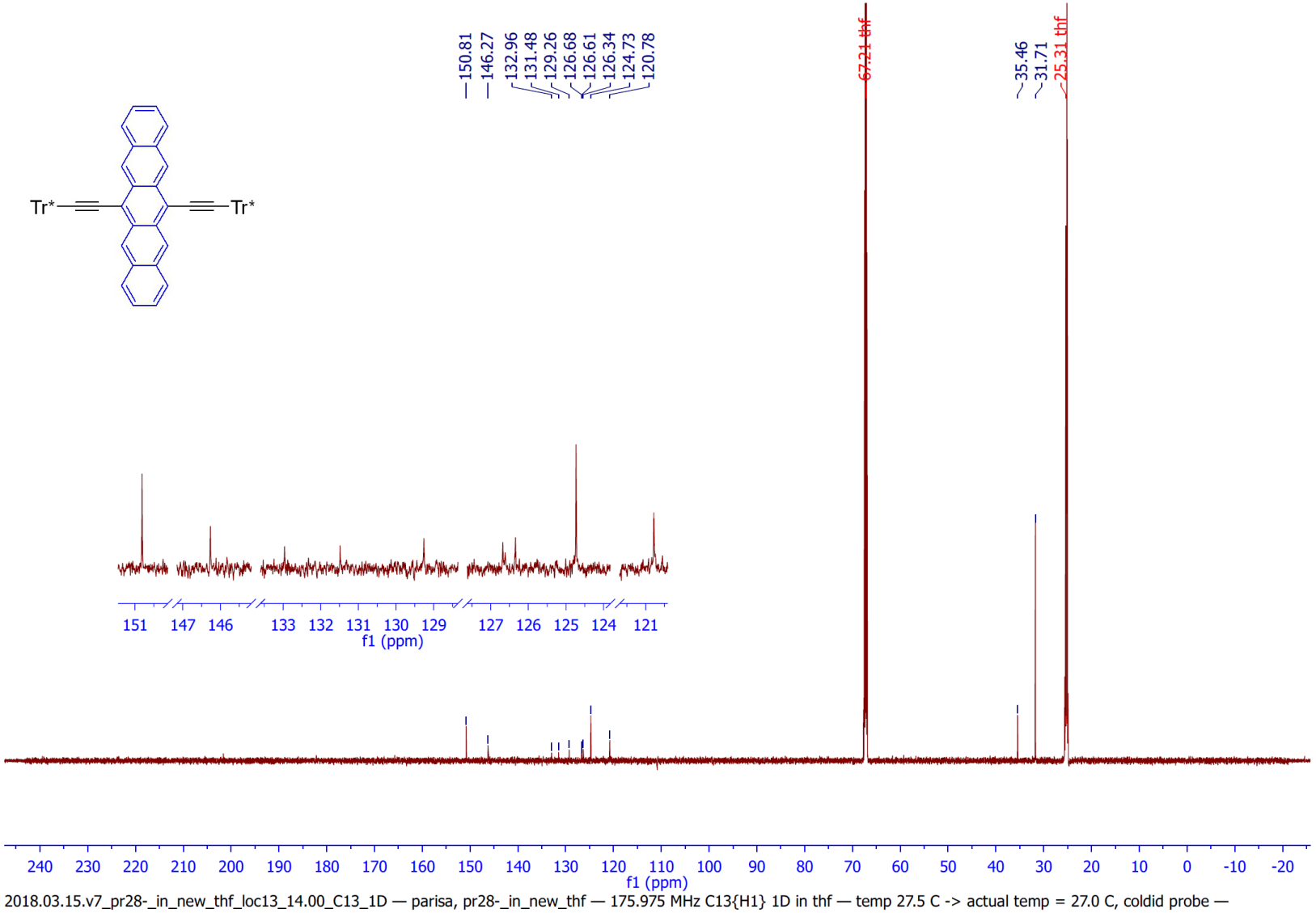

Figure N18. ^{13}C NMR spectrum of compound **2.3** by MestReNova software, 175 MHz, THF-d_8.

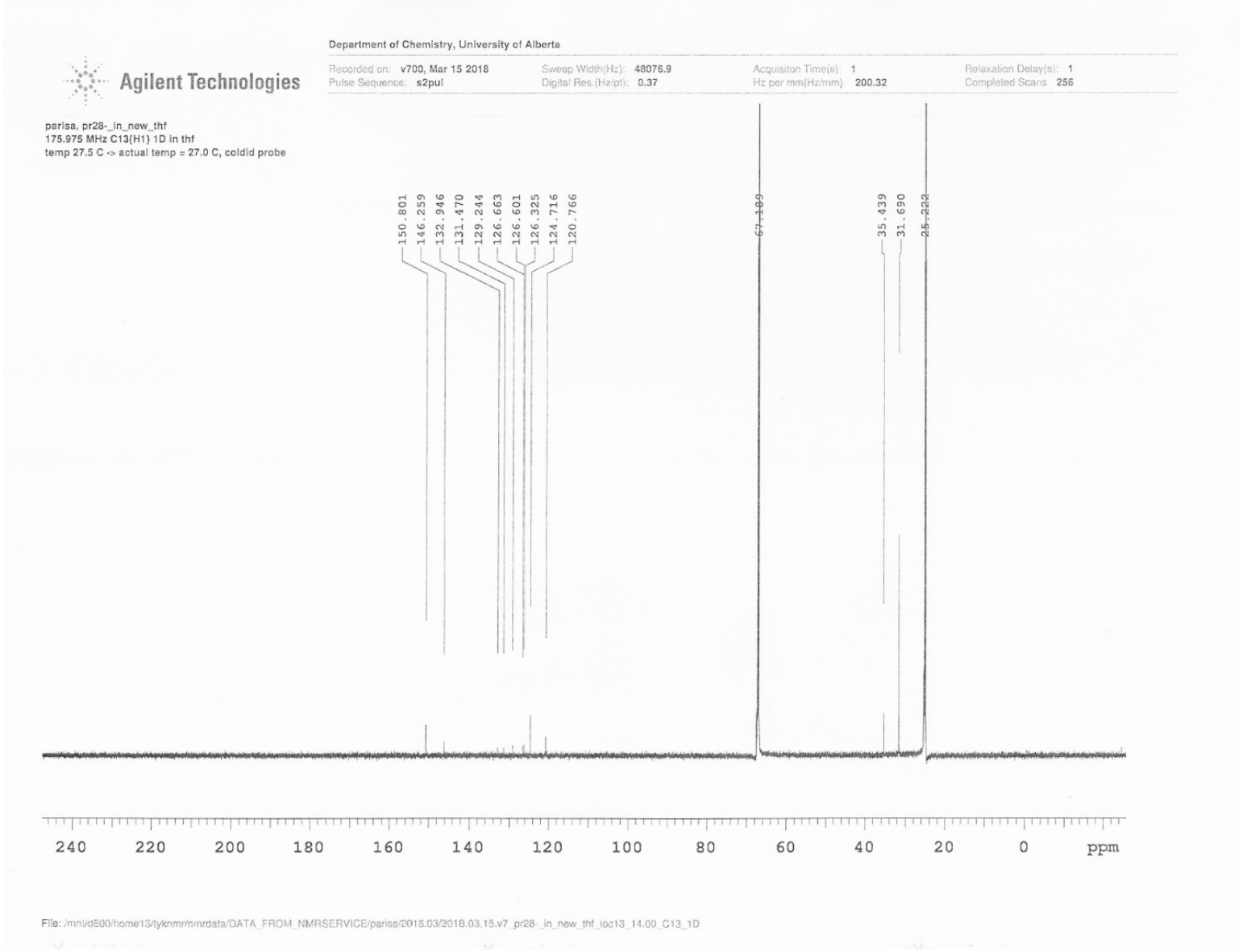

Figure N19. Original ^{13}C NMR spectrum of compound **2.3**, 175 MHz, THF-d_8.

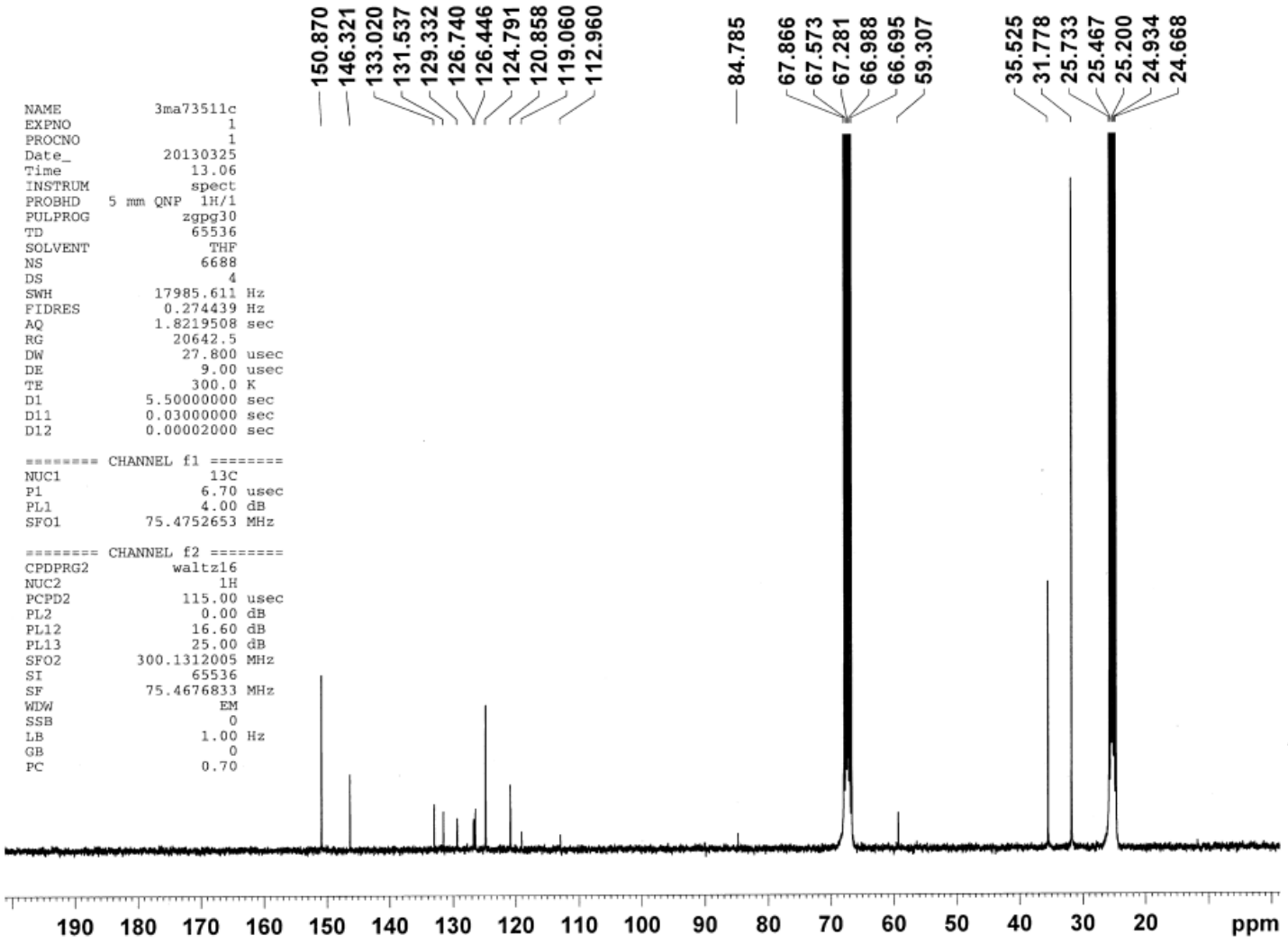

Figure N20. Original ^{13}C NMR spectrum of compound **2.3**, 75 MHz, THF-d_8.[10]

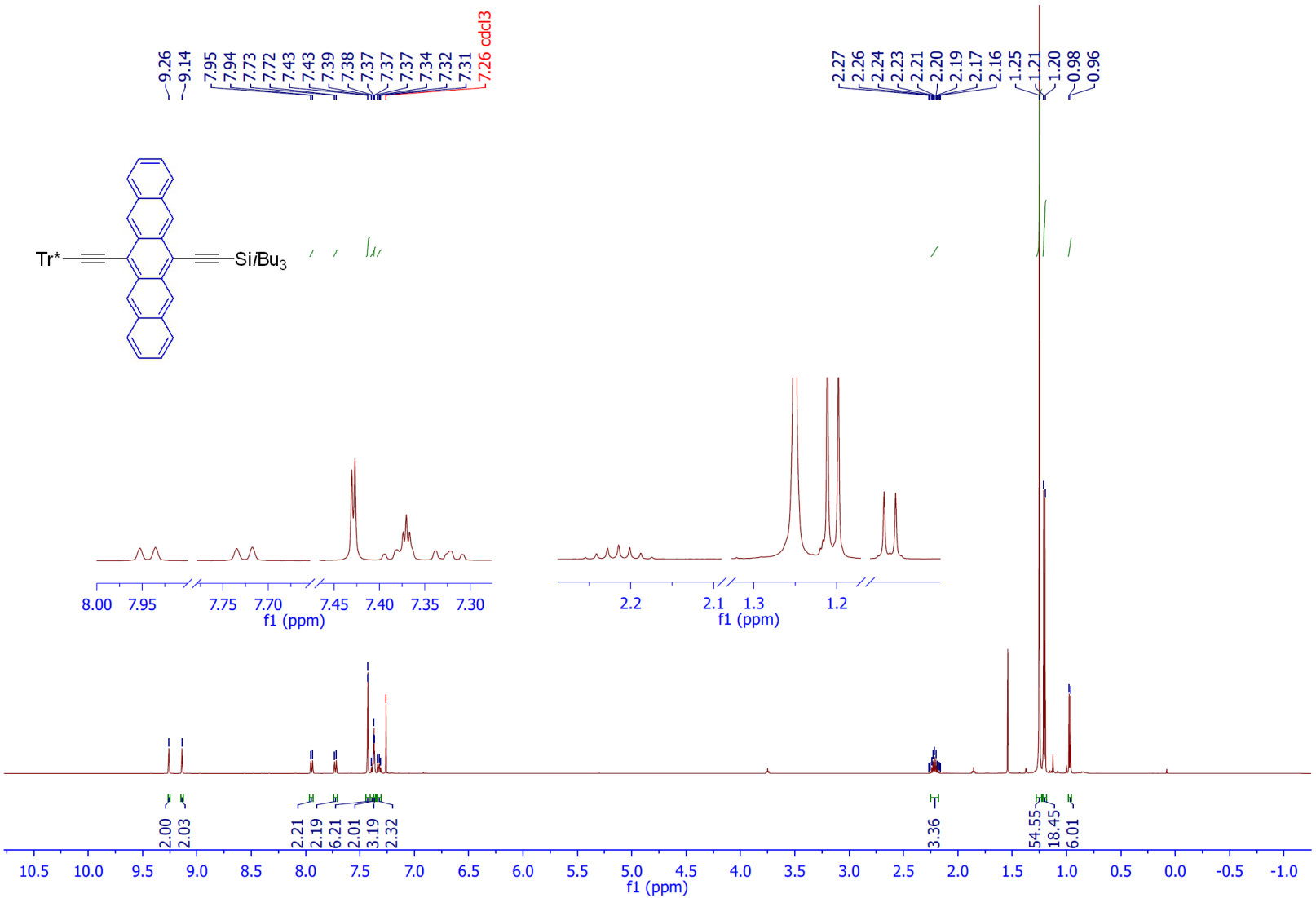

Figure N21. ^{1}H NMR spectrum of compound **2.4** by MestReNova software, 500 MHz, $CDCl_3$.

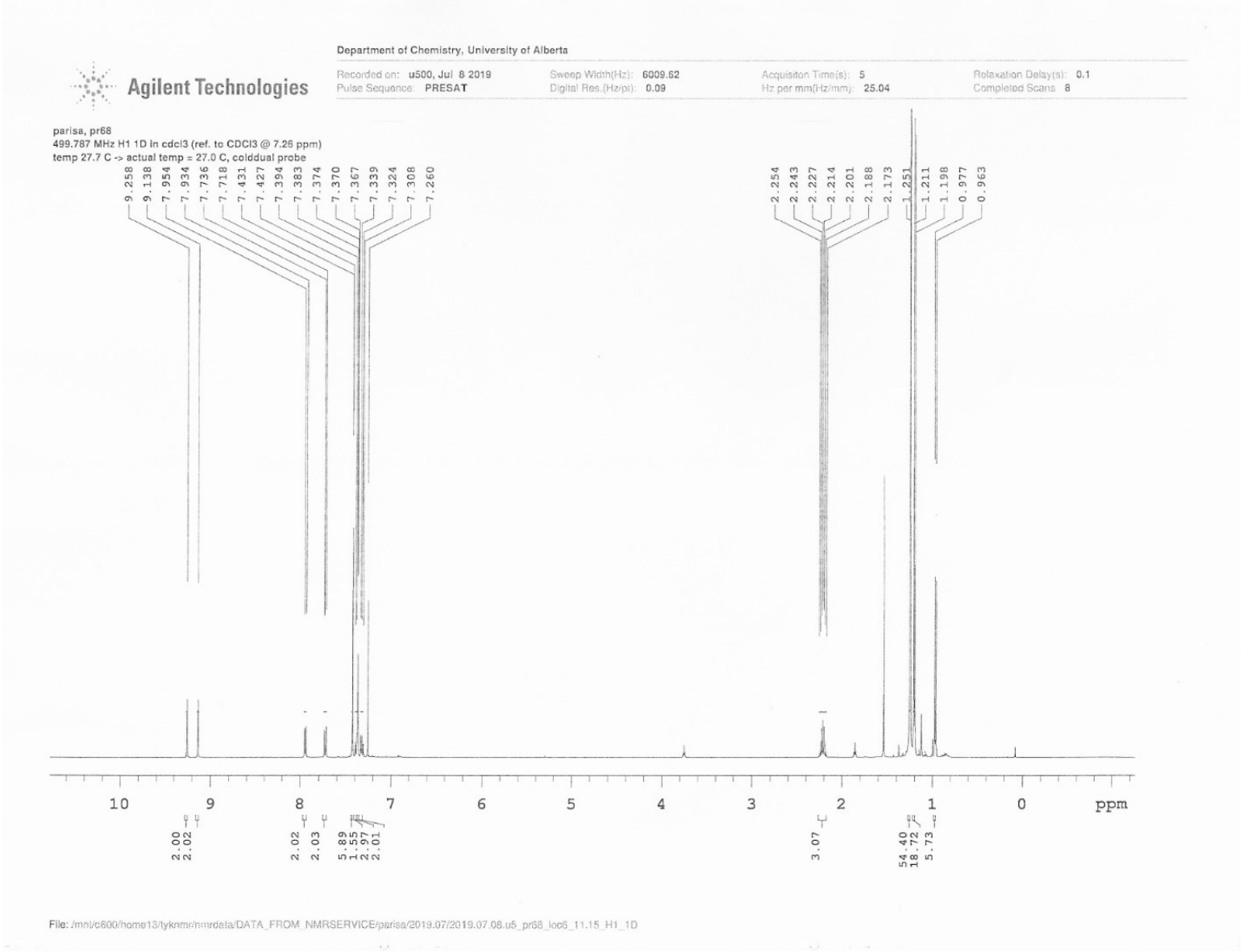

Figure N22. Original ^{1}H NMR spectrum of compound **2.4**, 500 MHz, $CDCl_3$.

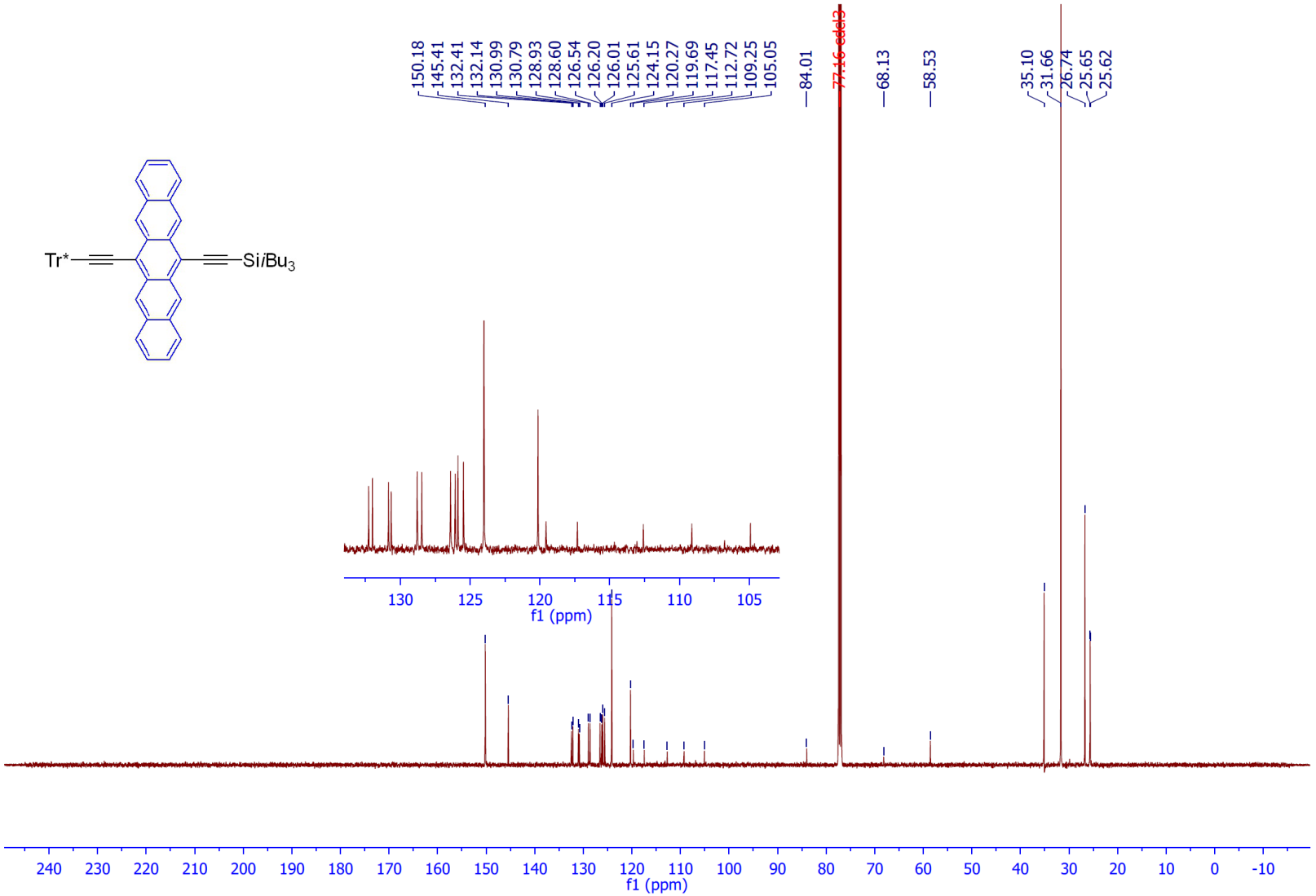

Figure N23. ^{13}C NMR spectrum of compound **2.4** by MestReNova software, 125 MHz, $CDCl_3$.

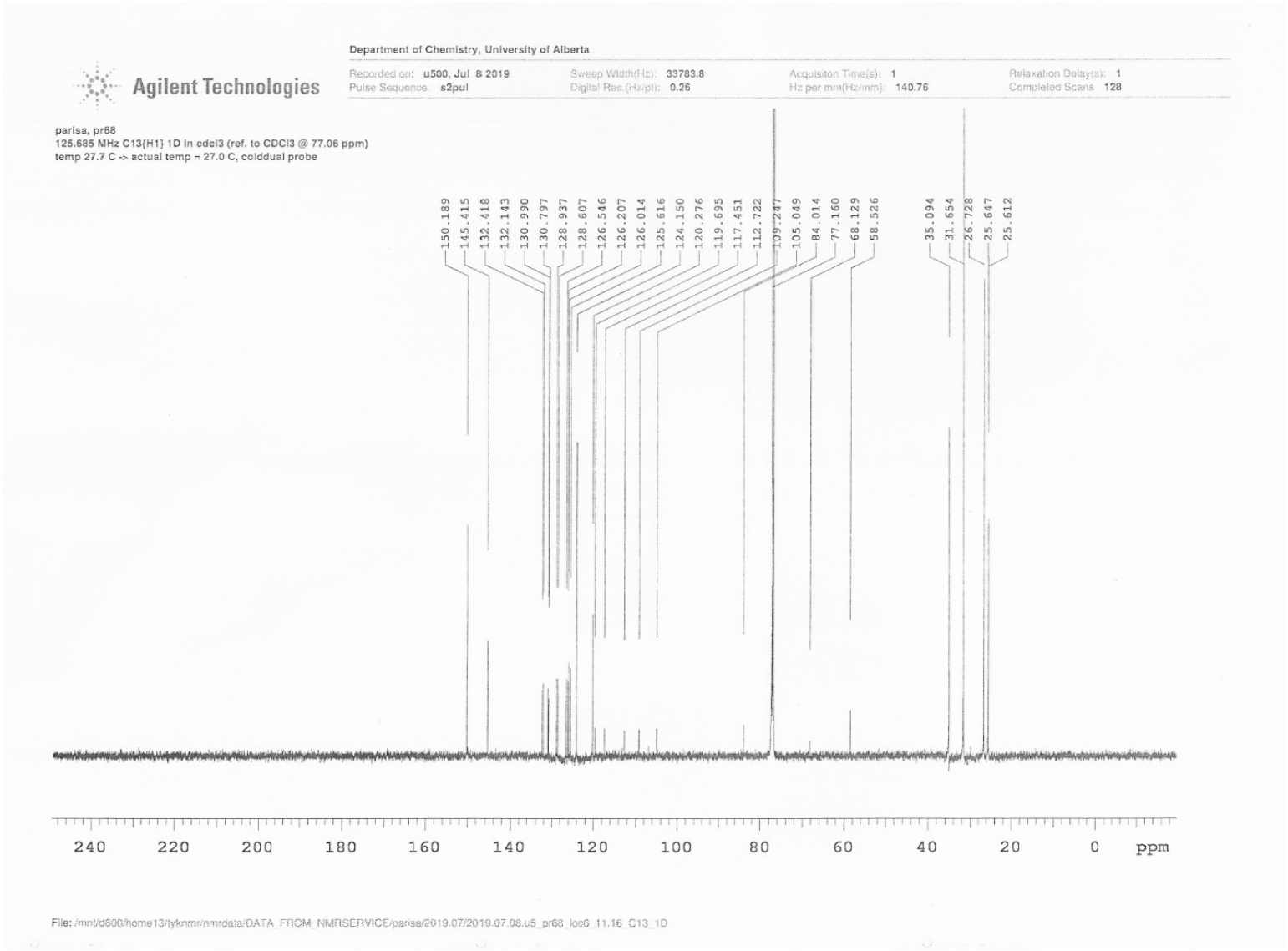

Figure N24. Original ^{13}C NMR spectrum of compound **2.4**, 125 MHz, $CDCl_3$.

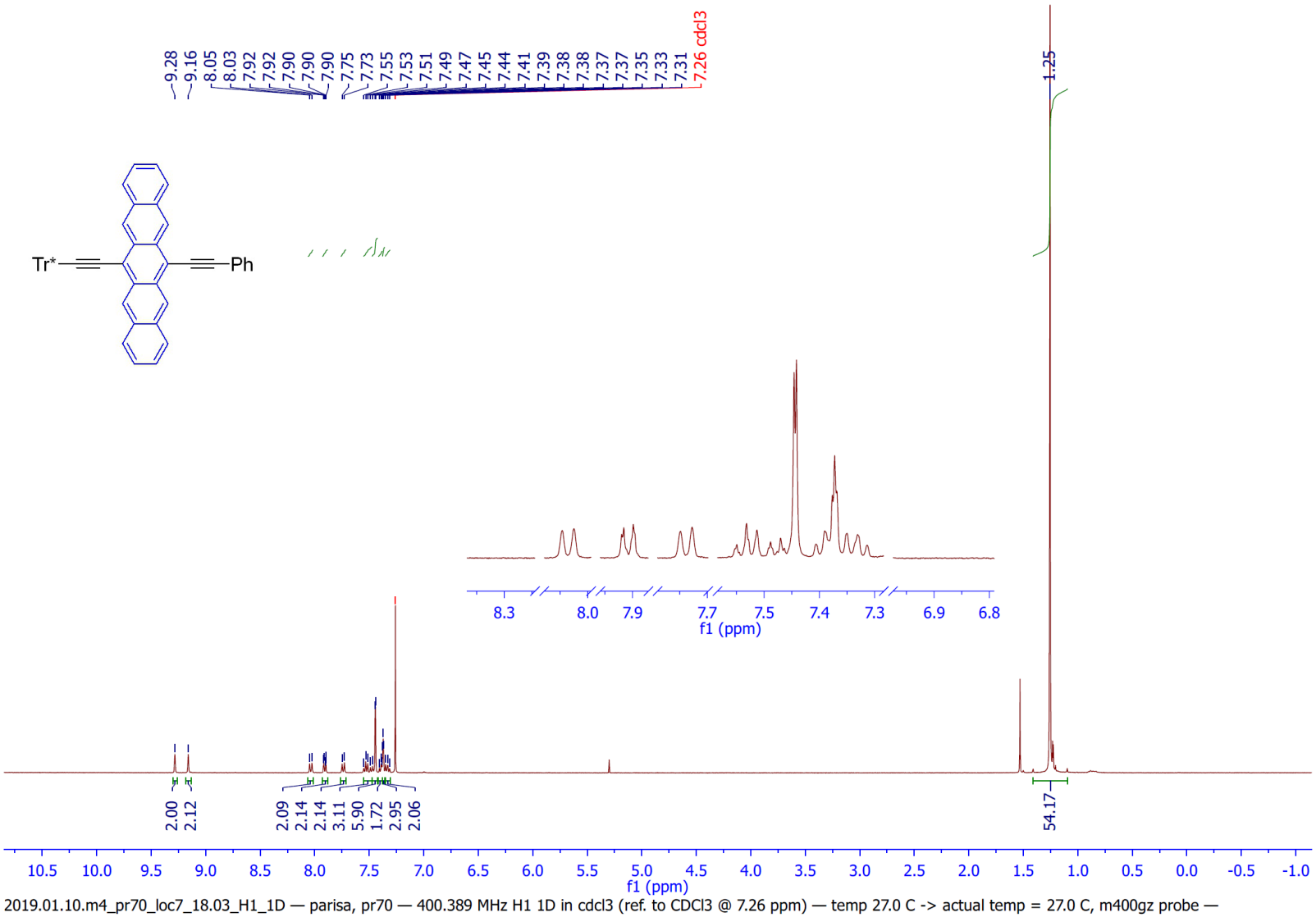

Figure N25. ^{1}H NMR spectrum of compound **2.5** by MestReNova software, 400 MHz, $CDCl_3$.

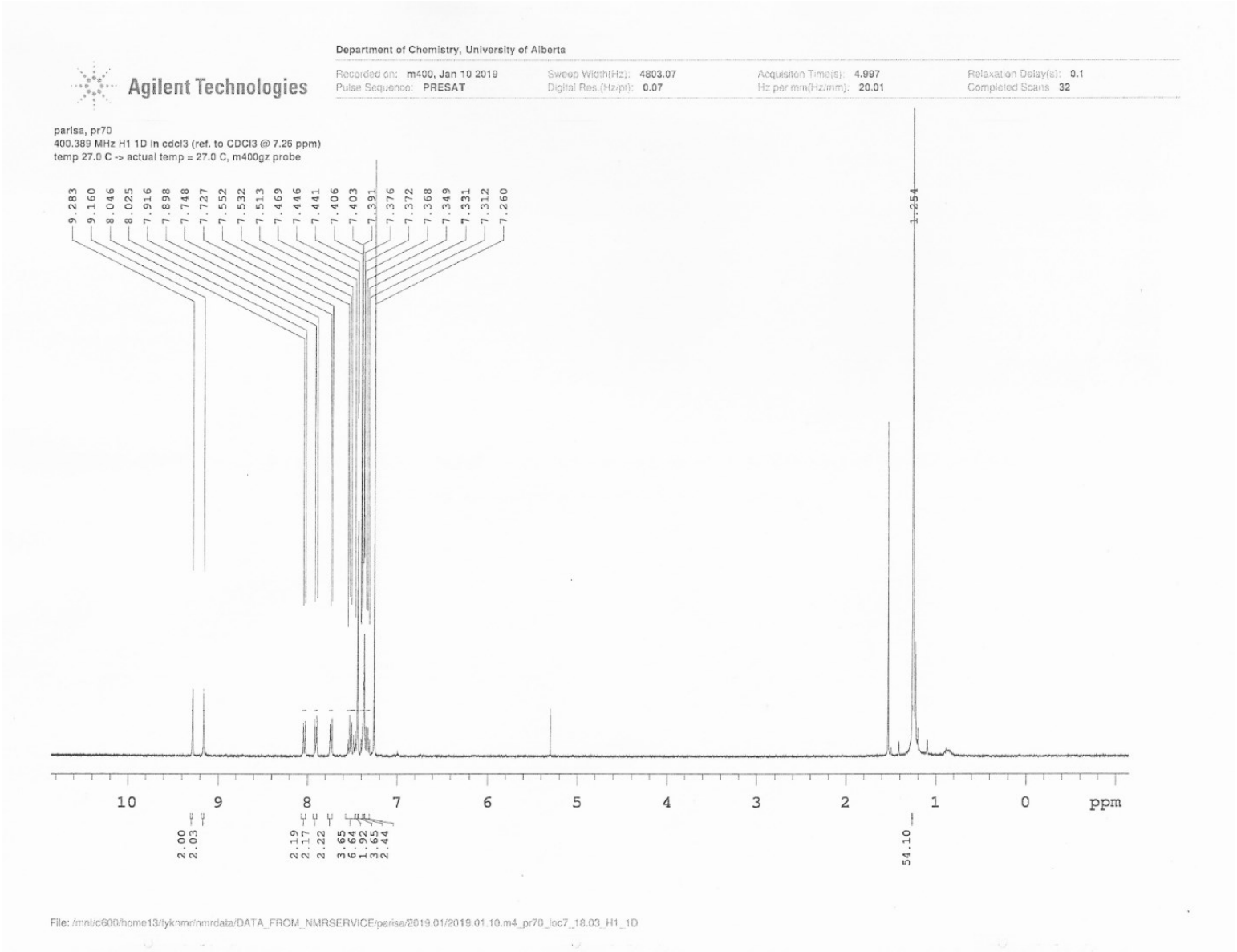

Figure N26. Original ^{1}H NMR spectrum of compound **2.5**, 400 MHz, $CDCl_3$.

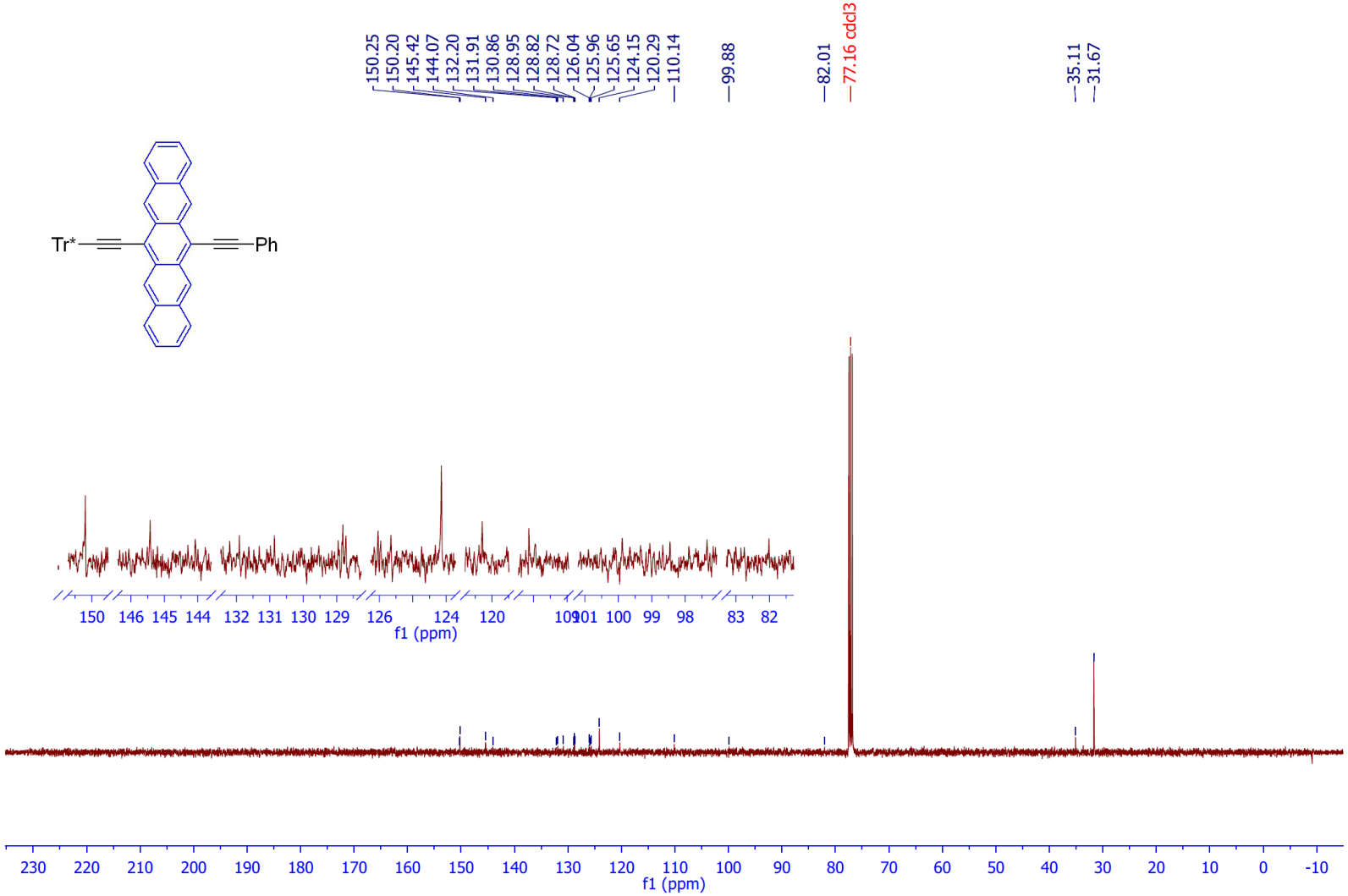

Figure N27. ^{13}C NMR spectrum of compound **2.5** by MestReNova software, 100 MHz, $CDCl_3$.

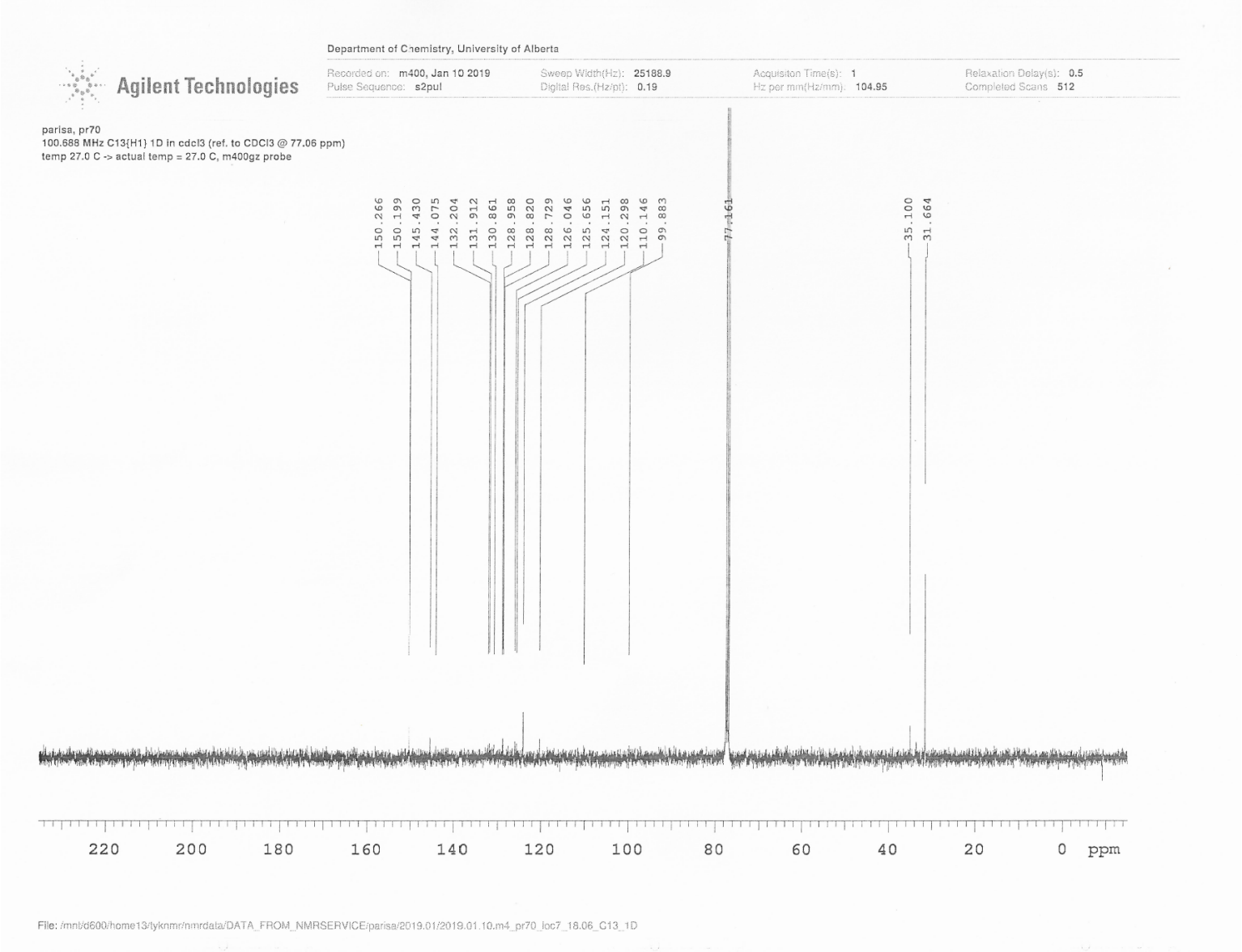

Figure N28. Original ^{13}C NMR spectrum of compound **2.5**, 100 MHz, $CDCl_3$.

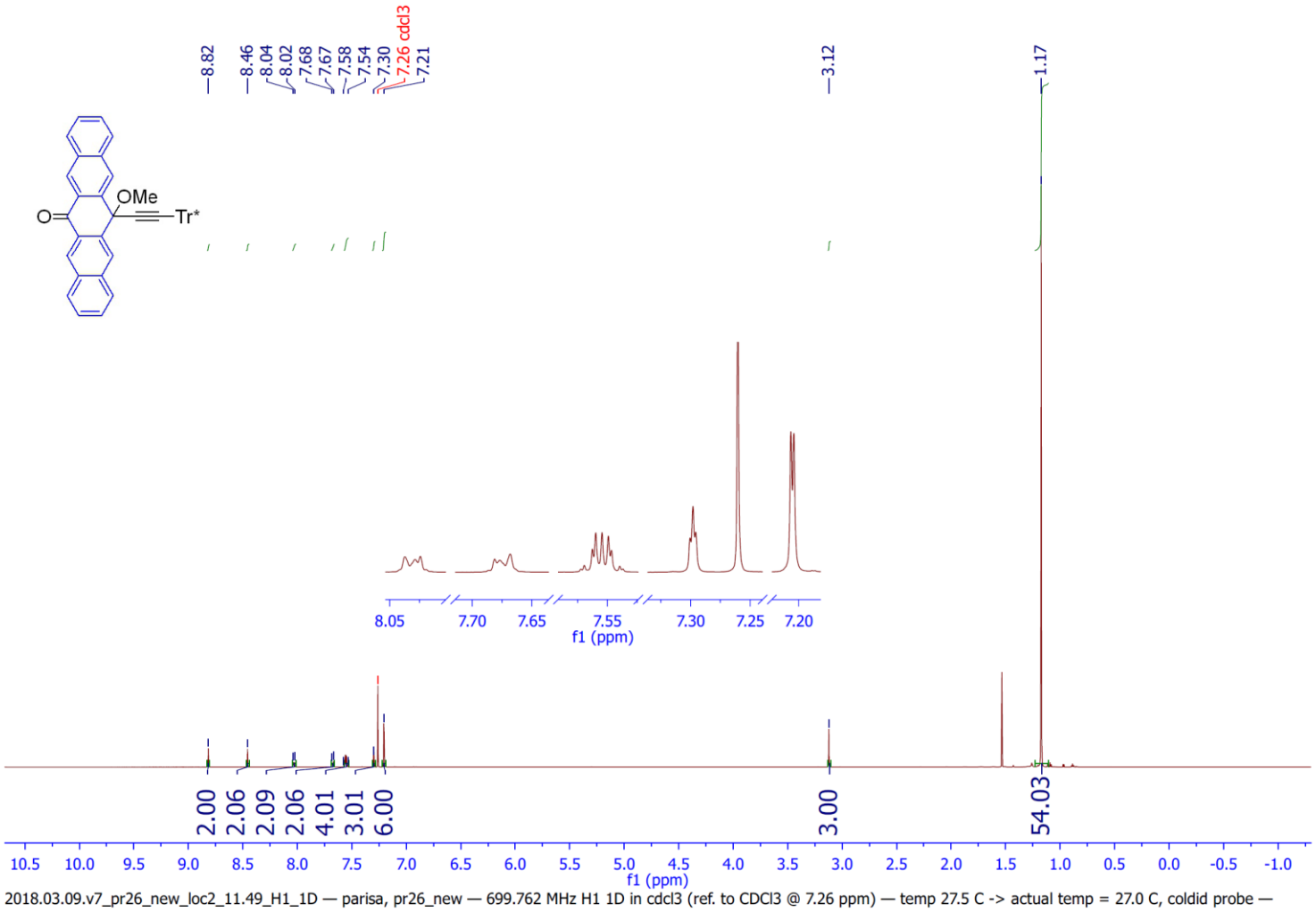

Figure N29. ^{1}H NMR spectrum of compound **2.15** by MestReNova software, 700 MHz, $CDCl_3$.

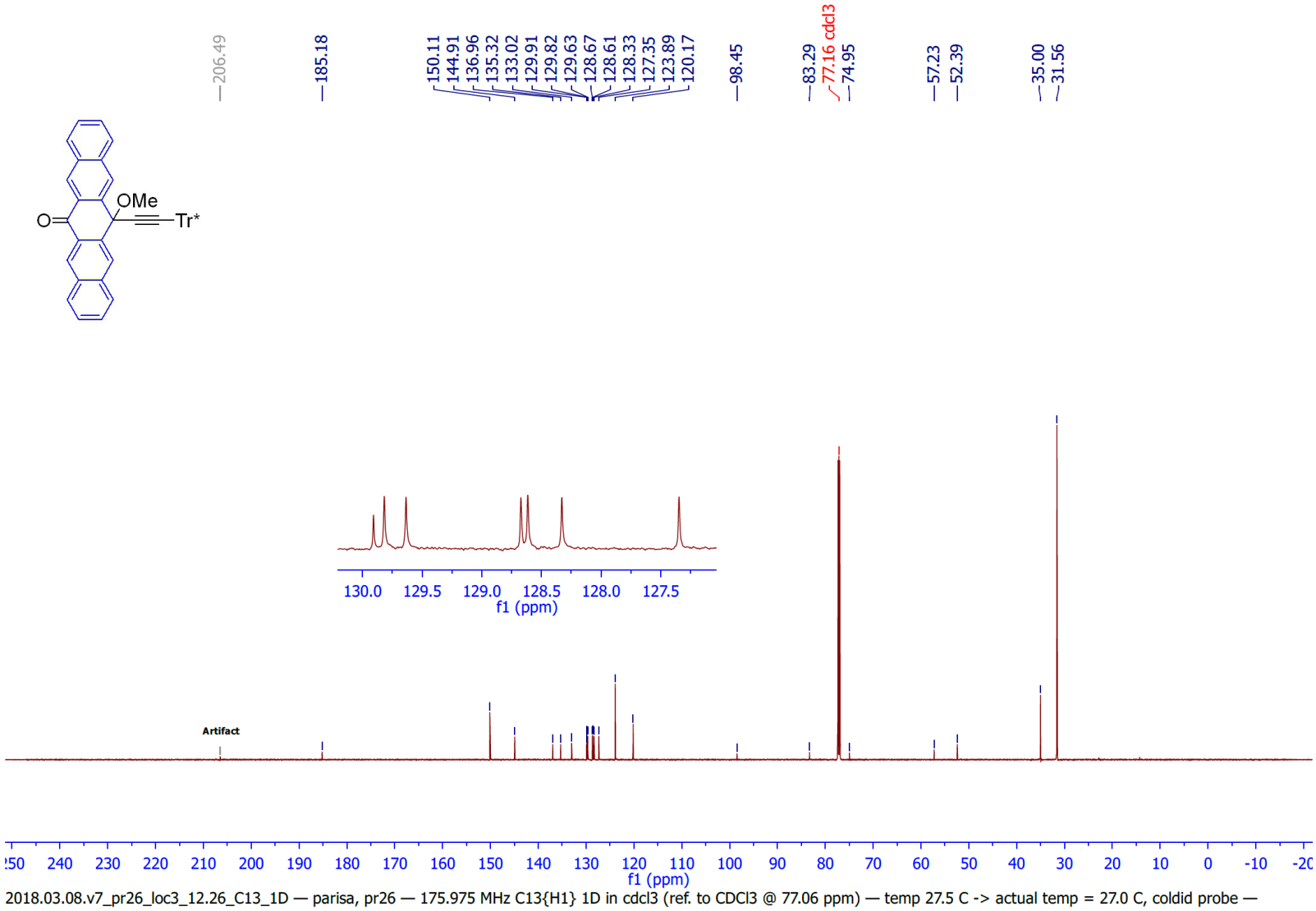

Figure N30. ^{13}C NMR spectrum of compound **2.15** by MestReNova software, 175 MHz, $CDCl_3$.

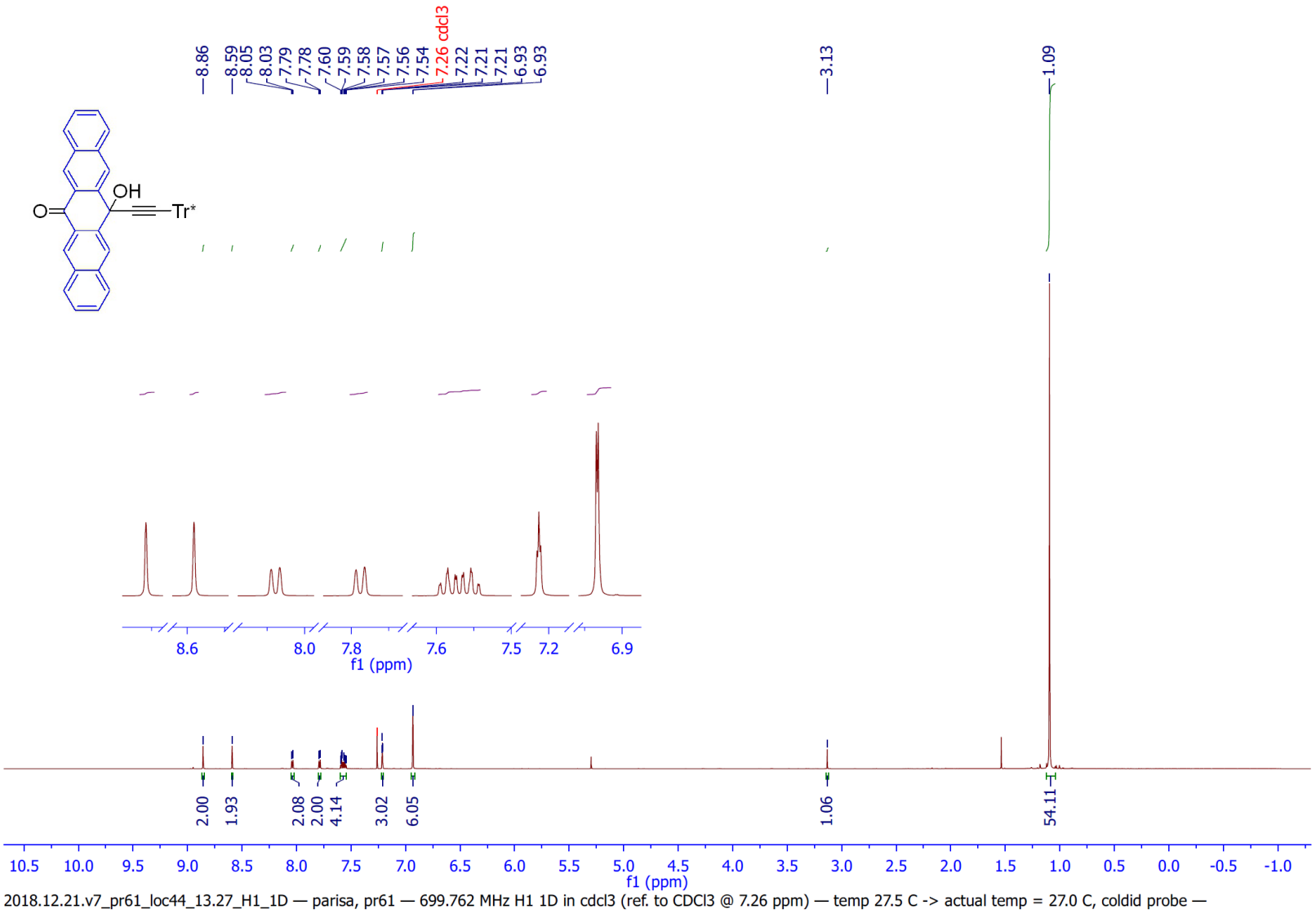

Figure N31. ^{1}H NMR spectrum of compound **2.16** by MestReNova software, 700 MHz, $CDCl_3$.

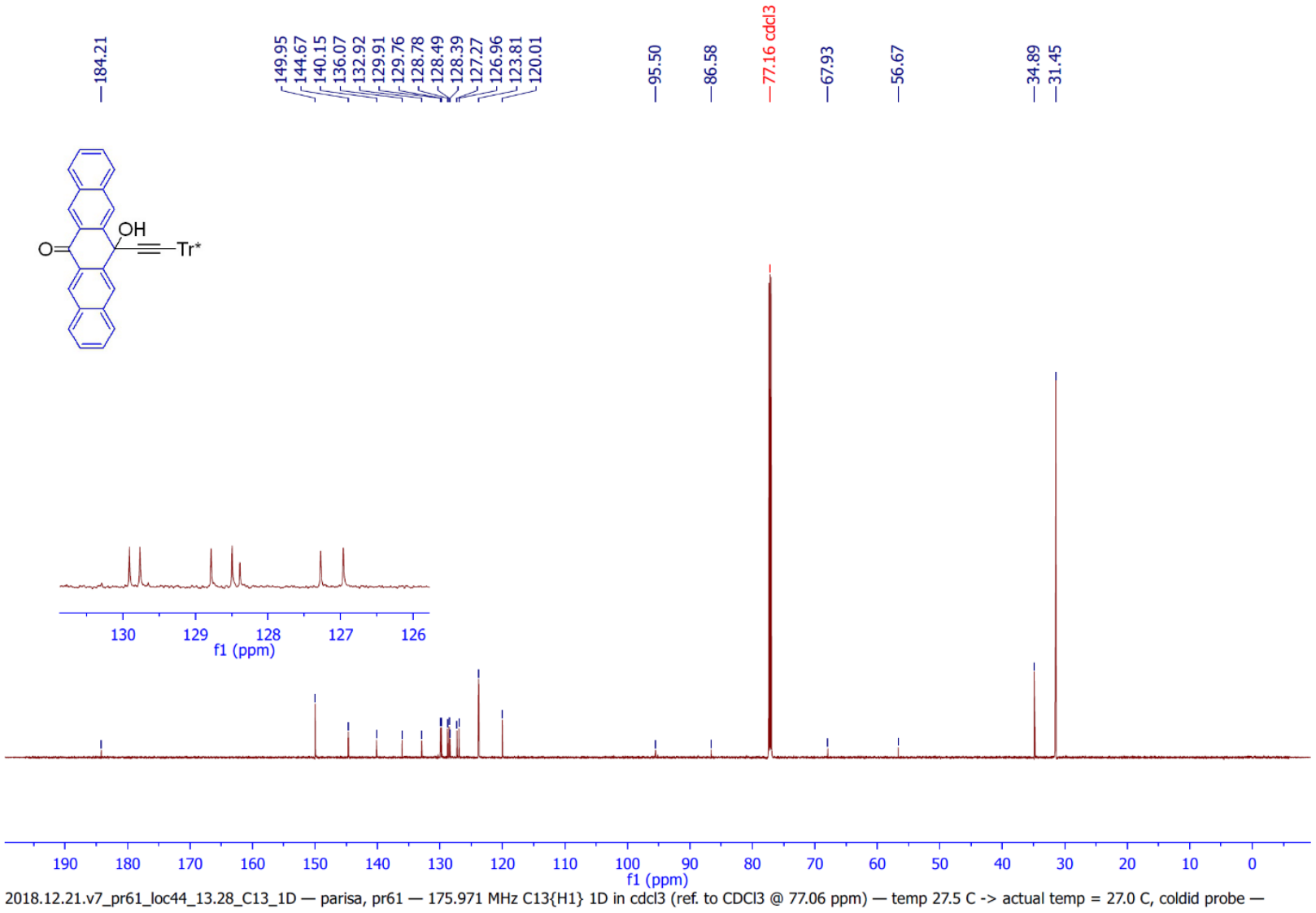

Figure N32. ^{13}C NMR spectrum of compound **2.16** by MestReNova software, 175 MHz, $CDCl_3$.

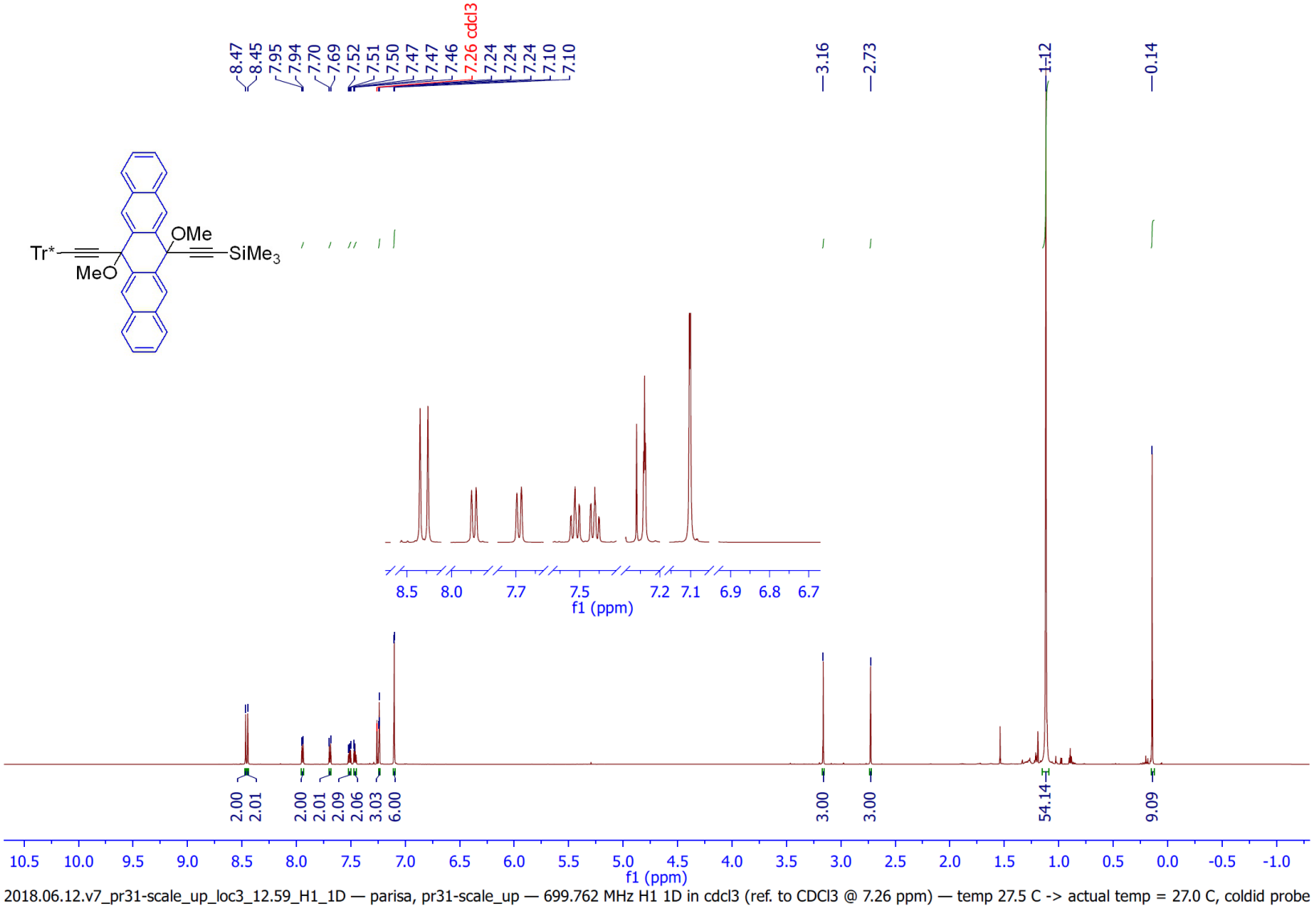

Figure N33. ^{1}H NMR spectrum of compound **2.17** by MestReNova software, 700 MHz, $CDCl_3$.

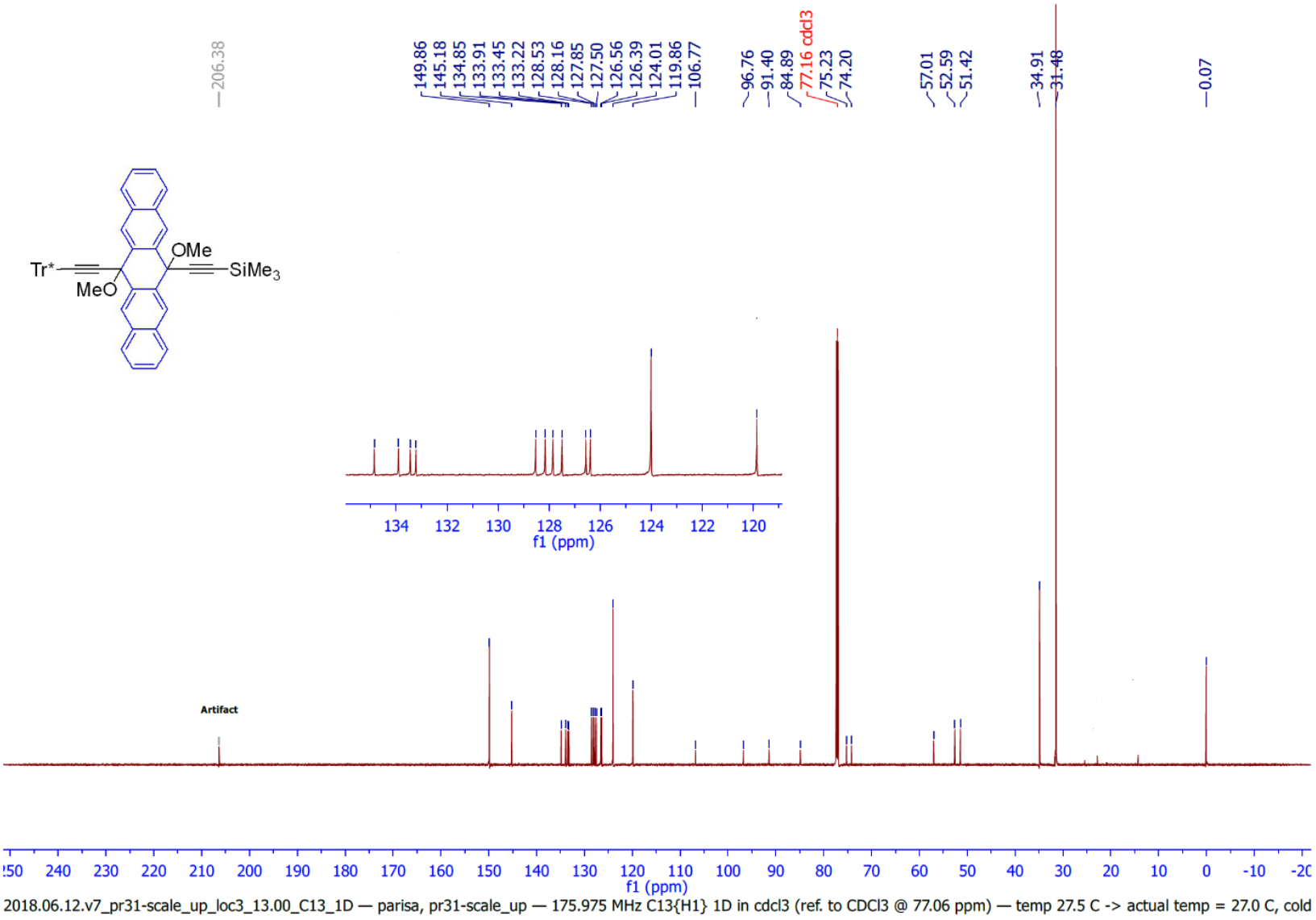

Figure N34. ^{13}C NMR spectrum of compound **2.17** by MestReNova software, 175 MHz, $CDCl_3$.

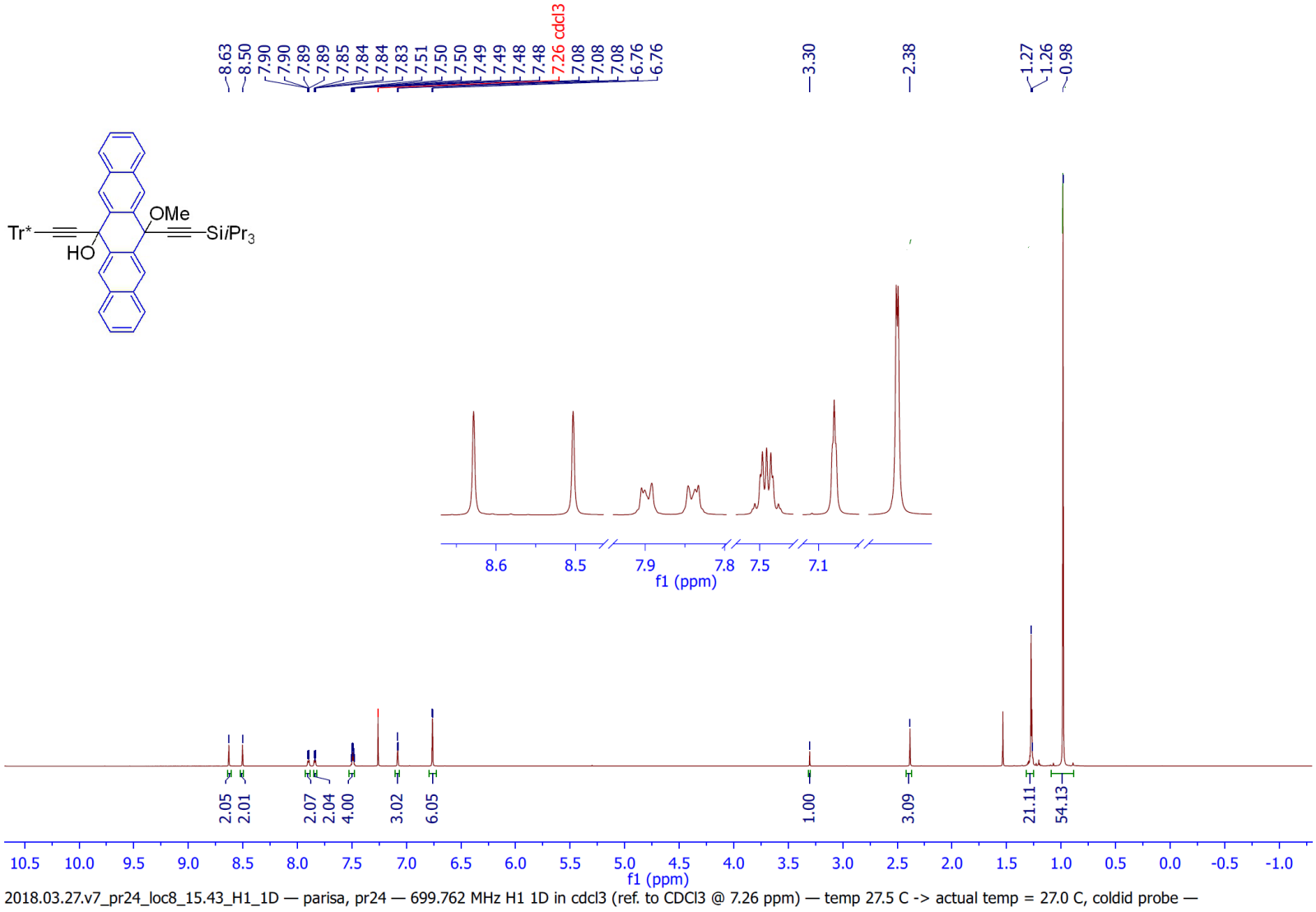

Figure N35. ^{1}H NMR spectrum of compound **2.18** by MestReNova software, 700 MHz, $CDCl_3$.

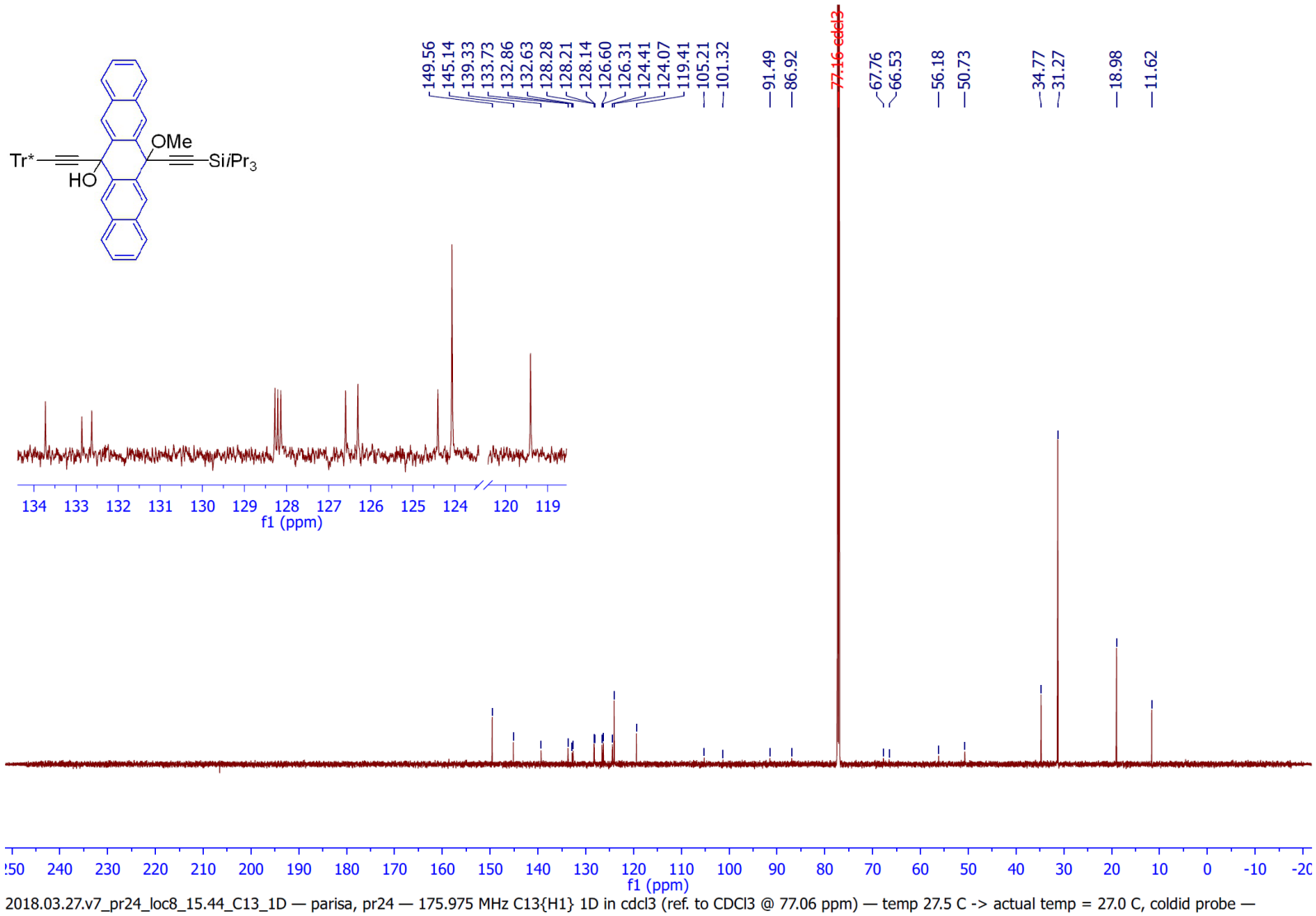

Figure N36. ^{13}C NMR spectrum of compound **2.18** by MestReNova software, 175 MHz, $CDCl_3$.

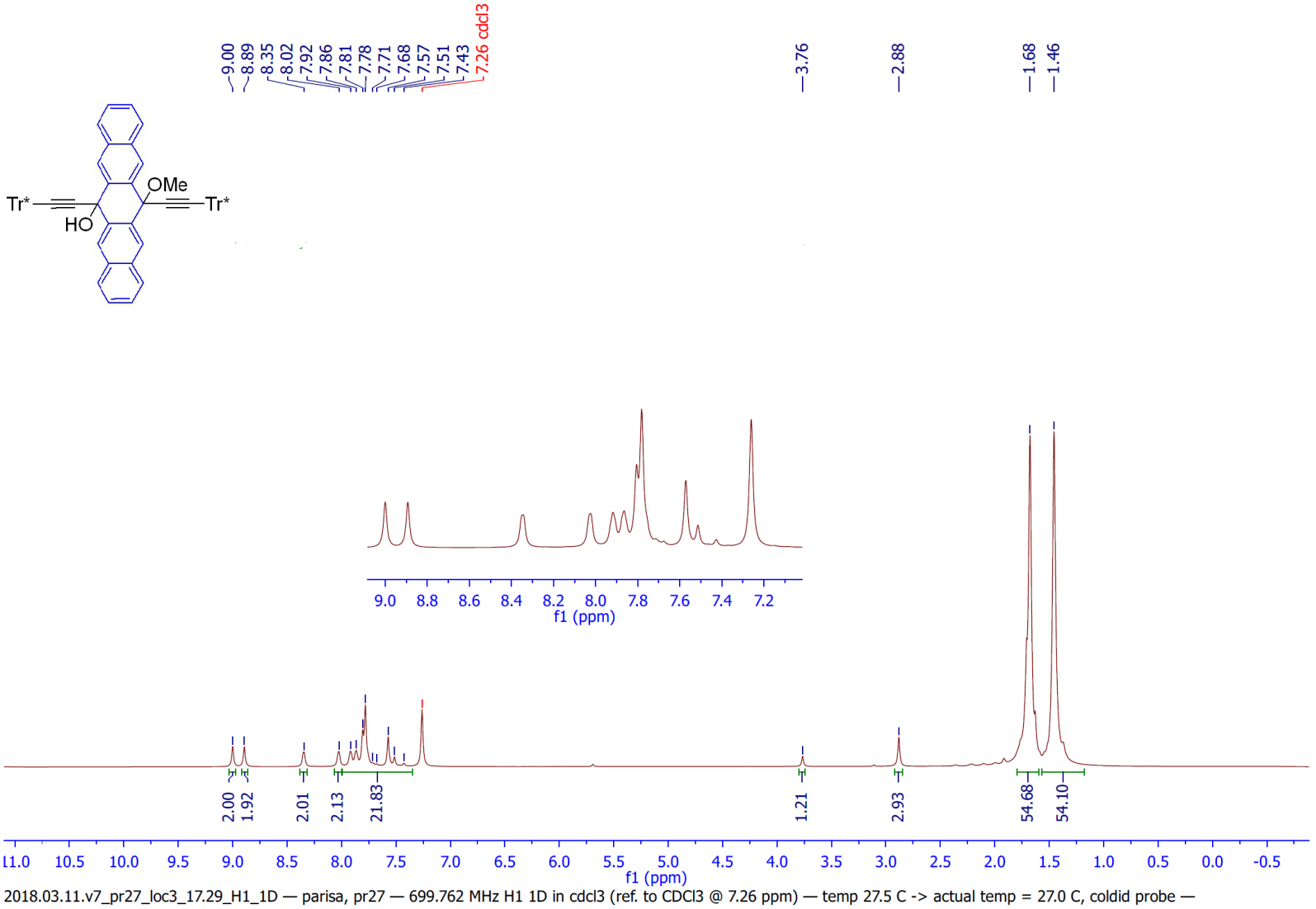

Figure N37. ^{1}H NMR spectrum of compound **2.19** by MestReNova software, 700 MHz, $CDCl_3$.

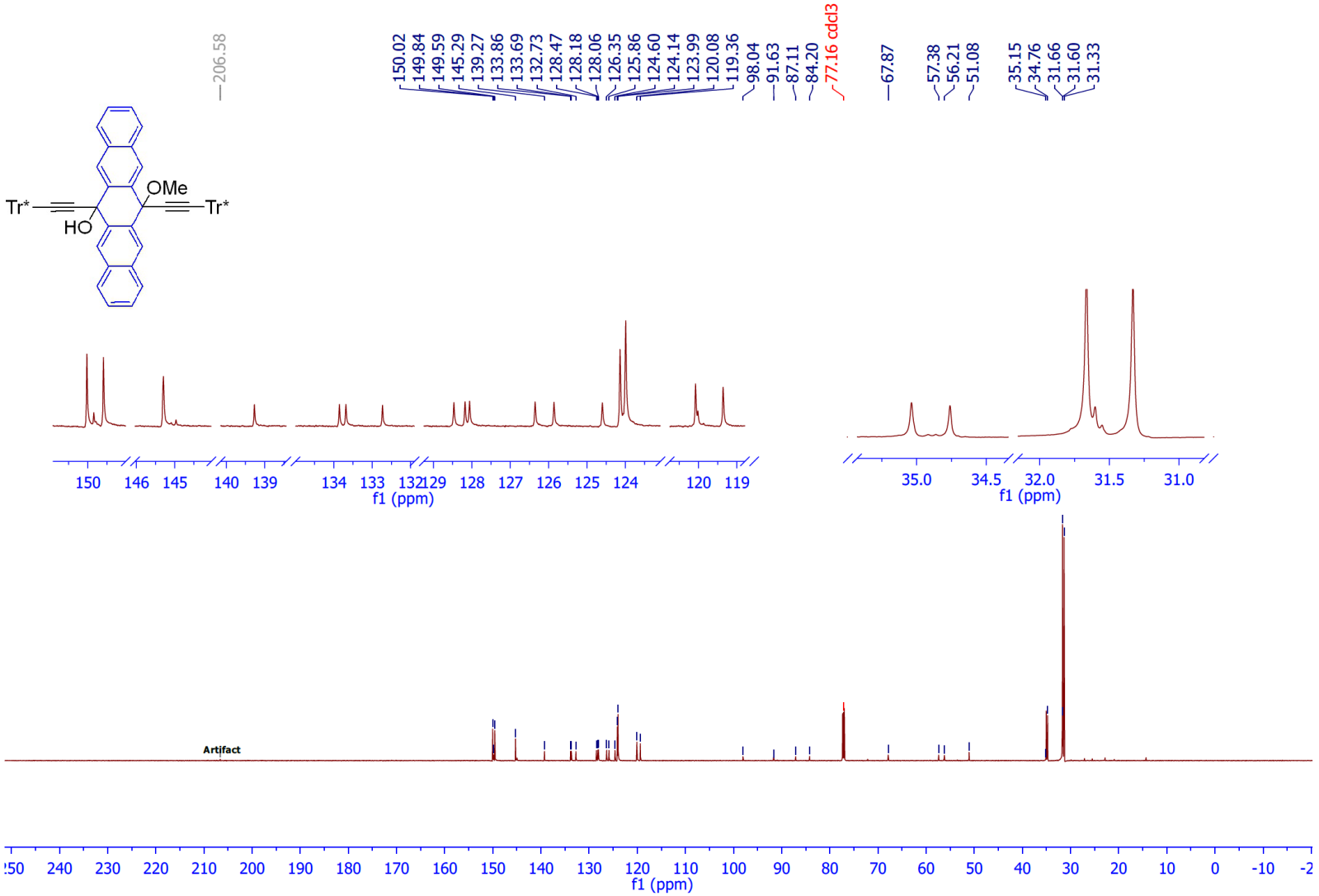

Figure N38. ^{13}C NMR spectrum of compound **2.19** by MestReNova software, 175 MHz, $CDCl_3$.

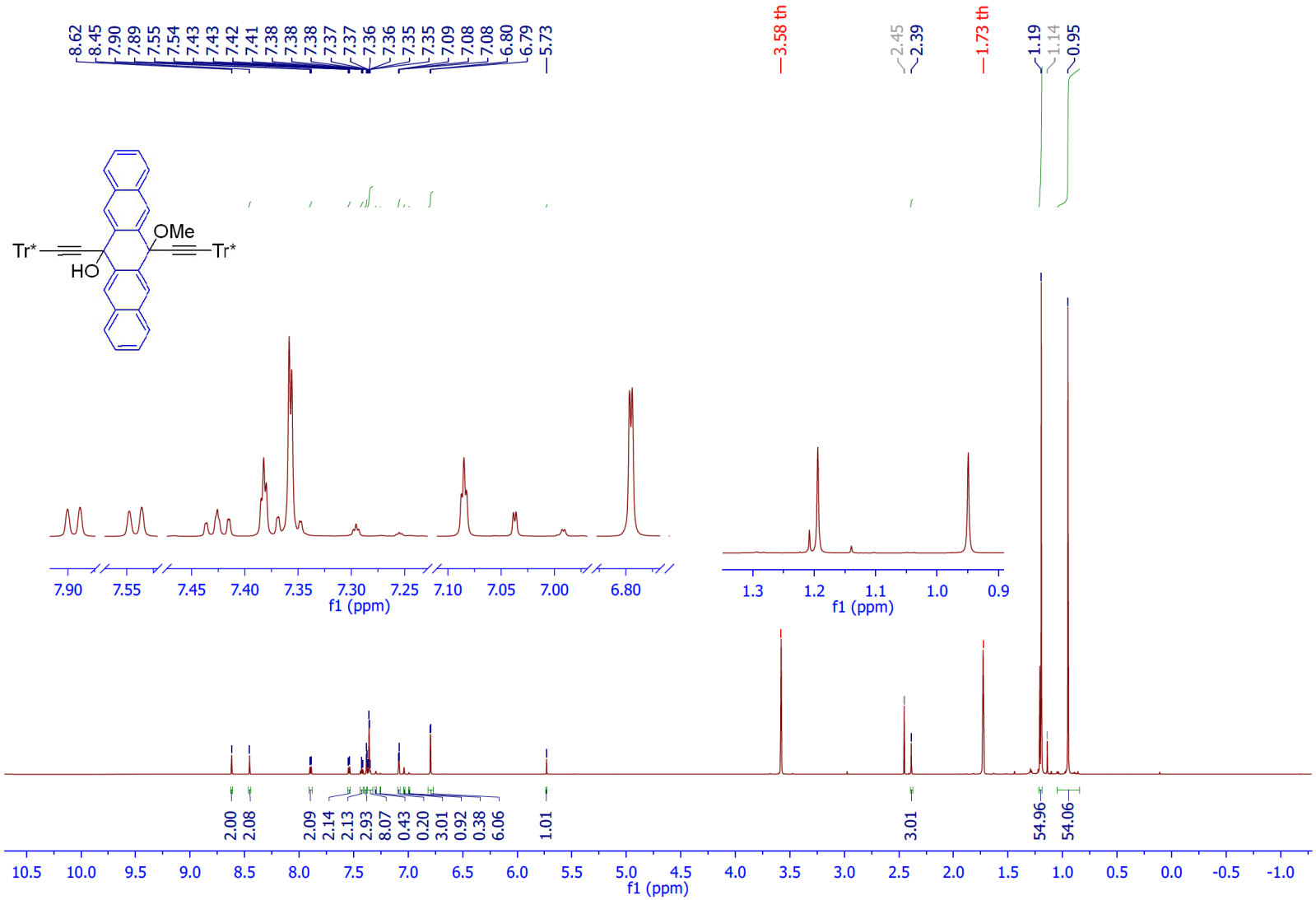

Figure N39. ^{1}H NMR spectrum of compound **2.19** by MestReNova software, 700 MHz, THF-d_8.

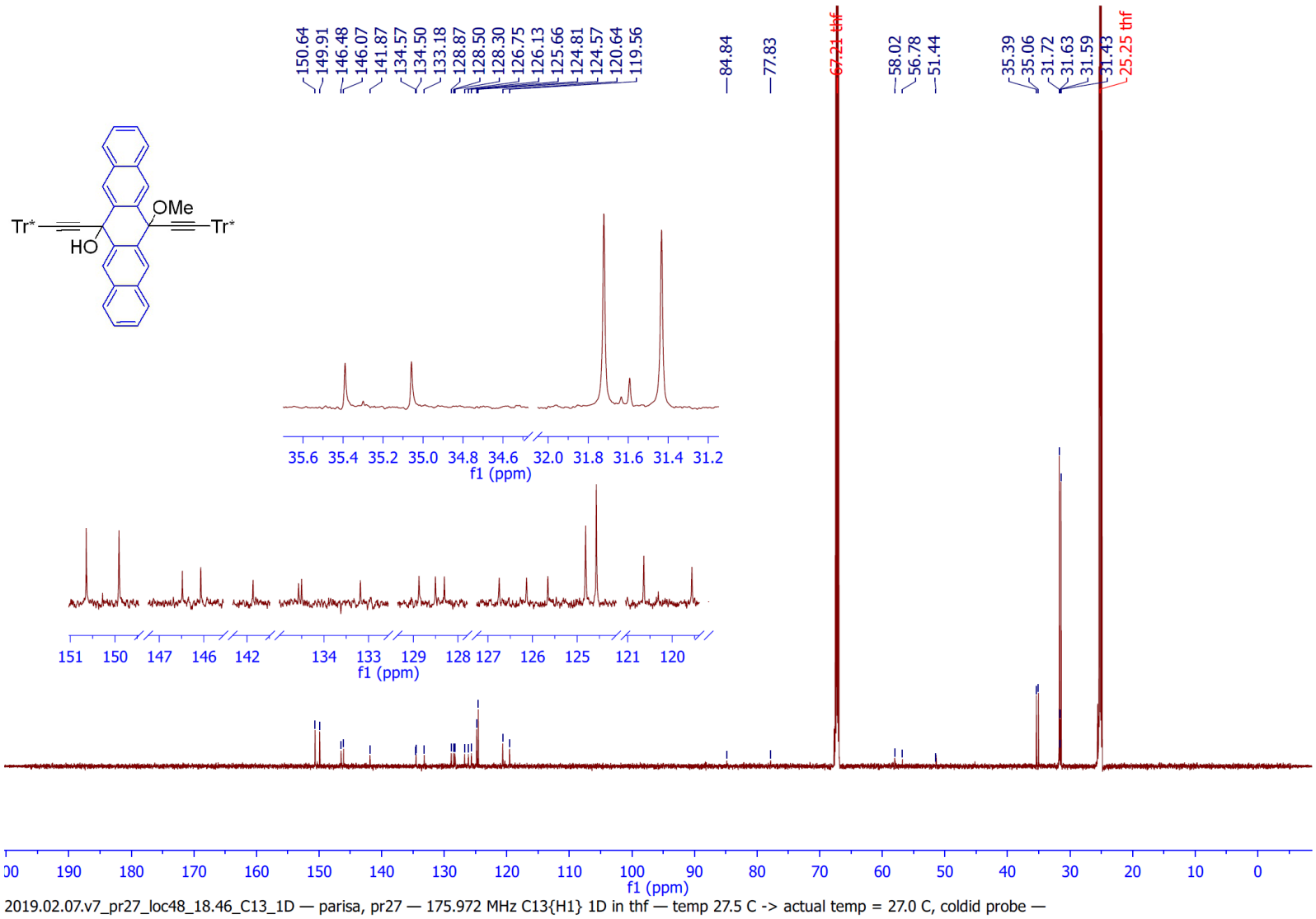

Figure N40. ^{13}C NMR spectrum of compound **2.19** by MestReNova software, 175 MHz, THF-d_8.

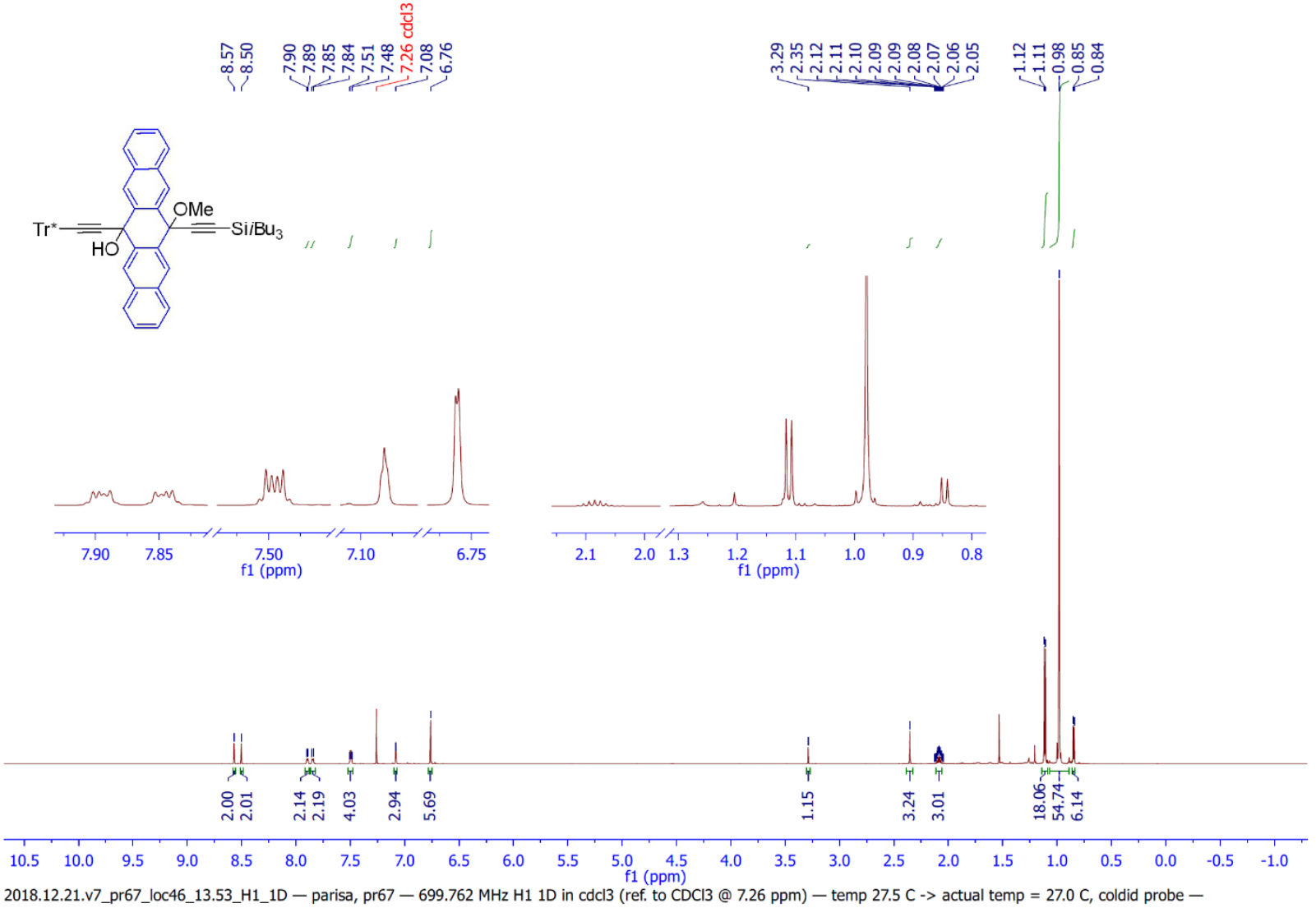

Figure N41. ^{1}H NMR spectrum of compound **2.20** by MestReNova software, 700 MHz, $CDCl_3$.

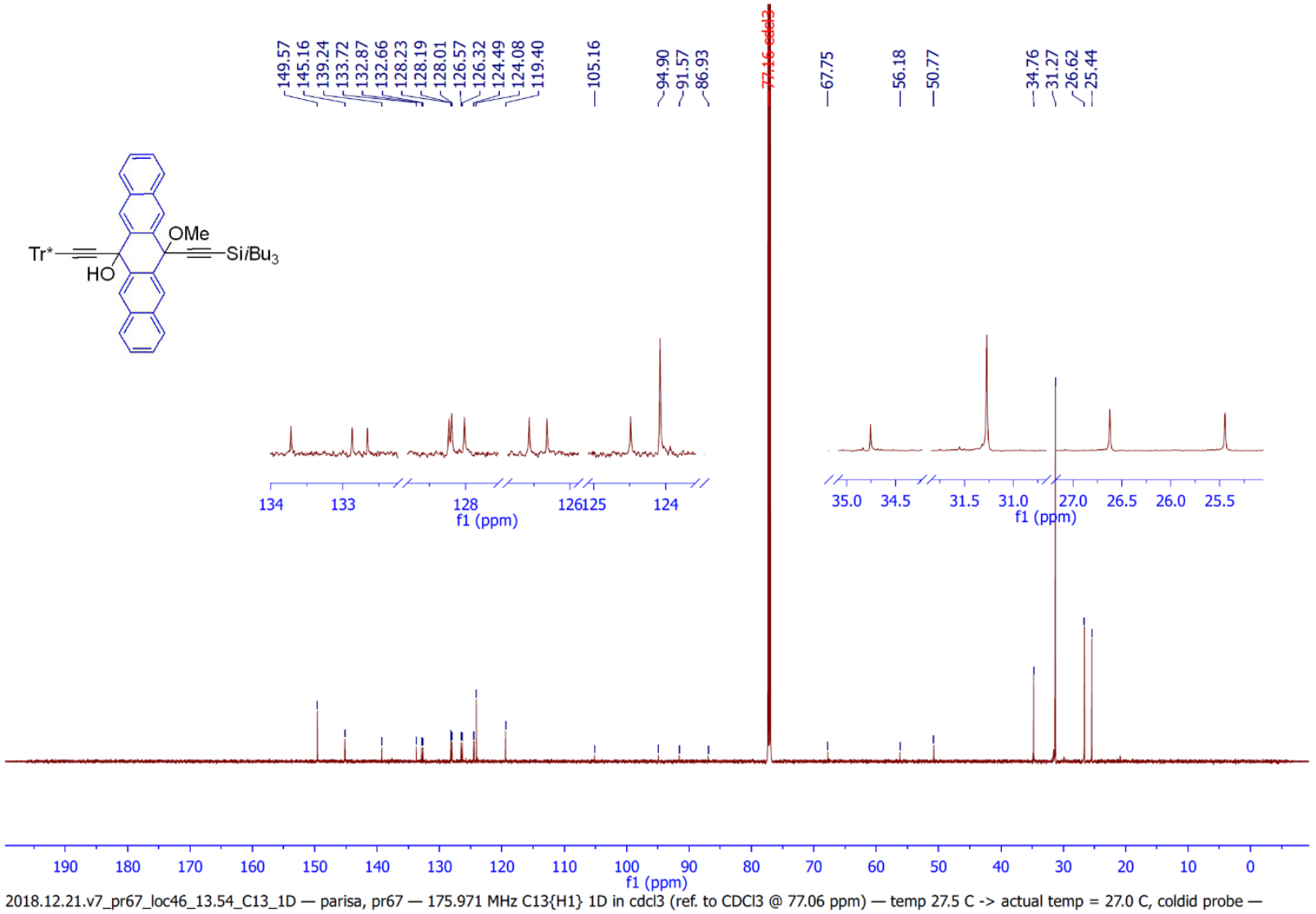

Figure N42. ^{13}C NMR spectrum of compound **2.20** by MestReNova software, 175 MHz, $CDCl_3$.

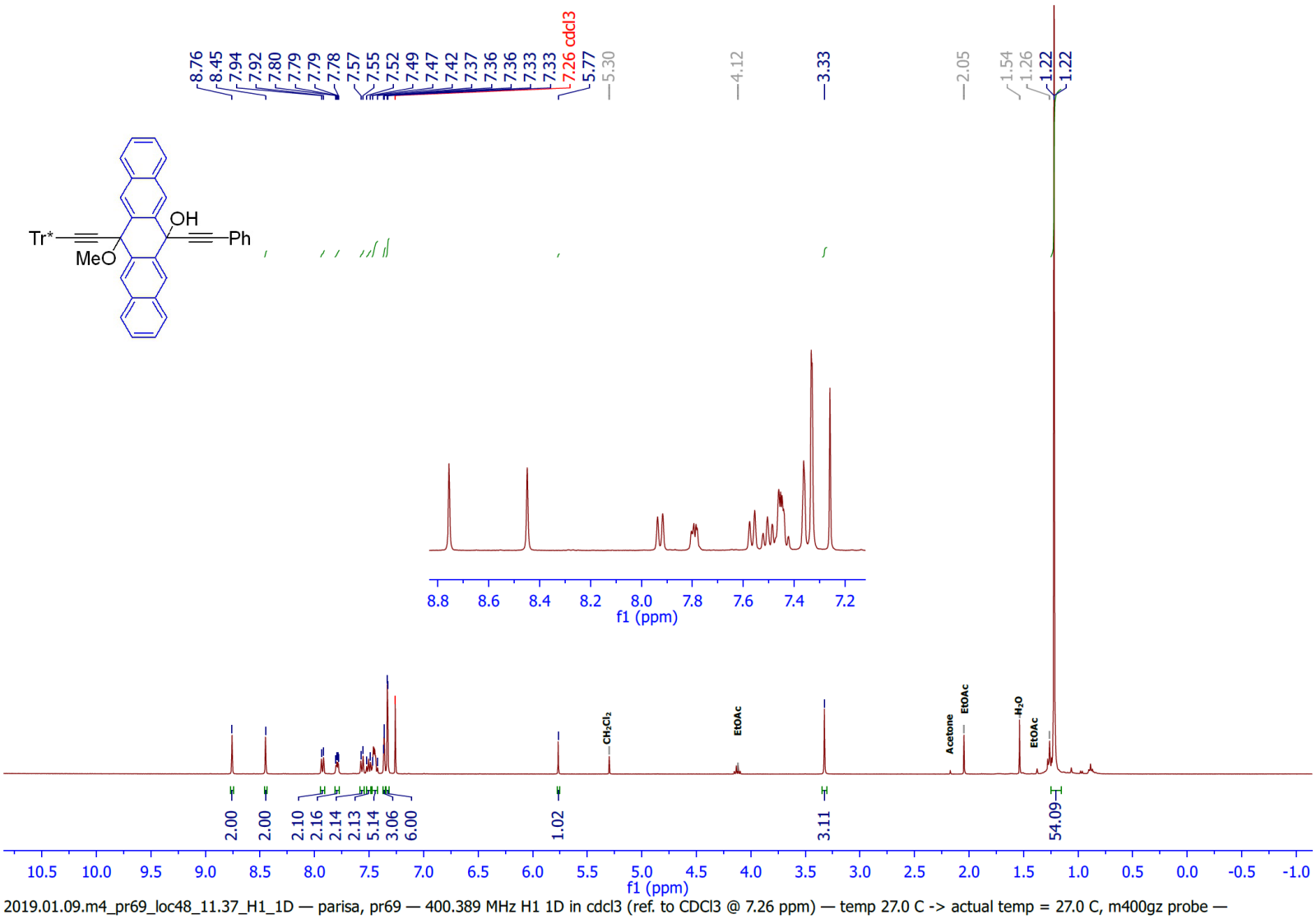

Figure N43. ^{1}H NMR spectrum of compound **2.21** by MestReNova software, 400 MHz, $CDCl_3$.

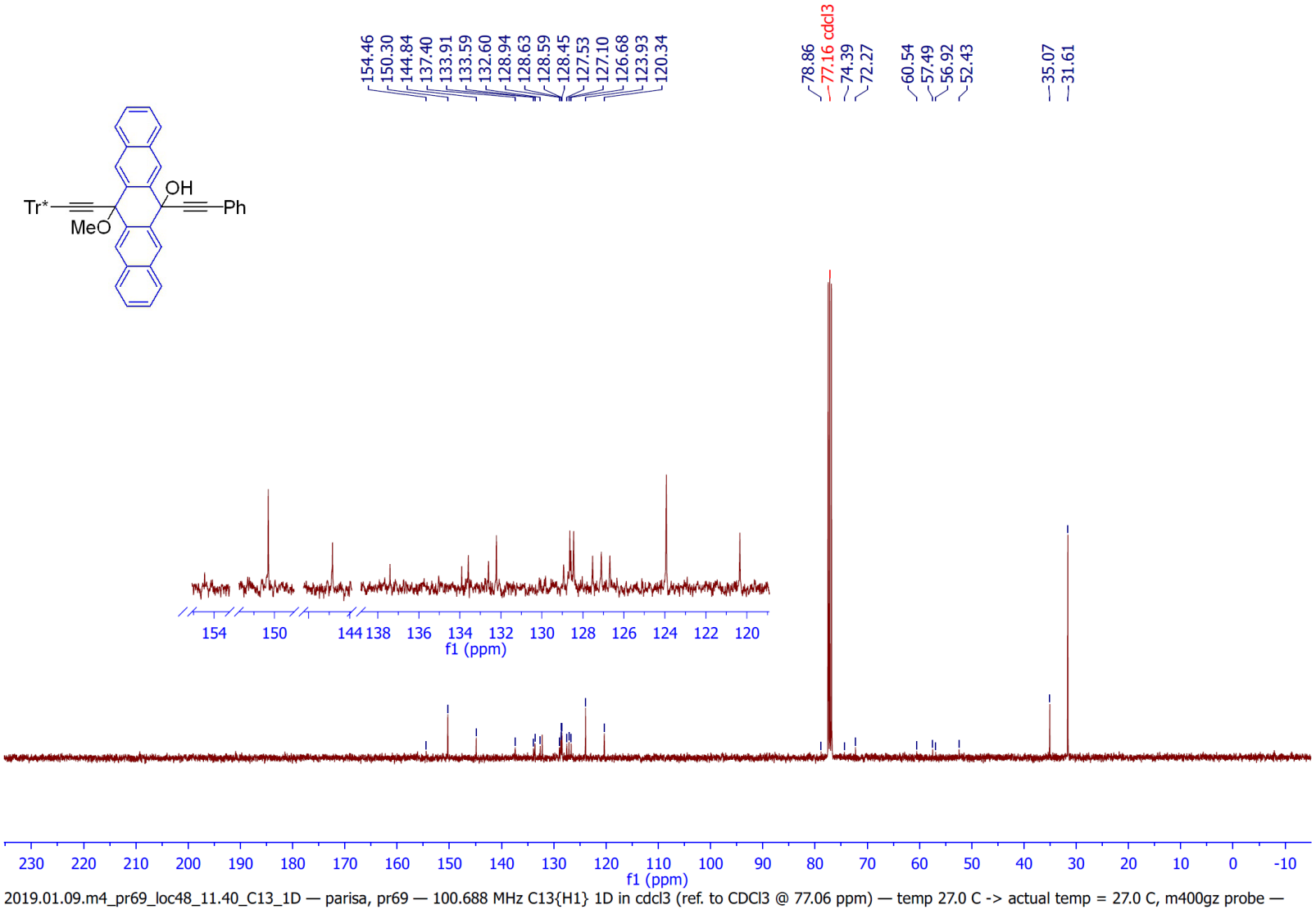

Figure N44. ^{13}C NMR spectrum of compound **2.21** by MestReNova software, 100 MHz, $CDCl_3$.

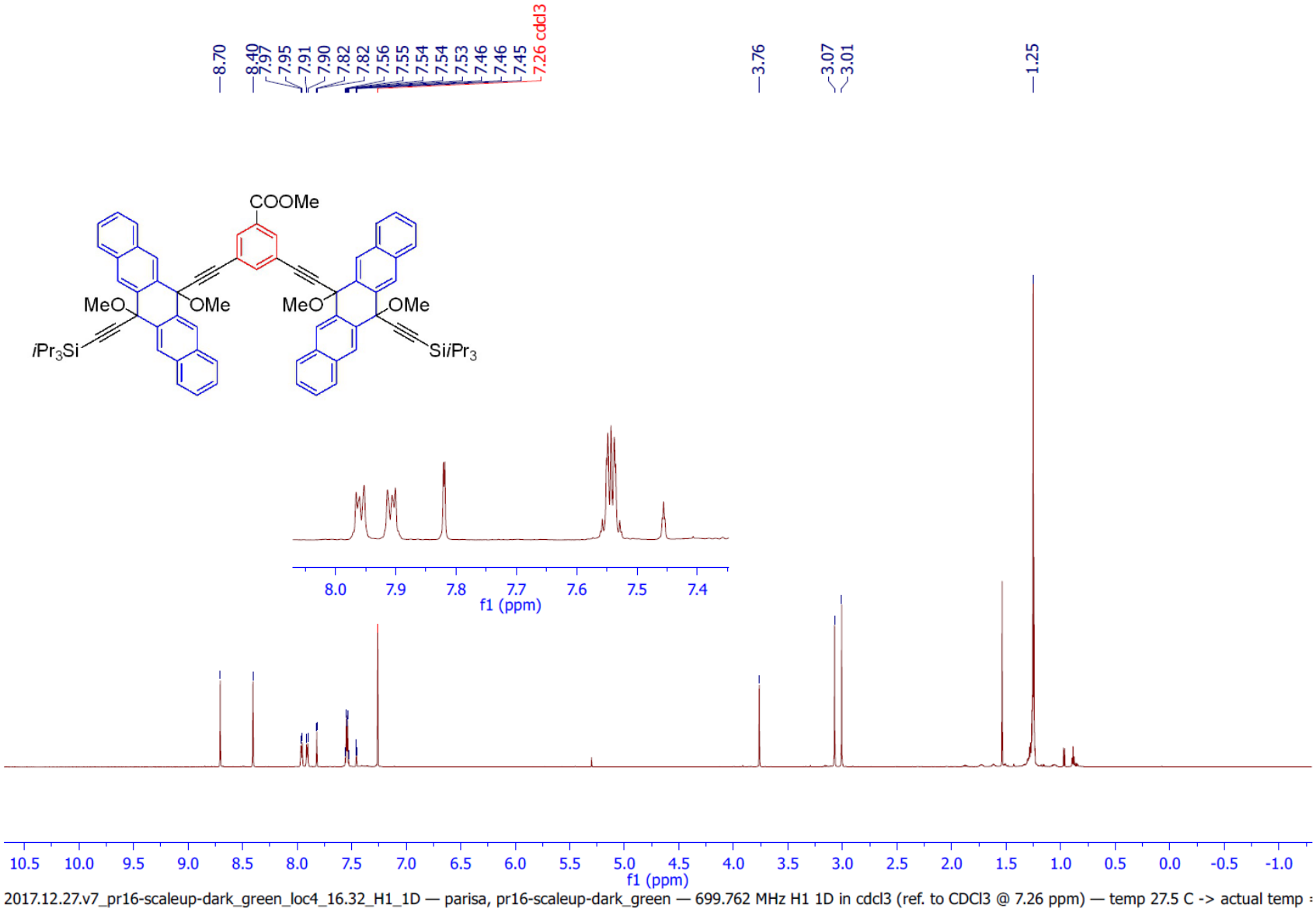

Figure N45. ^{1}H NMR spectrum of compound **3.1** by MestReNova software, 700 MHz, $CDCl_3$.

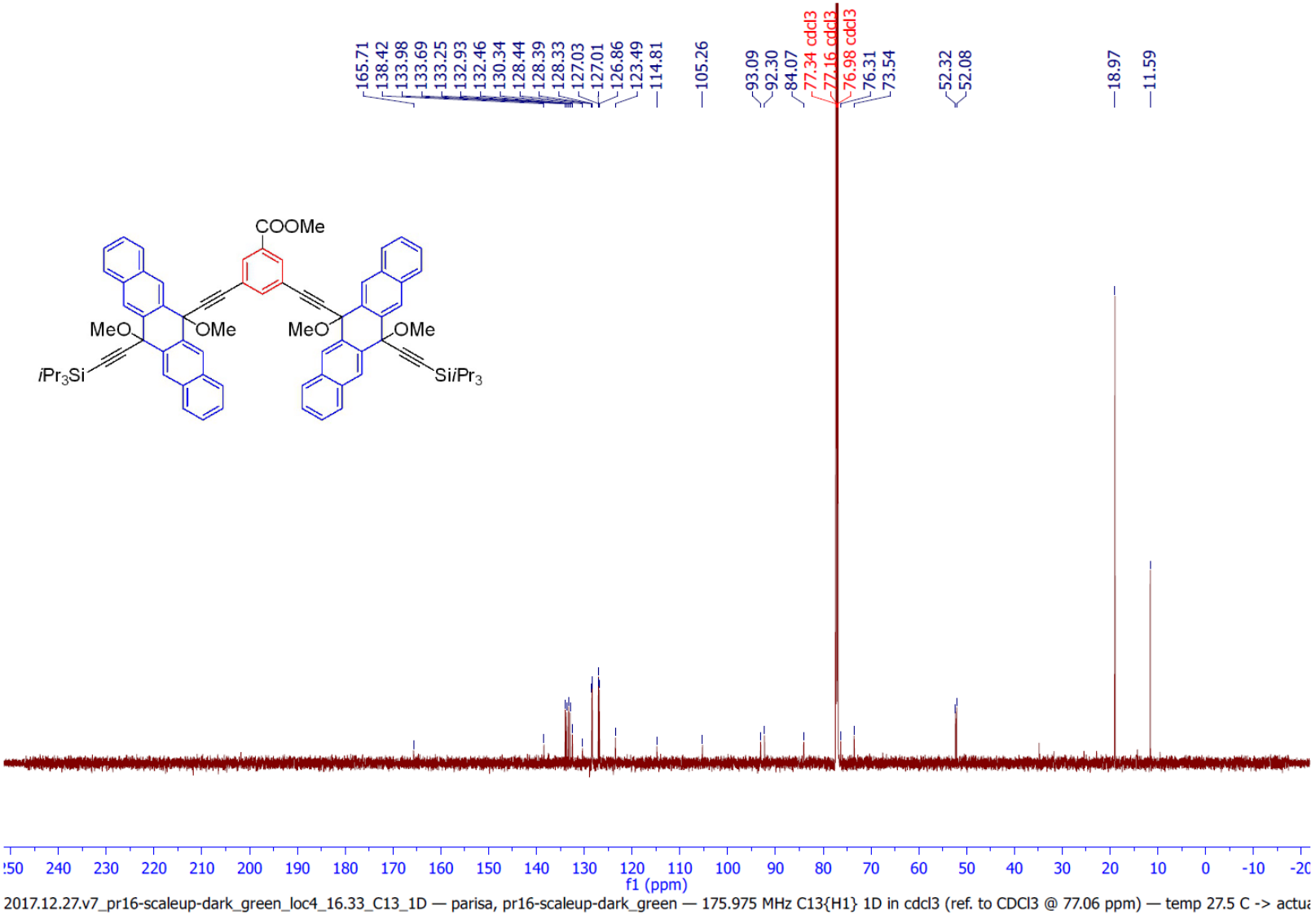

Figure N46. ^{13}C NMR spectrum of compound **3.1** by MestReNova software, 175 MHz, $CDCl_3$.

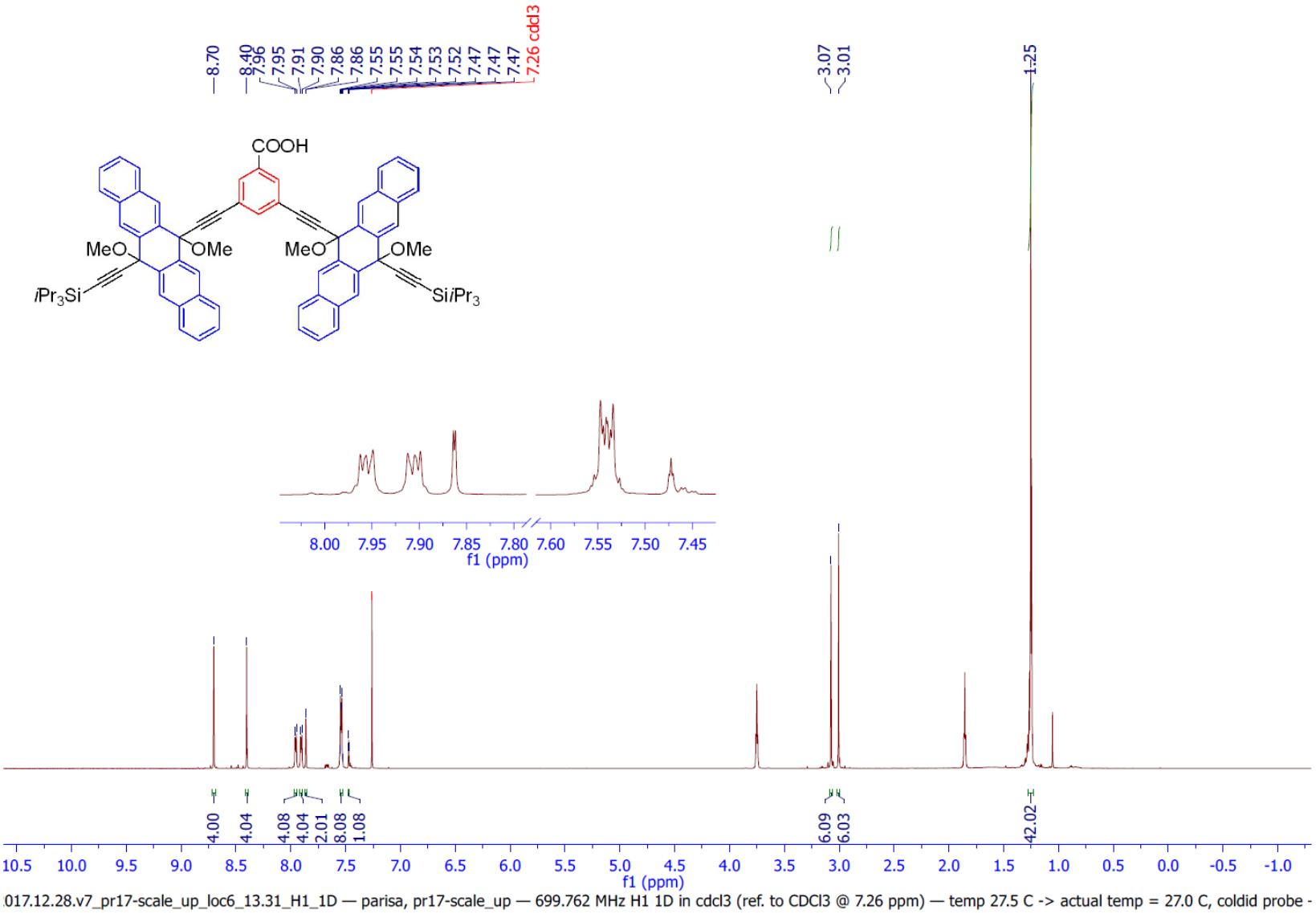

Figure N47. ^{1}H NMR spectrum of compound **3.2** by MestReNova software, 700 MHz, $CDCl_3$.

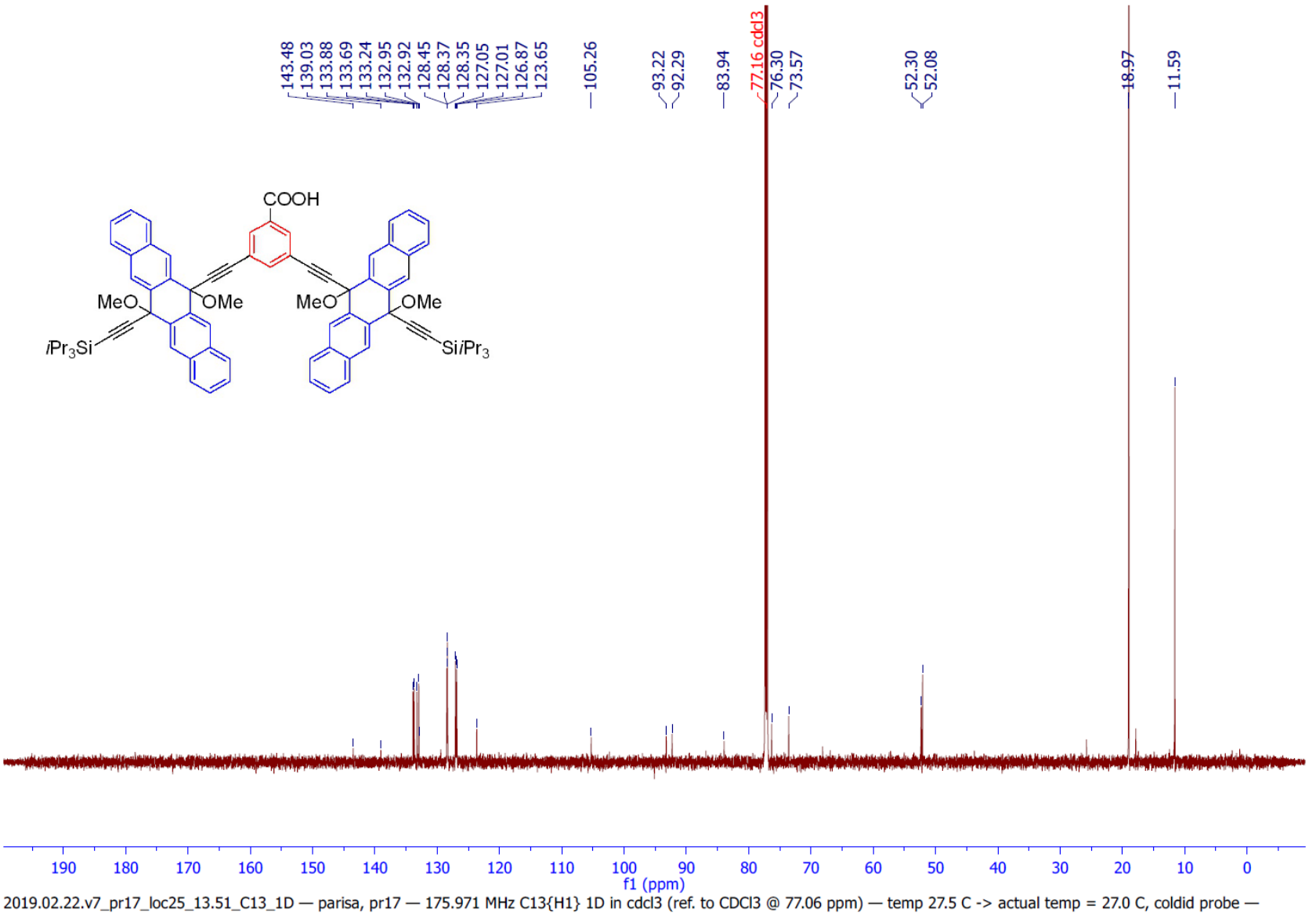

Figure N48. ^{13}C NMR spectrum of compound **3.2** by MestReNova software, 175 MHz, $CDCl_3$.

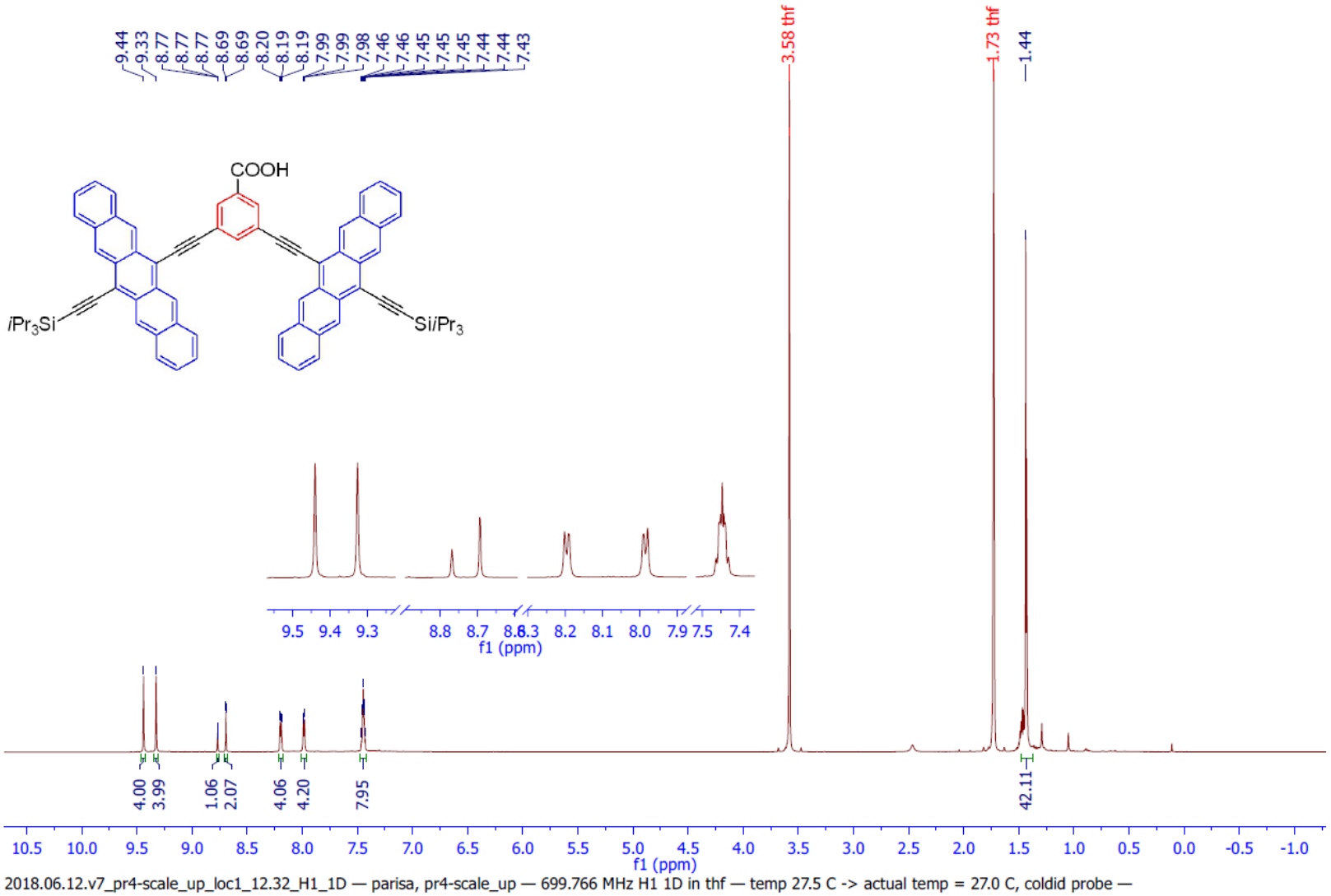

Figure N49. ^{1}H NMR spectrum of compound **TIPS-Pnc$_2$** by MestReNova software, 700 MHz, THF-d_8.

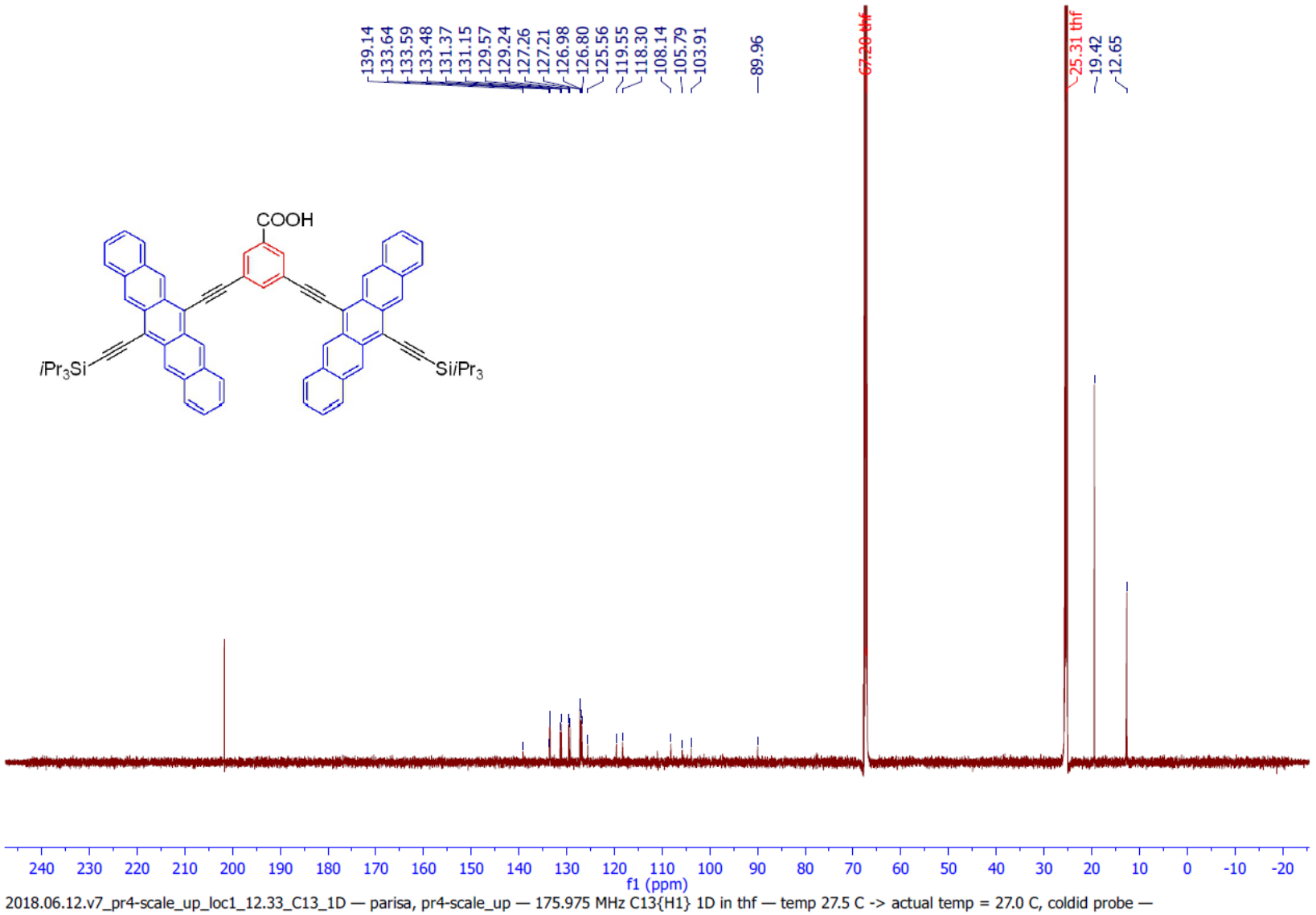

Figure N50. ^{13}C NMR spectrum of compound **TIPS-Pnc$_2$** by MestReNova software, 175 MHz, THF-d_8.

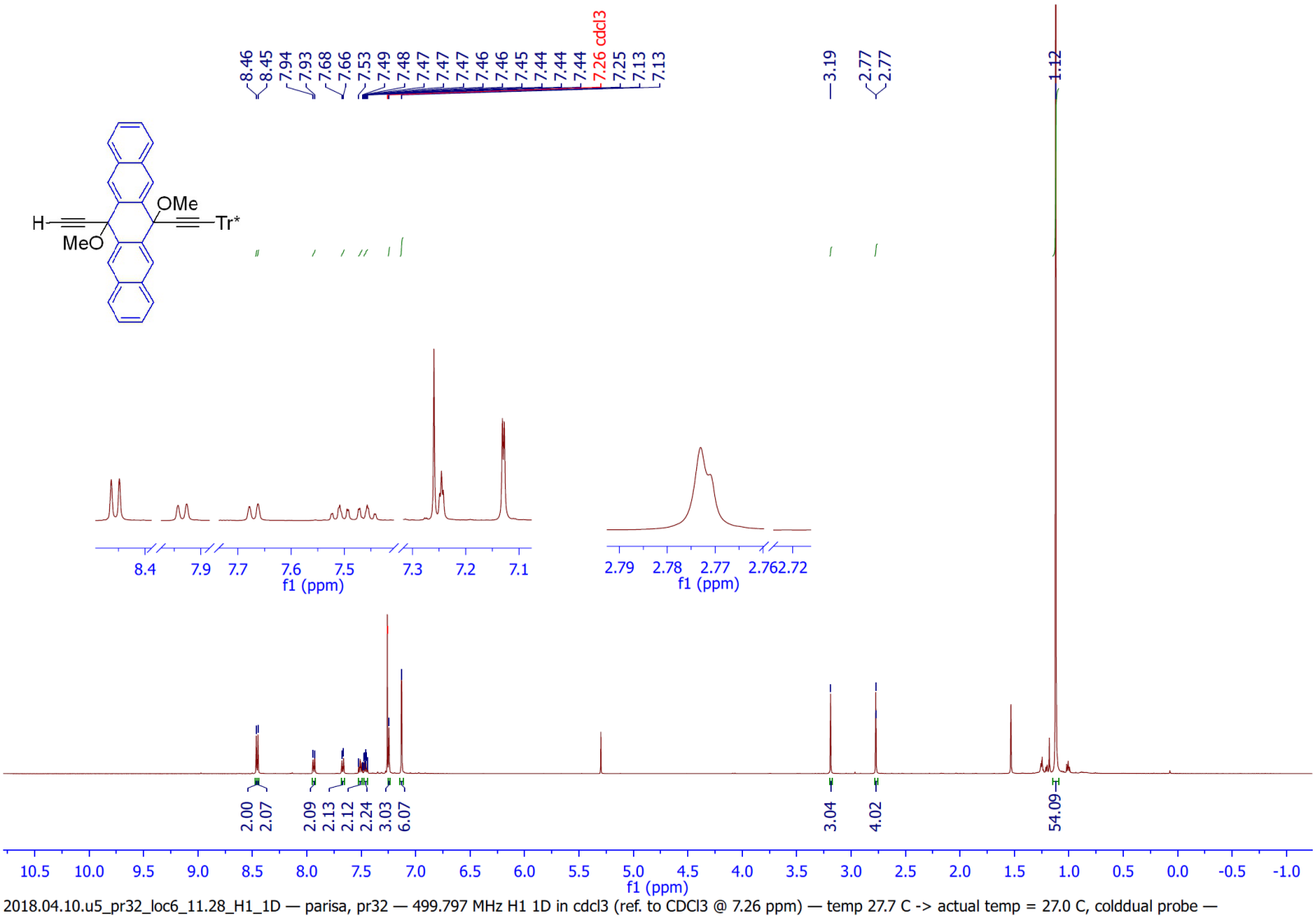

Figure N51. ^{1}H NMR spectrum of compound **3.3** by MestReNova software, 500 MHz, $CDCl_3$.

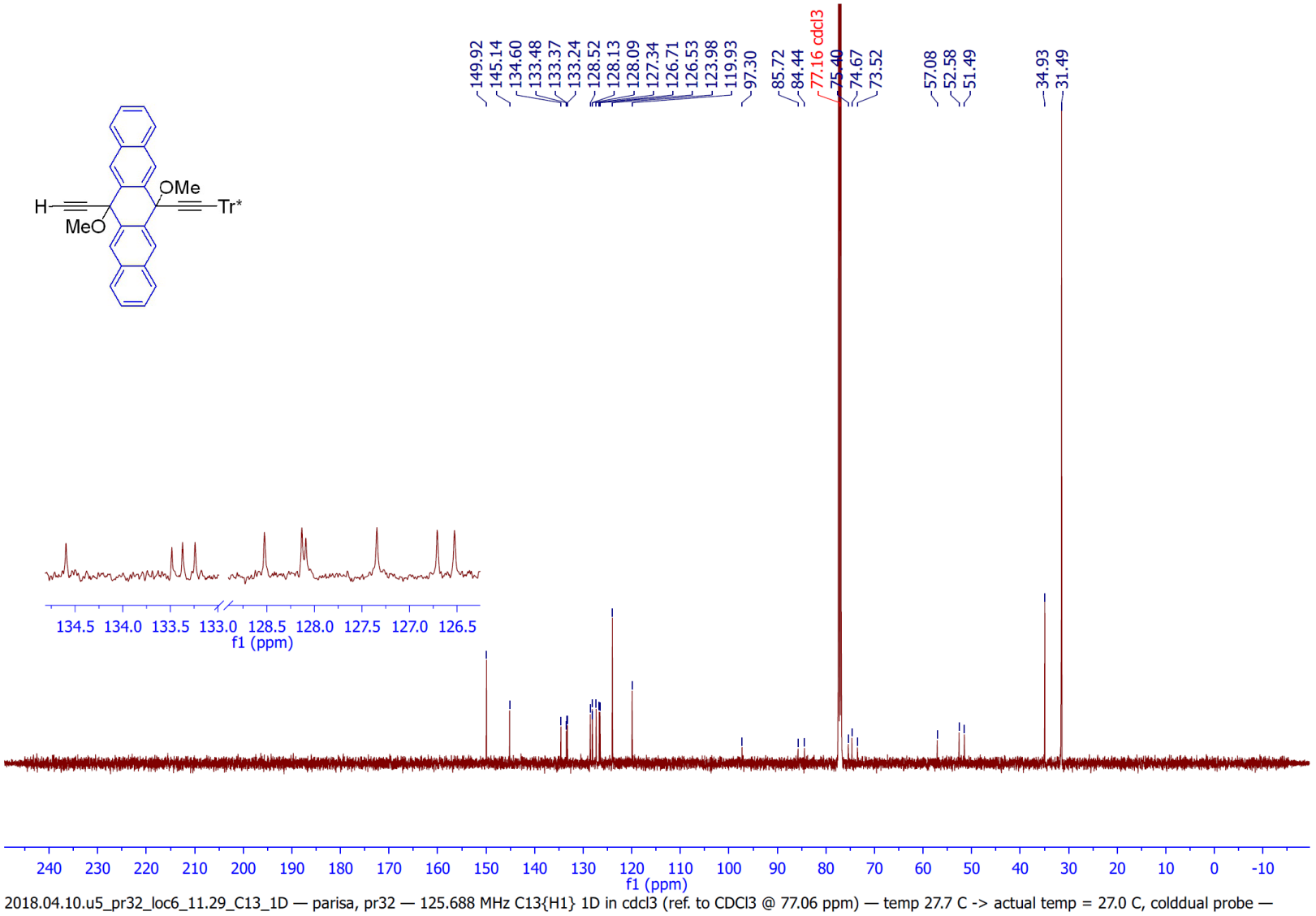

Figure N52. ^{13}C NMR spectrum of compound **3.3** by MestReNova software, 125 MHz, $CDCl_3$.

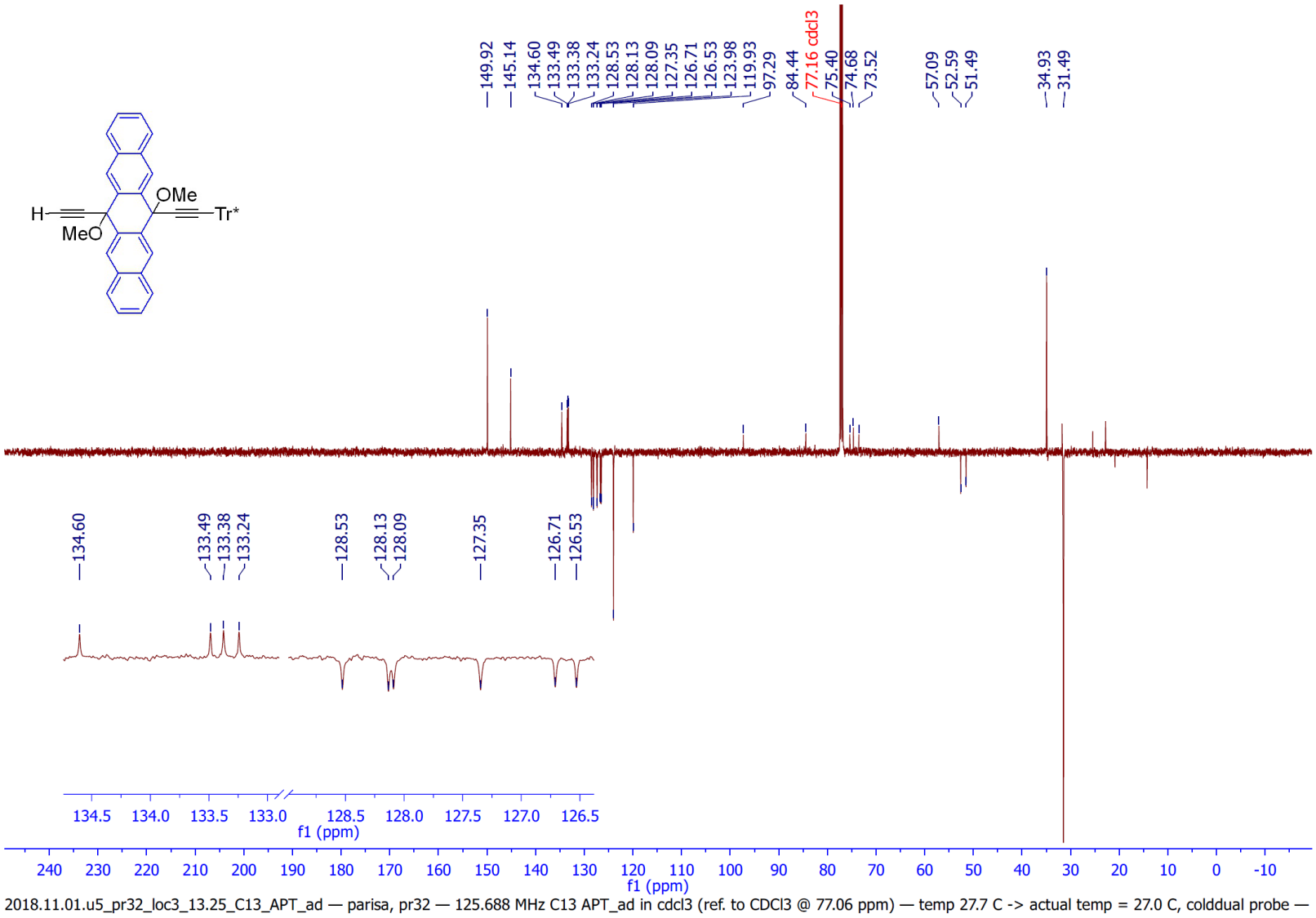

Figure N53. ^{13}C NMR APT spectrum of compound **3.3** by MestReNova software, 125 MHz, $CDCl_3$.

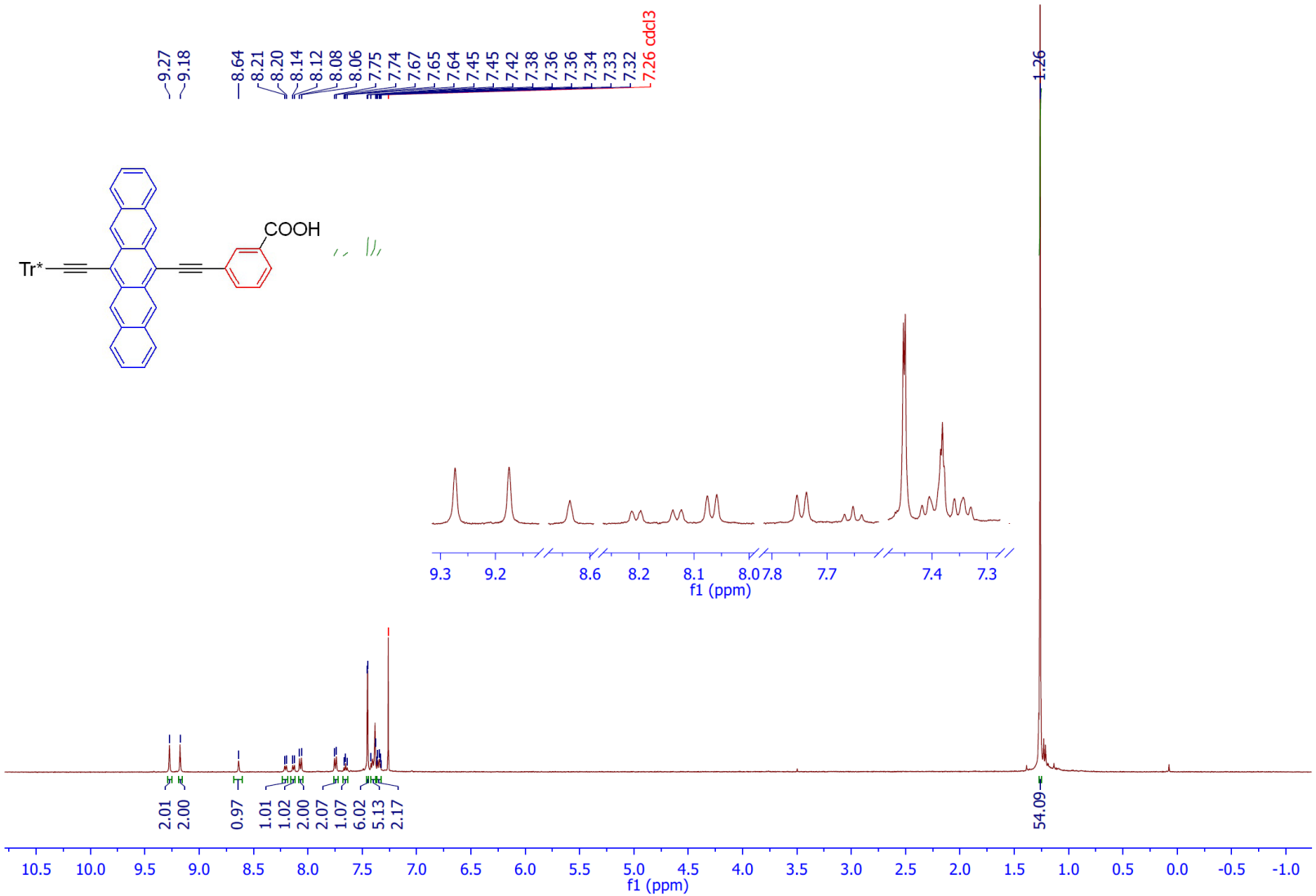

Figure N54. ^{1}H NMR spectrum of compound **3.4** by MestReNova software, 500 MHz, $CDCl_3$.

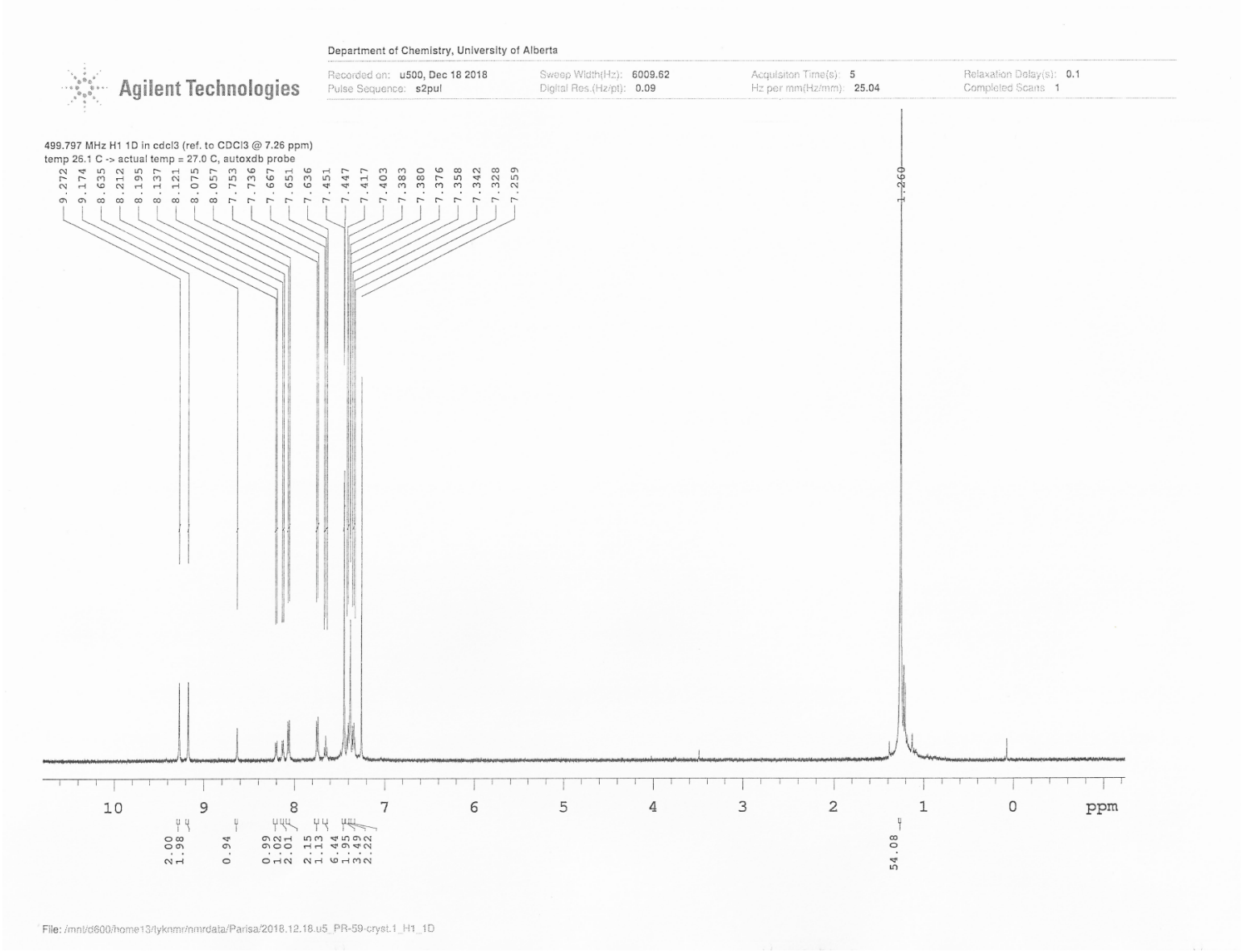

Figure N55. Original ^{1}H NMR spectrum of compound **3.4**, 500 MHz, $CDCl_3$.

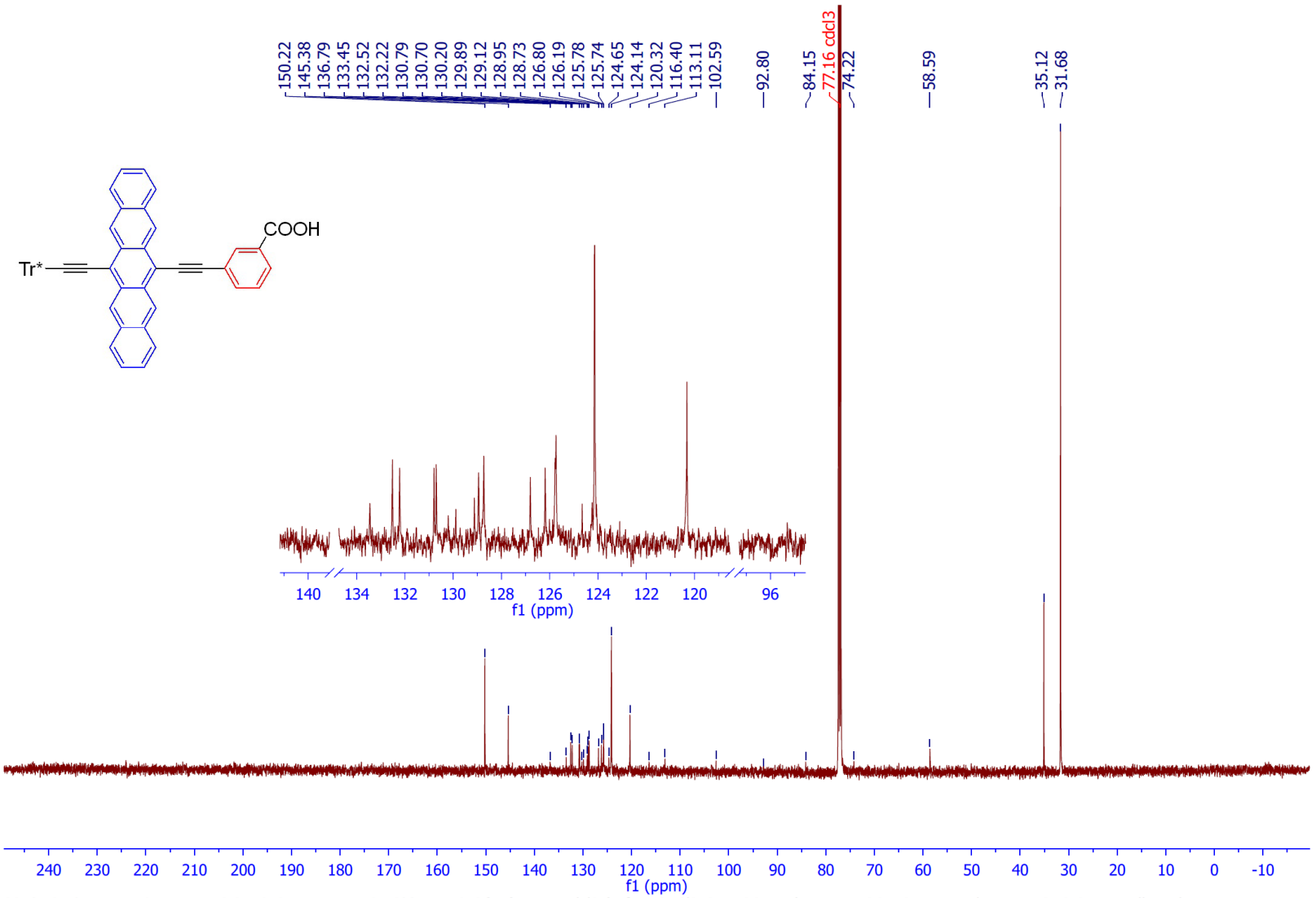

Figure N56. ^{13}C NMR spectrum of compound **3.4** by MestReNova software, 125 MHz, $CDCl_3$.

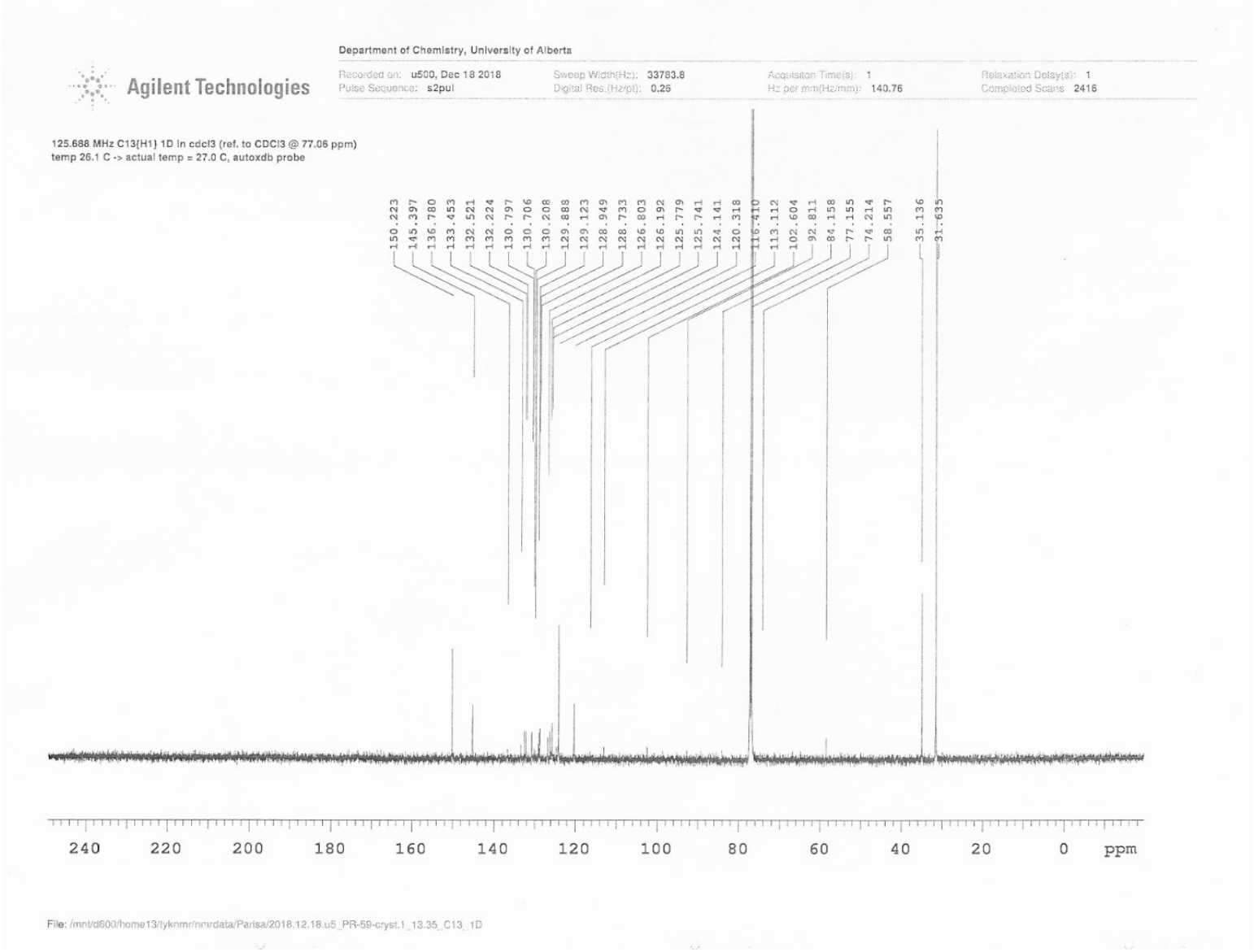

Figure N57. Original ^{13}C NMR spectrum of compound **3.4**, 125 MHz, $CDCl_3$.

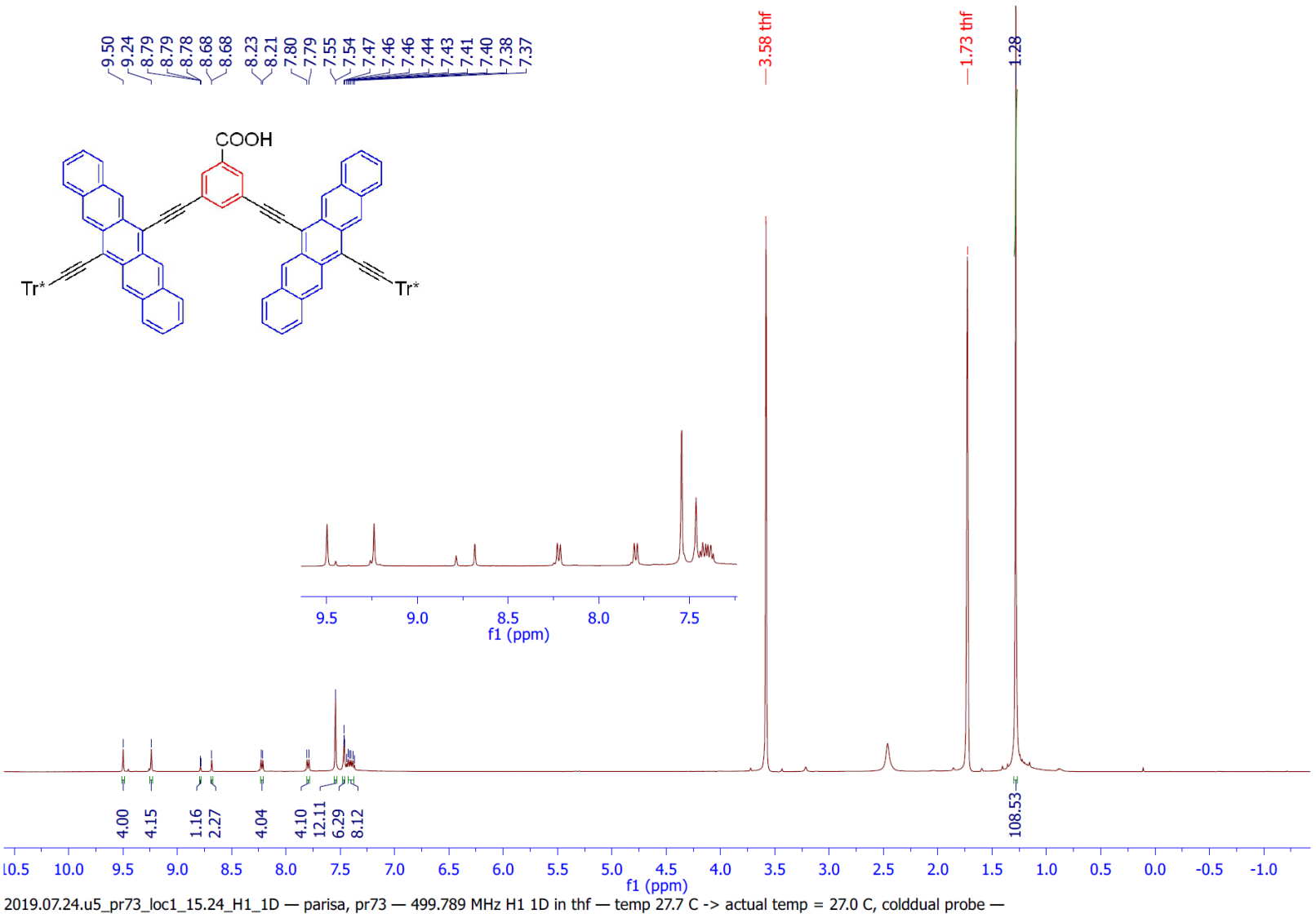

Figure N58. ^{1}H NMR spectrum of compound **Tr*-Pnc$_2$** by MestReNova software, 500 MHz, THF-d_8.

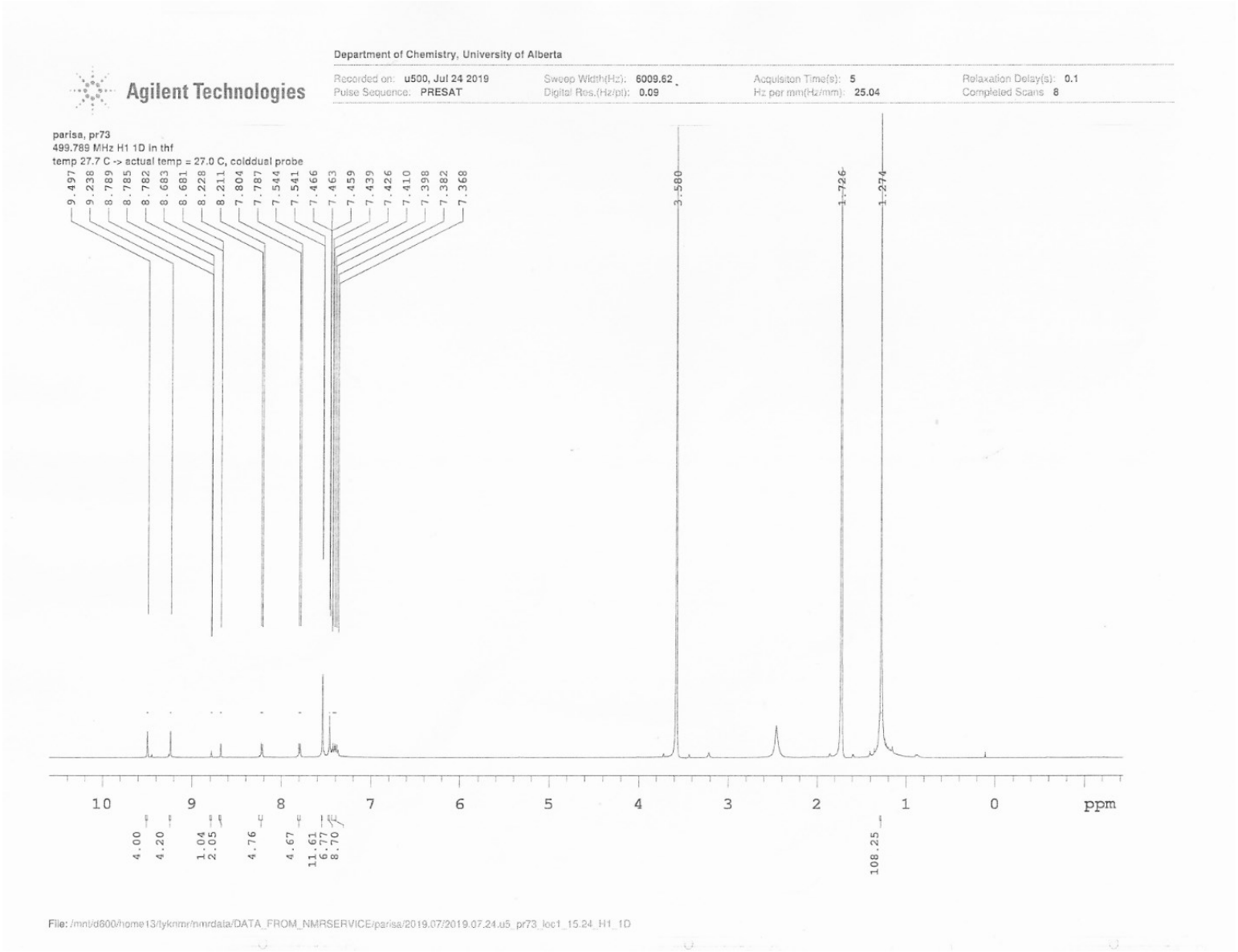

Figure N59. Original ^{1}H NMR spectrum of compound **Tr*-Pnc$_2$**, 500 MHz, THF-d_8.

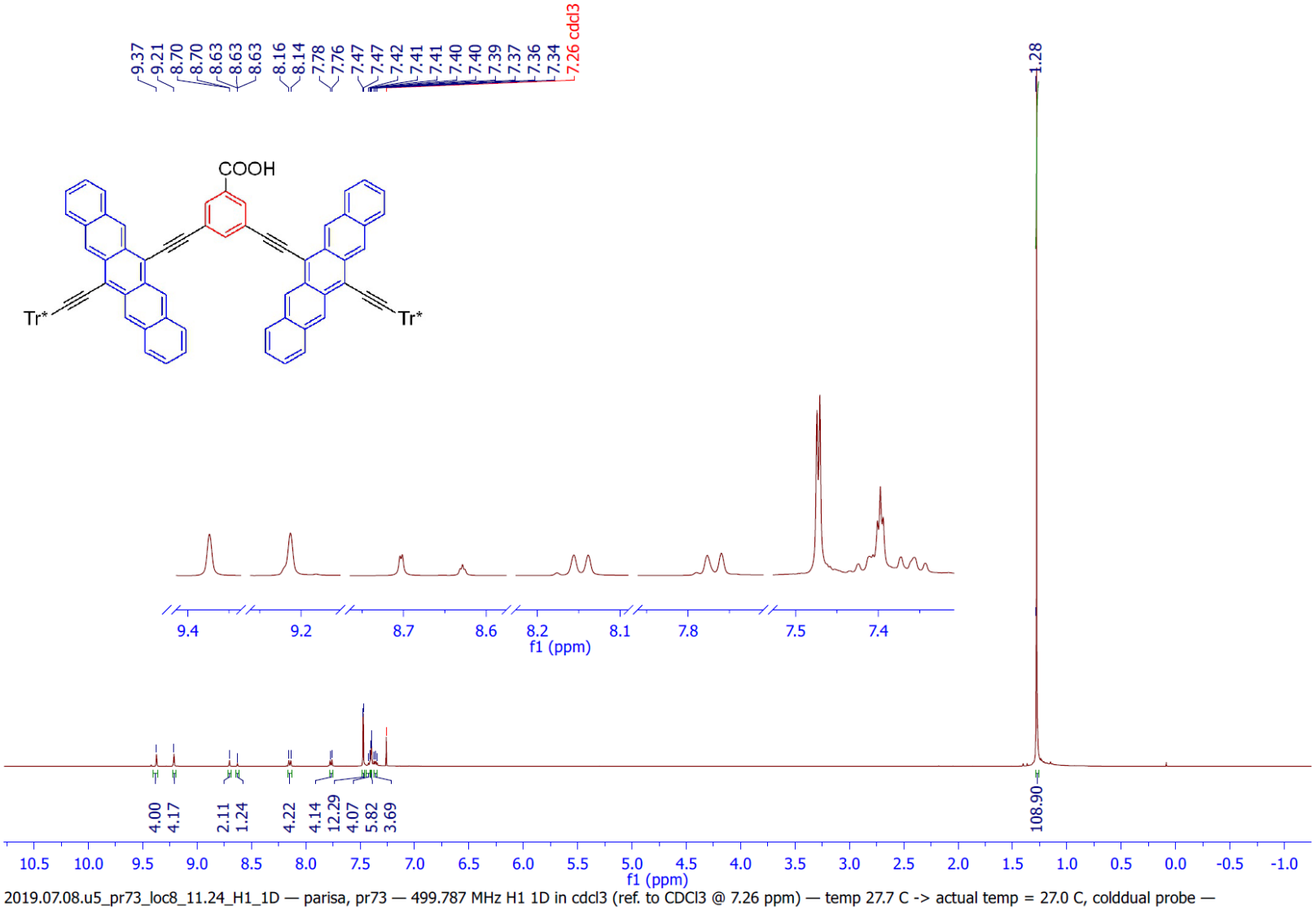

Figure N60. ^{1}H NMR spectrum of compound **Tr*-Pnc$_2$** by MestReNova software, 500 MHz, $CDCl_3$.

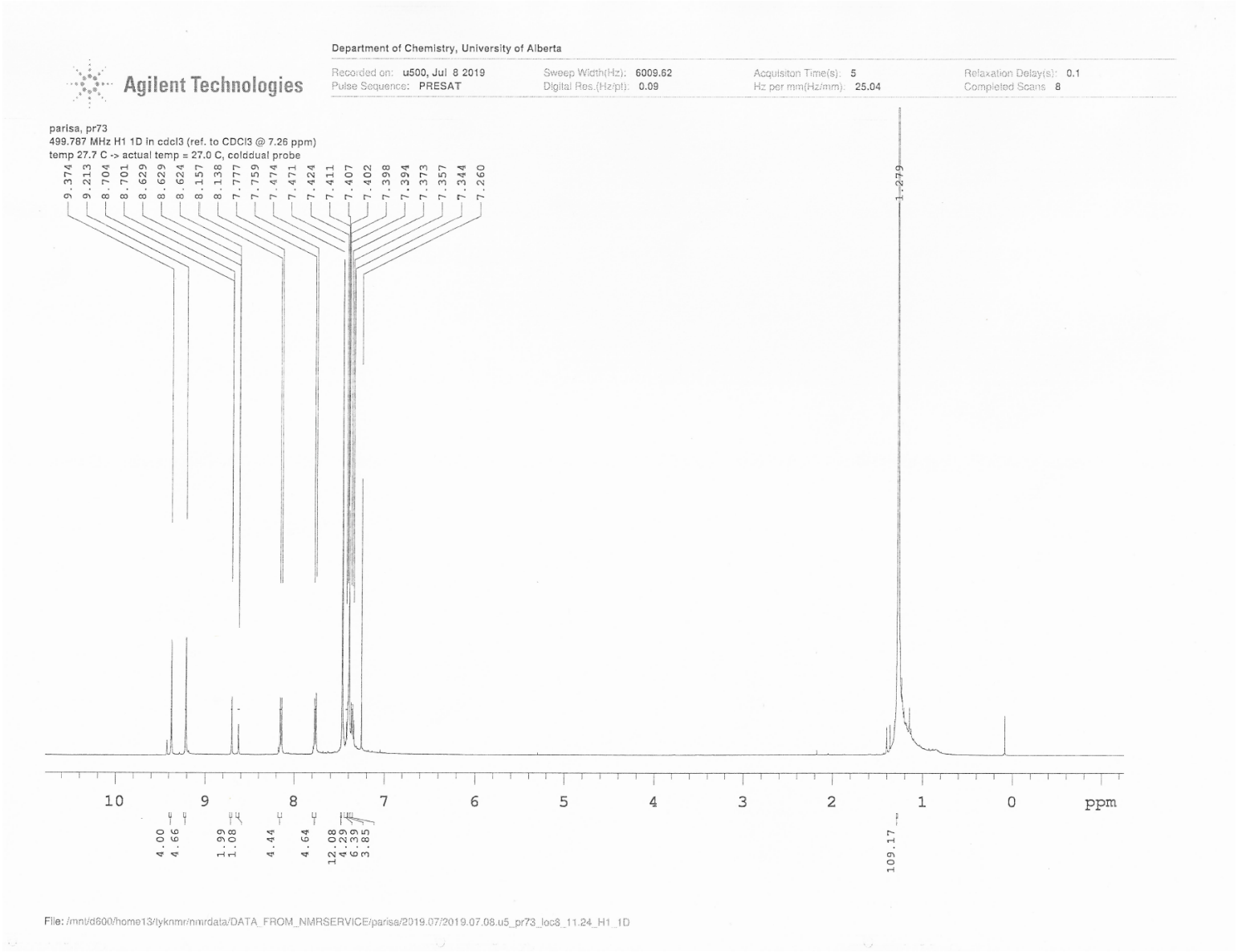

Figure N61. Original ^{1}H NMR spectrum of compound **Tr*-Pnc$_2$**, 500 MHz, $CDCl_3$.

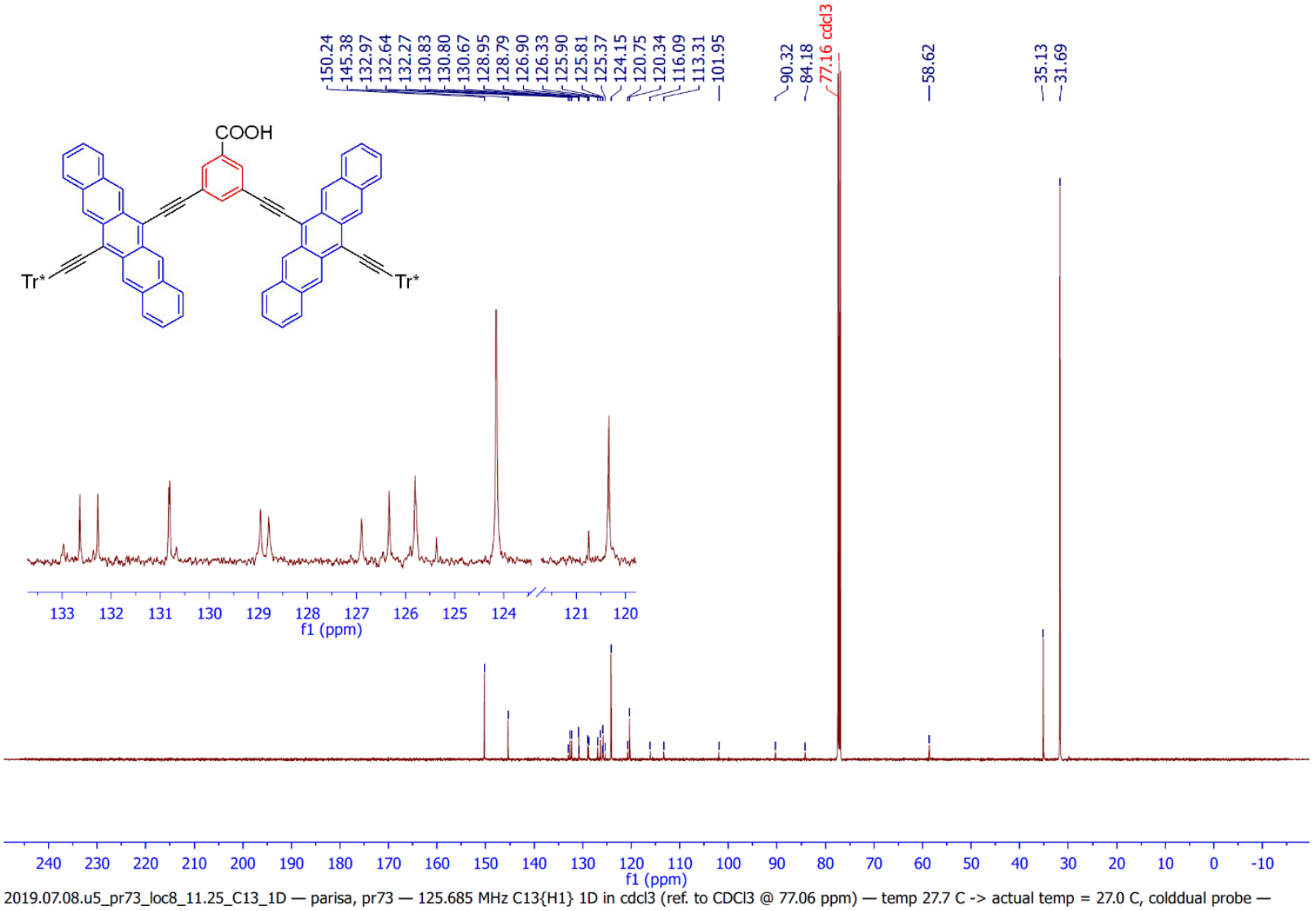

Figure N62. ^{13}C NMR spectrum of compound **Tr*-Pnc$_2$** by MestReNova software, 125 MHz, $CDCl_3$.

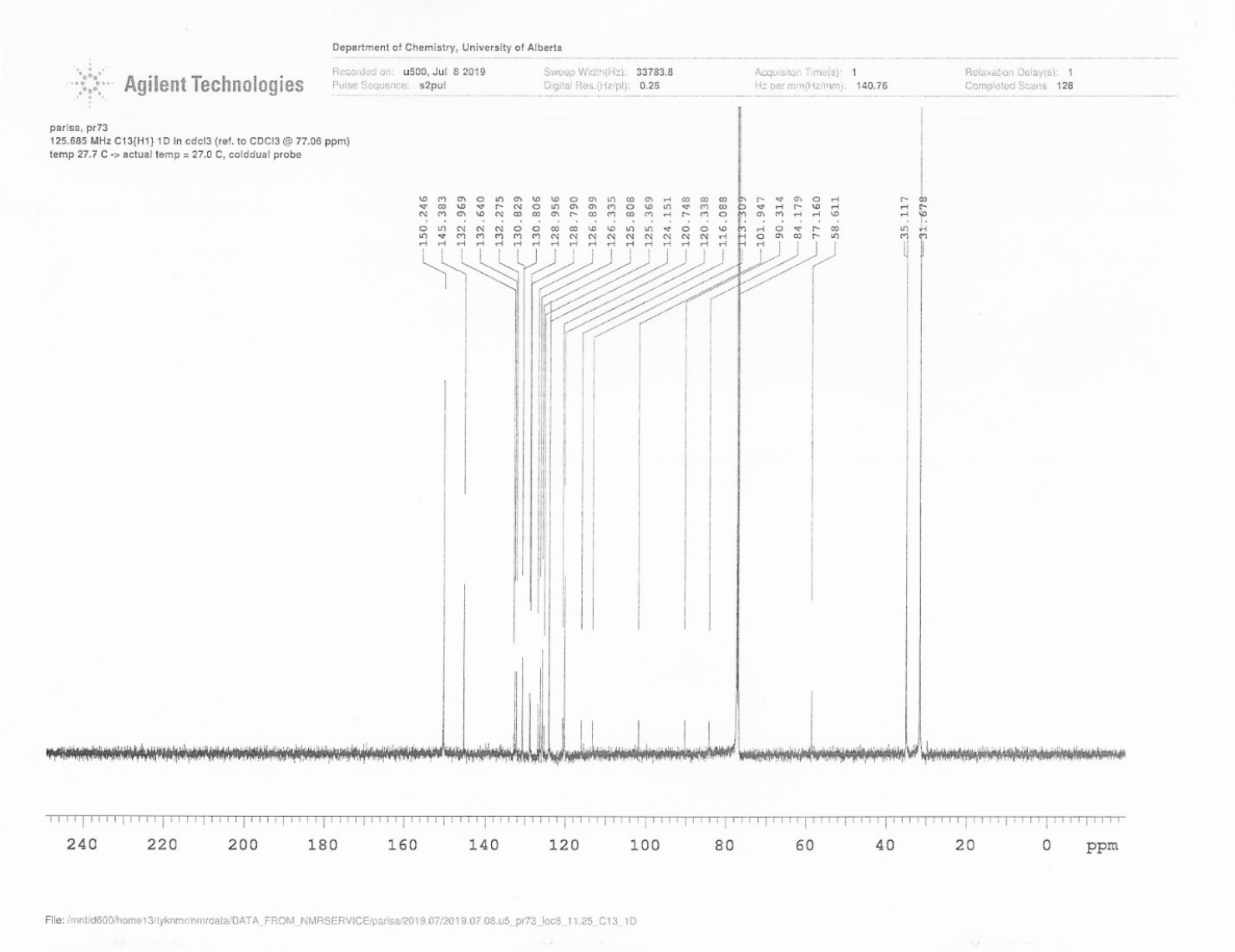

Figure N63. Original ^{13}C NMR spectrum of compound **Tr*-Pnc$_2$**, 125 MHz, $CDCl_3$.

Appendix II – Differential Scanning Calorimetry

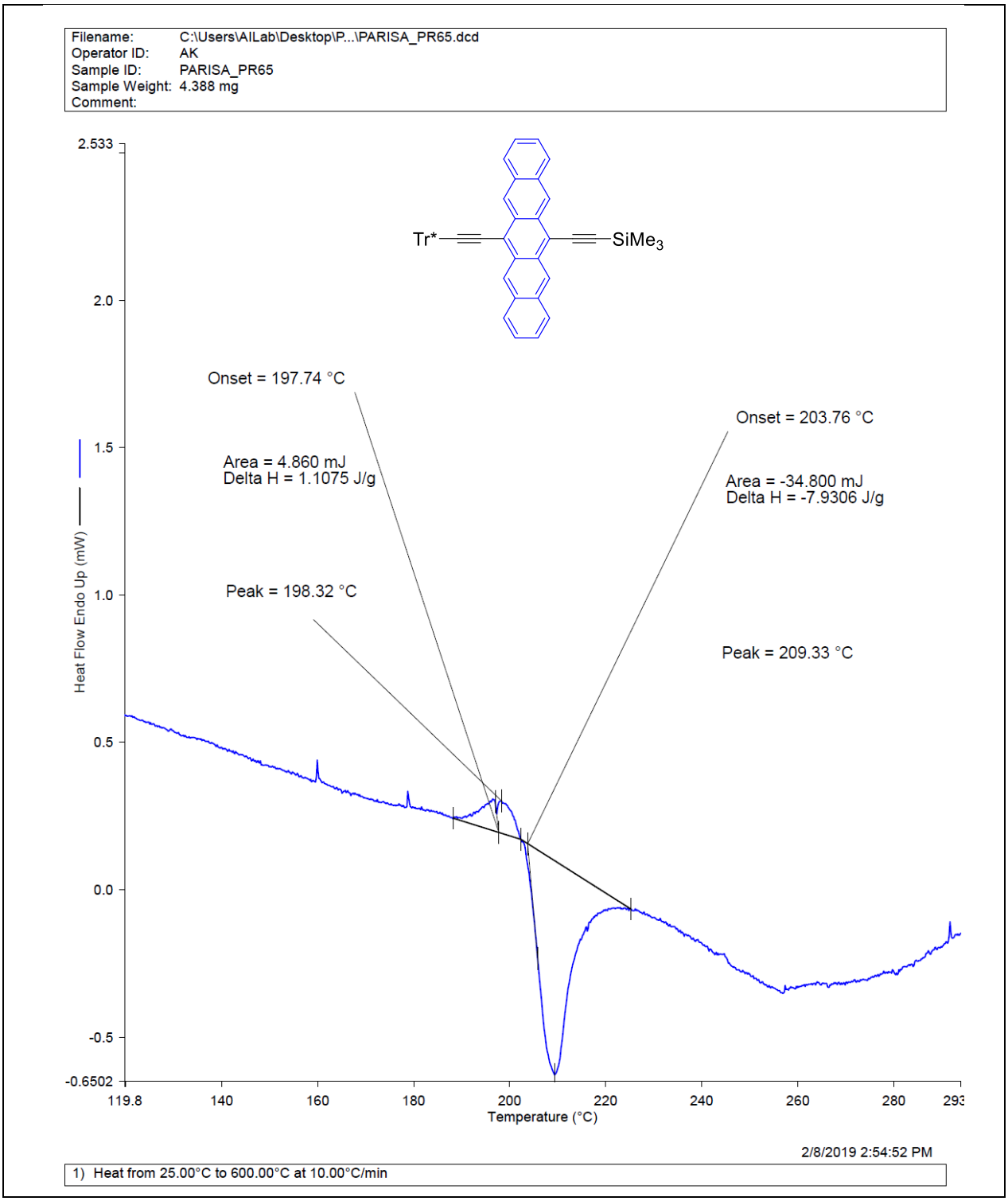

Figure D1. DSC analysis of compound **2.1**.

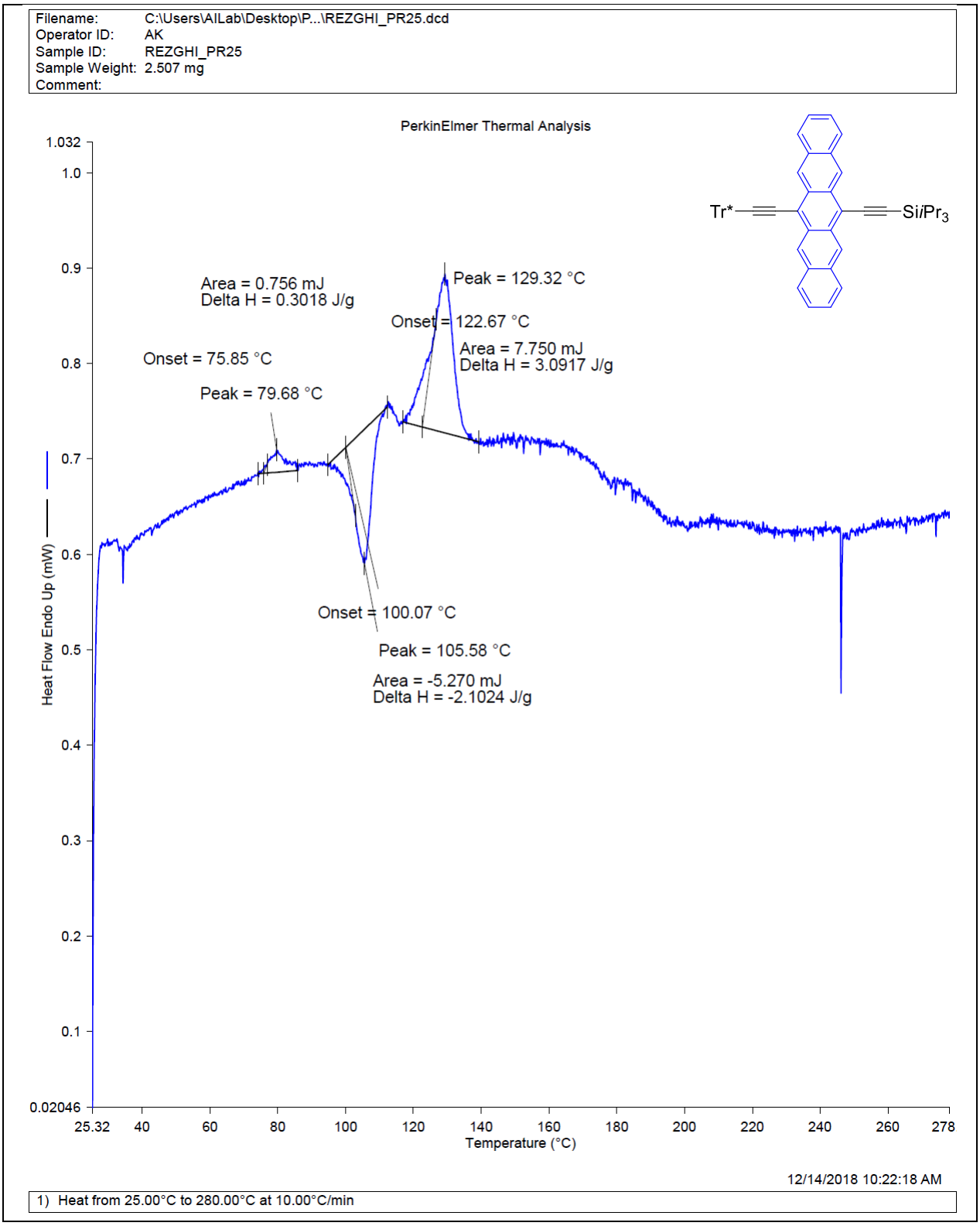

Figure D2. DSC analysis of compound **2.2**.

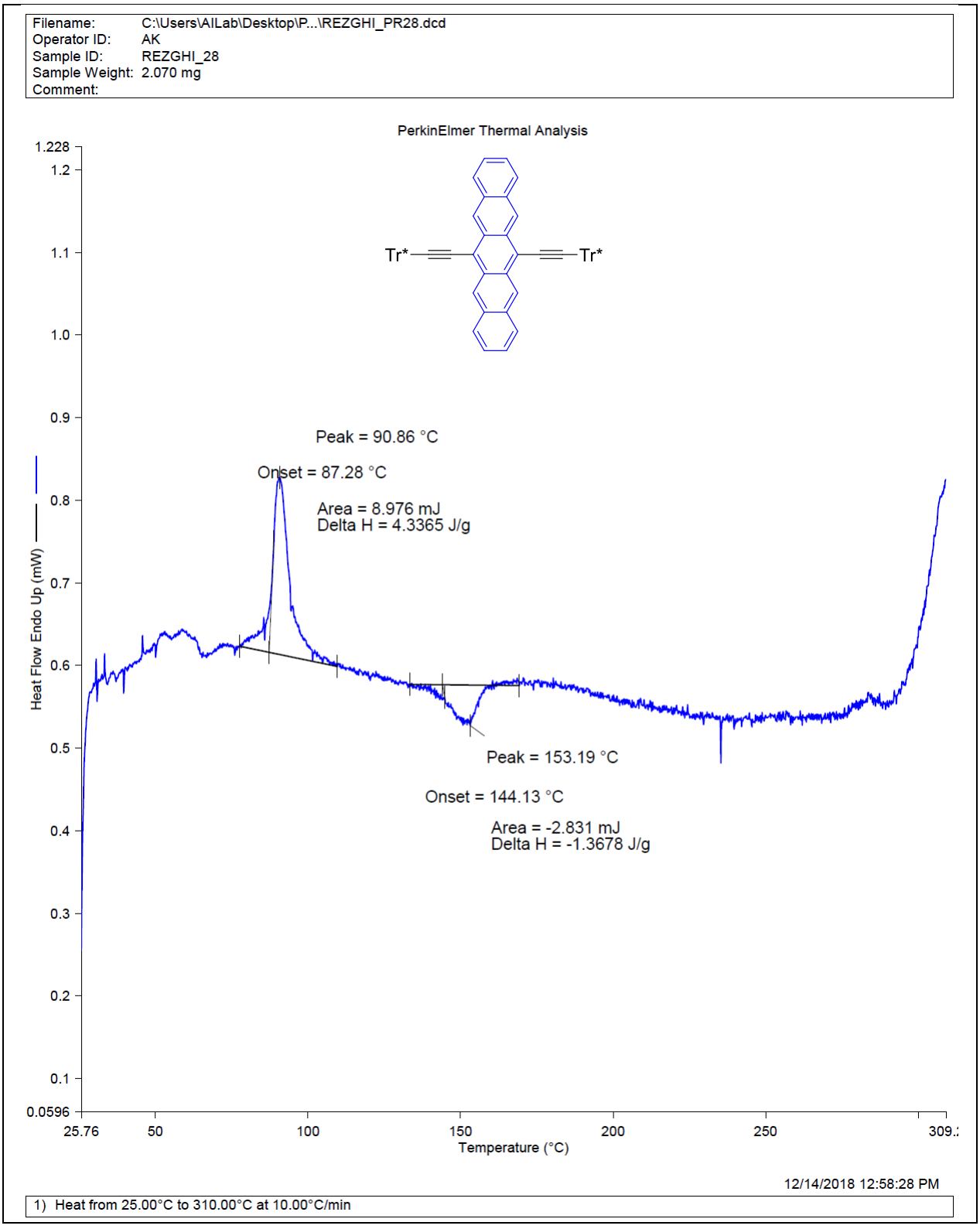

Figure D3. DSC analysis of compound **2.3**.

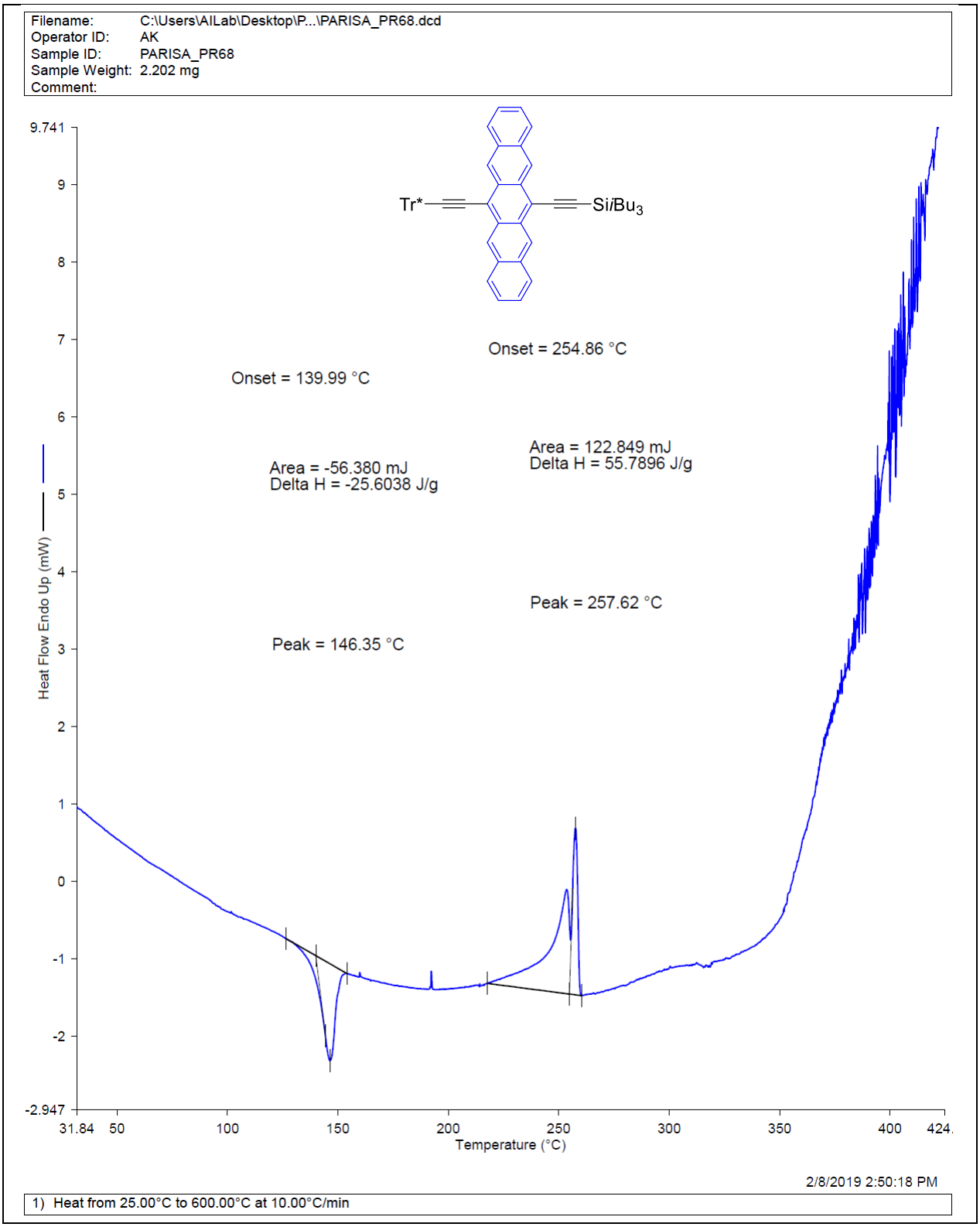

Figure D4. DSC analysis of compound **2.4**.

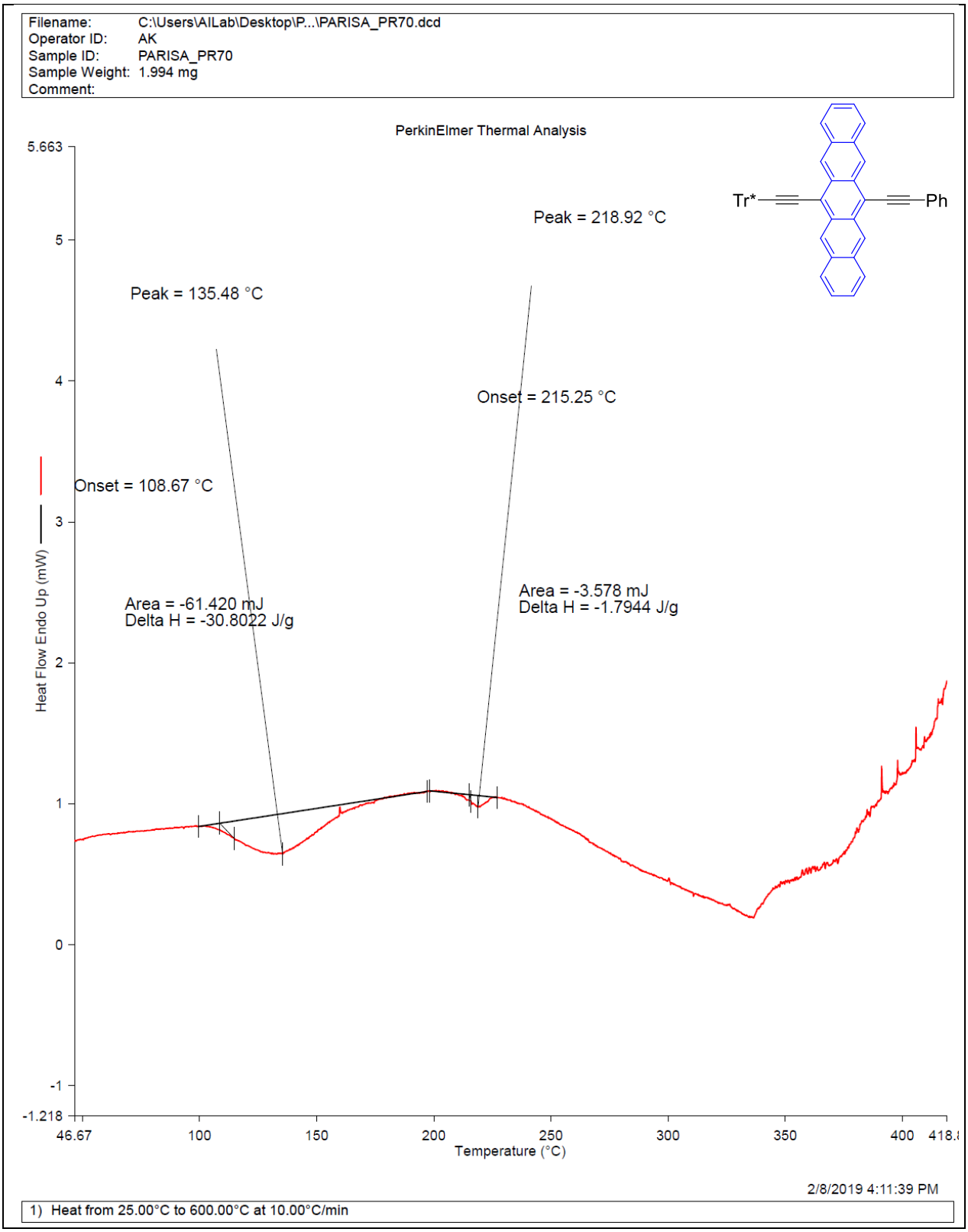

Figure D5. DSC analysis of compound **2.5**.

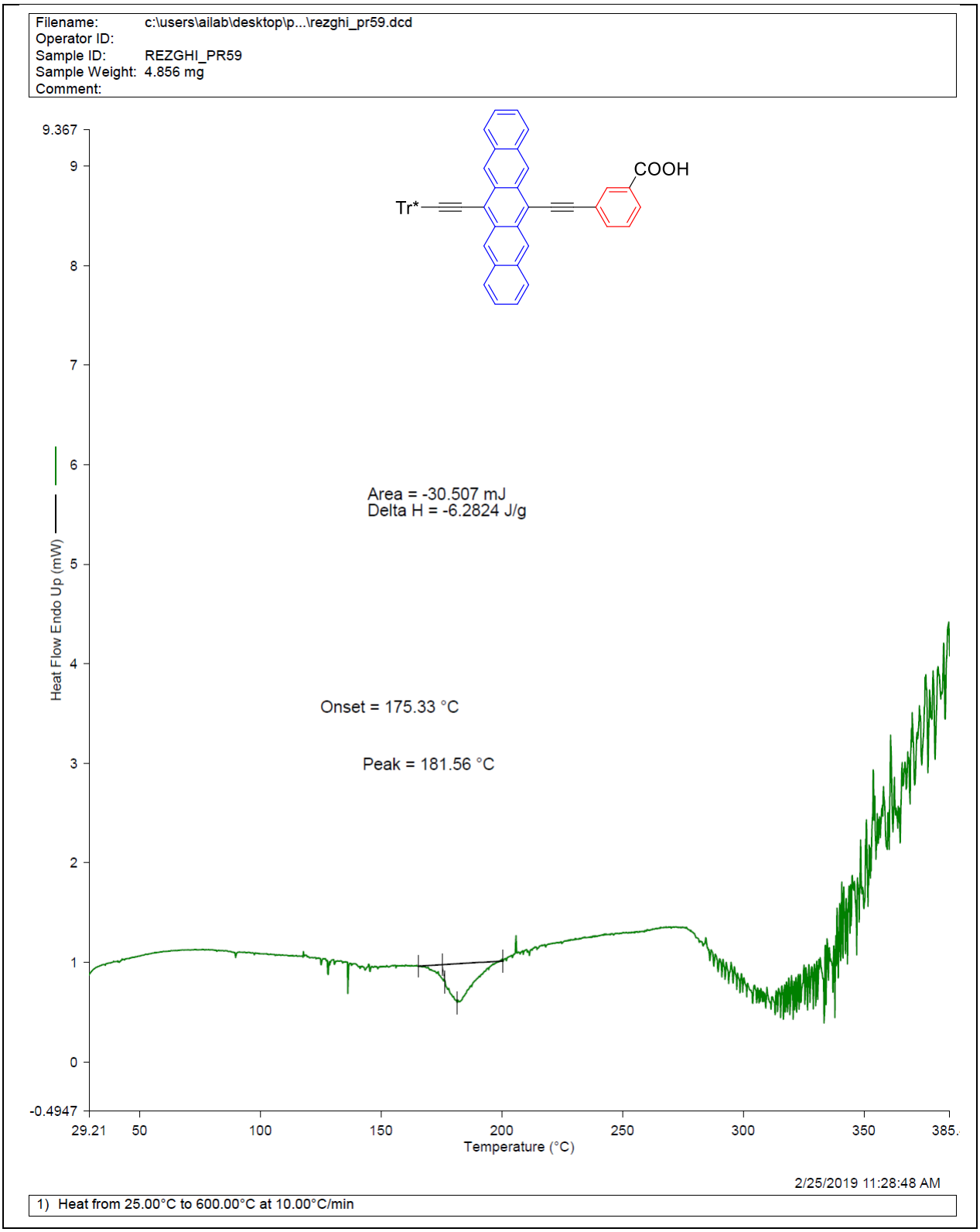

Figure D6. DSC analysis of compound **3.4**.

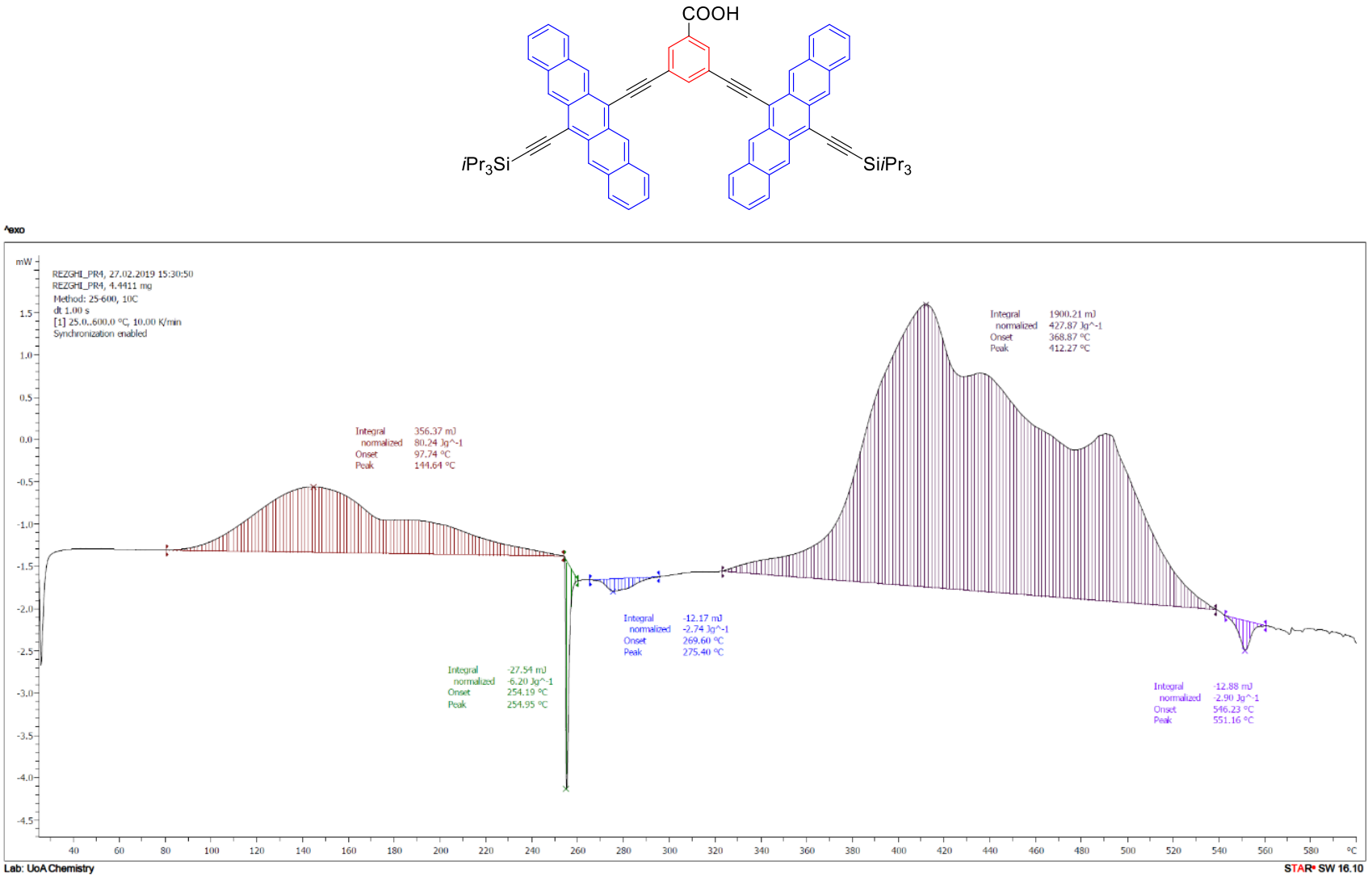

Figure D7. DSC analysis of dimer **TIPS-Pnc$_2$**.

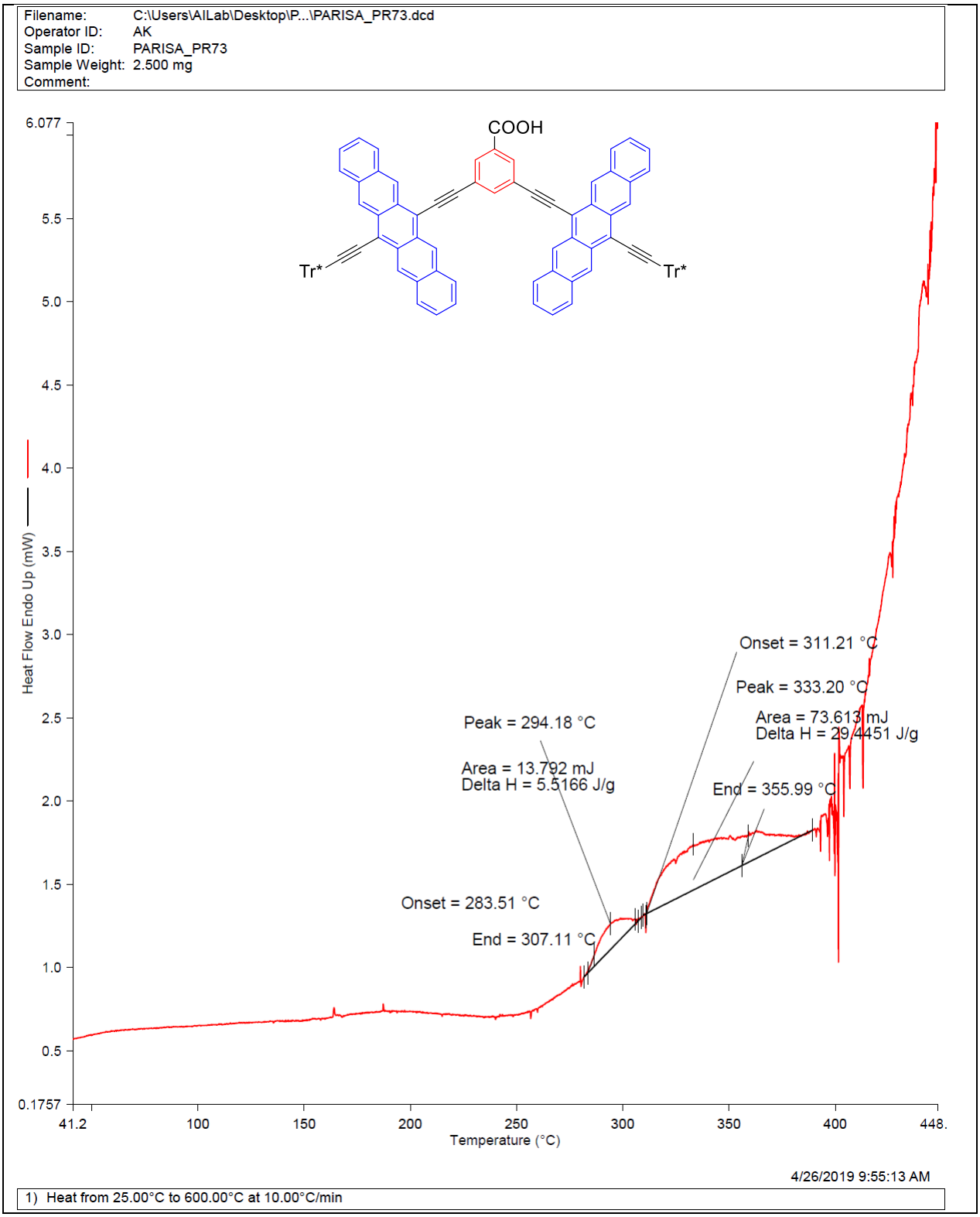

Figure D8. DSC analysis of dimer **Tr*-Pnc$_2$**.